THE REVERSED FIELD PINCH

L Marrelli, P. M. Martin, M E Puiatti, J S Sarff, B. Chapman, J R Drake, Dominique Escande, S Masamune

THE REVERSED FIELD PINCH

L. Marrelli[1,2], P. Martin[1,3], M.E. Puiatti[1,2], J. S. Sarff[4], B. E. Chapman[4], J. R. Drake[5], D. F. Escande[6], S. Masamune[7,8]

[1]*Consorzio RFX, Corso Stati Uniti 4, 35127 Padova, Italy*
[2] *CNR-ISTP, Corso Stati Uniti 4, 35127 Padova, Italy*
[3] *Dipartimento di Fisica e Astronomia, Università degli Studi di Padova, Padova, Italy*
[4] *Department of Physics, University of Wisconsin, Madison, WI, United States of America*
[5] *Royal Institute of Technology KTH, SE-10044 Stockholm, Sweden*
[6] *Aix-Marseille Universitè, CNRS, PIIM, UMR 7345, Marseille, France*
[7] *Kyoto Institute of Technology, Kyoto 606-8585, Japan*
[8] *Chubu University,1200, Matsumoto-cho, Kasugai-shi, Aichi 487-8501, Japan*

Abstract.

This paper reviews the research on the Reversed Field Pinch in the last three decades. Substantial experimental and theoretical progress and transformational changes have been achieved since the last review (Bodin, 1990). The experiments have been performed in devices with different sizes and capabilities. The largest one are RFX-mod in Padova (Italy) and MST in Madison (US). The experimental community includes also EXTRAP -T2R in Sweden, RELAX in Japan and KTX in China. Impressive improvements in the performance are the result of exploration of two lines: the high current operation with the spontaneous occurrence of helical equilibria with good magnetic flux surfaces and the active control of the current profile. A crucial ingredient for the advancements obtained in the experiments has been the development of state-of-art active feedback control systems allowing the control of MHD instabilities in presence of a thin shell. Contributions of the RFP line to the fusion grand challenge will be reported. The balance between achievements and still open issues leads us to the conclusion the RFP can be a valuable and diverse contributor in the quest for fusion electricity.

Contents

Introduction

This review paper describes the achievements of the Reversed Field Pinch configuration in the last thirty years, since the last review (Bodin, 1990) and the advancements in the understanding of its fusion potentialities. The RFP is a toroidal magnetic configuration alternative to the mainstream tokamak. We will summarize in the next seven points why the RFP is much more relevant for fusion and plasma physics than it was twenty years ago and why, in our opinion, it is worth going through the paper.

First, the RFP is not anymore a torus of plasma sitting in a stochastic magnetic field. For long the configuration was portraited like that, and there were some good reasons. The sustainment in time of the configuration against resistive diffusion was indeed due to electric field driven by a broad spectrum of magnetic field and velocity fluctuation, so stochasticity was a price to be paid. Now we know that this is not anymore the case. We have discovered a helical state where the RFP is maintained in time through a self-organised process and with good magnetic flux surfaces. Such a discovery is conceptually similar to that of the H-mode in the tokamak. In alternative, we know how to substitute that plasma generated electric field with an externally applied one.

Second, the confinement has significantly improved. With the reduction of magnetic stochasticity a major source of particle and energy transport was eliminated and confinement performance is better, both in the helical state and with the application of the external poloidal field. With the latter

values of confinement time comparable to those of tokamaks with scaled parameters have been obtained, though in a transient fashion.

Third, confinement can be even better. We have good reasons to believe that it can be strongly improved. The history of the RFP science described in this paper shows how RFP performance was often hampered by technological limitations. All operating RFP devices have originally been designed more than thirty years ago, with a much limited knowledge of the physics, leading for some aspects to solutions that today appear not to be the best. Now countermeasures and modifications have been implemented. The story of MHD stability active control, where RFPs have been successful pioneers, is a clear example. And the upgraded RFX-mod2 device will have most of the limitations due to a sub-optimal magnetic front-end removed.

Fourth, the aforementioned points have been supported by a diagnostic and modelling tool portfolio which is now fully comparable with those of tokamak and stellarator. Not surprisingly, diagnostics developed in RFPs have been moved to other configurations and mainstream codes are used and sometimes validated in the RFP, as for example the tools for helical equilibrium reconstruction.

Fifth, the RFP has bridged with the other two major magnetic configurations, providing profound insights in open problems for the stellarator and the tokamak. Some RFP devices have still the most complete system of coils for feedback control of MHD stability, and in using them have obtained seminal results in a crucial field for fusion. Just to make a couple of examples RFP has been the first to demonstrate simultaneous active suppression of multiple resistive wall modes. And results obtained with those systems have inspired the experiment which has proven the possibility of operating the DIII-D tokamak with a edge safety factor $q95<2$ through active control (Piovesan et al., 2014). Exploration of RFP helical states has provided insights into the understanding of helical equilibria and of helical self-organized processes central to the advanced tokamak operation.

Sixth, the major selling points of the RFP as a fusion configuration, i.e. the possibility of reaching thermonuclear regimes with ohmic heating only and the relatively simpler engineering due to the low magnetic field at the coils are worth to be explored again. The modern understanding of the configuration suggests revisiting them in the light of the new paths for confinement improvement (considering also that the route to a steady state fusion device with efficient auxiliary heating systems it is still not very clear).

Seven, diversity. The search for fusion electric energy is based on a grand experiment which includes devices, theories and modelling tools. While the roadmap to fusion is relatively clear, the issues to be solved to reach the final goals are still such that diversity may help both for solving them and as risk mitigation. While focussing most of resources on the tokamak is reasonable,

keeping an eye open on different regimes is crucial. In this respect the RFP covers a parameter region otherwise unexplored. We think that the RFP can be fusion relevant even if it will never reach fusion.

1 Narrative summary

Even if they are just a blink in the course of human history, thirty years in modern science are a period long enough to witness important changes and improvements. This is certainly true for magnetic fusion research where, during the last three decades, a huge amount of progress has been made. This is true also for the RFP, whose physical comprehension and experimental performance have considerably and sometimes even surprisingly improved.

The aim of this section is to provide the reader with a bird's-eye view of the entire paper. Given the length of the paper we feel it is important to grant access to its contents at different and clearly visible levels. We hope that the main message can be captured without too much technical detail – but with accurate links to the locations where the whole story can be found - and in a few minutes reading.

Having to pick the starting point for this narrative summary, the natural choice is the change of paradigm for the configuration description: from a plasma dominated by magnetic turbulence to one with closed flux surfaces, with dramatic improvement in plasma confinement.

The 1990 review was indeed describing the RFP as a Taylor relaxed state (Taylor, 1986), where the elegance of the physics description was accompanied by the belief that the level of magnetic turbulence implicit in the RFP dynamics would have significantly hampered the fusion ambition of the configuration. The RFP equilibrium was described at the first order as a Taylor state, but it was already very clear that in order to maintain in time the equilibrium with a reversed toroidal field a process to convert externally supplied poloidal flux into toroidal flux was necessary. This process was identified as the RFP dynamo, with analogy to astrophysical settings.

The "engine" of the RFP dynamo was described as powered by magnetic ($\tilde{b}$) and plasma flow fluctuations ($\tilde{v}$): both measurements and pioneering numerical simulations supported the picture of the coherent combination of $\tilde{b}$ and $\tilde{v}$ as the origin of the dynamo electric field. The RFP safety factor profile, while avoiding gross and disruptive instabilities, is rich of resonant surfaces for m=1 and m=0 MHD tearing instabilities, corresponding to rational values of the q parameter, which were routinely measured. The issue is that the radial component of the magnetic fluctuations, in particular, is breaking the toroidal symmetry of the magnetic field and causing broad regions of stochasticity. The breaking of nested flux surface and the wandering of magnetic field lines from

the plasma core to the edge produces a privileged and direct channel of energy and particle losses (parallel field transport), with painful consequences on confinement.

The turn between the 80's and the 90's marked the start of a new research programme, which overturned the previous expectations on the RFP confinement properties. Two large experiments, MST in Madison, Wisconsin and RFX in Padova, Italy started to operate. They produced an ample set of measurements. The experiments were driven by (and drove themselves) MHD numerical simulations which opened a completely new paradigm for the RFP description. Such simulations revealed a bifurcation from a magnetically stochastic to a helical and magnetically ordered plasma state, where sustainment in time was not coming at the expenses of broadband magnetic turbulence.

Now multiple MHD instabilities are no longer considered an essential ingredient of the RFP dynamics. These low magnetic turbulence states are basically of two kinds: those spontaneously achieved by accessing the single helicity regime and those obtained by means of inductive control of the plasma current profile. In single helicity the basic nature of the RFP is described as a self-organized helical state corresponding to the non-linear saturation of a single kink-tearing mode, called the dominant mode. The best experimental approximation of single helicity are quasi-single-helicity (QSH) states. In these states the innermost resonant $m = 1$ mode dominates over the others, the so-called secondary modes, which maintain a much smaller finite amplitude.

While theoretical and experimental studies of single helicity plasmas were progressing, a second approach to go beyond the paradigm of a stochastic RFP dominated by global core-resonant tearing modes has been advanced, relying on the modification of the current profile to mitigate such modes. The experiments of Pulsed Poloidal Current Drive led to a strong reduction of stochasticity and improvement of the plasma confinement scalings.

Parallel to the results obtained in MST, RFX and RFX-mod, the other RFP experiments were successful in reproducing the improved regimes resulting from current profile control and the transition to Quasi Single Helicity states, including TPE-RX in Tsukuba , EXTRAP-T2R in Stockholm, RELAX in Kyoto.A new large device, KTX, is in the first phase of operation in Hefei, China.

The advancement of the RFP performances obtained in the last decade motivated an upgrade of the RFX-mod device, presently underway, aiming at a further reduction of the magnetic turbulence and at a substantial improvement of the high current performance.

Chapter 2 gives a quick insight into the basics of RFP equilibrium and stability and a summary of the devices that since '90s contributed to the development and to the progress of the RFP

confinement scheme. They are spread in three continents, Europe, America, Asia, testifying and favouring the international character of this research line.

The RFP is a helical magnetic configuration in both the Multiple Helicity (MH) state, characterized by several MHD unstable modes of comparable amplitude producing magnetic chaos, and in the experimental Quasi Single Helicity (QSH) state, with a single mode dominating over the others thus producing ordered magnetic surfaces: in the MH state it is characterized by a toroidally localized helical deformation, in the QSH state it corresponds to a uniformly distributed one. This is discussed in chapter 3. It starts with recalling the developments based on the magnetic self-organization processes as derived from the original Taylor theory. Nonlinear, 3D, resistive magnetohydrodynamic computations show that the dynamo activity appears in two regimes: the discrete dynamo, where current density redistribution takes place quasi-periodically, and the continuous dynamo where no characteristic discrete behavior can be identified.

The dynamo field has then been reinterpreted with a unified description that allows to understand both turbulent and laminar dynamo. The origin of the dynamo velocity field is recognized to be an electrostatic drift and the experimental studies of the dynamo term are presented in detail. This approach to the RFP dynamo paves the way for a new vision where the MH and SH states are described by theory as the result of a bifurcation process ruled by the dissipation $d = \eta(0)\nu(0)$, also quantified by the Hartmann number $H = d^{-1/2}$: an increase of dissipation is favourable to a laminar behaviour of the system. The importance of this new vision has been fully recognized when Quasi Single Helicity (QSH) states emerged in the experiments, mainly in high current regimes. In particular, when in RFX-mod accurate active feedback control of the edge magnetic radial field allowed operating RFX-mod at its maximum current of 2 MA, a new topological bifurcation to a single helical magnetic axis was found to occur (SHAx states), with the spontaneous development of a helical equilibrium with a single helical axis, reduced magnetic fluctuations and strong transport barriers. The remarkable agreement between theory and experimental QSH states even improves when such states are produced by a magnetic edge perturbation, both in simulation and experiment.

The magnetic dynamics has a significant impact on the confinement and transport properties in the RFP, which are addressed in chapter 4. In the MH state the overlap of the magnetic islands due to the core resonant dynamo modes causes a broad region of stochastic magnetic field, where the temperature profile is observed to be flat. The analysis of the radial profile of the electron thermal diffusivity χ_e indicates a dependence on the relative magnetic fluctuation amplitude $\chi_e \propto (\tilde{b}/B)^{\alpha}$,with α ranging between 1.4 and 2. This scaling is similar to that described by Rechester and

Rosenbluth (Rechester and Rosenbluth, 1978), though the experimental values of χ_e are generally smaller than those predicted by the theory. In QSH states the temperature profile mirrors the magnetic topology: a small hot island is observed in a Double Axis state, when the QSH is characterized by the presence of two magnetic axes (the unperturbed axi-symmetric one and the axis related to the island of the dominant mode). A wider region with high temperature, involving most of the plasma core and encompassed by strong gradients, is instead observed in experimental SHAx states, when the magnetic separatrix of the island is expelled and a single magnetic axis survives. SHAxs are characterized by improved transport and confinement properties, and in the region of strong gradients the energy transport is strongly reduced by more than one order of magnitude. As to particle transport, the analysis of electron density profiles coupled to transport simulations show that the main drive remains the residual magnetic chaos also in QSH states, with the diffusion coefficient lower than in MH, due to the lower value of magnetic fluctuations. Indeed transient experiments by pellet injection in RFX-mod showed an enhancement of the global particle confinement time by a factor 2-3 in QSH. The impact of microturbulence on transport has been studied by gyrokinetic simulations. They show that in axisymmetric configuration the Ion Temperature Gradient (ITG) turbulence basically does not affect transport. Instead in helical states, where the temperature gradients are higher and stochastic transport is reduced, ITGs become an important contributor to transport. They act together with microtearing modes, which are unstable in the high temperature gradient region. Dedicated studies have been devoted to the effect on transport of magnetic reconnections, which are basic processes during which magnetic energy is dissipated or converted into kinetic energy or particle acceleration. Altogether it has been found that a significant fraction of the magnetic energy (30-50%) is released during reconnections and that a fraction ($\leq$ 30%) of such energy is converted into ion thermal energy. Detailed measurements of the evolution of the electron thermal diffusivity in the core during a reconnection event in MST have shown a strong enhancement at the crash followed by a minimum soon after. Studies performed on edge transport and turbulence aimed in particular at characterizing the effect on transport of the $m=0$ island chain corresponding to the $q=0$ surface, which basically acts as a transport barrier. Outside the reversal surface the RFP edge transport is mainly driven by electrostatic turbulence. A positive isotopic effect is observed, related to stronger temperature gradients at the edge. Fast ion confinement studies have been mostly carried out in MST, thanks to its beam injector. It is relevant that in MH states the confinement of fast ion is much higher than that of thermal particles and close to the classical values. This is due to a weaker effect of magnetic stochasticity related to their larger Larmor radius, which averages out a part of the magnetic fluctuations. In QSH states, fast ion confinement remains higher than the thermal ion one, but does not reach classical values.

The alternative approach to improved confinement in the RFP by stochasticity reduction, based on current profile control, is described in chapter 5. MHD computations demonstrated that tearing fluctuations responsible for magnetic field stochasticization could be reduced or even eliminated with a suitable modification of the current profile. A relatively modest local change in the edge current profile leads in fact to dramatic changes in the core-resonant tearing mode amplitudes, such that stochasticity is substantially reduced. Several approaches to inductive current profile control have been studied in experiments and simulations. All entail temporal variations in the toroidal and/or poloidal magnetic field. Pulsed Poloidal (or Parallel) Current Drive (PPCD) is the most successful technique. First studied in MST, it has been successfully tested also in RFX, EXTRAP T2-R and TPE-RX. The dynamo electric field during PPCD is observed to become very small, so that the resistive term in the Ohm's law is balanced by the applied electric field, and the measured fluctuation reduction is broadband and substantial. PPCD has led, though transiently, to large improvements in energy and thermal particle confinement time with substantial enhancement of electron and ion temperature and reduction of ohmic heating power. Moreover, the normalized electron density can exceed the Greenwald limit and an RFP-record beta exceeding the Mercier criterion (Mercier, 1960) has been obtained. The efforts undertaken on MST aiming at non-inductively (non-transiently) modifying the current profile will be described. Those efforts aim at driving current via electrostatic current sources inserted into the plasma edge and at launching lower-hybrid and electron-Bernstein waves from rf antennas.

Chapter 6 deals with the limits to plasma pressure. It is shown that the β limit is different in the RFP with respect to the Tokamak. The ideal β limit is much higher in the RFP. In MST values of total β as high as 26% have been measured, consistent with the Connor-Taylor scaling (Connor and Taylor, 1984) and exceeding the Mercier criterion governing the interchange stability (Mercier, 1960). High beta values are also associated to neoclassical bootstrap current effects. The chapter describes the experimental and modelling efforts to explain the high density limit. They contribute to the understanding of a still open issue for all magnetic configurations. In this context a new power-balance model is particularly interesting (Zanca et al., 2019), being able to reproduce the experiments in RFPs, Stellarators and L-mode Tokamaks up to now described by the empirical Greenwald law.

During the last 15 years RFP devices have become very attractive laboratories to study state-of-the-art active feedback control of MHD stability, in particular thanks to the very advanced active coil systems deployed in EXTRAP T2R and RFX-mod. To these studies is dedicated chapter 7. Theoretical studies on the stabilization of RWM are described together with the experimental demonstration of RWM control. The focus is on EXTRAP T2R and RFX-mod experiments: in fact

such devices are equipped with sophisticated active control systems based on 128 and 192 coils respectively, each independently driven and controlled. The chapter deals also with tearing modes, which in the RFP, are ruled by nonlinear MHD (in contrast to RWM). The constructive interference of the m=1 internally resonant modes produces a toroidally localized helical deformation of the plasma column (Slinky or Locked Mode, LM), which can rotate in the laboratory frame or wall-lock, depending on the level of plasma current, on the amplitude of magnetic fluctuations and on the properties of the device boundary. Such Locked Mode, especially when wall locked, produces negative effects on the plasma: increased plasma-wall interaction, increased fuel recycling, and increased loop voltage necessary to sustain the plasma. Several algorithms have been developed and tested to control the local deformation of the magnetic field induced by Locked Mode, mainly in RFX-mod, ultimately leading to its very effective reduction and slow rotation, which allowed safe plasma operation also at the highest current levels.

As in other magnetic configurations, the Plasma-Wall Interaction (PWI) plays a crucial role in determining the plasma behaviour and performance, in particular through the control of plasma density and impurity contamination. In the RFP PWI is related to the magnetic topology through the three-dimensional edge magnetic fields (Locked Mode). This is discussed in chapter 8. The MH RFP shows in fact a substantial evidence of asymmetries in the power deposition, correlated to the local deformation of the magnetic field. Power loads locally as high as ≈100 MW/m^2 are observed in the region where the bulge intercepts the wall. In RFX, with plasma current approaching 1 MA, in proximity of LM the graphite tiles reached the carbon radiation enhanced sublimation temperature, resulting in carbon blooming processes, observed as uncontrolled sudden increase of carbon, radiation and electron density. Feedback control of MHD stability has strongly reduced the issue of PWI, both in RFX-mod and EXTRAP-T2R. In RFX-mod, a large reduction of the radial deformation of Last Closed Magnetic Surface (LCMS) has been observed, and slow mode rotation has been obtained. This brings more uniform PWI and improved plasma performance. Similarly, in EXTRAP-T2R the active feedback stabilization of RWMs resulted in reduced impurity radiation and improved plasma performance. Due to the necessity of a close fitting conducting wall for MHD stability, the RFP devices have not been equipped with divertors so far. Only limited studies for small size devices were done and provided uncertain outcomes. The absence of an active control of neutral particles comes with the issue of fuel and impurity recycling control, which requires the study of innovative concepts for the active control of recycling and for the power exhaust. Some note on dust particle studies, performed on the EXTRAP T2 and T2R devices, is also given.

Chapter 9 summarizes the experimental and modelling studies made on a quasi-steady-state method of inductive current sustainment, called Oscillating Field Current Drive (OFCD), based on the

application of oscillatory toroidal and poloidal loop voltages, resulting in the generation of a dc current via the nonlinear relaxation processes. In principle for a future reactor, inductive current drive via a transformer does not introduce special plasma-boundary requirements or perforations in the blanket and shield. Modelling of the OFCD process and the experimental tests performed mainly on MST and marginally in RFX-mod are reported.

2 RFP basics

2.1 Cylindrical equilibrium and basic linear stability

The Reversed Field Pinch (RFP) is a toroidal magnetic configuration for the confinement of thermonuclear fusion plasma. The RFP shares several features with the well-known tokamak configuration. (i) It exploits the pinch effect, as a toroidal electrical current is driven in a plasma embedded in a toroidal magnetic field. (ii) It relies on a toroidally symmetric vacuum vessel surrounded by a set of toroidal field coils. (iii) A central solenoid provides the induced loop voltage necessary to trigger the plasma discharge and drive a current in the plasma. However, different from the tokamak the toroidal field coils do not play a key role in providing the total magnetic field, since most of it is instead generated by the currents flowing in the plasma. The toroidal and poloidal components of the RFP magnetic field are of comparable amplitude, a different situation than in a tokamak where a stabilizing toroidal magnetic field larger than the poloidal one is needed. This is shown in Fig. 2.1, where the poloidal and toroidal radial magnetic field profiles (normalized to the on-axis toroidal field) are reported for cylindrical RFP and tokamak configurations. Two features should be noted: first, the toroidal field amplitude in the RFP has a strong radial dependence, goes through zero and then negative at the edge, meaning that in the outmost part of the plasma the toroidal field has opposite direction with respect to the core. This feature, together with the poloidal magnetic field, guarantees a strong magnetic shear. Second, for the same plasma current the edge toroidal field is much smaller – almost zero – for the RFP in comparison with the tokamak. This latter feature is of course something that engineers love, since it means much lighter and cheaper coils. Historically the RFP the cylindrical 1-d equilibrium is described in terms of two edge and easily measurable quantities, the reversal parameter F and the pinch parameter Θ:

$$F = \frac{B_\phi(a)}{\langle B_\phi \rangle}, \quad \Theta = \frac{B_\theta(a)}{\langle B_\phi \rangle} \qquad 2.1$$

where $\langle B_\phi \rangle$ is the cross section average toroidal magnetic field and a is the plasma minor radius. While these parameters and in general the 1-d cylindrical description of the RFP equilibrium are in

fact any more used – and this will become clear in the following– it is worth mentioning them since elements of the work described in this paper refers to them.

The currents flowing in the plasma to generate the magnetic field are only partially driven by the applied inductive electric field. Already in the '80s it was in fact realized that in order to maintain in time the equilibrium with a reversed toroidal field a self-organized process to convert the externally supplied poloidal magnetic flux – driven by the applied toroidal electric field - into toroidal magnetic flux was necessary. This self-organization process was identified as the RFP dynamo, with analogy to astrophysical settings.

Not surprisingly safety factor profiles in tokamak and RFP are very different, too, as shown in Fig. 2.2 respectively. The RFP cylindrical safety factor $q(r) = rB_\phi/RB_\theta$ is positive and lower than 1 in the core ($q(0) \approx a/2R$, where a and R are the minor and major radius respectively) and negative at the edge due to the reversal of the toroidal field. This has profound consequences in terms of plasma magnetohydrodynamic (MHD) stability.

In the tokamak the radial force balance is achieved by equilibrating the radial kinetic pressure gradient with the stresses of the poloidal magnetic field. The large toroidal magnetic field has very little role in the radial pressure balance and in the toroidal force balance (Freidberg, 2013). Its main function is that of providing plasma stability against the kink mode. This action is ruled by the Kruskal-Shafranov limit, which dictates that the tokamak edge safety factor must be larger than unity. Allowing the edge safety factor to monotonically decrease from a value lower than unity in the core and become negative at the edge as in the RFP opens a new stability windows where the Kruskal Shafranov limit is not anymore an issue. For a given applied toroidal field the RFP does not have therefore the plasma current limitation of the tokamak and in principle fusion temperatures can be reached by ohmic heating only, which could be a significant simplification for future fusion plants (Werley, 1991).

On the other hand, the high magnetic shear cannot guarantee ideal stability of external m=1 low n pressure driven and current driven kink modes and therefore a relatively close-fitting conducting shell is required (Robinson, 1971). As the conductivity of any real shell is finite, the kink modes become unstable at a growth rate that depends on the shell time constant $\tau_w = \mu_o a \delta \sigma$ (where a is the minor radius, δ is the wall thickness and σ is the wall conductivity). Resistive Wall Modes were considered a serious issue for the RFP: as they cannot be stabilized by the sub-alfvenic plasma rotation, they require active feedback. After an early attempt by HBTX-1C, EXTRAP-T2R and RFX-mod proved the feasibility of magnetic feedback control, as will be shown in Chap.7.

The RFP configuration is tightly linked with resonant resistive instabilities, as it comes apparent by examiningthe location of rational surfaces in a typical RFP safety factor profile (Fig. 2.3). Resonant surfaces for m=1 modes with $n \geq 2R/a$ are present throughout the plasma (R is the plasma major radius and m and n are respectivel the poloidal and toroidal mode numbers in the usual cylindrical fourier modal decomposition) and the $q=0$ surface is resonant for m=0 modes.

Tearing instabilities strongly influences the plasma behaviour. While the RFP MHD instabilities are rarely disruptive for long time they have been a constant presence of the RFP operation. A spectrum of m=1 and m=0 modes with nonlinearly saturated amplitude of the order of 1% of the equilibrium field seemed to be indeed an universal and unavoidable feature of the RFP. Those multi-modes RFP scenarios where dubbed Multiple Helicity (MH). The fluctuating magnetic field and velocity field due to those instabilities was indeed considered to be the "engine" of the RFP dynamo, working by means of a mean electric field $\mathbf{E}_f = -\langle \tilde{\mathbf{v}} \times \tilde{\mathbf{b}} \rangle$ produced by the fluctuating velocity field $\tilde{\mathbf{v}}$ and fluctuating magnetic field $\tilde{\mathbf{b}}$, where the brackets indicate an appropriate spatial and time average. The downside of those magnetic fluctuations was the production of broad regions of stochastic magnetic field in the plasma, increasing the transport and spoiling the confinement.

Given that situation the understanding and its active and/or self-organized control has been a crucial challenge for the RFP research over the last twenty years. The community efforts have been successful and, as it will appear evident continuing the reading of this paper, a changed of paradigm occurred, driven by experimental and numerical work. Excellent capabilities for instability control and/or suppression have been developed and a helical self-organized RFP state with internal transport barrier has been discovered. This state, theoretically called Single Helicity (SH) state, allows for sustaining the RFP configuration thanks to a single dominant mode – thus accessing and helical equilibrium - and to drastically reduce the level of magnetic stochasticity, with consequent confinement improvement.

2.2 The RFP devices

Since the '90s, several RFP devices have been in operation developing strong collaborations and contributing to the aforementioned progress. Table 2.1 lists the machines presently in operation. The largest one is RFX-mod (formerly RFX, (Gnesotto et al., 1995)) at Consorzio RFX in Padova (Sonato et al., 2003), with major radius R=2m and minor radius a=0.459 m, equipped with a thin copper shell (τ_w=100 ms shell time) and able to produce plasmas with 2 MA maximum current. The device is being upgraded in order to improve its performance by improving MHD stability and reducing the plasma-wall interaction. MST, at the University of Wisconsin Madison , US (Dexter et al., 1991), (R=1.5 m, a=0.5 m) can operate up to 0.6 MA plasma current and its vacuum vessel

coincides with a thick (5 cm) conductive shell aluminium shell. EXTRAP-T2R (Brunsell et al., 2001) , in operation at the Royal Institute of Technology, Stockholm, Sweden, (R= 1.24 m, a=0.18m, maximum plasma current = 0.3 MA) is equipped with a copper shell with shell time 12 ms and focuses its experimental activity on the development of advanced tools for the feedback control of plasma MHD instabilities. RELAX is a low aspect ratio RFP (Masamune et al., 2007) (R= 0.51 m, a=0.25 m, maximum plasma current = 0.12 MA) is operated at the Kyoto Institute of Technology, Japan and is mainly dedicated to the study of Single Helicity plasmas. KTX (Zheng et al., 2012) is starting its operation at the University of Science and Technology in Hefei, China, (R=1.4 m, a= 0.4 m), has a magnetic boundary similar to the RFX-mod one and is foreseen to produce a plasma current of 0.5MA in phase 1 and 1 MA in phase 2

	RELAX	EXTRAP-T2R	MST	KTX phase1(phase2)	RFX-mod
R/a (m)	0.5/0.25	1.24/0.18	1.5/0.5	1.4/0.4	2/0.459
Shell time τ_w (ms)	5	12	several hundreds	40	100
Max I_p(MA)	0.12	0.3	0.6	0.5 (1)	2
Pulse length (s)	0.0035	0.1	0.1		0.5
Max T_e (keV)	0.3	0.3	2	0.3 (0.8)	1.2
n_e range $10^{19}m^{-3}$	0.2-3	0.5-2	1-3	1-10	1-8

Table 2.1 – Main parameters of present RFP devices

Based on the present understanding of the interplay between passive conductive boundaries and tearing modes in an RFP, an upgrade of RFX-mod machine assembly has been designed, dubbed RFX-mod2, and it is now being implemented (Lionello Marrelli et al., 2019; Peruzzo et al., 2019, 2017). Main aim of such upgrade is to modify the magnetic front-end in order to reduce the magnetic chaos. Indeed a reliable RFP operation at high current requires a reduction of the localized plasma-wall interaction by a decrease of the non-axisymmetric deformation of the Last Closed

Magnetic Surface (LCMS), which is related to the amplitude of tearing modes. In RFX-mod2, the stainless steel vacuum vessel containing the RFX-mod plasma will be removed, and the copper shell will become the first conductive surface for the plasma. The vacuum barrier will be provided by the properly modified toroidal support structure. The shell-plasma proximity will be reduced from b/a = 1.11 to b/a = 1.04 (with b shell radius). This design choice implies challenging modifications on the components of the machine close to the plasma, while maintaining the existing magnetic coil system. Innovative solutions have been conceived to fulfil vacuum and electrical requirements of the in-vessel components, in particular to ensure their reliability during the operation also in presence of abnormal events.

According to model simulations, this magnetic configuration will reduce the deformation of the LCMS by a factor about 3 with respect to RFX-mod, see Fig. 2.4 (Zuin et al., 2017). Moreover, the 3D nonlinear MHD Specyl, including realistic boundary conditions, predicts a reduction of the energy of unstable modes by about 30% (L. Marrelli et al., 2019).

3 Magnetic self-organization in the RFP

If the final state reached by a physical system is reproducible and independent of initial conditions that system reaches a self-organized state. Many natural plasmas exist in such states, whose properties are determined by boundary conditions and a few global parameters such as magnetic flux or current. The dynamical process of achieving these preferred states is often called *plasma relaxation*, thus they are referred to as relaxed states (Ortolani and Schnack, 1993; Schnack, 2009) .

The process controlling the redistribution between toroidal and poloidal current in a RFP, often named as dynamo and which is considered responsible for the sustainment of the configuration in time, is an example of self-organisation in plasmas. This mechanism has historically been called the "RFP dynamo," in analogy to various astrophysical phenomena in which magnetic fields are created and sustained due to a velocity field. However, the drive of the dynamo mechanism in the RFP is an externally provided toroidal electric field, not the velocity field as in astrophysical plasmas.

In the RFP, the edge poloidal magnetic field is of the same order of magnitude as the core toroidal field and the latter reverses at the edge. Therefore currents must flow in the plasma that cannot be ohmically sustained by the inductive electric field alone applied through the central solenoid. This indicates the presence of a current sustained by an additional, plasma driven electric field.

As reported in chapter 2, several Tearing Mode instabilities can be present in the RFP, producing magnetic and velocity fluctuations, associated to a dynamo electric field $\mathbf{E}_f = -\langle \tilde{\mathbf{v}} \times \tilde{\mathbf{b}} \rangle$ (the brackets indicate an appropriate spatial and time average). Their spectrum though can be very

different depending on the plasma state, and this has very different impact on plasma confinement, which will be described in the next chapter. When the dynamo is driven by a broad spectrum of magnetic Fourier modes resonating inside the plasma and producing magnetic stochasticity it is turbulent, and we say that it happens in the so called Multiple Helicity (MH) state. When the dynamo is based on an almost monochromatic spectrum, i.e. on a single tearing/resistive kink mode and its harmonics, it is laminar and works in the Single Helicity (SH) state.

For several decades, up to '90s, the MH state was considered as intrinsic to the RFP and due to the need for a dynamo. The SH state was predicted when MHD simulations revealed a bifurcation from the usual MH state to a different one, with the tearing mode spectrum dominated by a single mode (Cappello and Paccagnella, 1992), (Finn et al., 1992b) and experiments showed, under certain conditions, a drastic change in the MHD fluctuation. The occurrence of plasmas dominated by a single tearing mode was observed in RFX (Martin, 1999), (Escande et al., 2000b), and subsequently confirmed in almost all RFP experiments (Brunsell et al., 1993a), (Hirano et al., 1997), (Sarff *et al* 1997), (Ikezoe et al., 2012). It is worth noting that in both configurations, MH and SH, the RFP is a helical magnetic configuration: the MH state corresponds to a toroidally localized helical deformation (produced by the phase locking of several magnetic modes, (Kusano et al., 1991)), while the SH state, with one dominant mode, corresponds to a uniformly distributed one.

In this chapter, sec. 3.1 provides an introduction to the turbulent RFP dynamo in the single fluid approximation, then described in the double fluid approach in sec. 3.2. Experimental measurements of the RFP dynamo field are reported in sec. 3.3. The emergence of the helical state of the RFP as the result of a bifurcation from MH to SH is reported in sec. 3.4. The electrostatic dynamo is the framework where both turbulent and laminar dynamo can be described and is discussed in sec. 3.5, while sec. 3.6 describes the emergence of helical states in experiments. The tools developed to reconstruct the experimental 3D magnetic equilibria in the helical states are reported in sec. 3.7. The effect of an external 3D edge radial field, applied both in simulations and experiments, is discussed in sec. 3.8. Finally, miscellaneous theoretical studies concerning helical states are summarized in sec. 3.9.

3.1 The RFP turbulent dynamo in single fluid approximation

Plasma relaxation in a RFP was originally described by Taylor theory (Taylor, 1986). According to Taylor theory, isolated MHD systems minimize their magnetic energy (neglecting pressure) subject to the constraint that the total magnetic helicity remains constant. This results in the minimizing state $\nabla \times \mathbf{B} = \lambda \mathbf{B}$, where $\lambda = \mu_0 J_\parallel / B$ is a spatial constant ($J_\parallel$ is the current density parallel to the magnetic field).

From the Taylor theory point of view, relaxation in the RFP is both incomplete and cyclic (Kusano and Sato, 1990). It is incomplete in that, experimentally and numerically, both the pressure profile and the profile of the current parallel to the magnetic field, $p(r)$ and $\lambda(r)$ respectively, are approximately flat only in the core of the plasma. Toward the edge they both decrease to zero, thus showing a discrepancy between theory and experiments. It is cyclic in that relaxation is observed, in both experiment and simulation, to occur in discrete events generally called "sawtooth crashes" or "dynamo reconnection events" (Fig. 3.1) , which provide the generation of a substantial amount of toroidal flux by the destabilisation of tearing modes (Almagri et al., 1992), (Ji, 1994), (Hedin, 1998), (R Lorenzini et al., 2008). Experimental observations showed such events as characterized by large amplitude bursts of low (m,n) modes (Fig. 3.1a), and by the flattening of $\lambda(r)$ inside the $q=0$ surface (Brower et al., 2002). The flattening of $\lambda(r)$ inside the $q=0$ surface is a consequence of the relaxation due to large scale magnetic chaos, as was shown by Rusbridge in (Rusbridge, 1991): in the radial domain of chaotic magnetic field, transport is fast and equilibrium almost force-free, so that $\mathbf{J}=\lambda(r)\mathbf{B}$, where λ may be space dependent. Setting this in $\nabla \cdot \boldsymbol{J} = 0$ implies $\nabla\lambda(r) \cdot \boldsymbol{B} = 0$, which shows that λ must be constant along the field lines. Therefore λ is constant in the chaotic domain, which in presence of multiple magnetic components means in the $q>0$ domain. Meanwhile, there is a priori no reason for λ to stay constant where $q<0$.

In the light of visco-resistive MHD simulations performed from 90's, also other aspects of Taylor's theory have been criticized (Cappello et al., 2008). Among them, the fact that the timescale of relaxation turns out to be intermediate between ideal and resistive; the fluctuations involved in these processes are large scale (tearing and resistive modes). Also, the saturation of the pinch parameter Θ predicted at 1.56 by the Taylor's theory is not found in the experiments and, different from Taylor's theory, a linear relation between Θ and F is observed (Ortolani and Schnack, 1993). Furthermore, Taylor theory assumes a closed system, while the RFP is an open ohmic system.

In order to go beyond the simple Taylor theory several nonlinear numerical studies have been performed to describe the sustainment of the RFP. The first approach was based on single fluid MHD, which ignores the existence of separate ions and electrons. Collisions between particles are assumed to be relatively rare events. Resistivity induces a diffusion of the magnetic field, characterized by the timescale $\tau_R = \mu_0 L^2/\eta$, where L is the length scale of the structure and η is the resistivity. τ_R is often the longest time scale of interest in the plasma. The shortest one is instead associated with ideal MHD and is called the Alfvén time, $\tau_A = L/V_A$, where $V_A = B/\sqrt{\mu_0\rho}$. The ratio $S = \tau_R/\tau_A$ of the resistive and ideal timescales is called the Lundquist number. In RFPs

usually $S \gg 1$, thus the challenge in properly capturing the range of plasma dynamics with an MHD simulation.

In order to include the momentum transport and to avoid singularities in the dynamics of velocity, viscosity must be added to resistive MHD. By defining a fluid dimensionless number analog to the Lundquist number, $S_\nu = \tau_\nu/\tau_A = LV_A/\nu$, where ν is the kinematic viscosity, the non-dimensional visco-resistive MHD equations become

$$\rho\left(\frac{\partial \mathbf{V}}{\partial t} + \mathbf{V}\cdot\nabla\mathbf{V}\right) = -\nabla p + \mathbf{J}\times\mathbf{B} + \frac{1}{S_\nu}\rho\nabla^2\mathbf{V} \qquad 3.1$$

$$\frac{\partial \mathbf{B}}{\partial t} = \nabla\times(\mathbf{V}\times\mathbf{B}) + \frac{1}{S}\nabla^2\mathbf{B} \qquad 3.2$$

The inherent nonlinearity of these equations renders their analytical solution unworkable. MHD numerical simulations played a key role in displaying the RFP dynamics,(Schnack et al., 1987), (Cappello and Biskamp, 1996), (Caramana et al., 1983),(Sovinec et al., 2004), (Chacón, 2004), (Kusano and Sato, 1986), following Sykes and Wesson's pioneering work demonstrating robust field reversal in a simulation using a $14 \times 14 \times 13$ grid (Sykes, A. and Wesson, J., 1977). They identified the basic mechanism of field reversal as the nonlinear evolution of $m = 1$ kink instabilities in the presence of an externally applied toroidal voltage. As noted above, experimentally the sustainment of field reversal is a cyclic process. The reconnection driven by the kink modes occurs in a sawtooth crash that flattens $J_\parallel/B$ (in the q >0 domain) and increases field reversal (Caramana et al., 1983). It is worth noting that due to computational limits the first simulations above were already dealing with the Single Helicity RFP, though the awareness of the potentialities of such scenario was achieved only in subsequent years.

Fluctuations play a crucial role in generating the electric field which balances the effect of resistive diffusion. In fact within the context of MHD, a first view of the RFP dynamo was obtained by considering the simplest form of the Ohm's law. If **V** and **B** consist of both mean and fluctuating parts, then a mean electric field $\mathbf{E}_f = -\langle\tilde{\mathbf{v}}\times\tilde{\mathbf{b}}\rangle$ can be produced by the fluctuating velocity field $\tilde{\mathbf{v}}$ and fluctuating magnetic field $\tilde{\mathbf{b}}$, where the brackets indicate an appropriate spatial and time average. This $\mathbf{E}_f$ is often referred to as the "MHD dynamo electric field". Taking the parallel components of Ohm's law gives $E_\parallel - E_{f\parallel} = \eta J_\parallel$; thus the combination of externally applied $E_\parallel$ and dynamo field $E_{f\parallel}$ produces the observed current density $J_\parallel$. This is illustrated in Fig. 3.2 (3D visco-resistive MHD simulation) (Ho et al., 1989) and Fig. 3.3 (experimental equilibrium reconstruction) (Anderson et al., 2004). By itself, the applied $E_\parallel$ would create a peaked λ profile, and could not sustain a reversed magnetic field (note that $E_\parallel$ near the edge is in a direction to suppress $J_\parallel$). The

positive values of $E_{f\parallel}$ near the axis suppress parallel (axial) current, while negative values of $E_{f\parallel}$ near the edge drive parallel (poloidal) current. This is what is required to produce a reversed magnetic field.

3.2 The Hall dynamo in two-fluid MHD

In the framework of extended, or two-fluid, MHD, Ohm's law is generalized to (Spitzer L, Jr. , 1962):

$$\mathbf{E} + \mathbf{V} \times \mathbf{B} = \eta \mathbf{J} + \frac{\mathbf{J} \times \mathbf{B}}{ne} - \frac{\nabla p_e}{ne} - \frac{m_e}{e}\frac{d\mathbf{V}_e}{dt} \qquad 3.3$$

where $\mathbf{V}_e$ is the electron fluid velocity, $\mathbf{V} \approx \mathbf{V}_i$ (the ion fluid velocity), η is the resistivity, p_e is the electron pressure, n is the plasma density, m_e is the electron mass, and e is the electron charge. The last three terms on the right-hand side of Eq. 3.3 are the Hall term, gradient of electron pressure, and electron inertia. They represent effects beyond standard single-fluid MHD.

By splitting the quantities in Eq. 3.3 into mean and fluctuating parts, averaging over a flux surface, and taking parallel components, generalized parallel Ohm's law becomes (Ji et al., 1996)

$$\eta \mathbf{J}_\parallel = E_\parallel + \langle \tilde{\mathbf{v}} \times \tilde{\mathbf{b}} \rangle_\parallel - \frac{\langle \tilde{\mathbf{j}} \times \tilde{\mathbf{b}} \rangle_\parallel}{ne} \qquad 3.4$$

where the last term on the right-hand side is often referred to as the "Hall dynamo". Note that the electron inertia term is usually neglected as small, and the parallel component of the pressure gradient term vanishes upon flux-surface averaging.

Parallel Ohm's law represents the force balance on the electrons in the plasma, and as such describes the dynamics of the parallel current. In the generalization of Taylor relaxation theory to two-fluids, both the electron and ion helicities are conserved separately (Steinhauer and Ishida, 1997), (Hegna, 1998). In the resulting relaxed state, the spatial constant $J_\parallel/B$ is recovered from the standard MHD analysis, and represents the dynamics of the electrons. Additionally, a new spatial constant appears $nV_\parallel/B$, representing the dynamics of the ions and describing the relaxed state of the parallel plasma momentum profile.

Recent two-fluid computations (Sauppe and Sovinec, 2016), (Sauppe and Sovinec, 2017) have shown a significant contribution from the Hall term which may help or oppose the dynamo action in the process of parallel current profile relaxation, though it has to be mentioned that in the simulation the MHD dynamo results to be the dominant term, so that the total effect of Hall plus MHD dynamos was the same as the MHD dynamo in single fluid simulations. However, as will be reported in sec. 3.3, considering the Hall term allowed an experimental determination of the dynamo field.

In analogy to Ohm's law, the parallel momentum balance equation is

$$\rho \frac{\partial V_\parallel}{\partial t} = \langle \tilde{\mathbf{j}} \times \tilde{\mathbf{b}} \rangle_\parallel - \rho \langle \tilde{\mathbf{v}} \cdot \nabla \tilde{\mathbf{v}} \rangle_\parallel \qquad 3.5$$

where the left-hand side represents ion inertia with ρ as the mass density. On the right-hand side are the fluctuation-induced Maxwell and Reynolds stresses, respectively. Note that both the Maxwell stress and the Hall dynamo terms contain $\langle \tilde{\mathbf{j}} \times \tilde{\mathbf{b}} \rangle_\parallel$, indicating that dynamics of the parallel current and parallel plasma flow are coupled. In MHD simulations, the relaxation of the parallel momentum profile is driven by the same reconnection events causing relaxation of the parallel current profile (Ebrahimi, 2007). The effect of including a flow term in the magnetic equilibrium has been found to be an edge reversal of the toroidal velocity (Guazzotto and Paccagnella, 2009), consistent with experimental observations (Antoni et al., 1997), (Carraro et al., 1998), (Puiatti et al., 2001).

3.3 Measurements of the RFP dynamo and momentum transport

The first experimental determination of the MHD dynamo in the RFP was made via edge probe measurements of $\langle \tilde{\boldsymbol{E}}_\perp \cdot \tilde{\boldsymbol{b}}_\perp \rangle$ (Ji et al., 1996), (Ji, 1994). This quantity can be shown to represent the MHD dynamo by substituting the perpendicular component of generalized Ohm's law (Eq. 3.3) into Eq. 3.4. Fig. 3.4 shows this measured dynamo electric field in the edge of the MST RFP (r/a = 0.9), compared to the other terms in Ohm's law, where the resistivity η is calculated from measured local T_e and with estimated Z_{eff} = 2. The dynamo electric field increases during the sawtooth event to overcome the inductive backreaction produced by rapid changes in the plasma current profile.

The next step in RFP dynamo measurement was the direct measurement of plasma flow velocity fluctuations via ion Doppler spectroscopy in the core of MST (Den Hartog et al., 1999). The measured flow fluctuations were correlated with the magnetic field fluctuations due to the long-wavelength m = 1 tearing modes in the core of the plasma, enabling the contribution of individual tearing modes to the MHD dynamo to be quantified. Fig. 3.5 is an example of two components of the $\langle \tilde{\mathbf{v}} \times \tilde{\mathbf{b}} \rangle$ dynamo produced by the core-resonant m = 1, n = 6 tearing mode. This work also indicated that the velocity fluctuation eigenfunctions involved in the MHD dynamo were localized at the rational surfaces, with widths similar to the expected widths of the tearing islands (Fig. 3.6).

Spectroscopic investigation of the MHD dynamo was furthered by measurements with an optical probe inserted in the edge of MST (Fontana, 2000). At large r/a outside the q = 0 rational surface, the MHD dynamo term was large and balanced the Ohm's law as expected, with the dynamo being produced by m = 0 fluctuations resonant at the nearby $q = 0$ surface. However, at smaller r/a inside the $q = 0$ surface, the MHD dynamo term disappeared due to a change in sign of the $\tilde{v}_r \tilde{b}_t$ term, which canceled the contribution of the other term, $\tilde{v}_t \tilde{b}_r$. This observation suggested that other

dynamo mechanisms, such as the Hall dynamo, might be required to balance Ohm's law in the RFP, at least in some regions of the plasma.

In the Multiple Helicity RFP, whether the configuration is sustained by a series of discrete dynamo reconnection events (RE) or by a continuous series of bursts appears to be related with *m=0* mode stability, which in turn depends on the distance between the plasma and the first conductive wall (Paccagnella, 1998). In the MST device, where an ideally conducting wall is located close to plasma edge, during experiments at deep F values, it has been observed that during strong reconnections the *m=0* modes are driven by the nonlinear coupling of a broad *m=1* spectrum, while they are linearly unstable during the small bursts in-between the large REs (Piovesan et al., 2008).

In RFX or RFX-mod, where a conducting shell is located outside a thin vacuum vessel, the *m=0* modes are linearly unstable (Zanca et al., 2001b), (Fitzpatrick and Zanca, 2002), and typically the growth and subsequent reconnection takes place with shorter periods. (M. E. Puiatti et al., 2013).

The QSH dynamo was first measured in MST (Piovesan et al., 2004a), and showed: (i) the magnetic and velocity fluctuation spectrum to have the same dominant wave number; (ii) the corresponding component of the velocity to extend throughout the plasma volume and to couple with magnetic fluctuations, which produces a significant MHD dynamo electric field; (iii) the radial profile of this component to be consistent with the one obtained in QSH runs of the SpeCyl MHD code (Cappello, 2004). A similar study was performed in RFX-mod (Bonomo et al., 2011): a helical plasma flow was observed to form a $m = 1$ convective cell creating a localized sheared flow outside the eITB (Fig. 3.7); however, the experimental pattern revealed the maximum flow shear more external with respect to the predictions of 3D MHD simulations; this might be due to an ambipolar component of the helical electric field on top of the MHD one. Even weak external 3D fields can modify significantly the flow profile and in particular its shear (Piovesan et al., 2011a).

In RFX-mod, the edge flow displays a QSH modulation (Scarin et al., 2011). Probes have been used in low current discharges (up to 0.45 MA) of RFX-mod; this enabled to exhibit in forced QSH states a modulation of the perpendicular components of the flow (Vianello et al., 2015) concomitant with the density modulation along the toroidal angle (M. E. Puiatti et al., 2013).

3.4 Emergence of a new interpretation of viscoresistive simulations: the helical ohmic state

As mentioned above, the first numerical simulations of the RFP had already given some indication of the existence of helical ohmic states. Calculations assumed $\beta = 0$, and worked with a forced single helicity (SH): only one ratio m/n for the Fourier harmonics was retained beyond (0,0) in simulations based on the elementary visco-resistive compressible nonlinear MHD model in the constant-pressure, constant-density approximation, as in eq. 3.1 and 3.2 with $\nabla p = 0$ (Sykes, A. and

Wesson, J., 1977), (Caramana *et al* 1983) (Aydemir and Barnes, 1984) (Holmes et al., 1985) (Schnack et al., 1985), (Kusano and Sato, 1986). .

However, the initial numerical 2D SH states were deemed too far from the multiple helicity (MH), which were experimentally observed. When computational physicists, taking advantage of the increase of the power of computers, began to deal with the full 3D problem, the parameters of initial numerical simulations led them into the MH state, just converging with the then dominant MH experimental plasmas. Only in 1990, 3D numerical simulations revealed a bifurcation of the magnetic configuration from the MH state to the SH state, occurring when viscosity is increased and coming with magnetic order (Cappello, S. and Paccagnella, R., 1990), (Cappello and Paccagnella, 1992),(Finn et al., 1992b),(Cappello and Biskamp, 1996).

The favourable features of the helical ohmic states fully emerged by revisiting the '90-'92 simulations. An appropriate rescaling of time and velocity in the MHD equations shows that, for given radial distributions of η and ν, the dynamics is ruled by the magnetic Prandtl number $P = \nu(0)/\eta(0)$ and by the dissipation of the system $d = \eta(0)\nu(0)$, also quantified by the Hartmann number $H = d^{-1/2}$, a classical dimensionless number in conductive fluid MHD. Dissipation is the dominant parameter when the inertia term becomes negligible, which happens for a large range of simulation parameters (Cappello and Escande, 2000) . These simulations indicate d (or H) as the control parameter independently of P and Θ. Therefore, the previous high viscosity simulations turned out to be in reality high dissipation (or small H) simulations. As usual in nonlinear dynamics, an increase of dissipation is favourable to a laminar behaviour of the system. Depending on the initial conditions, two nearby different helicities were found to be selected by the plasma when relaxing to SH (Cappello and Escande, 2000) (Cappello, 2004).

As *d* decreases, the pure helix (single helicity) develops a toroidally (axially) localized bulging; this bulged helix is interrupted by longer and longer intermittent phases, in which secondary modes with other helicities show up in the Fourier spectrum. The bulged helix corresponds to a Quasi Single Helicity (QSH) state where secondary modes are not zero but smaller than the dominant one. When at least two modes have similar amplitudes the plasma switches to the MH state. With decreasing *d*, the duration of the QSH phases decreases, as well as the percentage of time where QSH dominates, and after a transition region corresponding to $10^3 \le H \le 10^4$, the system reaches a non-stationary MH regime (Cappello and Escande, 2000). This is shown in Fig. 3.8 where the energy of the $m = 0, n \neq 0$ modes is used as an order parameter for the SH-MH transition; indeed these modes vanish in the SH state, since they result from the beating of at least two different helicities. Furthermore, magnetic chaos sets in progressively during the transition. However, very recent

extended analysis including a large set of simulations actually shows that a second low dissipation region exists where SH states also develop (Veranda et al., 2020).

On top of the MHD bifurcation leading from MH to SH, another one is predicted, suppressing the magnetic island and making the magnetic topology kink-like. When the amplitude of the SH mode increases, the island X-point collides with the unperturbed axis of the configuration, which leads to a topology with a single helical axis corresponding to the former island O-point (Escande et al., 2000c) (Fig. 3.9). Such a magnetic topology, which has been dubbed SHAx (R. Lorenzini et al., 2008), occurs because the inner loop of the separatrix becomes tighter and tighter about the former axisymmetric O-point and vanishes when its inner area vanishes.

Incidentally, it has to be mentioned that, while in the first simulations the plasma current and the axial magnetic flux were taken as constant, which implies the constancy of the pinch parameter Θ ((Cappello, 2004) and references therein), from 2008 on, subsequent simulations with the SpeCyl and PIXIE3D (Chacón, 2008) (Bonfiglio et al., 2010a) codes were performed with a constant loop voltage instead of a constant Θ.

3.5 Electrostatic nature of the RFP dynamo

Both in SH and MH states, the spatially fluctuating component of the velocity may be seen as an electrostatic drift velocity related to an electrostatic field which is spatially modulated (Bonfiglio et al., 2005), (Cappello et al., 2006), (Cappello et al., 2011). This comes quite natural in SH: the helical displacement of magnetic surfaces causes a modulation of the parallel current density along each flux tube, which requires the build-up of a helical electrostatic potential producing the dynamo flow as an electrostatic drift (laminar MHD dynamo). This statement is supported by an elementary calculation in cylindrical geometry in (Cappello et al., 2011): in the parallel Ohm's law (scalar product of eq. (3.3) with $\boldsymbol{B}$), the $\boldsymbol{v}$ x $\boldsymbol{B}$ term and the Hall term $\boldsymbol{J}$ x $\boldsymbol{B}$ bring vanishing contributions. The gradient of electron pressure vanishes too, because it is perpendicular to magnetic surfaces. Moreover, electron inertia is generally neglected in the RFP. If the magnetic field is known, the parallel Ohm's law enables the calculation of the electrostatic potential ϕ since $\boldsymbol{E} = E_0 \hat{\boldsymbol{e}}_z - \nabla\phi$, with E_0 the inductive (loop) electric field. Finally, the full Ohm's law eq. (3.3) yields the velocity field, which turns out to be slaved to the magnetic field. In the plasma core, the contribution from the loop voltage is larger than that from the mean parallel current density, but it is smaller in the edge. The difference is balanced by the electrostatic term, which provides an anti-dynamo contribution in the core and a genuine dynamo contribution in the edge. The same interpretation can be applied to the MH case, where the electrostatic field is due to charge separation patterns produced by the periodic

relaxation events and is again the main contributor to the fluctuating velocity field (Bonfiglio et al., 2005), (Bonfiglio, D. et al., 2006b), (Cappello et al., 2006).

The pinch velocity leads to a build-up of the plasma density on the helical axis in MHD simulations where density is free to evolve (Onofri et al., 2008). This does not occur in a genuine plasma, where the central density profile is flat. This inconsistency was avoided in (Delzanno et al., 2008) by adding a diffusive term in the continuity equation for the density.

3.6 Emergence of helical states in experiments

Just after the first numerical indications, since 1993 transient QSH states were detected and found to last for several energy confinement times in all large RFP devices (Brunsell et al., 1993a), (Nordlund and Mazur, 1994), (Hirano et al., 1997), (Sarff *et al* 1997), (Martini et al., 1999b), (Martin 1999). Plasmas with long lasting QSH states over the whole current flat-top phase were present in the RFX data base at about 1 MA plasma current (Escande et al., 2000b), (Martin et al., 2000). The dominant magnetic mode had an amplitude 1 to few percents of the central magnetic field, and several times that of the other secondary modes (Piovesan et al., 2004a) (Martin et al., 2002). For such states, termed Double Axis (DAx) states (Puiatti et al., 2009a), the magnetic field displays two magnetic axes: the unperturbed axis-symmetric one and the axis related to the island O-point (R. Lorenzini et al., 2008).

When RFX was upgraded into RFX-mod, QSH states were rapidly recovered above the current threshold of ≈0.6-0.8 MA, and at shallow reversal ($F > -0.2$) (Ortolani and team, 2006), (Paccagnella et al., 2006). The main features of the new machine were a lower aspect ratio and a state-of-art real time control system, as described in chap. 7. The plasma current operational range was extended with respect to RFX, reaching 2 MA (nominal maximum current value of the machine). An example of long-lasting spontaneous QSH in RFX-mod at high current is given in Fig. 3.10.

After the observation of long lasting QSHs in RFX and RFX-mod, experimental studies on such regimes were extended in all other RFPs: in MST (Marrelli et al., 2002), (Piovesan et al., 2004a), in TPE-RX (Piovesan et al., 2004b), in EXTRAP T2R (L. Frassinetti et al., 2007), and in RELAX (Ikezoe et al., 2012). In TPE-RX, long-lasting highly reproducible QSH states were obtained by applying a delayed reversal of the toroidal field at the edge (Hirano et al., 2005), and were systematically triggered by applying a small positive pulse in the initially weakly reversed edge magnetic field (Hirano et al., 2006). The end of the QSH phase came with a distortion of the $m = 0$ magnetic island chain, and the occurrence of a chaotic region, expelling energy at the location of the slinky (Frassinetti et al., 2006). In RELAX, QSH states lasting above 30% of the flat-top duration

can be obtained (Oki et al., 2012): such good features of QSH in RELAX suggest an advantage of a low aspect ratio configuration to reach QSH, as expected from the scarcer density of the central m = 1 tearing modes in this case (Oki et al., 2013, 2012).

The results obtained in the various RFPs have common features: QSH is favoured by shallow reversal and when the dominant mode resonates near the magnetic axis (Hirano et al., 2006) (Oki et al., 2013, 2012) (Sarff et al., 2015). It has to be mentioned that this latter point is in contrast with the outcome of numerical simulations with a vanishing edge radial magnetic field (Cappello and Escande, 2000). Moreover, there is a higher probability to obtain QSH spectra with higher plasma current (Marrelli et al., 2002) (Bolzonella and Terranova, 2002) (Martin et al., 2003), (Valisa et al., 2008), which will be discussed with more detail in chap. 4.

First observations of the separatix expulsion turned out to be done in RFX-mod (R. Lorenzini et al., 2008), (Lorenzini et al., 2009b). An initial small localized hot island is replaced by a large plateau which is then warmed up, see Fig. 3.11c. Such plasmas featuring a single magnetic axis were dubbed SHAx states. SHAx states were obtained either spontaneously, at plasma current above ≈ 1.4 MA, offering a further example of self-organisation (Bonomo et al., 2009), or stimulated by an external magnetic perturbation, or triggered by a oscillating poloidal current drive (R. Lorenzini et al., 2008),(Lorenzini et al., 2009a).

SHAx states also occur in MST, at similar Lundquist number S despite lower plasma current (about 0.5MA) than in RFX-mod (Auriemma et al 2011), (Bergerson et al., 2011). The dominant $m=1$,$n=5$ helical mode grows as large as 8% of the axisymmetric field; when S increases, the secondary $m=1$ modes decrease, which implies reduced magnetic chaos (Sarff et al 2013).

QSH (including both SHAxs and DAxs) periods end by crashes where the amplitude of secondary modes increases, inducing magnetic reconnection with the formation of poloidal current sheets (Zuin et al., 2009). This is shown in fig. Fig. 3.10b and Fig. 3.14c.

3.7 Experimental reconstruction of helical equilibria

The reconstruction of the experimental internal magnetic field in QSH states has been obtained by several tools. A first approach based on field line tracing codes has been applied to various RFP devices (White and Chance, 1984), (P Innocente et al., 2017), (Martin et al., 2003). The internal magnetic field profiles were computed from the axisymmetric cylindrical α-θ_0 model (Antoni et al., 1986; Ortolani and Schnack, 1993). The magnetic fluctuation spectrum measured at the plasma edge was used as a boundary condition for the calculation of the radial perturbations. This is done by solving the Newcomb equation (Fitzpatrick, 1993; Sadao Masamune et al., 1998; S Masamune et al., 1998; Newcomb, 1960; Robinson, 1978; Paolo Zanca et al., 2007). The Poincarè map showed a

magnetic island with the helicity of the dominant mode embedded in magnetic chaos. Such island corresponds to a “bean”-like hot structure featuring strong electron temperature gradient at the edges (Martin et al., 2000) (Escande et al., 2000b) (Piovesan et al., 2004a) (Marrelli et al., 2002) (Franz et al., 2006).

In SHAx states, if only the dominant mode eigenfunction is considered, the magnetic topology consists of nested helical surfaces; it has been calculated by the SHEq code in RFX-mod (Martines et al., 2011) and in MST (Auriemma et al., 2011). SHEq reconstructions show that the electron temperature is a magnetic flux function, see Fig. 3.12 (Lorenzini et al., 2009b). In MST, the magnetic field reconstruction by SHEq has been compared with a direct measurement of the internal magnetic field (Bergerson et al 2011).

As a result of the magnetic topology reconstruction, the helical safety factor profile has been calculated and goes through a maximum located in the vicinity of the temperature gradient region, as shown in fig. Fig. 3.11b (Momo et al., 2011), (Gobbin et al., 2011b). Similar q profiles have been also found in numerical simulations by the SPECYL code. This non monotonic behaviour has been interpreted as a minimum of the rotation frequency of the pendulum-like Hamiltonian describing the SH dynamics. When the amplitude of the SH mode increases further after the separatrix disappearance, a stronger amplitude of secondary modes is required to produce chaos about the maximum of the helical safety factor (Escande et al., 2000c). As a result, SHAx states are typically more resilient to chaos than DAx ones (Escande et al., 2000c) (Bonfiglio et al., 2010b) (Cappello et al., 2011) (Veranda et al., 2013).

Given the 3D nature of the SHAx states, the VMEC equilibrium code, originally developed in the Stellarator community, has been applied and enhanced in order to deal with the reversal of the toroidal field (Terranova et al., 2010), (Gobbin et al., 2011a). This allowed the reconstruction of the magnetic equilibrium surfaces. The resolution of the equilibrium reconstruction has been then improved by coupling VMEC with the V3FIT code (Terranova et al., 2013), able to include internal and external measurements as constraints. As an example, Fig. 3.13 shows the comparison of the electron temperature profile from a Thomson scattering diagnostic remapped by the V3FIT code: when the flux radial coordinate is calculated as a force free equilibrium taking into account only magnetic measurements the reconstruction fails, while it is successful when also temperature and density are included as constraints.

3.8 Driven helical states.

The SH ohmic state can be described analytically as a small helical perturbation of an axis-symmetric ohmic pinch with small edge axial magnetic field and conductivity. This description uses

the pinch-stellarator equation, which shows how the axial field of a cylindrical SH RFP evolves radially because of the pinch effect and of a stellarator contribution due to the helical deformation of the plasma (Pustovitov, V.D., 1982),(Finn et al., 1992b), (Bonfiglio et al., 2011). Reversal is due to the edge stellarator contribution, which is more efficient when the edge pinch contribution is weak. The latter condition corresponds to a resistive edge plasma. Furthermore, simulations performed with a flat resistivity profile display a reduction of the dynamo action, which brings to marginally-reversed or even non-reversed equilibrium solutions (Bonfiglio, D. et al., 2006a) (Onofri et al., 2008) (Onofri et al., 2009) (Onofri et al., 2010a). This occurs because with a larger resistivity at the edge, the electrostatic field is larger too, in order to balance parallel Ohm's law; the electrostatic drift due to such larger electrostatic field provides an enhanced dynamo action, which is sufficient to sustain the reversed configuration (Bonfiglio, D. et al., 2006a) The edge resistivity of RFPs is high enough for the reversed axis-symmetric part of the toroidal field to be rather constant in the reversal domain after a steady decrease in the non reversed. The pinch-stellarator equation enables the derivation of a necessary criterion for the reversal of the edge axial field (Bonfiglio et al., 2011), which in combination with MHD simulations shows that a finite edge radial magnetic field of given helicity is favourable for field reversal. The criterion is found to be satisfied in RFX-mod when a finite edge radial magnetic field is applied, but only marginally in spontaneous QSHs (Bonfiglio et al., 2011).

Though MHD simulations were able to predict QSH states, in the first SpeCyl calculations they had a temporal behaviour different from the experimental one. The reason is that the former had a vanishing radial magnetic field at the edge, while the latter correspond to a finite one, since in experiments the time discretization of a digital feedback control system prevents the achievement of zero radial field at plasma radius (Zanca, 2010). Indeed a better agreement with the experimental QSH dynamics was obtained in simulations including a small m=1,n=7 resonant magnetic perturbation (RMP), with an amplitude similar to the experimental one (about 1.5% of the central magnetic field) and with $S=10^7$ (Bonfiglio et al., 2013). An example is shown in Fig. 3.14. A more recent work shows that the similarity with experiments bears on several features (Bonfiglio et al., 2015): (i) the dependence of the temporal behaviour of QSH states on the RMP amplitude, (ii) the dependence of the amplitude of the dominant mode on the same parameter, (iii) that of the position of shear reversal and maximum q, (iv) the amplitude of the dominant mode is independent of dissipation, whereas the amplitude of secondary modes decreases with increasing resistive and viscous Lundquist numbers. Numerically, a stationary state is reached for a RMP of 10%.

In experiments the effect of a feedback controlled 3D field on QSH states has been studied too. A controlled helical boundary has been applied, stationary or rotating to a prescribed slow (up to 50-

100Hz) frequency, provided that the reference radial field amplitude is sufficiently high (L Marrelli et al., 2007), (Piovesan et al., 2011b). This is different from Resonant Magnetic Perturbation (RMP) or Resonant Field Amplification (RFA) experiments (see e.g. (Evans et al., 2004) or (Munaretto et al., 2015)) where the currents flowing into the control coils are pre-programmed: in RFX-mod experiments they are adjusted by feedback in order to keep the measured radial field at the prescribed reference level (L Marrelli et al., 2007). The application of a *m=1, n=7* field in plasmas with shallow reversal, strongly increases the persistence of the helical state (Piovesan et al., 2011a). Furthermore, QSH states can be obtained at higher densities ($n/n_G \approx 0.5$, (with $n_G[10^{20}m^{-3}]=I_p[MA]/\pi a^2$ Greenwald density)) than in the spontaneous case (Piovesan et al., 2013). While first RFX-mod experiments with the application of an external 3D field resulted in a significant increase (up to 50%) of the loop voltage necessary to sustain the plasma current, such effect has then been minimized, provided that a relatively low value of the radial field is set (Gobbin et al., 2015). An increase of the QSH probability up to 10% and a larger magnetic island occurred in EXTRAP T2R by applying a resonant magnetic perturbation with the corresponding helicity (Frassinetti et al., 2009b).

As predicted by numerical simulations (Veranda et al., 2013), by providing a corresponding helical boundary condition in RFX-mod, it is possible to excite non internally resonant QSH *n=6* states (Cappello, S. et al., 2012). When a non-resonant boundary condition is applied the area with well conserved magnetic surfaces is larger and the transport of magnetic field lines is reduced (Fig. 3.15) (Veranda et al., 2017). This has been related to the existence of Cantori, encompassing the region characterized by conserved magnetic surfaces, which act as barriers to transport of magnetic field lines.

3.9 Further theoretical results

A simple *toy model* makes magnetic field reversal intuitive: it consists in a current-carrying resistive wire initially placed on the axis of a cylindrical flux conserver, whose spontaneous kink leads to the reversal of the edge axial magnetic field, and not to a "disruption" (Escande, D. F. and Bénisti, D., 1997) (Escande et al., 2000a). This effect is present in a genuine RFP, but most of the current corresponds to the paramagnetic pinch component of the configuration, as discussed in section 3.8.

When performed in toroidal geometry, 3D nonlinear visco-resistive MHD simulations show that toroidal coupling prevents the system from reaching a pure SH state when dissipation increases, but that magnetic chaos due to toroidal coupling stays limited in the close to SH states for the aspect ratios of the largest present RFP's (Sovinec et al., 2003). This is confirmed by toroidal simulations with the PIXIE3D code, also showing an m=0 islands chain induced by the toroidal coupling at the

q=0 reversal surface (Cappello, S. et al., 2012). Incompressible 3D nonlinear visco-resistive MHD simulations show that, in contrast with the cylindrical case, the toroidal one presents a double poloidal recirculation cell with a shear localized at the plasma edge (Morales et al., 2014).

Analytical calculations in (Cappello et al., 2011) show that (i) the SH state is the same on using single or two-fluid Ohm's law, which backs up a numerical result (section VA of (King et al., 2011)); (ii) the SH mode amplitude is insensitive to *S*, which backs up experimental (Piovesan et al., 2009) and numerical results in a two-fluid context (King et al., 2011). Adding gyroviscosity in the force balance equation enables to get the experimental ratio of secondary to primary modes, while it is twice too large otherwise (King et al., 2011). More analytical results can be found in the course (Escande, D. F., 2015)

QSH states were obtained in simulations performed with an anisotropic thermal conductivity, and using a multiple-time-scale analysis to this end; the temperature distribution indicates the existence of closed magnetic surfaces, and there is a hot confined region (Onofri et al., 2010b). When resistivity increases steeply at the edge, SH states are obtained for parameters similar to the case without thermal transport (Onofri, 2011) (Onofri and Malara, 2013).

The magnetic topology of both SHAx and DAx states of RFX-mod can be reproduced by a one parameter fit of a minimally constrained equilibrium model using only five parameters, and resulting from a two-domain generalization of Taylor's theory. Both states appear as a consequence of the formation of a transport barrier in the plasma core, in agreement with experimental results (Dennis et al., 2013).

Recently, a new MHD approach was proposed to explain why high current is favourable to SHAx states, why the innermost resonant m = 1 mode is the spontaneous dominant mode, and why there are crashes of this mode. It invokes the shear stabilization associated with the 3D structure of the dominant mode to interrupt the nonlinear mode–mode coupling occurring in the MH regime (Terry and Whelan, 2014). This kind of ideas had been first introduced in (Kim and Terry, 2012). The crashes can also be interpreted as the consequence of pressure-driven resistive modes, which introduce a feedback between transport and the MHD stability of the system (Paccagnella, 2014).

The aspect ratio scaling law for the toroidal mode number of experimental QSH states was shown to be close to the one corresponding to the optimal electromagnetic response of the toroidal shell surrounding the plasma (R. Paccagnella, 2016). The observed scaling with the aspect ratio and reversal parameter for the dominant mode in the Single Helical states can be obtained (Roberto Paccagnella, 2016) by minimizing the distance of the relaxed state described in (Bhattacharjee et

al., 1980) from a state which is constructed as a two region generalization of Taylor relaxation model (Tassi et al., 2008).

4 Transport and confinement in the Multiple Helicity and Quasi Single Helicity RFP

In the RFP, around the field reversal surface strong temperature and density gradients are observed (Biewer et al., 2003), (Canton et al., 2004), (Agostini et al., 2010), which naturally lead to distinguish two domains in describing transport: a core region, inside the reversal surface, and an edge region outside.

In the edge, transport is strongly influenced by a chain of m=0 magnetic islands developing at the reversal surface (Spizzo et al., 2006), (Vianello et al., 2009), and forming in fact a transport barrier corresponding to the *q=0* surface.

In the core, the figure of merit as transport drive is the amount of magnetic chaos. As discussed in chap.3, the magnetic field configuration in the RFP is characterised by several internally resonant Fourier modes. When the deformation produced by the interaction of such modes grows above some critical amplitude the magnetic field lines tend to become stochastic. The degree of stochasticity can be characterized by the Chirikov parameter *s,* defined as (Chirikov, 1979)

$$s = \frac{1}{2}\frac{|W_{mn} + W_{m'n'}|}{|r_{mn} - r_{m'n'}|} \qquad 4.1$$

where *m* and *m'* (*n* and *n'*) are the poloidal (toroidal) mode numbers, W_{mn} is the width of the magnetic island related to the *(n,m)* mode, and r_{mn} the radial location of the resonant surface. The magnetic island overlap takes place when *s~1*, and the field lines develop to highly stochastic state when *s>>1*.

In the domain where *s>1*, the traditional paradigm describing transport in the RFP is based on the assumption of diffusion in a stochastic field, as derived by Rechester and Rosenbluth theory (RR) (Rechester and Rosenbluth, 1978), developed for an isotropically fully stochastic region in collision-less regime and based on a random walk approach. According to RR, the thermal diffusivity depends on the amplitude of the magnetic fluctuations as:

$$\chi_{RR} = v_{th,e}(\tilde{b}/_B)^2 L_c \qquad 4.2$$

where $\tilde{b}$ is the magnetic fluctuation amplitude, *B* the average field, $v_{th,e}$ the electron thermal speed, and L_c the auto correlation length of magnetic fluctuations. For particle fluxes the RR theory is complemented with the Harvey equation (Harvey et al., 1981) in a diffusive-convective scheme for fluxes

$$\Gamma = -D \nabla n + v \cdot n \qquad 4.3$$

where *D* is the diffusion coefficient and *v* the convective velocity. Assuming that the thermal energy is lost via the electron channel and particles are lost through the ion channel, the ambipolarity condition leads to $\chi_{RR}/D = (m_i/m_e)^{1/2}$.

The reduction of magnetic field stochasticity corresponds to a mitigation of transport. Indeed, if the level of magnetic fluctuations becomes sufficiently low, the RFP transport regime can go away from the RR paradigm. This has been achieved in Quasi Single Helicity states. Improved confinement states have been also obtained when fluctuations are reduced by current profile control, which will be described in chapter 5.

However, magnetic chaos, when weak, is not necessarily related to poor confinement: in weakly chaotic regimes small leakage surfaces acting as confining structures can be present (Pegoraro et al., 2019),(Di Giannatale et al., 2018).

In the following, heat transport properties are described in sec. 4.1, both in Multiple Helicity and Quasi Single Helicity states. Particle transport properties are instead discussed in sec. 4.2. The studies of the effect of microsinstabilities on transport in RFP geometry, are summarized in sec. 4.3. The effect on transport of reconnection events involving magnetic topology re-arrangement and magnetic energy conversion is drawn in sec.4.4. The main features of transport in the edge region are reported in sec.4.5. Sec. 4.6 gives a short summary of the isotopic effect in the RFP. Finally, sec. 4.7 summarises the observations related to fast particle confinement in the RFP.

4.1 Core heat transport and confinement

4.1.1 *Multiple Helicity states*

Fig. 4.1 shows an example of the radial extent of the magnetic islands superposed to the *q* profile in a MST plasma and the related temperature profile (Biewer et al., 2003); in this example, with reference to eq. (4.1), *m=m'=1* and *n'=n+1*. The islands are calculated by the nonlinear 3D MHD code DEBS (Schnack et al., 1987), being the width estimated in the saturated phase. In the core region inside the innermost resonant surface, the *s* parameter is ~1, while in the intermediate region where several m=1/n>>1 modes resonate, *s*>>1, and the field lines are likely to be stochastic. Accordingly, the temperature profile is flat inside the reversal surface, due to the overlap of magnetic islands.

The radial profile of the electron thermal diffusivity χ_e has been analyzed in various experiments by expressing $\chi_e \propto (\tilde{b}/_B)^{\alpha}$, inspired by the RR scaling: while a dependence on magnetic fluctuations has been confirmed in all devices, the α exponent has not always been found to be 2 as in eq. 4.2.

In MST, when comparing the experimental core heat flux with the amplitude of the magnetic fluctuations, the scaling with $\tilde{b}/_B$ was found to be consistent with the RR prediction if the thermal ion (instead of electron) velocity is assumed in eq. 4.2. This has been interpreted by a model where the ambipolar constraint is recovered through nonlinear bunching of electrons (Terry et al., 1996): a bunch of ions is formed along a stochastic stream line and interacts with electrons; the energy transport is dominated by the flow velocity of ion bunches. Also referred to an MST plasma, in (Biewer et al., 2003) an estimate of χ_e is given, based on a steady state power balance where the electron temperature and density profiles are the measured ones. Fig. 4.2 shows the corresponding experimental thermal diffusivity compared to DEBS simulations and to the RR theory, with a remarkable agreement.

In RFX and RFX-mod, where electron and ion temperatures are close (Paccagnella et al., 2006), steady state analyses of the electron thermal transport adopted a single fluid approach. An effective thermal diffusivity χ_{eff} has been calculated, whose dependence on the magnetic fluctuations has been found to be $\chi_{eff} \propto (\tilde{b}/_B)^{1.4}$, (Intravaia et al., 1999), (Terranova et al., 2000), not fully consistent with RR predicted exponent. This result has been interpreted by a model taking into account the effect of mode spectrum on field line stochasticity (D'Angelo and Paccagnella, 1996).

A perturbative approach was applied to evaluate the thermal diffusivity in the TPE-RX device, based on the analysis of the radial propagation of a cold pulse during pellet injection (L Frassinetti et al., 2007a). In the scaling with magnetic fluctuations $\alpha \sim 1$.

Nonlinear MHD computations of the electron energy transport in a stochastic field were also applied to characterize energy confinement in MH RFPs. When using the classical (Braginskii) parallel electron thermal diffusivity to estimate the parallel heat diffusion, the experimental energy confinement scal-ing was well reproduced (Scheffel and Liu, 1997),(Scheffel and Schnack, 2000a), (Scheffel and Schnack, 2000b).

Studies on ion thermal energy transport have been affected by the fact that ion heating sources are still not well understood. Both in MST and RFX ion and electron temperatures have close values, which is not compatible with a collisional heating. In (Scime et al., 1992) a correlation between ion heating and dynamo fluctuations is shown, suggesting that a dissipation mechanism based on

fluctuations could contribute to ion heating in the RFP. As will be discussed in sec. 4.4, anomalous ion heating is experimentally observed corresponding to reconnection events.

4.1.2 *Quasi Single Helicity states*

To highlight the effect of the magnetic equilibrium, Fig. 4.3 shows the profiles measured by the Thomson scattering diagnostic in MH, QSH and SHAx plasmas in RFX-mod. Data refer to three times during the same plasma discharge. The first bifurcation, from a MH state (blue crosses) to a helical state characterised by two magnetic axes (DAx) (black squares) corresponds to the development of a hot island involving a small fraction of plasma radius. When the magnetic separatrix is expelled and the transition to a SHAx state occurs, the hot island becomes wider and encompassed by strong electron temperature gradients (red diamonds), establishing an electron thermal transport barrier (eITB) (Valisa et al., 2008), (Lorenzini et al., 2009b), (Puiatti et al., 2009a),(Carraro et al., 2009), (Puiatti et al., 2011). In agreement with the theoretical description (Escande et al., 2000c), a threshold has been found for the occurrence of the transition DAx/SHAx, which is observed when the dominant mode amplitude, normalized to the edge magnetic field, is larger than about 3-4%. In SHAx states, crucial in determining the radial extent of the hot region is the amplitude of the secondary modes: in particular, the widest thermal structures are related to the stabilisation of the two innermost resonant secondary modes, see Fig. 4.4 (Lorenzini et al., 2016).

As plasma current increases, long-lasting QSH states occur more frequently and their total persistency increases. In RFX-mod above 1.5 MA the latter exceeds 90% of the plasma current flat-top (Valisa et al., 2008), (Carraro et al., 2013). The amplitude of the dominant mode and that of the secondary modes scale in opposite ways with the current and with the Lundquist number, as observed both in RFX-mod and in MST and reported in Fig. 4.5 (Piovesan et al., 2009), (Sarff et al., 2013).

The DAx states observed in RFX were characterised by increased temperature and soft X-ray emissivity in the core magnetic island (Escande et al., 2000b). In RFX-mod, at high current (above 1.1 MA), core gradients are steeper and electron temperature higher, exceeding 1 keV; the heat diffusivity ranges between 6 and 35 m^2/s approaching the tokamak range. Despite the small size of the island, the corresponding electron confinement time is higher than in MH states (about a factor 2), with a best electron energy confinement time of about 1.3 ms (Alfier et al., 2008). Simulations of test ion and electron transport show the average diffusion coefficients inside the helical core to be about one order of magnitude lower than those found in MH plasmas (Gobbin et al., 2007). When DAx states are stimulated by a helical edge toroidal magnetic field, the magnetic chaos decreases also, involving the region outside the island, and allowing for a global enhancement of confinement by about 50% (Terranova et al., 2007). A similar behaviour is found in self-similar current decay

experiments, where an initial fast decrease in the mode amplitudes is observed (about 40% of the initial value) (Zanca, 2007).

Regarding the confinement in SHAx states, in MST the global energy confinement improves by about 50 %. A three-fold improvement in confinement is obtained by forcing a slow decay of the plasma current (Sarff et al., 2013). In RFX-mod, where extensive experiments and analysis involving SHAx states have been carried out, eITBs are characterized by an electronic thermal diffusivity lower than $20 m^2/s$, with minimum values approaching 2 m^2/s, still higher than neoclassical predictions (under 1 m^2/s). Such a minimum χ_e value (of the same order in SHAx and DAx states) is much lower than outside the barrier or in MH states, where χ_e ranges around 100 m^2/s (Gobbin et al., 2013), (Franz et al., 2013), (Fassina et al., 2013). Both thermal diffusivity and electron temperature gradient length scale with the total amplitude of the secondary $m = 1$ modes (Puiatti et al., 2011) (Lorenzini et al., 2012). So does the inverse of the maximum electron temperature gradient (Carraro *et al* 2013) (Lorenzini et al., 2012). These scalings indicate a strong link between the level of magnetic chaos and the strength of the barrier, though it has to be mentioned that in helical states the electron temperature gradients show a time behaviour not necessarily related to the dynamics of secondary modes: they are the highest (above keV/m) in the rising phase of the QSH state, and start decreasing 0.5 to 1 keV/m before the destabilization of secondary modes (Carraro et al., 2013). However, despite this intermittent behavior of eITBs, there are examples of long-lasting eITBS, up to 18ms in deuterium plasmas, in particular with QSH stimulated by 3D magnetic perturbations externally applied (Gobbin et al., 2015).

In RFX-mod, in SHAx states the highest τ_{Ee}'s values are obtained. This is shown in Fig. 4.6, where a clear relation between the electron energy confinement time and the secondary mode amplitude appears (Piovesan et al., 2009) (Martin et al., 2009), (Puiatti et al., 2015), (Carraro et al., 2013) , (Martin et al., 2009). This is also found in a three parameter fit of the energy confinement time with plasma current, average density and amplitude of secondary modes b_r, which yields a scaling $\tau_{Ee} \approx I^{0.81\pm0.02} \langle n_e \rangle^{0.28\pm0.02} b_r^{-0.88\pm0.03}$ (Innocente et al., 2009). This result strongly motivates the upgrade of the RFX-mod magnetic front-end presently under implementation, whose main aim is to obtain a decrease of b_r by moving the plasma edge closer to the thin shell (Peruzzo et al., 2017).

In RFX-mod, the best plasma performances at high current in QSH regimes have been reached with shallow reversal *(-0.01 < q(a) < 0*) coupled to low amplitude of secondary modes (Carraro et al 2013). It is worth noting that, as shown in (Bonfiglio et al., 2011), shallow reversal comes also with a lower amplitude of the dominant mode, which favours a lower plasma-wall interaction. As yet, spontaneous helical states are observed at plasma densities $n/n_G \leq 0.35$ (Spizzo et al., 2010). Such a

limit has been related to the effect of an anomalous viscosity due to microturbulence which can act outside the reversal region, (M. E. Puiatti et al., 2013), (Spizzo et al., 2015) (Puiatti et al., 2015).

To interpret the flat temperature profile of the hot region encompassed by the temperature gradients in SHAx states, transport related to self-consistently generated vortical drift motions due to electrostatic turbulence was proposed (Sattin et al., 2011).

4.2 Particle transport and confinement

In the RFX device, an interpretative analysis of the electron density profiles measured by the 13 chord two color interferometer (Innocente et al., 1997) in multiple helicity plasmas yields a particle diffusion coefficient of ≈ 10-20 m^2/s in the core decreasing to about 5 m^2/s towards the edge. The same analysis also indicates the presence of a particle outward pinch, necessary to reconstruct the hollow or flat experimental profiles (Gregoratto et al., 1998). The ratio of thermal to particle diffusivities turns out to be consistent with RR theory in the core. A more recent analysis carried out in RFX-mod both in Multiple and Single Helicity plasmas also yields $\chi/D = (m_i/m_e)^{1/2}$and a dependence $D^* \propto (\tilde{b}/_B)^{1.5}$ (with D^* core diffusivity normalized to the thermal velocity) (Auriemma et al., 2015). This implies that, though residual magnetic chaos remains the main drive for particle transport also in QSH plasmas, the diffusion coefficient is lower, due to its dependence on magnetic fluctuations: Fig. 4.7 shows that the same power law is able to describe the behaviour of D^* in both MH and SHAx states, with $\alpha = 1.5$ in eq. *4.2*. This again indicates that the reduction of stochasticity expected in the RFX-mod2 device could have a beneficial effect on confinement.

The fact that in RFX and RFX-mod the scaling of particle diffusivity is weaker than in RR theory has been related to a sub-diffusive nature of transport. In (Spizzo et al., 2007) and (Spizzo et al., 2009) the ORBIT code (White and Chance, 1984) is applied, showing that the velocity in eq. 4.3 can be interpreted as a sub-diffusive correction to the diffusive evaluation of fluxes. Indeed in RFX-mod the magnetic field is chaotic, but not much above the stochastic threshold, so that hidden structures are anyway present and the RR assumption of random phase approximation and fully isotropic stochasticity might be questionable.

Simulations in (Predebon et al., 2004) predict a strong improvement of particle confinement in QSH with respect to MH. This has been experimentally confirmed in several devices: in TPE-RX, the transition from MH to QSH came with an enhancement of the particle confinement time τ_p by about 30%, together with strong indications of a higher energy confinement (Frassinetti et al., 2006). The improvement was confirmed in RFX-mod, in particular by using pellet injection (Terranova et al., 2010). A pellet entering the central hot region in a SHAx plasma induces a higher density with a

possibly peaked profile, which triggers both an enhancement of τ_{Ee} by a factor 2 to 3, and an increase of τ_p , with a maximum value of 12 ms obtained at 1.5 MA (Terranova et al., 2010).

Single particle trajectories numerical studies applied to RFX-mod plasmas show that, while passing particles are confined for a very long time, particle trapping dominates transport across the helical structure at the rather low collisionality of QSH regimes. The neoclassical diffusion coefficient is one order of magnitude larger than the classical one (Gobbin et al., 2007), (Gobbin et al., 2009). When trapped particles drift out of the helical core, at $r/a \approx 0.6$, they become almost passing without being lost, because the helical distortion decreases when going outwards. This results in a very low population of superbanana particles at the experimental levels of helical magnetic field (about 10% of the total) (Gobbin et al., 2010). Therefore, transport is proportional to the collision frequency, in contrast with unoptimized stellarators where the lower bound of transport scales inversely with this frequency (Gobbin et al., 2010). The diffusion coefficients computed by this approach were confirmed by local neoclassical transport calculations including the radial electric field. A comparison with power balance estimates shows that residual chaos due to secondary modes and small-scale turbulence still drive anomalous transport in the barrier region. For an ion temperature of 0.7 keV, in the absence of chaos and of impurities, the radial electric ambipolar field near the eITB is about -2kV/m. The toroidal and poloidal flows are ≈10-20 km/s and ≈ 2-8 km/s respectively, decreasing with lower ion temperature gradients (Gobbin et al., 2011a).

The computation of single particle trajectories exhibits a different influence of helical states on main gas and impurity transport (Gobbin et al., 2007). Several studies of impurity transport have been carried out, both in MST and in RFX and RFX-mod (see for example (Barbui et al., 2015),(Carraro et al., 2000b),(Barbui et al., 2014), (Gobbin et al., 2017)). In MH regimes, similar results have been obtained: the experimental impurity diffusion coefficient is around 10-20 m^2/s, and the convective term in eq. 4.3 is outward. An example for RFX-mod is given in Fig. 4.8. These values are larger than the values calculated according to the stochastic model (also shown in the figure). The analysis of impurity behaviour in RFX-mod QSH and SHAx states shows that inside the core region the confinement of impurities does not increase, which makes unlikely their central accumulation (Carraro et al., 2009). A core impurity diffusivity one order of magnitude higher than at the edge has been estimated (Menmuir et al., 2010), with an outwardly directed pinch velocity over the whole plasma featuring a strong maximum around the core/edge transition point of the diffusivity, much wider than in MH.

4.3 Effect of microinstabilities

Gyrokinetic numerical simulations and analytical analyses have been applied to study the role of microturbulence as a driving mechanism of transport in the RFP. In axisymmetric configurations, the Ion Temperature Gradient (ITG) mode threshold is larger than in the Tokamak by a factor R/a, due to a strong Landau damping related to short field connection lengths of plasmas acting in low-q configurations (Guo, 2008), (Predebon et al., 2010a),(Sattin et al., 2010). In addition, non-linear calculations show that in axisymmetric plasmas the impact of residual Zonal Flow, beneficial in controlling ITG, can be strong (Predebon and Xanthopoulos, 2015). The ITG stability decreases in helical states, because of the enhancement of temperature gradients in the outer part of the helical deformation where magnetic surfaces are close-packed (Predebon and Xanthopoulos, 2015). Therefore, ITG turbulence might be an important contributor to the total heat transport in helical states, also in combination with a decreased impact of the stochastic transport related to magnetic chaos. The stability of ITG modes might be further decreased in the presence of strongly outwardly peaked impurity profiles (Liu et al., 2011). However, quasilinear and nonlinear three-species simulations of ITG turbulence prove that the inward impurity flux corresponding to a strong ITG would not be compatible with the measured positive impurity peaking (Predebon et al., 2011).

Linear gyrokinetic simulations of RFX-mod SHAx states show that microtearing (MT) modes are unstable at the eITB, as shown in Fig. 4.9. For the strongest eITB's, quasi-linear estimates of the associated transport show MT-driven thermal transport to be comparable to the experimental one (Predebon et al., 2010b). It has to be noted that MT modes have actually been experimentally observed in RFX-mod helical states, with amplitude well correlated to the electron temperature gradient (Zuin et al., 2013).

Microturbulence in MST plasmas has been modelled (Terry et al., 2015), (Carmody et al., 2013), and the effect of ITG and microtearing has been analysed. A role of the β parameter, already well known in the Tokamak (Zonca et al., 1999), has been envisaged also in the RFP, with ITG unstable at low β (vanishing around β =6-10%) and MT unstable at high β.

The occurrence of collisionless microtearing instabilities has been studied in RFX-mod (Predebon and Sattin, 2013) and MST (Carmody et al., 2013), indicating that the high magnetic drifts in the RFP could favour such microinstabilities.

4.4 Effect of reconnection events

As discussed in chapt.3, magnetic reconnection in plasmas is a process by which the plasma relaxes to a state of lower magnetic energy, which is converted to kinetic/thermal energy. In the RFP reconnection events (RE) occur both in MH plasmas, where they are often called sawthooth (ST)

(see Fig. 3.1) and in QSH, where they correspond to a back transition to the MH state. In the MST experiment, the total amount of magnetic energy lost during sawthooth in a plasma discharge has been estimated to be of the order of 50% (Ji, H et al., 1995). Recently, the same kind of evaluation has been made for RFX-mod back transitions QSH/MH, estimating that ≈30-40% of magnetic energy is lost during reconnections and does not contribute to ohmic plasma heating. This is similar to the MST result. A fraction of the energy dissipated during reconnections could be converted into ion thermal energy: strong ion heating corresponding to reconnection events has been observed in MH RFP plasmas (Scime et al., 1992), (Hörling et al., 1996), (Gangadhara et al., 2007), (Gangadhara et al., 2008). In MST, the fraction of magnetic energy converted to ion heating has been evaluated to be ≤ 30% and increases with the square root of the ion mass (Fiksel et al., 2009). An example of the time behavior of ion temperature during a ST in MST is given in Fig. 4.10, showing that ion temperature can increase by a factor 2 or more. It has to be mentioned that only events accompanied by a significant drop of magnetic energy exhibit such ion heating (Gangadhara et al., 2007).

In order to investigate the effect of relaxation events on electron thermal transport, a time dependent model has been applied to RFX-mod and Extrap T2R MH plasmas (Frassinetti et al., 2008), (Frassinetti et al., 2009a). The χ_e radial profile is divided into three regions: (a) the core, where $\chi_e = k_1 (\tilde{b}/B)^{1.4}$ is assumed; (b) the reversal region, with $\chi_e = k_0$; (c) the edge region, where a much higher diffusivity is assumed. Fig. 4.11 shows an example of the χ_e profile reconstructed before and after a RE (Frassinetti et al., 2008), with enhanced core thermal diffusivity just after RE. The same model also gives good agreement with the experiments when applied to the EXTRAP T2R MH plasmas (Frassinetti et al., 2008). Experimentally, as reported in (R Lorenzini et al., 2008), enhanced non axisymmetric particle losses are observed in RFX-mod during RE localised at the toroidal angle where MHD tearing modes lock in phase and to the wall.

An enhanced convective electron particle flux during magnetic reconnections has been measured in MST (Ding et al., 2008a), (Ding et al., 2008b), where a high time resolution Thomson scattering system has been also exploited to estimate the electron thermal diffusivity during a reconnection event in MST (Reusch et al., 2011). It was found (see Fig. 4.12) that χ_e varies by two orders of magnitude in the core region, with a peak at the sawtooth crash followed by a minimum shortly after. Such results can be well simulated by the DEBS code in the middle-radius region if the effect of trapped particles is taken into account, leading to $\chi_e = f_c v_{th,e} D_{RR}$, with f_c passing particle fraction and D_{RR} magnetic diffusivity as in the original formula by RR. Instead, in the centre the

simulation cannot reproduce the χ_e dynamics before the crash, indicating that other mechanisms dominate electron heat transport.

The thermal diffusivity inside a magnetic island close to the axis has been measured in MST, showing flat temperature profiles with rapid parallel heat conduction along helical magnetic field lines in-between the reconnection events. Instead, just after a RE, a temperature gradient develops inside the island, suggesting reduced thermal transport (Stephens et al., 2010).

4.5 Edge transport and turbulence

The m=0 island chain which develops at the field reversal surface strongly influences the edge transport, both in the MH and QSH state. Tearing modes, which are certainly detrimental for confinement when producing intense magnetic chaos in the $q>0$ region, have also a secondary positive effect, allowing for the formation of good magnetic surfaces close to $m=0$ islands, which indeed act as a transport barrier and have a direct impact on plasma pressure profile (Spizzo et al., 2006), (Spizzo et al., 2009). An example is given in Fig. 4.13.

The change in the pressure profile, whose gradient increases when the magnetic shift is outward (Agostini et al., 2012), influences the edge turbulence. In particular in RFX-mod it is found that the radial correlation length of the fluctuations increases with the characteristic radial pressure length, indicating that the latter drives the radial dimension of turbulent structures (Agostini et al., 2012).

In fact outside the reversal surface the RFP edge transport is mainly driven by electrostatic turbulence and, similar to Tokamak and Stellarator, is characterized by a highly sheared v_{ExB} flow (Carraro et al., 1998), (Antoni et al., 2005), (Antoni et al., 2006), (Puiatti et al., 2001), (G Fiksel et al., 1996), (Fiksel et al., 1994). Experiments on the Extrap-T2R device showed that Reynolds stress, driving the E x B flow against anomalous resistivity, features a high gradient in the edge region where the flow shear is large, and is mainly related to the electrostatic component, despite the high magnetic fluctuations in this region (N. Vianello et al., 2005), (N Vianello et al., 2005). Coherent structures emerge as bursts in the turbulent background, with rotation direction determined by the local velocity shear: in RFX and Extrap-T2R they have been identified as dipolar and monopolar vortices, contributing by about 50% to the radial diffusivity (Spolaore et al., 2004). Such turbulence shares common features with other magnetic configurations (Sattin et al., 2006). In particular, the edge electromagnetic turbulence measured in RFX-mod when operated as a RFP and as a Tokamak has been compared (Vianello et al., 2016) (Spolaore et al., 2015). Electrostatic fluctuations in both configurations reveal a strong degree of intermittency with very similar scaling of the shape of the PDF of fluctuation increment, while magnetic fluctuations behave differently, with a lower degree of intermittency in the Tokamak case, consistent with the lower β. In particular, the study of

turbulence in the SOL of RFX-mod Tokamak plasmas allowed the validation of the GIBS code (Ricci et al., 2012), used for Tokamaks (Riva et al., 2018).

The edge electrostatic properties are strongly related to the underlying magnetic topology. When 3D non-axisymmetric magnetic perturbations (MP) are applied in RFX-mod, though they have a main $m=1$ periodicity, at the edge the flux induced by electrostatic turbulence results to be modulated by an $m = 0$ magnetic island, with an enhancement close to the O-point and a reduction at the X-point; transport is due to fluctuations propagating in the electron diamagnetic drift direction (Rea et al., 2015). Also, the connection length to the wall of the edge magnetic field L_{cw} is the result of the interaction between the applied dominant $m=1$ and the $m= 0$ modes and has a complex structure, responsible for an impure $m=1$ behaviour observed for floating potential, electron pressure, perpendicular flow, high frequency magnetic turbulence (Agostini et al., 2017). The edge flow pattern in presence of a MP has been reconstructed and shows a convective cell structure, with the toroidal flow moving to an outer region when the deformation related to the MP (Δ_{MP}) is positive (outwards) and to a more internal one when $\Delta_{MP} <0$ (Masi et al., 2013).

As in the core, at the edge the reduction of TM amplitude is related to an improved confinement: the temperature gradient, which scales almost linearly with plasma current, increases at low secondary mode amplitude, and so does the thermal diffusivity, as shown in Fig. 4.14 (Vianello et al., 2009).

Recent research in RFX-mod (Scarin et al., 2019) points out the crucial role of the secondary modes in influencing the plasma performance (electron temperature and confinement time, particle influx and plasma-wall interaction, radiated power). During QSH discharges with a well-formed helical state, despite secondary mode amplitude is kept low by the feedback system, a deformation related to a non-stationary "locked mode" remains present, similar to MH plasmas (Valisa et al., 1997), though with a strongly reduced size of the displacement (< 1 cm). In Fig. 4.15(b) such a locked mode is observed as an interference pattern (black curve), which corresponds to two dips of the magnetic field connection length to the wall, L_{cw} (see panel (a)). These "holes" can be seen as homoclinic lobes ("fingers") at two toroidal positions ($\phi \approx 110°$ and $\phi \approx 133°$) (Scarin et al., 2019).

The analysis of RFX-mod data suggests a threshold of ≈0.3 in terms of the ratio between secondary locking size and displacement of the helical structure, $S_k = \Delta_{sec}/\Delta_{1,7}$ to completely avoid the detrimental effect of the secondary mode locking, which is important in perspective of the RFX-mod upgrade, where a reduction by a factor~2 in secondary mode amplitude is expected (Zuin et al., 2017).

4.6 Isotopic effect

The comparison of plasmas with hydrogen and deuterium as filling gas carried out in RFX-mod has shown a positive isotopic effect on the confinement of SHAx states similar to the one in tokamaks. For plasma currents around 1.5 MA, the energy confinement time scales as $M_i^{0.3}$, where M_i is the ion mass; the particle influx is significantly reduced and the particle confinement time scales as $M_i^{0.45}$. The effect on confinement is mainly due to the mitigation of transport at the edge (Lorenzini et al., 2015). In deuterium plasmas, the electron temperatures are higher by about 0.2 keV over most of the plasma volume ($r \approx 0.365$m, corresponding to $r/a < 0.8$), as shown in Fig. 4.16; the numerical calculation of particle orbits shows that the loss time in QSH regimes is about 1.3 times higher in deuterium than in hydrogen for both spontaneous and induced helical states (Gobbin et al., 2015).

4.7 Fast ion confinement

The experimental exploration of fast ion behavior in the RFP and its understanding is still preliminary. In the MST device, the tangential injection of a 0.5MW, 25 keV neutral beam allowed the study of fast ion confinement by measuring the decay of the fusion D-D neutron flux. In the Multiple Helicity state, the confinement time of fast ions has been found to be much higher (by an order of magnitude) than that of thermal particles, and consistent with the classical ion energy loss rate, in particular when injected in the direction of plasma current (Fiksel et al., 2005). Indeed the confinement of fast ions is even less affected by magnetic stochasticity than that of thermal ions. This can be explained by the fact that their larger Larmor radius averages out a part of the magnetic fluctuations and guiding center islands can differ significantly from magnetic islands, affecting the interaction between fast ions and magnetic fluctuations. In MH MST discharges, the fast ion particle confinement can be ≈10–20 ms, to be compared to ≈1 ms for thermal particles. The TRANSP code (Budny et al., 1992) has been applied to model the behavior of fast ion populations, indicating that they are core localized with an high pitch $v_{||}/|v|$ (Anderson et al., 2013). Due to the good confinement of the beam-produced particles, a consistent population can develop during neutral beam injection, with significant impact on the bulk plasma. There is a stabilizing effect on the most internally resonant tearing mode, whose amplitude results to be strongly suppressed, while the outer modes are basically unaffected. However, this reduction of the most-core resonant mode is related to a change in the magnetic equilibrium such that the width of the core island and the core stochasticity do not basically change. A destabilizing effect is also present at the same time, since Energetic Particle Modes and Alfven instabilities are excited (Koliner et al., 2012), leading to a saturation of the core fast ion population.

The behavior of fast ions is different in QSH regimes (Anderson et al., 2014). In fact, beam-produced fast ions make more difficult the transition from MH to QSH states, which is delayed in presence of beam injection at a given current level. In addition, the fast ion confinement, though larger than the thermal ion one, does not reach classical values as in MH. This is shown in Fig. 4.17, where the fast ion confinement time is plotted as a function of the normalized amplitude of the most-core resonant mode ($m=1,n=5$ in MST), which corresponds to MH plasmas at the lowest values and to QSH at the highest ones. In (P. J. Bonofiglo et al., 2019), (P. J. Bonofiglo et al., 2019) the fast ion transport associated with energetic particle driven Alfven instabilities, stochasticity induced by tearing modes and neoclassical effects has been investigated by 3D MHD simulations coupled to the STELLGAP code (Spong et al., 2003). It is found that in QSH the residual stochasticity governs the fast ion confinement.

5 Current profile control

In addition to helical states, a second approach has been successfully explored to go beyond the paradigm of a stochastic RFP dominated by global core-resonant tearing modes driven unstable by the radial gradient in the current flowing parallel to *B.* It relies on the modification of the current profile for reduction of these modes, which has been experimented with: (1) external field coils, (2) insertable current sources, and (3) rf antennas. The inductive approach with external field coils, the primary focus of this chapter, has been the most successful, leading to a strong reduction of stochasticity and tokamak-like energy confinement, along with the emergence of tokamak-like micro-scale fluctuations. These advances are important for development of the RFP and for the advancement of toroidal fusion science.

The theoretical and experimental foundations for current profile control are described in section 5.1. In section 5.2 we describe four inductive techniques, and in section 5.3 we describe measurements of the modified current profile and fluctuation reduction. Improvements in RFP fusion performance and work toward fusion parameter scaling are described in sections 5.4 and 5.5. The emerging role of micro-instability is described in section 5.6. Results with insertable current sources and rf antennas are described in section 5.7. Section 5.8 contains other related routes to improved confinement, and section 5.9 discusses questions and future directions.

5.1 Foundations for current profile control

Comparison between experiment and nonlinear MHD established that the multiple core-resonant modes are current-gradient-driven tearing fluctuations (or resistive kinks), well described by resistive MHD (Caramana et al., 1983), (Prager, 1990). As described in previous chapters, these relatively large (~ 1%) magnetic fluctuations can stochasticize the magnetic field in the core, leading to rapid field line diffusion (Rosenbluth et al., 1966), (Filonenko et al., 1967) and rapid transport of particles and energy (Rechester and Rosenbluth, 1978), (Schnack, 1992) .

MHD computations demonstrated that these tearing fluctuations could be reduced or even eliminated with a suitable modification of the current profile (Ho, 1991), (Sovinec, 1995), (Sovinec and Prager, 1999), (Prager, 1999). The essential idea is captured in Fig. 5.1 showing results from the DEBS code. On the left are profiles of the plasma current flowing parallel to *B*. The standard profile results from steady induction, while the controlled profile results from the addition of current in the plasma edge, implemented in the simulations with an *ad-hoc* electron force profile. The local change in the edge current profile leads to dramatic changes in the core-resonant tearing mode amplitudes, such that stochasticity, Fig. 5.1(c), is substantially reduced, Fig. 5.1(b). The fact

that a change to the edge current profile can affect core-resonant tearing modes stems from the global character of these modes, such that they are sensitive to the shape of the current profile everywhere in the plasma. The added current can either be stabilizing or destabilizing, depending on its magnitude and profile (stabilizing in the case of Fig. 5.1). This auxiliary current replaces the fluctuation-based dynamo that helps maintain the RFP configuration.

5.2 Inductive techniques

Four approaches to inductive current profile control have been studied experimentally and in most cases computationally. All entail temporal variations in the toroidal and/or poloidal magnetic field. Two of the techniques are transient. Pulsed poloidal (or parallel) current drive (PPCD) primarily entails a ramp down of the toroidal magnetic field, and self-similar current decay (SSCD) entails a ramp down of both fields. The other two techniques are quasi-steady-state. Oscillating poloidal current drive (OPCD) entails oscillation of the toroidal magnetic field, and oscillating field current drive (OFCD) entails oscillation of both fields. The most thoroughly developed and successful of these techniques is PPCD. Hence, PPCD is the primary focus of this chapter.

The PPCD technique was first studied experimentally on MST (Sarff et al., 1994) and computationally in DEBS soon thereafter (Sovinec, 1995) and in later work (Svidzinski and Prager, 2007),(Reynolds et al., 2008). Electric and magnetic field waveforms from one of the highest-performance MST PPCD plasmas are shown in Fig. 5.2. Sustained reduction of both m=1 and m=0 fluctuations was found to require $E_{//} \geq 0$, where $E_{//} = E_{//}(a) = E \bullet B/B^2 = (E_\theta B_\theta + E_\phi B_\phi)/B$ is the surface parallel electric field, and the subscripts θ and ϕ refer to the poloidal and toroidal direction (Chapman et al., 2002). $E_{//} > 0$ is maintained initially through E_θ via a ramp down in B_ϕ. Later in time, E_ϕ is reversed in order to prolong the control period. The ramp down in B_ϕ brings about a rather extreme RFP equilibrium, with the toroidal field reversal parameter, F, reaching about -2 and the pinch parameter, Θ, reaching about 3.5. In addition to the $E_{//}$ criterion, the production of high-quality PPCD plasmas is subject to a number of other conditions, e.g., avoiding an overly large E_θ (Sarff et al., 1995), providing a well-conditioned plasma-facing boundary and sufficiently low initial plasma density (Chapman et al., 2002),(Frassinetti et al., 2003),(Frassinetti et al., 2004), avoiding sawtooth crashes at the initiation of PPCD (Chapman et al., 2002) , and assuring a good control of magnetic error fields and locked modes (Chapman et al., 2002),(Frassinetti et al., 2005b).

The SSCD technique was first considered in two independent theoretical studies (Watterson and Gimblett, 1983), (Caramana and Nebel, 1988) in which it was recognized that a particular prescribed self-similar ramp-down of both B_θ and B_ϕ can yield an inductive electric field profile which can maintain an MHD stable current profile. The RFP dynamo is thereby suppressed, and the

RFP configuration is maintained purely inductively with a magnetic equilibrium approximately constant in time. The ramp-down rate is set by the instantaneous value of the resistive diffusion time (Nebel et al., 2002). The loop voltage programming required for SSCD, originally dubbed "catching" (Watterson and Gimblett, 1983), was attempted on the HBTX device at Culham, but the results were never published.

The OPCD technique was first tested experimentally on RFX (Bartiromo et al., 1999a) and later examined with a 1D model simulating magnetic field profiles (Martines and Spagnolo, 2008). Entailing a siniusoidal oscillation of B_ϕ, half of each OPCD cycle is PPCD-like in the trajectory of B_ϕ, and magnetic fluctuations can be reduced in an oscillatory fashion. Finally, the OFCD technique entails oscillations in both B_θ and B_ϕ. It will be extensively described in chap. 9.

5.3 Current profile modification and fluctuation reduction

In this section some examples are provided of the experimental current profile control and of fluctuation responses to current profile control, primarily from PPCD plasmas but also from SSCD. Direct internal measurements of the current profile during PPCD were made possible on MST by a combination of laser polarimetry (Brower et al., 2003) and 2D RFP equilibrium reconstruction (Anderson et al., 2003). Fig. 5.3 compares profiles of $\lambda = \mu_0 a(J_{//}/B)$ during PPCD (λ is the same quantity plotted in Fig. 5.1) to profiles before and after sawtooth crashes, each of which leads to flattening of the current profile in steady-induction plasmas (Brower et al., 2002), (Terry et al., 2004). Measured with approximately 0.08 m spatial resolution, λ during PPCD falls between the pre-crash and post-crash profile for $r > 0.3\ m$, while the PPCD profile is more peaked than either profile in the center of the plasma. Such peaking was also observed in MHD modeling of PPCD plasmas in RFX with the SpeCyl code (Puiatti et al., 2003), showing that during PPCD a significant reduction of magnetic perturbation is accompanied by a shrinking of the magnetic profiles. Measurements of the current profile were also made in the outer 10% of MST plasmas by an inserted probe (Chapman et al., 2000) with 0.01 m spatial resolution. In this region λ *decreases* when PPCD is applied. This initially surprising result was interpreted as being due to measured drops in the dynamo electric field and the electrical conductivity, the latter resulting from a drop in the electron temperature. Overall, the change in the λ profile is fairly modest with PPCD, but additional measurements in MST showed that there are much larger changes to the inductive electric field profiles, (Sarff et al., 2003b) (Anderson et al., 2005). Hence, there is a much greater change in the current drive than in the driven current.

Fluctuation measurements with current profile control are numerous, and show a significant drop in magnetic fluctuations. Fig. 5.4, representing data from RFX-mod OPCD plasmas, shows that the

innermost resonant $m = 1$ mode gradually increases while the remaining $m = 1$ modes with higher-n decrease, which also corresponds to higher electron temperatures (Terranova et al., 2007). The reduction of higher-n modes is a feature of plasmas with improved global confinement (Sarff et al., 2003b) (Sarff et al., 2003a). While most measurements of magnetic fluctuations are restricted to magnetic sensing coils at the plasma boundary, the polarimeter in MST allowed for first time the measurement of the fluctuation reduction in the core (Ding et al., 2003), (Terry et al., 2004) which has been found to be broadband and substantial.

Ohm's law in steady-induction RFP plasmas is balanced by the dynamo electric field arising from fluctuations, e.g. (Ho et al., 1989), see chap. 3. In plasmas with substantial fluctuation reduction, such as with PPCD, the dynamo electric field becomes small. This was demonstrated by measurements in PPCD plasmas in MST, Fig. 5.5 (Anderson et al., 2004) (Anderson et al., 2005). In this figure the two terms in simple Ohm's law are shown to be approximately equal over the entire plasma, implying that these plasmas are dynamo free. Consistent with the discussion earlier in this section, the $\eta_{neo}J_{//}$ term does not change much between steady-induction and PPCD plasmas, but $E_{//}$, along with the dynamo electric field, changes substantially (Anderson et al., 2004a (Anderson et al., 2005).

With the drop in the core-resonant magnetic fluctuations, other changes occur in the fluctuation behavior. For example, in the core of MST PPCD plasmas, density fluctuations, measured with interferometry and a heavy ion beam probe, are found to drop precipitously (Lanier et al., 2000) (Lanier et al., 2001), (Lei et al., 2002). Potential fluctuations drop as well, both in the core (Lei et al., 2002) and in the edge (Chapman et al., 1998a). This is not unexpected given the previously measured correlation between core-resonant magnetic fluctuations and edge-localized potential fluctuations in steady-induction plasmas in the Extrap T1 RFP (Li et al., 1995). There is also a more localized tapering of the fluctuations in MST correlated with a region of strong flow shear (the flow shear is addressed further in sec. 5.8). Measurements in the edge of MST PPCD plasmas also reveal that higher-frequency magnetic turbulence is much less intermittent and has a statistical behavior typical of self-similar turbulence expected in systems exhibiting self-organized criticality (Marrelli et al., 2005). A similar conclusion was drawn for both magnetic and potential fluctuations in the edge of TPE-RX PPCD plasmas (L Frassinetti et al., 2007b).

The drop in core-resonant tearing fluctuations also brings about an important change to the core magnetic topology. Tomographic x-ray measurements in the core of MST PPCD plasmas revealed two discrete, non-overlapping islands, corresponding to the two innermost resonant $m = 1$ modes (Franz et al., 2004) (Franz et al., 2006). This is shown in Fig. 5.6 and is a direct evidence of decreased stochasticity in the core. High-energy runaway electrons also emerge in these plasmas, as

described in more detail in the next section, further indicating that stochasticity no longer dominates core transport.

5.4 Improved fusion performance

This section describes improvements in fusion performance brought about by SSCD, OPCD and PPCD. Most of the results are from plasmas with PPCD, and with only two exceptions, noted below, the results described here are from ohmically heated plasmas. The papers cited herein contain results from both hydrogen and deuterium plasmas.

The only published test of SSCD occurred in RFX-mod (Zanca, 2007). The simultaneous decay of B_θ and B_ϕ is provided primarily by actively reversing the sign of the surface toroidal voltage. This affects both the toroidal and poloidal current flowing in the plasma. As magnetic fluctuations drop, poloidal beta, $\beta_p = 2\mu_0 \langle p \rangle / B_\theta^2(a)$, and the global energy confinement time increase by approximately 50%. A crude approximation of SSCD was also tested on MST, with the decay of B_θ and B_ϕ provided passively by the external poloidal field circuit. The energy confinement time in such plasmas is estimated to triple.

The quasi-steady OPCD technique was tested in both RFX (Bartiromo et al., 1999a), (Bolzonella et al., 2001), (Carraro et al., 2002) and RFX-mod (Terranova et al., 2007) . One signature of OPCD is an oscillation in the central electron temperature, which increases in the PPCD-like half of OPCD cycle and then decreases in the other half. In plasmas with OPCD during the PPCD-like phase, the toroidal mode spectrum becomes peaked, and a T_e structure emerges in the core. The width and height of the structure varies. In the region where ∇T_e is largest the electon thermal diffusivity χ_e can drop to as low as 10 m^2/s. The global energy confinement time increases by about 60%. Indeed in the phase with the thermal structure the behaviour of T_e profile and mode spectrum is the same as during QSHs, so that OPCD has been suggested as a means to favour the occurrence of QSH states (Terranova et al., 2007).

The PPCD technique has been the most widely applied and studied of the inductive approaches, and it has brought about the most substantial improvements in RFP fusion performance. PPCD has been tested in MST, RFX, RFX-mod, EXTRAP T2R, and TPE-RX, and it has led to (1) improvements in energetic electron and ion particle confinement and in thermal electron particle confinement, (2) large values of the normalized electron density, substantially exceeding the Greenwald limit, (3) classical confinement of impurity ions, (4) RFP-record values of electron and ion temperature, with a simultaneous reduction in Ohmic heating power, (5) an RFP-record beta that exceeds the Mercier criterion, (6) an RFP-record tokamak-like energy confinement time, and (7) the emergence of two new regimes for the RFP, with the prominence of micro-instability in lower-beta plasmas and

pressure-driven macro-instability in higher-beta plasmas. We expand upon each of these results in what follows, with detailed discussion of micro-instability and pressure-driven macro-instability in sections 5.6 and chapter 6, respectively.

One of the key PPCD results was the observation of runaway electrons in the core of MST plasmas (O'Connell et al., 2003). In a stochastic magnetic topology, the rate of electron transport increases with the electron velocity. Hence, while the Dreicer criterion for runaway electrons can easily be satisfied in low density RFP plasmas, electrons are lost more and more quickly as they accelerate. Fig. 5.7 contains x-ray bremsstrahlung emission from PPCD and steady-induction plasmas. The rate of electron particle diffusion is $\sim (v_{//}/v_{th})^{\alpha}$, where $v_{//}$ and v_{th} are the parallel and thermal electron velocities, respectively. The x-ray energy spectrum from steady-induction plasmas is well fit with α=1, consistent with stochastic transport, while the spectrum from PPCD plasmas is well fit with α=0, indicating that stochastic transport is no longer playing an important role. High-energy (20keV) beam-injected ions may also be modestly better confined during PPCD (Hudson, 2006); however, it has to be mentioned that beam ions are already well confined in steady-induction MST plasmas (Fiksel et al., 2005).

	w/o pellets	With pellets	w/o pellets	With pellets
I_p (MA)	0.21	0.17	0.53	0.48
$n_e(0)$ ($10^{19}m^{-3}$)	0.9	3.5	1.2	4
$<n_e>/n_G$	0.26	1.2	0.13	0.66
P_{oh} (MW)	1.0	2.2	2.3	4
$T_e(0)$ (keV)	0.6	0.17	1.9	0.7
$T_i(0)$ (keV)	0.18	0.19	1.3	0.6
β_{tot} (%)	15	26	10	17
τ_E (ms)	10	>5	12	7

Table 5.1: PPCD plasmas in MST with and without pellet injection at low (columns 1 and 2) and high (columns 3 and 4) plasma current. Reproduced from (Chapman et al., 2009)

Thermal electron particle confinement is also improved with PPCD. From measurements in MST, the particle flux decreases everywhere in the plasma, with a drop of almost two orders of magnitude in the core. Correspondingly, the global particle confinement time is estimated to improve eight-fold (Lanier et al., 2000), (Lanier et al., 2001). The rate of particle diffusion also drops by about a factor of two in RFX plasmas (Puiatti et al., 2003). The combination of PPCD and frozen-deuterium

pellet injection in TPE-RX brought about an estimated five-fold improvement in the global particle confinement time (Koguchi et al., 2006). Absent pellet injection, the global confinement time improved in TPE-RX by an estimated factor of ten (L Frassinetti et al., 2007b), (Auriemma et al., 2009).

Frozen pellet injection allows a substantial increase in the density attainable in PPCD plasmas, while still retaining reduced fluctuations and improved confinement. Raising the density with edge-deposited fueling techniques such as gas puffing bring about increased fluctuations and degraded confinement (Koguchi et al., 2006), (Wyman et al., 2008a),(Wyman et al., 2008b) ,(Chapman et al., 2009). Pellet injection can fuel the plasma core without substantially impacting the edge or degarding confinement. The synergy between pellet injection and PPCD was first noted in RFX (Lorenzini et al., 2002), (Puiatti et al., 2003), where the density doubled, reaching about 4×10^{19} m^{-3}. Pellet injection into TPE-RX brought about a similar doubling of the density (Koguchi et al., 2006), and injection into MST plasmas initially quadrupled the density, surpassing the Greenwald density limit (Wyman et al., 2008a),(Wyman et al., 2008b) ,(Chapman et al., 2009). Shown in table 5.1 are central densities and densities normalized to the Greenwald limit in MST. Subsequent injection of larger pellets in MST has resulted in an absolute density up to 9×10^{19} m^{-3} and a normalized density up to ~ 2 (Caspary, K.J., 2014), (Sarff et al., 2015).

The confinement of impurity ions also improves. In steady-induction RFX plasmas, the impurity particle diffusion coefficient profile drops from 20 m^2/s in the core to 1 m^2/s in the outer 10% of the plasma. With PPCD, the lower diffusivity region widens to encompass the outer 20% of the plasma (Carraro et al., 2002), (Puiatti et al., 2003. In EXTRAP T2R, the rate of impurity diffusion decreases by about a factor of two in the core with no change in the edge (Kuldkepp et al., 2006) . In MST, impurity transport drops down to the classical value (Kumar et al., 2012a), (Kumar et al., 2012b), (Barbui et al., 2014). Dominated by Coulomb collisions rather than neoclassical particle drift effects, impurity ions are convected outward, and the impurity density profile, along with the Z_{eff} profile (Galante et al., 2015), become hollow, consistent with the temperature screening mechanism of classical transport.

One common feature of PPCD plasmas is an increase in the central electron temperature, e.g., (Sarff et al., 1997), (Stoneking et al., 1997), (Bartiromo et al., 1999b), (Chapman et al., 2001),(Cravotta et al., 2003) (Yagi et al., 2003). This is in spite of the fact that the Ohmic heating power commonly drops, e.g., (Sarff et al., 1994), (Telesca and Tokar, 2004). The largest central $T_e \sim 2$ keV was achieved in MST, table 5.1 (Chapman et al., 2010). This is the largest electron temperature achieved

thus far in the RFP. Neutral beam heating has also been applied to PPCD plasmas in MST, increasing the central electron temperature by about 100 eV (Waksman et al., 2012). This is the only example thus far of auxiliary (non-Ohmic) heating of an RFP plasma.

In contrast to electron temperature, the evolution in the ion temperature in low-density PPCD plasmas is typically fairly small. The only localized measurements of the ion temperature in the core of PPCD plasmas were made in MST using neutral-beam-based charge-exchange-recombination spectroscopy. Initial measurements in low density plasmas showed that the central T_i changes very little between steady-induction and PPCD plasmas, with a value of about 300 eV in the core of plasmas with a central $T_e > 1$ keV (Chapman et al., 2002) . The Ohmic heating power channeled from the electrons to the ions is quite small. A roughly four-fold increase in the ion temperature, to about 1.3 keV (table 1), was achieved by triggering large amplitude sawtooth crashes shortly before the start of PPCD (Chapman et al., 2010). The ion heat generated during the crashes is trapped in the plasma with the onset of PPCD and the ion energy confinement time is estimated to improve ten-fold. With pellet injection and substantially higher density, the ion temperature increases with time during PPCD plasmas in MST (Wyman et al., 2008a). This is due both to a larger Ohmic input power and a larger rate of energy transfer from the electrons to the ions.

Another common feature of PPCD plasmas is an increase in beta. There are examples of this from RFX, TPE-RX, EXTRAP T2R, and MST, e.g., (Martini et al., 1999b) ,(Chapman et al., 2001), (Yagi et al., 2002), (Cecconello et al., 2003). This will be discussed in detail in chapter 6.

In PPCD plasmas an increase in the global energy confinement time is observed in all RFP devices. The confinement time in RFX and EXTRAP T2R as much as doubled (Martini et al., 1999b), (Cecconello et al., 2003), while in TPE-RX it increased as much as five-fold (Yagi et al., 2003), (L Frassinetti et al., 2007a). The largest increase in confinement, as well as the largest absolute RFP confinement time was produced in MST. The energy confinement time increased by more than ten-fold, reaching about 12 ms (Chapman et al., 2009), (Chapman et al., 2010). The global electron thermal diffuvisity drops to about 5 m^2/s, with a local minimum of about 2 m^2/s in the region of large ∇T_e. The values of confinement times reached in MST are tokamak-like (Sarff et al., 2003b), (Sarff et al., 2003a), (Chapman et al., 2010). This is illustrated in Fig. 5.8, where MST standard and PPCD confinement data is compared to what is predicted by the IPB98(y,2) ELMy H-mode tokamak confinement scaling formula. Both of the PPCD data points lie within a factor of two of the scaling prediction. This is not meant to imply that this tokamak scaling applies to the RFP. Rather it demonstrates that the best RFP energy confinement is comparable to that in an equivalent tokamak, with a much smaller toroidal field.

5.5 Confinement scaling

Considering plasmas with PPCD, for which there are results from multiple RFP devices, there is not as yet a firmly established universal scaling for energy confinement time, although basic parameters such as plasma minor radius very likely play a role. As suggested by Fig. 5.1(b), even with current profile control, there may be regions of the plasma where stochasticity still plays a role in energy transport. In addition, as discussed in the next section, in lower-density (lower-beta) PPCD plasmas, micro-scale fluctuations due to instabilities like the trapped electron mode may be important, while, as described in the next chapter, in higher-beta PPCD plasmas, macro-scale pressure-driven tearing may play a role. Hence, confinement physics in PPCD plasmas is complicated. Nonetheless, there has been noteworthy effort on this topic.

As reported in Fig. 5.9, for low-density and high-density PPCD plasmas in MST, the improved energy confinement fell above, and in one case well above, the empirical Connor-Taylor scaling which was based on the best standard-plasma confinement results from a variety of RFP devices (Chapman et al., 2001), (Chapman et al., 2002),(Wyman et al., 2008b). Hence, PPCD plasmas represent a break from the previous trend.

The dependence on the dimensionless Lundquist number S, which was introduced in chap.3 and varies as $I_p T_e^{3/2}/n_i^{1/2}$, was examined based on data from RFX (Intravaia et al., 1999), (Terranova et al., 2000). While magnetic fluctuations were smaller (and the energy confinement time larger) in RFX PPCD plasmas, the fluctuations exhibited the same amplitude scaling with S as steady-induction plasmas.

The factor by which the energy confinement time improves with PPCD in *low-density* TPE-RX, RFX, and MST plasmas, including results up to 2002, was found to be well represented by the change in $\gamma = (1 - F)/\Theta$ from the beginning to the end of PPCD (Yagi et al., 2002), (Yagi et al., 2003), (Martini et al., 1999b). This parameter is linked to the shape of the current profile and hence MHD stability. Later work included additional TPE-RX data and data from EXTRAP T2R and found that an empirical scaling including a Θ^3 dependence, encompassed fairly well all of the PPCD results from various devices (Yagi et al., 2005).

The scaling of various RFP confinement-related parameters was evaluated numerically for generic current profile control with single-fluid resistive MHD modeling (Scheffel and Dahlin, 2006), (J.-E Dahlin and Scheffel, 2007). An auxiliary electric field profile is applied in the model that, on the resistive time scale, substitutes for the dynamo electric with the aim of eliminating tearing fluctuations. The energy confinement time scales as $196\Theta^{1.0} a^{1.5} \mu^{0.25} Z_{eff}^{-0.50} (I/N)^{0.50} I^{0.50}$, where μ is the fuel-ion to proton mass ratio, and N is the line density.

5.6 Emergence of microinstability in PPCD plasmas

As when in helical states stochasticity is not the only mechanism driving transport and microinstabilities become significant contributors (see sec. 4.3), the role of microinstabilities has been explored in low-density MST PPCD plasmas . both theoretically and experimentally work (Terry et al., 2015).

The theoretical work is based on gyrokinetic modeling with the codes GYRO and GENE using toroidal equilibrium reconstructions of PPCD plasmas from MST. The simulations predict unstable density-gradient-driven trapped-electron modes (TEMs) (Carmody et al., 2013). They also predict that the critical gradient is larger than for a typical tokamak plasma by roughly the aspect ratio, R/a, consistent with the relative difference in magnetic field scale length. Nonlinear simulations show that the Dimit's shift due to strong zonal flows is relatively large and persists even at finite beta (Carmody et al., 2015).

The first experimental work focused on density fluctuations, measured by FIR forward scattering in MST PPCD plasmas (Sarff et al., 2015). A broadband decrease in fluctuation amplitude is observed relative to steady-induction plasmas, but the spectrum exhibits a new peak around 100 kHz, Fig. 5.10. The fluctuations at this new peak have $k_\phi \rho_s \sim 0.2$, propagate in the electron diamagnetic drift direction, and are localized in a region $r/a \sim 0.8$ where the equilibrium density gradient is maximum. The fluctuation amplitude also correlates with the experimental gradient scale length, exhibiting a threshold onset at $R/L_n \approx 35$. These characteristics are all consistent with the density-gradient-driven TEM.

5.7 Toward non-inductive (dc) current profile control

Three additional efforts were undertaken on MST with the goal of noninductively (non-transiently) modifying the current profile and will be briefly summarized in this section: driving current via electrostatic current sources inserted into the plasma edge and launching lower-hybrid and electron-Bernstein waves from rf antennas.

Edge electrostatic current drive was tested with 16 miniature plasma sources inserted into the outer 10% of the plasma (Craig et al., 2001). When the sources were inserted but inactive, they caused a perturbation leading to an estimated 50% drop in particle and energy confinement. When biased negatively to emit electron current, each source injects roughly 0.5 kA, and when the current is injected parallel to the background edge parallel current, magnetic fluctuations are reduced, and the particle and energy confinement are restored to approximately their unperturbed values. The restoration of confinement is linked to a time-averaged drop in magnetic fluctuation amplitude, due

primarily to an increase in the time between sawtooth crashes. Although the plasma sources did not prove a viable means of achieving a net confinement improvement, they did demonstrate the principle of current profile control.

The foundation for lower-hybrid (LH) wave injection stemmed in part from theoretical studies (Uchimoto et al., 1994), (Shiina et al., 1995). It was predicted that the location of the driven current can be controlled by choice of parallel wave number and rf frequency, and that the predicted efficiency of current drive is sufficient for tearing suppression with 1-2 MW of rf power. Experimentally, an interdigitial-line antenna mounted on the inner surface of MST launched the correct $n_{//}$ spectrum and was well loaded by the plasma (Kaufman, 2005), (Kaufman et al., 2007). With the source of rf power exceeding 200 kW, substantial x-ray emission from the plasma was observed (Burke et al., 2007). However, robust operation at this high source power did not prove feasible, implying that a large number of antennas would be required to inject sufficient power to affect tearing mode stability.

The foundation for the injection of the electron-Bernstein wave (EBW) was laid in part by computational studies showing that there is a directional component to the absorption of the wave, which can be controlled by the poloidal angle at which the wave is launched, so that directed current drive is possible (Forest et al., 2000). The conversion of Bernstein waves generated within the plasma to electromagnetic waves was confirmed by measurements of thermal emission at the plasma boundary (Chattopadhyay et al., 2002). By reciprocity, this implies that externally launched electromagnetic waves can couple to the Bernstein mode. Starting with very low power (< 10 W), coupling of rf was studied experimentally with a waveguide antenna and found to agree with full-wave modelling (Cengher et al., 2006). Coupling efficiency exceeding 80% was observed under certain conditions, though coupling can be degraded by effects such as edge density fluctuations (Bilato et al., 2009). The available power for injection was increased to several hundred kW, and electron energization in the plasma is evident from x-ray emission (Seltzman et al., 2016). However, recent modeling with a Fokker-Planck, rf-altered electron distribution coupled into a single-fluid MHD simulation indicates that much larger power (~ 10 MW) would be needed to produce an observable effect on the tearing modes (Hendries et al., 2014).

5.8 Other routes to improved confinement

In addition to QSH, described earlier in this paper, there are other routes to improved confinement in the RFP that do not entail active control, *per se*. We mention these here, given an observed partial synergy with and partial similarity to PPCD plasmas in MST.

Both in TPE-1RM20 and MST, spontaneous periods of improved confinement were observed in conjunction with strong toroidal magnetic field reversal and a relatively large pinch parameter. Dubbed "improved high theta mode" in TPE-1RM20 (Hirano et al., 1996) and ultimately "enhanced confinement" (EC) periods in MST (Chapman et al., 1996), (Chapman et al., 1998b), magnetic fluctuations drop, and both the electron temperature and the energy confinement increase, doubling in TPE-1RM20 and tripling in MST. Magnetic fluctuations drop, the electron temperature increases, and energy confinement is improved up to 20%. Improved confinement was observed later still in TPE-RX, corresponding to slow decay (toward zero) of the edge toroidal field (Yambe et al., 2014).

The EC periods in MST are characterized in part by regularly occurring bursts of $m = 0$ mode activity. Each burst causes a temporary degradation of confinement (Piovesan et al., 2008). Such bursts can also occur in PPCD plasmas, with a similar effect on confinement (Frassinetti et al., 2005a). The hottest, highest confinement PPCD plasmas are entirely free of such bursts (Chapman et al., 2001), with reduction of both $m = 1$ and $m = 0$ occurring almost immediately after the start of PPCD (Chapman et al., 2002) . This immediate reduction occurs when an EC period is produced leading into the start of PPCD. In fact a possible explanation of the lower effect of PPCD in RFX and RFX-mod with respect to MST has been ascribed to a lower reduction of $m=0$ modes. Furthermore, EC periods can terminate with very large amplitude sawtooth crashes, contributing to the pre-PPCD ion heating described above (Chapman et al., 2010). Initiating PPCD with (EC-like) strong toroidal magnetic field reversal also led to the best PPCD performance in EXTRAP-T2R (Cecconello et al., 2003).

The physics of these spontaneous periods of improved confinement, and the $m = 0$ bursts occurring in EC and PPCD plasmas in MST, is not well understood. However, based on the fact that the bursts bear some resemblance to edge-localized modes in tokamak H-mode plasmas (Chapman, 1997), (Piovesan et al., 2008), it was hypothesized that $E \times B$ flow shear could play a role. And in the PPCD case, this would not be overly surprising given the emergence of tokamak-like micro-instability. Strong flow shear was measured in the edge of both EC and PPCD plasmas (Chapman et al., 1998a), (Chapman et al., 1998b). Later modeling of the impact of various flow profiles on tearing stability showed that the flow shear in EC and PPCD plasmas could play a role in governing the $m = 0$ bursts (Gatto et al., 2002). Modifications to $E \times B$ flow shear were also measured during PPCD in RFX (V. Antoni et al., 2000a), (V. Antoni et al., 2000b). Finally, it is worth mentioning that biasing the edge of MST brought about a reduction of electrostatic fluctuations and an improvement in particle confinement (Craig et al., 1997). Electrostatic fluctuations and the edge particle flux were also affected by biasing in RFX (V Antoni et al., 2000).

5.9 Open questions and future directions

There are many questions in the realm of current profile control. For example: (1) what is the optimal inductive $E(a)$ waveform for sustained fluctuation reduction and improved confinement, and can the degree and duration of improved confinement be increased? (2) how does the improved energy confinement time scale with parameters like I_p? (3) what would be the impact of an advanced, low-recycling boundary on plasmas with current profile control? (4) how are PPCD/OPCD plasmas associated to the onset of QSH states? (5) what is the role of $m=0$ modes? Though the comprehension of these plasmas has significantly progressed, further computational and experimental work is required to fully address these points.

While MHD computation provided the foundation for current profile control, experimental progress to date has been almost entirely empirical. This is due in part to the fact that fully nonlinear simulations of RFP plasmas require considerable raw computing power, the need for which increases, for example, with S. The most recent modeling of PPCD with the NIMROD MHD code was conducted with $S < 10^4$ (Reynolds et al., 2008), much lower than in the hottest PPCD plasmas in MST. The importance of $m = 0$ bursts in MST plasmas was described above, but such bursts are not typically observed in MHD computation, implying unrealistic input parameters or missing physics.

However MHD computation has pointed ways forward. The concept of "advanced current profile control" was examined with MHD modeling wherein a generic auxiliary electric field is feedback-adjusted during a time-evolved simulation to minimize the MHD dynamo electric field (Dahlin and Scheffel, 2005), (Dahlin et al., 2007), (J.-E Dahlin and Scheffel, 2007), (Jon-Erik Dahlin and Scheffel, 2007) (Scheffel et al., 2013), and scaling based on this work predicts that RFP-reactor relevant central temperatures can be obtained with Ohmic heating alone (Scheffel and Dahlin, 2006), (J.-E Dahlin and Scheffel, 2007). Reactor-relevant simulations were also conducted for SSCD, showing that appropriately applied inductive waveforms can lead to a pulsed reactor system with significant net energy gain (Nebel et al., 2002).

Gyrokinetic modeling is also likely to be important. The potentially missing physics noted above might be related to micro-instability. Hence, understanding present day experimental results and projecting to the future will likely require both MHD and gyrokinetic work.

In present-day RFP devices, current profile results have for the most part stemmed from simple, passive power supplies comprised of capacitors and inductors. The future of current profile control lies in digitally programmed, feedback-controlled power supplies, which are in use on RFX-mod and are being developed on MST. In agreement with the modeling described just above, the power

supply waveforms can in principle be adjusted in real time based on measurements, for example, of the MHD dynamo, or at least the constituent fluctuations. But additional inductive and/or non-inductive control may also be needed for micro-scale fluctuations.

Scaling can, in principle, be assessed empirically to some extent in present-day devices, but such scaling would ideally be based on a single optimal means of controlling macro- and micro-scale fluctuations. Ultimately, RFP devices with access to much higher I_p will be required for scaling studies, and such devices might also allow for non-inductive control techniques like rf, which would help further probe and optimize scaling.

With respect to power and particle handling, RFP devices have to date operated with primitive boundaries that would be irrelevant in a reactor setting. While substantial progress in fusion performance has nonetheless been possible, it was noted above that a crucial requirement for high-quality PPCD plasmas is a "well-conditioned boundary," meaning minimized contamination by atmospheric impurities and low recycling. Indeed MHD modeling showed that changing the edge resistivity changes magnetic fluctuation amplitudes (Sätherblom et al., 1996). It is customary to think of current profile control in terms of changing the inductive electric field, but the current profile can be altered equally well by a change in resistivity. Together with the already mentioned possible effect of the m=0 modes (sec. 5.8), also the need for low recycling in PPCD may explain in part the fact that the confinement improvements in TPE-RX and MST were greater than that in RFX and RFX-mod. With full graphite coverage of the plasma-facing boundary, RFX had large recycling, in contrast to the other two devices with their metallic boundaries. RFX-mod has a boundary similar to RFX, but the upgraded device RFX-mod2 (Peruzzo et al., 2017) aims at a reduced recycling, which would provide a critical test for PPCD. It has also been hypothesized that an advanced, low-recycling boundary, comprised, e.g., of liquid lithium, could have a profound effect on the RFP plasma, particularly in conjunction with current profile control (Munaretto et al., 2012), (Innocente et al., 2015), (M. E. Puiatti et al., 2013).

In this chapter and in the previous one two ways of reducing stochasticity and improving the performance of RFP plasmas have been presented: the helical states and the current profile control. Still an open issue is if they could act in synergy when applied together. Due to the non stationary character of both, an extended experimental investigation is difficult and not done yet. In RFX-mod at plasma current $I_p < 1$MA, OPCD favoured the development of QSH leading to an enhancement in confinement by ≈50% (Terranova et al., 2007). At high current QSHs spontaneously develop, so that their time phasing and duration with OPCD is difficult to control. New insights into the combined effect of QSH and OPC/PPCD will come from RFX-mod2, where more stationary helical states are expected to occur.

6 β and density limit

In the Tokamak, the total β is limited basically by ideal stability, which sets a disruptive limit around 5%, depending on current and aspect ratio. In addition, limitations of achievable β related to neoclassical pressure driven resistive tearing modes have been observed in several devices, and compared to theory, see for example (Chang, 1995),(Kislov et al., 2001), (Koslowski et al., 2000). In the Stellarator, ideal interchange modes are a major concern for high β plasma production, leading to a non disruptive limit similar to the Tokamak one (Weller et al., 2006), (Sakakibara et al., 2015), though violations of the Mercier criterion (Mercier, 1960) have been observed in some experiments and interpreted as a local effect (Okamura et al., 1999), (Carreras et al., 2001). Instead, plasmas characterized by high β values are a peculiar feature of the RFP configuration, where, due to the edge magnetic field nearly poloidal, the total β is almost equal to the poloidal one. As reported in papers as (Merlin et al., 1989), the ideal limit is much higher than in Tokamaks, $\beta_p=50\%$ for $m=0$ instabilities and $\beta_p=100\%$ for $m=1$ (with m poloidal mode number and β_p poloidal beta value). However, current experiments achieve β values that, though high compared to the tokamak and stellarator, are still well below the ideal stability limit.

At variance with beta limits, the high density limit is nearly the same for the RFP and the Tokamak, associated to a radiation barrier and traditionally described by the empirical Greenwald law (Greenwald, 2002), though recently a power balance model accounting for neutrals and impurity radiation has been developed and successfully describes the high density limit in the Stellarator, RFP and L-mode Tokamak (Zanca et al., 2017), (Zanca et al., 2019).

6.1 High β plasmas

Experimentally, high beta values are usually related to high density and low fluctuation (i.e. low transport) regimes. In the TPE-1RM20 RFP, in the so-called Improved High Theta Mode the highest $\Theta=B_\theta(a)/\langle B_\Phi\rangle \approx 2$ has been found to correspond to increased densities and temperatures, and therefore to the highest values of $\beta_p \approx 18\%$ (Hirano et al., 1996). This regime was related to a reduction of dynamo activity, measured as a large reduction of magnetic fluctuation power around 70 kHz. Similar β_p values have been measured in TPE-RX when the electron density was increased by fast gas puffing (Sakakita et al., 2004). Indeed, in most RFPs increasing density in improved regimes by pellet injection or fast gas puffing has been applied as a means to improve confinement and achieve record β values. In RFX-mod, the highest poloidal beta values of ≈15% have been observed when n/ n_G approaches 1 (Innocente et al., 2007); a statistical analysis in terms of global parameters and assuming ion temperature as a constant fraction of the electron temperature, yields

$\beta_p \approx I_p^{-0.23}\ (n/n_G)^{0.58}$, which indicates a small degradation of β_p with plasma current and a more significant increase with n/n_G (Innocente et al., 2009). Instead, 3D resistive MHD simulations by the DEBSP code, based on stochastic transport scalings (Scheffel and Schnack, 2000a) predict a dependence of β_p on I_p more negative than the experimental RFX-mod data ($\beta_p \approx I_p^{-0.56}\ (n/n_G)^{0.56}$). In MST also a modest decrease of β_p with the current, $\beta_p \approx I_p^{-0.23}$ at high n/n_G, was reported in (Stoneking et al., 1998).

In several RFP devices the maximum achieved β has been transiently enhanced by the combination of high density plasmas and active control of the current profile (see chap. 5). In RFX, when an Oscillating Poloidal Current Drive was applied, β_p was enhanced by a factor 50% (Martini et al., 1999a). In the TPE-RX device, double β_p (13%) and β (11%) values have been measured during PPCD with respect to standard plasmas. In MST, the application of PPCD leads to enhanced total beta of 11-15 % (depending on plasma current), to be compared to 5-9% in standard plasmas (Sarff et al., 2003a). When during the active current profile control phases deuterium pellets were injected, thus increasing density and its gradient, record β values have been obtained (Chapman et al., 2009).

The TPE-RX experiment achieved increased density operation with improved confinement and β_p up to the record value ≈ 34%, by the injection of a deuterium pellet during PPCD (Koguchi et al., 2009).

In MST, dedicated studies on β limit have been performed, optimizing pellet parameters in PPCD plasmas in order to produce its ablation in the core and maximize β (Sarff et al., 2015). In these experiments, as introduced in chapter 5, while density increases the electron temperature decreases, and a large fraction of ohmic power (higher at higher density) is collisionally transferred to ions. The larger stored energy leads to high beta values, $\beta_{tot} \approx 26\%$, corresponding to a total poloidal beta ≈ 40%. The latter value of poloidal beta coincides with the maximum beta predicted by the Connor-Taylor scaling, $\beta \approx (m_e/m_i)^{1/6}$ (m_e and m_i electron and ion mass respectively), which gives 25.4% for MST (Wyman et al., 2009). In such plasmas, pressure gradients exceeding the Mercier limit have been produced (Wyman et al., 2008b), (Chapman et al., 2009), see Fig. 6.1, similar to what observed in stellarators (see for example (Sakakibara et al., 2015), (Aguilera et al., 2015)).

The Mercier criterion governs the interchange stability, and can be expressed as:

$$\frac{r\,B_\varphi^2}{4\pi}\left(\frac{q'}{q}\right)^2 + 8\,p'(1-q^2) > 0 \qquad 6.1$$

with the first term related to the stabilizing effect of the magnetic shear and the second one to the destabilizing effect of pressure gradient when $q < 1$.

Theoretical computations by the DEBS code have shown that in these high β regimes both pressure-driven interchange modes and tearing modes are linearly unstable (Chapman et al., 2009). In MST high beta plasmas, interchange modes have not been observed (possibly due to limits of the diagnostics), so that an open issue remains whether the driving modes are interchange or global tearing modes: in (Paccagnella, 2013) it is found that at low β the parity of pressure driven modes is the tearing parity. At β values around 20% the interchange modes appear, to become dominant around 40%. Indeed in RFX-mod the observed edge magnetic fluctuations corresponding to linearly unstable pressure driven modes have the tearing parity, though they were in a first time interpreted as g-modes (Zuin et al., 2010).

A disruptive limit of β does not occur, even when the control of the current profile with the related reduction of current driven modes and increase of beta leads to a destabilization of pressure driven modes: at very high β a 'soft' degradation of confinement is observed, likely related to increased fluctuations at high density.

At variance with tokamaks, shaping effects have not been found in RFPs to enhance the β limit for both ideal (Paccagnella et al., 1991) and resistive β modes , due to a poloidal mode coupling stronger than in the circular topology (produced by the variation of the poloidal field along the poloidal angle) and to the development of multiple trapping regions (Guo et al., 2013).

6.2 Density limits

Since 80's, the operational range of RFP experiments has been found to be limited both at low and high electron density (Ortolani and Rostagni, 1983), (Hokin et al., 1991). The low density limit was related to the acceleration of slide-away electrons and to a growth of the magnetic fluctuations. In RFX-mod the longest durations of helical states featuring ITBs have been obtained when the careful design of the magnetic boundary and the consequent reduction of the edge radial field by a proper tuning of the feedback MHD control system has allowed the extension of the density operational range towards the lower values (Gobbin et al., 2015).

Similar to tokamaks, the high density limit in RFPs has been instead associated to a radiation barrier, dependent on plasma current (Perkins and Hulse, 1985). In RFX-mod, the high density limit was compared to the Tokamak empirical Greenwald limit (Greenwald, 2002):

$$n_e[10^{20}m^{-3}] < n_G = I_p[MA]/\pi a^2 \qquad 6.2$$

with n_e average plasma density, I_p plasma current. It was found that in the RFP as in the Tokamak the upper boundary of the density operating space is limited by the Greenwald density (Valisa et al., 2004). The same empirical limit was also observed in the MST RFP in standard plasmas (Wyman et

al., 2008b), see Fig. 6.2. The fact that the same representation, based on averaged global plasma quantities, matches well data from devices characterized by different size, performances, magnetic topology and transport quality suggested that a common physics could underlie the phenomenology of the Greenwald limit. Indeed, the point of view of the RFP configuration has been compared to those of the Tokamak and Stellarator, significantly contributing to the general understanding of the high density limit (Puiatti et al., 2009b).

Recently, a new theory able to describe the density limit in RFPs, L-mode Tokamaks and Stellarators (where the density is constrained by the Sudo limit, (Sudo et al., 1990)) has been proposed, simply based on a radiative limit and taking into account the radiation from impurities and neutrals (Zanca et al., 2017), (Zanca et al., 2019). The model leads to a constraint for the edge density, ruled by radiation losses from light impurities. For ohmic tokamak and RFPs the limit scales linearly with the plasma current, as the empirical Greenwald one. The auxiliary heating adds a further dependence, scaling with the power as $P^{0.4}$, in agreement with L-mode tokamak experiments. Compared to previous works with a similar approach and applied to ohmic tokamaks (Wesson, 2004), this model is able to take into account profile-dependent terms.

In RFX-mod, when the density approaches the Greenwald value, the temperature decreases, while the density increases at the edge (Spizzo et al., 2010). Such edge density accumulation takes place after a back transition from the QSH (Quasi-Single-Helicity) to the MH (Multiple Helicity) regime, which occurs at $n/n_G \approx 0.35$ (Scarin et al., 2011). Due to the edge density accumulation radiation increases, in the shape of a poloidal radiating belt (Valisa et al., 2004) , (Puiatti et al., 2009c), which resembles the MARFE phenomenology observed in Tokamaks (with poloidal and toroidal coordinates exchanged due to the poloidal nature of the magnetic field in the RFP edge) (Lipschultz, 1987) or Serpens in LHD Stellarator (Miyazawa et al., 2006). An important difference between RFPs and Tokamaks is that the density limit is not disruptive in the RFP: when the Greenwald density is approached, due to plasma cooling and resistivity increase, the toroidal flux decreases, resulting in the shrinking of the current profile with soft decrease of plasma current. Indeed, in the RFP when density increases, the input power necessary to sustain the discharge increases as well, so that the density limit can be also regarded as a power limit , governed by the volt-seconds stored in the magnetizing circuit of the device (Spizzo et al., 2010). Only in some circustances, at high current and density, fast terminations have been observed in RFX-mod and MST (Bartiromo et al., 2000), (Wyman et al., 2008b). In particular, in RFX, where they occur mainly at very high current and in conditions of saturated graphite wall, they have been related, more than to a radiative instability, to strong localized plasma-wall interactions in the region of wall

mode locking, where severe power loads are dissipated, leading to a sudden particle release, locally enhanced radiation and temperature drop.

Dedicated experiments in RFX-mod led to the interpretation of the density limit based on the relation between the above mentioned localized accumulation process and the *m=0* mode magnetic topology. The main experimental observations are summarized in Fig. 6.3 as a function of the helical angle (Puiatti et al., 2013). The Hα emission (green line in top panel) shows a maximum localized at the helical angle of the *m=1* mode bulge due to mode locking (red line), thus indicating at that location the main particle source; at the edge, corresponding to the field reversal surface, a chain of *m=0* islands grows up (black line, middle panel); the plasma flow, measured by the Gas Puffing Imaging diagnostic (blue line) (Agostini et al., 2009), reverses at the X-point of *m=0* island: particles are carried from the source point ($\pi \pm 0.15\pi$) to a stagnation point (at $3\pi/2$) where density accumulates (bottom panel). The understanding of these observations relies on the application of the guiding-centre code ORBIT (White and Chance, 1984), modified to include the effect of a recycling wall (Spizzo et al., 2012). The whole process is triggered by a charge separation, induced by a differential diffusion between ions and electrons, which at high density leads to small order ($\approx 10^{14}$ m^{-3}) electron accumulation at the m=0 island X-point. To ensure ambipolarity, a radial electric field develops, which originates a convective cell, ultimately producing the macroscopic density accumulation (order 10^{20} m^{-3}). In (Spizzo et al., 2014) the model has been generalized to any kind of perturbation: it is shown that in any kind of device if a perturbation breaks the toroidal symmetry with a drift depending on the gyroradius (larger for ions than electrons), an ambipolar potential, with the same symmetry as the perturbation, is produced to balance the drifts.

It is well known that in Tokamaks the Greenwald limit has been exceeded in several conditions, in particular including additional heating and peaking of density profile in enhanced transport regimes and the modification of the source (pellet injection, strong Neutral Beam injection, supersonic molecular beam), as for example reported in (Greenwald, 2002) and (Lianghua et al., 2010). The same is true for RFPs, where also plasmas with $n/n_G > 1$ have been produced in several conditions.

In RFX-mod, where the operation at the highest densities is limited by the power available in the plant, the Greenwald value can be often exceeded at low current levels ($\leq$ 0.3 MA)(Spizzo et al., 2015). Discharges with He as filling gas have been found to be favourable for $n/n_G > 1$ plasmas (Valisa et al., 2004). This finding, similar to what previously observed in Asdex-Upgrade (Stabler et al., 1992), is attributed to a less localised PWI in the region of locked modes and, in the case of He, to a different edge flow pattern (De Masi et al., 2012).

The injection of hydrogen/deuterium pellet did not lead to overcoming the Greenwald limit in RFX-mod: this has been ascribed to the available pellet sizes, too large to penetrate into the plasma without destroying the helical core or too small to reach the plasma centre before the complete ablation. Pellets have rather been injected in RFX in order to study particle transport, comparing different plasma regimes, and in particular characterizing the enhanced particle confinement time in helical states (from ≈3-4 ms in Multiple Helicity to ≈12 ms in QSH) (Terranova et al., 2010) and with PPCD (Lorenzini et al., 2002).

Instead, as discussed in chapter 5, in MST $n/n_G = 1.4$ ($n_e = 0.9\ 10^{20}\ m^{-3}$) at a plasma current of 0.5 MA in pellet fuelled PPCD phases has been observed (Sarff et al., 2015), and in discharges with gas puffing through a high throughput valve $n/n_G = 1$ has been achieved (Wyman et al., 2008b).

The radiative limit is not the only high density boundary in RFPs: indeed a soft density limit has been observed both for the efficient poloidal current drive and for QSH state development. The former ((Wyman et al., 2008b),(Cecconello et al., 2003)), weakly increasing with plasma current, is related to the onset of burst m=0 activity, and in MST requires to start the current drive with a density below 0.8-1.1 10^{19} m^{-3} in the current range 0.2-0.5 MA (Chapman et al., 2002). The latter is also linked to a threshold in $m=0$ mode amplitude and requires $n/n_G \leq 0.35$ for the spontaneous development of QSH (Puiatti et al., 2013).

Given the relationship between $m=0$ modes and upper density limit, the effect of the reversal parameter has been studied too, both in RFX-mod and MST. As predicted in (Cappello, S. and Biskamp, D., 1996), the magnetic equilibrium plays an important role in governing the $m=0$ modes. Their amplitude is lower when the field reversal is shallow; indeed in RFX-mod the operation at high current is compatible with higher densities when the F parameter is close to zero. Therefore the operation at shallow F is the preferred one to perform discharges at high current, since it helps in operating below the density threshold for spontaneous QSH states. On the other hand, in such condition the distance of the reversal from the wall is small and the islands easily overlap the wall, which makes more difficult the control of the density and easier the onset of the radiative instability (Spizzo et al., 2010). In MST, results reported in (Sarff et al., 2015) show a modestly larger density limit with $F \approx 0$.

6.3 Neoclassical bootstrap current at high β

The bootstrap current J_{BS} depends on temperature and pressure normalized profiles and on the trapped particle fraction:

$$< \boldsymbol{J_{BS}} \cdot \boldsymbol{B} >= L_{31}\left[\frac{p_e'}{p_e} + \frac{1}{Z}\left(\frac{p_e'}{p_e} + \alpha\frac{T_e'}{T_e}\right)\right] + L_{32}\frac{T_e'}{T_e} \qquad 6.3$$

With L_{31}, L_{32},α functions depending on the trapped particle fraction and on the magnetic equilibrium (Hirshman, 1988),(Sauter et al., 1999). In an axisymmetric RFP, the fraction of trapped particles in the core is similar to the fraction in a tokamak with the same aspect ratio, while it becomes lower at the edge, depending on the current profile (Stoneking et al., 1998). The corresponding bootstrap current is instead much lower than in tokamaks, due to the higher poloidal field. In (Gobbin et al., 2009), it has been calculated by two different codes (RFXTOR, based on RFX-mod magnetic measurements (Zanca and Terranova, 2004) and FLOW, solving a generalized version of Grad-Shafranov equation,(Guazzotto et al., 2004)). The result is shown in Fig. 6.4 and confirms that in present day circular RFPs only a negligible additional current can be provided by the bootstrap mechanism (Guazzotto and Paccagnella, 2009). The total fraction of trapped particles increases in the presence of a helical structure, as in RFP Quasi Single Helicity states, basically due to an additional field ripple introduced by the helical geometry, evaluated from 30% in the axisymmetric case to 40% in the helical configuration in (Gobbin et al., 2009). This suggests a modest increase of the bootstrap current. The shaping effect is also related to some increase of the fraction of bootstrap current: in (Guo et al., 2013) it is evaluated to be of the order of 10-30%, which maintains the total fraction very low.

A more relevant effect is instead expected in a low aspect ratio equilibrium, mainly due to enhanced neoclassical viscosity (Sanpei et al., 2009). More specifically, in (Shiina et al., 2005) it has been found that, in a reactor relevant range of parameters with an aspect ratio 2, ellipticity 1.4 and triangularity 0.4, if the pressure profile is flat and thanks to a decreased magnetic shear, an equilibrium with 94% bootstrap current and extremely high values of $\beta = 63\%$ stable to ideal kink and Mercier localized modes can be maintained .

7 Active control of MHD stability

It has been know for a long time that the ideal MHD stability of the RFP requires a close fitting conducting shell

Sec. 7.1 deals with Resistive Wall Modes while sect. 7.2 with Tearing Modes.

7.1 Resistive Wall Modes

The limitations to pulse length imposed by RWM instabilities was considered a serious issue for the future of the RFP configuration: in order to characterize the dynamics of RWMs, several RFP

experiments with conducting walls were fitted with resistive walls, sometimes referred to as thin shells, with wall time constants shorter than the discharge pulse length. These early RFP experiments with resistive walls were commissioned in the late 1980's and included the OHTE device at General Atomic (Goforth et al., 1986; La Haye et al., 1988), the Reversatron at the University of Colorado (Greene and Robertson, 1993a) and the HBTX-1C device at Culham (Alper et al., 1989).

A convincing experimental demonstration of the RWM instability was achieved in the HBTX-1C experiment. The wall time constant $\tau_w = \mu_o a \delta \sigma$ (where a is the minor radius, δ is the wall thickness and σ is the wall conductivity) for HBTX1C was $1\,ms$. The discharge was sustained for about $4\,ms$. Non-resonant ideal kinks (RWMs) were observed with growth rates about a factor of three times the wall time constant consistent with theoretical studies assuming typical current profiles. The OHTE experiment did not report evidences of RWMs (La Haye et al., 1988), but the EXTRAP T2R experiment (based on OHTE but without helical coils), rebuilt in 1999-2000 with a resistive wall, actually did show clear RWMs (Brunsell et al., 2003).

The wall penetration time for EXTRAP T2R was selected to be $12\,ms$, which was relatively long compared to the earlier resistive shell experiments in OHTE; the observed growth rates of the RWMs were on the time scale as the wall penetration time: the normalized RWM growth rates spectrum $\hat{\gamma}^{m,n} = \tau_w \gamma^{m,n}$ for a typical RFP EXTRAP-T2R equilibrium are shown in Fig. 7.1.

Shortly after the experimental evidence for the existence of RWMs the first attempt of a simple active feedback experiment was performed in HBTX-1C (Alper, 1990). Two helically wound coils (sine and cosine configuration) outside the outer shell of the vessel were incorporated in order to control the $(m, n) = (1,2)$ mode. When the mode amplitude reached a pre-set value (below the level corresponding to discharge termination), the helical coil with the correct phase was activated to suppress the growth. With this feedback algorithm, the targeted mode was suppressed below the pre-set level. While encouraging, the feedback experiment on HBTX-1C using helical coils also made clear the technical limitations of using multiple helical coils for stabilizing multiple RWM. Although the early demonstration of active feedback of a single RWM in HBTX-1C was noteworthy, suppression of only one RWM mode did not substantially improve the RFP performance.

7.1.1 *Theoretical studies on RWM stabilisation*

Theoretical studies of RWM instability properties were carried out to determine the requirements for active control. In (Ho and Prager, 1988) the effect of shell resistivity and distance of the

boundary on linear stability of RWMs was investigated. Analytical studies developed further the stability analysis of the RWM, taking into account rotational stabilization and wall distance, (Jiang et al., 1995), (Guo et al., 1999), and supported the conclusion that active feedback was necessary for long pulse operation in the RFP.

The three dimensional, time-dependent, non-linear, resistive MHD code DEBS was modified to include resistive wall boundary conditions and investigate nonlinear aspects of RWM stability. Nonlinear numerical simulations of an RFP with the RFX geometry performed by this code provided estimates of performance degradation due to an increase in fluctuation amplitudes (Schnack and Ortolani, 1990), both due to Resistive Wall Modes and Tearing Modes, on time scales larger than the shell time. The code was further modified adding a "virtual" set of helical coils in order to perform RWM stabilization studies (Paccagnella et al., 2002b). In particular, each virtual helical coil was independently acting on a different Fourier harmonic, a feedback algorithm named Mode Control, because each mode was independently controlled with a different gain. An extensive scan of parameters for DEBS runs showed that the external kinks are always unstable if the wall surrounding the plasma is not ideal. The instability was found independently of the initial condition, the plasma equilibrium or the plasma physical conditions, described in viscoresistive MHD by S (the Lundquist number) and P (the Prandtl number).

A significant finding was that the external kinks are well described within the framework of linear theory: their nonlinear interactions are, in fact, almost negligible during their growth phase. More generally, linear theory gives a good prediction for the m=1 spectrum, eigenfunctions and growh rates. As far as feedback control is concerned, feedback stabilization of external kink modes was possible, provided that carefully chosen gains were simultaneously set on 4 or 5 unstable modes.

An experimental verification of the linear RWM behavior was obtained in EXTRAP-T2R (Brunsell et al., 2003), further experiments performed in RFX-mod (Bolzonella et al., 2008) confirmed the linear behavior of the RWM.

7.1.2 *The Intelligent Shell geometry*

As an alternative to helical coils, a concept for feedback stabilisation of the RWM instabilities called the *intelligent shell* (IS) or *virtual shell* (VS) was proposed by Bishop (Bishop, 1989) at about the same time as the experiments on HBTX-1C were carried out. The Intelligent Shell is composed by a set of saddle coils that surround the plasma. The amount of current driven in each coil is determined by sensors located at the same position as the coil and with an identical shape: from a control theory point of view, this scheme consisted of a series of independent Single Input Single Output (SISO) circuits. The aim of the Intelligent Shell concept is to 'freeze' the magnetic

flux linking the powered coil, i.e. the system of coils mimicks eddy currents and behaves as a perfectly conducting shell. The array includes a finite number of control coils in the poloidal direction, M_c, and in the toroidal direction N_c. In Bishop's paper, the voltage detected by the sensor coil due to the change of the flux is fed to an amplifier that drives current in the corresponding saddle coil aiming at reducing the measured flux.

The finite number of control coils sets a first limitation of the IS scheme, as already pointed out by Bishop: unstable modes with wavelengths shorter than the actuator coils spacing (i.e. with toroidal mode number $n > N_c/2$) would be largely unaffected.

A more stringent criterion on the minimum number of coils arises when multiple modes are simultaneously unstable. An early semi-analytical study by Fitzpatrick and Yu (Fitzpatrick and Yu, 1999) modelled the linear RFP RWM feedback stabilization with an ideal proportional control in the Intelligent Shell scheme (i.e. flux sensors of the same geometry of saddle loops). A successful stabilization of multiple modes was possible if the number of coils in the toroidal direction N_c was always greater than, or equal to, the range of toroidal mode numbers Δn of the multiple intrinsically unstable RFP Resistive Wall Modes. This is because a discrete saddle coil system always generate toroidal harmonics n together with toroidal sidebands $n+hN_c$ (where h is an integer number) whose amplitudes are not independent: the aforementioned criterion states that if n characterizes an unstable mode, then no sideband, in particular the first one $n+N_c$, should correspond to another unstable mode. A clear illustration of the violation of this criterion was obtained in initial EXTRAP-T2R active feedback operations with a limited number of active coils (Brunsell et al., 2004): two unstable modes were, in fact, observed to grow with phases aligned in such a way to generate zero flux below the control coils.

The conceptually simple Intelligent Shell feedback approach cannot be directly implemented in a toroidal device,because it interferes with the control of plasma position and equilibrium by means of an applied external vertical field, which corresponds to an *m=1,n=0* harmonic of the radial field. In order to circumvent this basic limitation, the feedback system needs the implementation of a Multiple Input Multiple Output scheme: a centralized digital controller (Cavinato et al., 2006a, 2006b) is necessary in order to process simultaneously in real-time all signal inputs and to generate the required references for the currents in the control coil. In the variants of the Intelligent Shell (named Selective Virtual Shell (Martini et al., 2007) or Wise Shell (Drake et al., 2005)), the feedback variables are "virtual" measurement $\tilde{b}^{i,j}$ (where the indices i,j refer to the spatial location of the sensor). Such "virtual" measurements are obtained by inverse Fourier transforming a suitably modified version $\tilde{b}^{m,n}$of the Fourier coefficients of raw measurements. For example, in order to remove the vertical field, $\tilde{b}^{m,n}$ is equal to the input $b^{m,n}$ for all *(m,n)* except the (1,0) coefficient,

which is instead set to 0. Selective Virtual Shell was also used to let selected unstable *(m,n)* modes grow uncontrolled while keeping all others at negligible levels (Bolzonella et al., 2007; Ortolani and team, 2006).

7.1.3 *The Mode Control algorithms*

Based on nonlinear feedback studies recalled in previous sections, a feedback system with a realistic geometrical description of the coils and of the sensors was studied in (Paccagnella et al., 2002a), by applying standard control theory techniques as previously adopted for tokamaks (Bondeson et al., 2002). The geometry of the Intelligent Shell was adopted: i.e. a finite and equal number of sensors and active coils, both in poloidal and toroidal directions were considered, but the control scheme was different. In the Mode Control scheme, the feedback variables $b^{m,n}$ are the Fourier coefficients of the flux loop sensor signals $b^{i,j}$, while the current harmonics $I^{m,n}$ correspond to the coefficients of the Fourier decomposition of the currents flowing into the control coils. The current flowing on each control coil is determined by an inverse Fourier transform of the spectrum of $I^{m,n}$ current harmonics, which is proportional to the corresponding feedback variable. This mode of operation was also defined targeted-mode control (Drake et al., 2005). Due to the linearity of the Fourier transform, it can be shown that the Mode Control feedback scheme is equivalent to the Intelligent Shell, if the same gains are set for all modes in Mode Control or for all positions in Intelligent Shell. In Mode Control a different gain for each mode can be applied, and in particular it can be set to 0 in order to let the corresponding harmonic uncontrolled. As Fourier coefficients are complex numbers, Mode Control gains can be complex. Experiments have been performed with the proportional component set to complex values (Bolzonella et al., 2008; Martini et al., 2007): this technique has been used to induce slow rotations of MHD modes (both TM and RWMs).

7.1.4 *Influence of control coils field sidebands and their aliasing on MHD control*

Due to its finite number, whenever the control coil system generates an *(m,n)* harmonic aimed at cancelling a corresponding unstable plasma mode, it also creates sidebands with helicity $(m+kM_c, n+hN_c)$ where k and h are integer numbers. If the number of sensors is equal to the number of coils (as in the Intellingent Shell geometry) all of the sidebands are aliased into the *(m,n)* coefficient of the Discrete Fourier Transform of the measurements $b^{m,n}$. In other words, measured harmonics are polluted by the field generated by control coils. Equivalently, the perfect cancellation by the feedback coils of the sensor fluxes does not correspond to the cancellation of the plasma or error field harmonics. This effect was simulated for RWM control in (Fitzpatrick and Yu, 1999) and in (Paccagnella et al., 2002a) and determined the optimal number of actuator and sensor coils. Both studies indicated that, when using a control system with the same number of sensors and actuators (i.e. with an Intelligent Shell geometry), the first sideband should not correspond to an unstable

mode. This determines the choice of the number of coils. Given that the RWM spectrum of poloidal modes in the RFP corresponds to *m=-1,0* and *1*, at least M_c=3 coils in poloidal direction are necessary, but practical mechanical considerations suggest to adopt M_c=4. As far as the toroidal number N_c is concerned, for the aspect ratio R/a=4, as in RFX, the minimum number of coils is 24, in order to avoid the generation of a sideband in the Tearing Mode part of the spectrum while stabilizing an RWM. In RFX-mod, in order to increase the stable operation window for radial sensors without overlapping coils, N_c was increased to 48.

A different approach to deal with sidebands aliasing, dubbed Clean Mode Control (Paolo Zanca et al., 2007), was developed for RFX-mod in the context of Tearing Modes, but successfully applied to the current driven q(a)<2 tokamak RWM (Zanca et al., 2012b). In CMC, the centralized RFX-mod digital controller implements a simplified vacuum cylindrical model that uses real time measurements of currents flowing in control coils in order to subtract the sidebands contribution to the measurements.

7.1.5 *Experimental demonstrations of RWM stabilization*

Two RFP experiments, EXTRAP T2R in Stockholm and RFX-mod in Padua, were specifically rebuilt to provide platforms to address experimental studies of active feedback to suppress RWM instabilities. RFX-mod was equipped with a thin copper shell (with $\tau_w = 100ms$), which replaced the thick aluminum shell of RFX, while the copper shell wall time constant of EXTRAP-T2R was $\tau_w = 12ms$. As far as feedback was concerned, both experiments implemented the Intelligent shell geometry: EXTRAP-T2R (Fig. 7.2) had $M_c = 4, N_c = 32$ saddle coils and corresponding saddle loop sensors, while RFX-mod was equipped with a matrix of $M_c = 4, N_c = 48$ (Fig. 7.3) active coils and sensors.

First experiments on simultaneous stabilization of multiple RWM in the RFP have been performed with a limited number of active coils in EXTRAP-T2R, i.e. N_c*=16,* M_c*=4* (Brunsell et al., 2004), i.e. half of the installed ones (Figure 7.3). In order to reduce power supply requirements, four coils at each toroidal position were hard-wired into two pairs forming $m = 1$ active coils. The sensor coil array was ($N_s = 32$, M_s*=4*) and the four sensor coils at each toroidal position were also hard-wired forming $m = 1$ sensors (Drake et al., 2005). With this configuration, mode coupling of n and $n + 16$ modes due to the sidebands generated by the coil array could be partially resolved by the sensors coils, although not controlled by the active coils. The Intelligent Shell experiments clearly illustrated the effect of the violation of the stabilization criterion $N_c > \Delta n$ derived in (Fitzpatrick and Yu, 1999) and explained in the previous section: the flux through all the sensors could be

maintained at zero although two unstable modes, separated by $\Delta n = 16$, were not zero but with phases aligned to compensate for each other at sensors locations.

After the upgrade of the coil power supply system to $M_c=4$, $N_c=32$, complete stabilisation of the unstable spectrum of RWMs was achieved (Brunsell et al., 2005). With the optimised feedback parameters, pulse lengths of 90 ms were achieved (Fig. 7.4), corresponding to about ten wall times. The pulse length was limited by power supplies (Drake et al., 2008).

The RFX-mod device resumed operations after the substantial modifications to RFX in 2005 (Sonato et al., 2003) and it also reported clear evidences of unstable RWMs when operating without feedback (Ortolani and team, 2006).

Feedback operations used since the beginning the full coverage by the saddle coil array with $N_c=48$ and $M_c=4$, giving a total of 192 independently controlled coils was installed. The same hardware and the same control algorithms developed for the EXTRAP-T2R device were adopted. Initial operations, based on the Selective Virtual Shell approach, allowed extending the RFX-mod discharge duration from 150ms to more than 300ms, with a significant loop voltage reduction, as reported in (Paccagnella et al., 2006). Differently from EXTRAP-T2R, RFX-mod (as previously RFX) was affected by the wall-locking of Tearing Modes (as will be described in the tearing mode section later on): therefore, the feedback system was also limiting the radial field penetration of wall locked Tearing Modes.

RFX-mod has also been operated as a circular ohmic tokamak with toroidal field of 0.5T. Its particular combination of the copper shell and of the Inconel vacuum vessel geometry is able to convert the $m= 2,n = 1$ external ideal current-driven kink that always occurs when q(a)<2 into a Resistive Wall Mode. The number of actuator coils was not designed to satisfy the stabilization criteria of this mode: in fact, the standard Mode Control scheme that was successful for RFP RWMs proved insufficient for the q(a)<2 RWM in the tokamak (Zanca et al., 2012b), no matter what gain was used. A simple stabilization criterion for standard Mode Control has been derived in (Zanca et al., 2012a). Once the Clean Mode Control feedback algorithm was put in place, the RWM was routinely kept at a negligible level for the whole duration of the discharge.

7.1.6 *Advanced topics in RWM control*

The demonstration of feedback stabilization of RWM instabilities was very important for the RFP concept. After RWM stabilization became routine for the RFX-mod and EXTRAP T2R RFP experiments, the comprehensive and flexible control systems have been used for a range of additional technology and physics developments of general interest forRWM physics in fusion experiments.

Resonant Field Amplification (a.k.a. Plasma Response): The capability of resolving modes and targeting modes using the control system opened up the possibility to study resonant field amplification (RFA) (Gregoratto et al., 2005). A broad spectrum of field errors is ubiquitous and field error harmonics are certainly present in the range of the RWM spectrum. In particular, it was experimentally observed that the spectrum of RWMs, both in amplitude growth rate and phase, was very reproducible when active control was not operating. This implied the existence of a reproducible field error spectrum, acting as a reproducible seed to the RWM dynamics. The observed growth rate spectrum was not in agreement with the theoretical predictions: in particular, low n modes $n = \pm 1, \pm 2$, which according to theory were marginally stable, had high growth rates. The field error spectrum contains low n modes associated with shell gaps, leakage flux from the iron core or lack of symmetry in toroidal coil positioning, which should result in RFA. Because the mode growth and phase was reproducible, separate modes could be targeted using an open loop configuration. Transient external control field harmonics were produced and the response of the plasma-shell system was analyzed. The growth and the damping rate of modes could be distinguished from the RFA effects and evaluated, giving good agreement with the theoretical predictions.

An important issue in all magnetic configurations is the assessment of error fields during plasma operation, which can be significantly different from error fields measured in vacuum conditions (Volpe et al., 2013). This was fulfilled by using the reference output tracking capability to produce a simulated external static field error harmonic with controlled amplitude and phase and, simultaneously, the same harmonic rotating with controlled amplitude and phase. The effect of the rotating harmonic on the static field error harmonic depends on the relative phase difference. As the phase of the rotating harmonic passes the phase of the static harmonic, growth and suppression produce an oscillation in the measured harmonic amplitude, which can be used to estimate the phase and amplitude of the field error harmonic.

RWM control with partial coverage: A general issue is the development of a control system when the number and placement of control coils is limited for technical reasons. The RFX-mod and EXTRAP T2R experiments have full active coil coverage but the reduction of coverage can be simulated in the control algorithm software. Furthermore, both devices have well developed control models, so that extensive studies of partial or few-coils coverage can be performed numerically. In RFX-mod, control with reduced coil coverage in the RFP was studied and compared with simulations using the flight simulator with encouraging results (Baruzzo et al., 2012; Marchiori et al., 2012). Similar studies were performed in RFX-mod tokamak discharges: as low as 6 active coils located in the outboard midplane were sufficient to stabilize the current driven m=2,n=1 unstable

mode that occurs when q(a) decreases below 2 (Baruzzo et al., 2012). In EXTRAP T2R an attempt to address RWM stabilization with few coils and low coverage was made incorporating the empirically derived model-based control to simulate the control with reduced coverage (Olofsson et al., 2012). Full control was not achieved in these first attempts, though the capability for studies was demonstrated.

Modelling of the control system: An example of the integration of the control system in the demanding technology of a fusion device has been performed at RFX-mod (Villone et al., 2008), by the adaptation of the CarMa code (Portone et al., 2008). This allowed to study the influence on the control system performance of the 3D passive structures surrounding the plasma using the finite element electromagnetic code Cariddi (Villone et al., 2008)[446][446](Villone et al., 2008)(Villone et al., 2008)(Villone et al., 2008) and a 2D model for RFP plasma stability (MARS-F) (Liu et al., 2000). In this way, the MHD stability analysis includes the effects of the 3D conducting structures on the control fields. Alternatively to this white-box approach, empirical data can be experimentally collected and a model created for the case without a plasma (black box model) and compared to a model created using the CarMa code (white box model). The models could be compared by running simulations incorporating a conceptual helical harmonic with qualitative agreement (Soppelsa et al., 2009). A further advancement in the capability to simulate experimental conditions was the development of a full dynamic flight simulator which includes the features of the CarMa code and a model of the RFX-mod control system (Marchiori et al., 2012).

Advanced System Identification Methods (SIM): The characterization of the RWM dynamics has been performed either theoretically by MHD modelling, or experimentally by observing the mode evolution without feedback control. An alternative estimate approach has been actively developed in EXTRAP-T2R: the RWM dynamics is probed during the feedback stabilized operations in the real system by simultaneously and pseudo-randomly exciting the RWM spectrum in the spatial sense (dithering). A minimal physics-based linear model is assumed to represent the data while all parameters (such as the RWM growth rates and the vacuum field penetration time) are extracted from the measurements (Olofsson et al., 2009, 2013a). The model includes also a prescribed number of aliased sidebands. An important aspect of this kind of technique is that it allows constructing a model that captures the dynamics of the plasma system, including the real 3D wall effects. At the same time, it naturally gives a reasonably small state space (Olofsson et al., 2011) representation that can be implemented in real time. An example of the estimated RWM spectrum is shown in Fig. 7.5.

The use of closed-loop system identification techniques to enable experimental modal analysis derived solely from empirical data was extended in an experimental study in RFX-mod (Olofsson et

al., 2013b). Contary to EXTRAP-T2R, the stabilisation diagram for RFX-mod showed unstable activity in the eigenvalue range corresponding to Tearing Mode values. This could be attributed to the fact that Tearing Modes are typically not rotating in RFX-mod. Therefore, the corresponding radial fields (that are well described by a nonlinear dynamic model, as will be shown in next section) are detected by the sensor system and negatively affect the parameters estimate of the linear control model.

The estimated SIM model enables the synthesis of a controller that implements the Multiple Input Multiple Output capability of the system. A further refinement based on modern control theory is the development of a Model Predictive Control (MPC) methodology which employs the SIM model for prediction and computes in real time optimal control inputs that satisfy a performance criterion (Setiadi et al., 2015). Since the control model is updated in real time, MPC could have advantages for long pulse operation where discharge parameters, such as equilibrium profiles, change in time.

7.2 Tearing Modes in the RFP

Contrary to RWMs, nonlinear MHD rules Tearing Modes dynamics. Moreover, the amplitude of tearing modes in the RFP is not described by the Rutherford equation (Rutherford, 1973) but it corresponds to a nonlinearly saturated level.

Multiple Tearing Modes have been observed to *phase-lock,* due to non-linear coupling, in RFP experiments, causing a toroidally localized deformation defined “slinky” (or Locked Mode in RFP literature). After first reports of toroidal asymmetries of the magnetic fluctuation behaviour in ZT-40M (Howell et al., 1987), the phenomenon of the phase-locking of m=1 modes was reported in the OHTE experiment (Tamano et al., 1987). It was then observed in other RFPs such as TPE-1RM15 (Hattori et al., 1991), Reversatron II (Greene and Robertson, 1993b), MST (Almagri et al., 1992; Hokin et al., 1991), TPE-1RM20 (Brunsell et al., 1993b), TPE-RX (Yasuyuki Yagi et al., 1999), EXTRAP-T2R (Malmberg et al., 2000), RFX (Buffa et al., 1994; Zanca et al., 2001b) and RFX-mod (Martini et al., 2007; Ortolani and team, 2006).

The Slinky or Locked Mode is a toroidally localized helical deformation of the plasma column due to the constructive interference of the helical deformations generated by the *m=1* internally resonant modes. The Locked Mode has been observed to rotate in the laboratory frame or to *wall-lock*, depending on the level of plasma current, on the amplitude of magnetic fluctuations and on the properties of the device boundary such as the resistivity of the conducting shell, the presence of error fields and the shell plasma distance. RFX was the only experiment in which rotation was never observed. Rotating Locked Modes have been observed in RFX-mod at plasma currents of 80-100kA (Innocente et al., 2014), a regime that was not explored by the RFX device.

Wall locking leads to negative local effects, such as enhanced plasma wall interaction, overheating of the first wall (Valisa et al., 1997; P. Zanca et al., 2007), increased impurity influxes and total radiation (Marrelli et al., 1999). On the other hand, wall locking also affects global quantities, such as increase of loop voltage, increased fuel recycling, subsequent difficult control of density (more details in Plasma Wall Interaction chapter).

7.2.1 *Wall and phase locking of Tearing Modes*

A basic phenomenological analytical model of the mechanism of wall locking of a single rotating tearing mode was described in (Fitzpatrick, 1993) for the case of tokamak geometry. An adaptation for the m=1 modes in the RFP has been described in (Fitzpatrick et al., 1999), in order to explain the different dynamic behaviour of tearing modes in the RFP experiments MST and RFX.

The model assumes that the phase dynamics of a single tearing mode depends on the balance between the electromagnetic torque, produced by the eddy currents on the resistive shell surrounding the plasma, and a phenomenological viscous torque tending to restore the natural rotation frequency of a mode when it is not wall locked.

Being nonlinear, multiple stationary solutions for the same amplitude of a mode are possible, exhibiting a bifurcation behaviour. For a vanishingly small mode amplitude, the rotation corresponds to the natural frequency. The rotation frequency decreases when the mode grows but it abruptly stops for mode amplitudes above a threshold (a transition from the rotating branch to the locked branch occurs Fig. 7.6.). A back-transition from the locked branch to the rotating branch takes place when mode amplitude decreases below a significantly lower mode threshold.

The absolute value of the mode amplitude for the locking threshold depends on the resistivity of the closest continuous conducting structure surrounding the plasma. In fact, even though both RFX and MST were equipped with a thick aluminium stabilizing shell, RFX plasma was contained by a vacuum vessel made by Inconel 625 alloy (Gnesotto et al., 1995). The significantly higher RFX liner resistivity was at the origin of the lower mode amplitude threshold for wall locking (short dashed line in Fig. 7.8). The TPE-RX device, whose plasma was contained by a stainless steel vacuum vessel (two times less resistive than Inconel), exhibited an intermediate wall locking behaviour between RFX and MST.

A more complete time dependent model was developed for MST (together with a correction for the estimates of wall locking threshold formulas) (Chapman et al., 2004), in order to simulate the deceleration curve due to a growing amplitude Tearing Mode.

Error fields are another important actor in the TMs wall locking process (Fitzpatrick, 1999). They are non axisymmetric magnetic fields generated, e.g., by eddy currents induced in the non-

homogeneous conductors surrounding the plasma due to the unavoidable gaps in the shells (Werley et al., 1985) or by a static misalignment of external coils. When the component of an applied error field resonant with tearing modes is above a certain threshold, wall locking is forced (Fitzpatrick and Zanca, 2002; Hansen et al., 1998), because TM braking due to eddy currents is more effective when error fields are present. In RFX-mod, EXTRAP-T2R and MST, thanks to active control coils it was possible to study the braking of plasma rotation when controlled external perturbations are applied (Frassinetti et al., 2015). In particular it was possible to measure the dependence of the perpendicular viscosity on the magnetic fluctuation amplitude (Fridström et al., 2018) and compare it with the predicted rate of stochastic field line diffusion (Finn et al., 1992a).

The phase alignment among different TM modes was analytically explained in term of electromagnetic torques due to three wave nonlinear coupling among tearing modes (Fitzpatrick, 1999; Fitzpatrick and Zanca, 2002; Guo and Chu, 2004; Hegna, 1996). The aim of the analytical model was to investigate the formation and breakup of the slinky mode in the RFP, in order to complement 3D non-linear visco-resistive MHD simulations (Schnack and Ortolani, 1990). The model considered the internally resonant *m=1* modes and the *m=0, n=1* resonant at the reversal radius (Fitzpatrick, 1999). A quasi-linear approach was used: non-linear coupling terms were computed adopting the linear Tearing Modes eigenfunctions (Robinson, 1978), (Newcomb, 1960). The electromagnetic torque in the region near a given resonant surface is ascribed to the modification of the linear δJ and δB caused by to the three-wave nonlinear coupling among *(1,n), (1,n+1)* and *(0,1)* modes. In the analysis, the *m=1* modes are assumed to be saturated at some level, therefore their amplitude is considered a fixed parameter. Instead, the m=0 modes are taken intrinsically stable and only driven by the nonlinear interaction of the *m=1* modes. The model predicts that when the ‘‘amplitude’’ of two coupled tearing modes exceeds a critical value (locking threshold) the two modes phase-lock, while when they are below a much lower critical value (unlocking threshold) their phases are not coupled anymore. In between the two thresholds, both locked and unlocked solutions can occur, depending on the initial conditions.

A thorough analysis of RFX magnetic measurements to characterize the measured MHD Tearing Mode spectrum along with the experimental features of the mode phase-locking phenomenon was documented in (Zanca et al., 2001b) and compared with both the nonlinear Fitzpatrick analytical theory and nonlinear numerical visco-resistive simulations. A partial agreement between the analytical theory and experimental data was found: the residual discrepancy was ascribed to the m=0 modes, which are not linearly stable in RFX due to the large shell-plasma distance (b/a=1.18).

A refined theory of mode locking was proposed in (Fitzpatrick and Zanca, 2002): at high mode amplitudes the various tearing modes phase-lock together minimizing the magnitude of the

electromagnetic torques exerted at the mode rational surfaces. In particular, the phase of m=0 modes was assumed to remain constant in time at the value observed experimentally and that was found to correspond to the minimum absolute value of the electromagnetic torque. This model explained the successful forced Locked Mode rotation experiments performed in RFX (Bartiromo et al., 1999b).

Active feedback with Clean Mode Control in RFX-mod, modified the wall locking behaviour of Tearing Modes. During optimization experiments of He discharges with very low plasma current (I_p < 150 kA a regime that was never investigated in RFX) the spontaneous rotation of TM was observed (Fig. 7.7) for the first time (Innocente et al., 2014). Such a low wall-locking threshold was expected, due to the high resistivity of Inconel vessel. On the other hand, a new unexpected feature of these RFX-mod experiments was the observation that the fast natural rotation can be recovered by a plasma current decrease *identical* to the current increase that slowed down the rotation. As in RFX-mod TM amplitudes scale almost linearly with plasma current I_p, the reversibility of the locking threshold with plasma current reflects a reversibility with mode amplitude: this was a marked difference with respect to the hysteresis observed in all other passive RFP experiments.

7.2.2 *Mitigation techniques of TM wall locking*

In RFX (Bellina et al., 1997; Gaio et al., 1999) and in MST (Munaretto et al., 2015), the intrinsic error fields were reduced by analog magnetic feedback systems using local saddle coils. Passive reduction of error fields, by means of an overlap of the shell edges, was implemented in TPE-RX (Y. Yagi et al., 1999) and in RFX-mod (Baker et al., 2002).

In RFX, active control of the position of the Locked Mode was obtained by means of an external m=0 magnetic perturbation (Bartiromo et al., 1999b). In particular, it was shown that, by modifying the dynamics of the m=0 tearing mode, it was possible to simultaneously affect the behaviour of the m=1 Tearing Modes. The main result was the possibility to change the position of the Locked Mode during the discharge through the control of the phasing of the m=0 mode. This phasing has been changed in two different ways: by transiently stabilizing the m=0 mode, by which a jump of the Locked Mode toroidal position was induced, or by applying an electromagnetic torque on the m=0 mode, which causes its continuous rotation and simultaneously drags the m=1 modes through nonlinear interaction.

In RFX-mod active feedback further mitigated the effects of wall locked Tearing Modes.

Initial passive shell operation of RFX-mod proved that the thin shell of RFX-mod produces an RFP with performance close to that of a thick shell, as in the RFX experiment, with some degradation occurring after one copper shell time due to the penetration of MHD instabilities (both RWM and

wall locked TMs) (Martini et al., 2007). The application of active feedback significantly improved discharge performance compared to RFX and to passive RFX-mod operations. (Ortolani and team, 2006). Even though the sideband's aliasing deleterious effect on tearing modes control was not known at that time, the reduced first wall interaction and the better magnetic boundary of RFX-mod, allowed performing long and well-controlled 1MA pulses, where the on axis loop voltage was in the range 20–30V. Nonetheless, the tearing modes were still phase and wall-locked, hence the incomplete field error correction by the saddle coils still caused the Plasma Wall Interaction to concentrate in the toroidally localized region of the Locked Mode (P. Zanca et al., 2007). Several forced rotation algorithms were implemented (Martini et al., 2007), taking advantage of the direct coupling of each m=1,n Tearing Mode with the corresponding feedback generated harmonic. Slow Tearing Mode rotations up to 40 Hz were observed together with a movement of the localized bulging due to phase locking of TM.

The real-time correction of the systematic error due to the aliasing of control coils sidebands (Paolo Zanca et al., 2007), described previously, led to a significant improvement of RFX-mod discharges (L Marrelli et al., 2007). A clear illustration of the systematic error for the tearing mode part of the spectrum in a Virtual Shell controlled discharge is shown in Fig. 7.8. The estimate of this corrected spectrum is based on the reasonable assumption that the pollution of the Discrete Fourier Transform (DFT) harmonics is only due to the vacuum saddle coils sidebands and not to MHD modes. A cleaning algorithm has been developed exploiting the measurement of the currents flowing into the control coils and computing by a simple vacuum cylindrical model the time behaviour of the relevant sideband amplitudes in order to subtract them from the DFT of the measurements (details are described in (Paolo Zanca et al., 2007)). A Mode Control on Clean harmonics approach was adopted (hence the name Clean Mode Control, CMC), instead of the Virtual Shell scheme, where the gain of each control coil could be adjusted. With CMC it was possible to set a different proportional gain value for each Tearing Mode to reduce its edge value to a threshold, after which modes began to slowly rotate.

7.2.3 *Modeling of TM phase dynamics under feedback control: limits of CMC control*

The rotation of Tearing Modes subject to CMC feedback control was initially reproduced by a stationary nonlinear model (Paolo Zanca et al., 2007), basically based on the same physics mechanisms describing the single TM wall locking in RFX as in (Fitzpatrick and Zanca, 2002). The active control coils are modelled as a harmonic error field whose amplitude and phase are determined by a prescribed feedback law. By assuming a time-constant mode amplitude at the resonant surface, above the wall locking threshold, in the absence of feedback the mode would be strictly wall-locked. Instead, by applying feedback, the model shows the existence of equilibrium

solutions, corresponding to uniform rotations of the mode with frequencies larger than $1/\tau_w$, for gains above a threshold value. These rotations establish with low edge amplitude: this is the advantage of the feedback with respect to feed-forward techniques to induce locked mode rotations.

Subsequently, a time dependent code including nonlinear phase coupling among multiple m=1 tearing modes, dubbed RFXLocking, was developed (Zanca, 2009). In this code the m=0 low n modes are assumed to be always phase locked, consistent with the experimental RFX findings. As in previous wall-locking studies, the model evolves the mode edge amplitudes and phases under the action of the feedback coils, while the mode amplitudes at the resonant surface are estimated from the experimental measurements.

Thanks to a modified version of RFXLocking, implementing the multiple-shell structure of RFX-mod, a model-based optimization has been performed (Piron et al., 2010), in order to find an optimal gain set and reduce the edge radial magnetic field amplitude of each tearing mode to the lowest possible value compatible with the tearing mode dynamics.

The model also reproduces rather well the tearing mode dynamics as a function of the feedback gains. The effect of the proportional gain on the (1,−7) mode angular frequency, the normalized edge radial magnetic field and the coil current is shown, for example, in Fig. 7.9. The experimental data (full circles) are compared with the model prediction for the same type of discharges (red dashed line). Each point represents a time average over the discharge flattop. A reduction in the total edge radial magnetic field has been obtained with the model-based set, with respect to the empirically optimized one.

The RFX-mod CMC experiment has shown some limitations in the possibility of reducing the edge radial field even when using the radial field harmonics extrapolated at the plasma surface (L Marrelli et al., 2007) as the feedback variable. The edge radial field cannot be reduced below a minimum non zero value for each tearing mode. This limitation is not related to the coils' amplifiers, but is physically based, as it can be reproduced by the RFXlocking code that shows the existence of a radial field minimum in an optimum gain region. (Zanca et al., 2012a). More precisely, simulations with RFXLocking showed that the ultimate CMC possibilities are fixed by the plasma–shell proximity: no matter the radius where the virtual sensors are located, the actively controlled radial field is always higher than the one obtained by an ideal shell that replaces the resistive one.

Based on these findings, an upgrade of RFX-mod is being designed (Peruzzo et al., 2019, 2017): the shell-plasma proximity decreases from b/a = 1.11 to b/a = 1.04 and copper, instead of Inconel, is foreseen be the continuous conducting structure nearest to the plasma. The non axi-symmetric

deformation of plasma column is expected to decrease by a factor 2-3 (Zuin et al., 2017); MHD non-linear simulations show that secondary tearing modes amplitude and the edge bulging due to their phase locking will decrease; moreover the plasma current threshold for tearing modes wall locking will also significantly increase (L. Marrelli et al., 2019).

8 Plasma-wall interactions

As in other magnetic confinement devices, in the RFP the plasma-wall interaction (PWI) plays a crucial role in determining plasma behaviour and performance through the control of plasma density and impurity contamination. In RFPs, PWI is strictly dependent on the magnetic topology, being strongly influenced by the three-dimensional edge magnetic fields related to the phase locking of Tearing Modes (TM) which produce a deformation of the Last Closed Magnetic Surface (LCMS). When such bulge of the LCMS is wall locked, a largepower is deposited onto the wall, with uncontrolled release of main fuel and impurity particles. It is therefore crucial keeping the Locked Mode (LM) into rotation, which can occur spontaneously at low plasma current (fast rotation branch), or thanks to the feedback control system (slow rotation branch).

8.1 Effect of magnetic topology on plasma-wall interaction

Since 80's in the ZT-40 device, a substantial evidence of asymmetries in the power deposition was correlated to the local magnetic field error (Weber, 1985). This kind of observations were extended and deepened especially in the RFX device, which in its first arrangement was not equipped with the MHD active control system, and where a spontaneous rotation of TM was never observed (Carraro et al., 1995),(Valisa et al., 1997),(Marrelli et al., 1999),(Tramontin et al., 1999),(Zanca et al., 2001a),(Valisa et al., 2001), (Spizzo et al., 2001). In addition, RFX was operated at higher plasma current levels with respect to other RFPs (up to 1MA), and this made even more severe the effect of the interaction associated with the deformation due to Locked Mode as described in chap. 7. As a consequence, the LM drove , large localized power fluxes onto the wall in the region intersected by the distorted magnetic surfaces. An example of the footprint on the first wall in a RFX discharge is shown in Fig. 8.1, compared with the reconstruction of the magnetic perturbation.

In RFX (and in RFX-mod afterwards), the plasma wall is fully covered by polycrystalline graphite tiles, to protect the Inconel vacuum vessel and avoid metal contamination. Though local field errors introduced by the insulating poloidal gap (allowing for the penetration of the magnetic field) were reduced by a local active control system, locked modes still produced a large radial displacement of ≈2cm (Zanca and Martini, 1999), determining power loads locally as high as ≈100 MW/m^2 in the

region where the bulge intercepted the wall (Marrelli et al., 1999). This was associated to local enhancement of electron density and density fluctuations, suggesting a continual ionization and loss of neutrals, and to increased transport and impurity influxes. Carbon and oxygen influxes from the LM region were estimated to be of the order of 20-40% of the total; however, tomographic measurements of total radiation showed that, due to the relatively small region of interaction, the radiation enhancement produced by LM was a fraction of the total input power of the order of ≈10%, leading to the conclusion that the main loss term is due to the local increase of transport and particle fluxes (Marrelli et al., 1999). With plasma current approaching 1MA, in proximity of LM the graphite tiles reached the carbon radiation enhanced sublimation temperature, producing carbon blooming processes, observed as sudden increase of carbon, radiation and electron density. Such strong particle release locally cooled the plasma, leading to the loss of density control and to the premature decay of the plasma current (Carraro, L. et al., 1995), (Carraro et al., 1996) (Valisa et al., 1997). An example of carbon behavior when such blooming processes occurred is given in Fig. 8.2. A rather crude means to mitigate PWI and carbon blooming was found by applying a toroidally rotating m=0 perturbation, thus forcing a rotation of the bulge associated to LM (Bartiromo et al., 1999b). This technique increased the amplitude of *m=0* modes, with associated confinement loss, but the enhanced interaction region was distributed in time over all toroidal angles, allowing reproducible operation up to 1.2 MA. A different approach to mitigate PWI in RFX was adopted by increasing the power radiated at the edge by impurity seeding (in particular Neon) (Carraro et al., 2000a). This operative scenario did not affect confinement properties, while both poloidal and toroidal asymmetries of radiated power were reduced, in particular in the high density regime. Though these experiments have notbeen subsequently investigated in RFX-mod or in other RFPs, they should be further explored in next devices as a means to control the power exhaust.

Despite all these issues related to the strong PWI induced by the presence of LM, in RFX quite low effective charge values have always been observed, Z_{eff}≈1.5 (except for very low density regimes, where the bremsstrahlung measurements become anyway difficult), independent of plasma current. This result has been interpreted as due to a screening mechanism, modelled by a Monte Carlo calculation, associated to a low ratio between impurity ionization length and Larmor radius, and to the presence of a radial electric field which points inward at the wall andoutward in the edge plasma (Carraro et al., 1999).

The above observations imply that in order to mitigate PWI the non-axisymmetric deformation introduced by TM phase and wall locking should be reduced. This has been accomplished in RFX-mod (Martini et al., 2007) by replacing the previous thick conducting shell with a thin close fitting one (50ms penetration time) with an active feedback control by external coils to mimic an ideal

shell on longer timescales, as described with more detail in Chap.7. To reduce PWI further , the shape of carbon tiles has also been optimized in order to avoid strong interactions at the edges. As a result, a large reduction of the radial deformation of LCMS has been observed related to reduced TM amplitude, and mode rotation (wall unlocking) has been obtained, with a consequent more uniform PWI. The plasma performance improved (Paccagnella et al., 2006), showing lower loop voltage, higher temperatures and confinement, purer QSH regimes, and plasma currents as high as 2MA have been produced and sustained (Martin and 133 others, 2011). It is worth mentioning that anyway, TMs are only partially phase unlocked, since spontaneous rotation has been observed only at very low current, (Innocente et al., 2014), also when the aliasing of the sideband harmonics due to the discrete saddle coils are compensated (L. Marrelli et al., 2007). The ratio between the maximum wall temperature increase and the total energy input times the discharge duration $\Delta T_{max}/(\Delta t_{pulse}\, \Delta E_{pulse})$ has been taken as an indicator of PWI intensity in (P. Zanca et al., 2007), where it has been found to be correlated with the maximum of the radial field associated to m=0 modes (Fig. 8.3), thus implying a dependence of the edge transport on m=0 modes, non linearly coupled to m=1 ones.

Similarly, in the EXTRAP T2R device a strong improvement of the performance has been obtained when the active feedback stabilization of RWM was applied (Brunsell et al., 2004); indeed spectroscopy and collector probe measurements showed larger metal emissions without feedback (Mo and Cr), and arcing was identified as an important contributor to metal release(Bergsåker et al., 2008).

The above considerations indicate that, due to a strong mitigation of the plasma wall interaction related to an ameliorated magnetic boundary, a significant enhancement of the performance will be obtained in the upgraded RFX-mod device, RFX-mod2 (Zuin et al., 2017).

In the RFX-mod helical improved regime (QSH states), the plasma edge is modulated by a helical ripple, thus wetting the wall over a helical region much larger than in the multiple helicity (MH) state. In such regimes, edge plasma parameters are helically modulated too (Scarin et al., 2011). In QSH, the power load in the portion of the wall wetted by the helix is ≈5MW/m^2 also at the highest current levels (M.E. Puiatti et al., 2013), and the plasma radiation is globally more symmetric than in MH (Spizzo et al., 2001). On average, in QSH states an improvement of PWI by at least a factor of three has been evaluated with respect to MH states (and the previous RFX device) (Scarin et al., 2019). However, when a back transition from QSH to MH occurs, the interaction region shrinks, and power loads can locally increase up to tens of MW/m^2, inducing again uncontrolled impurity and density release, with consequent decay of the plasma current. In some circumstances (at the highest currents with a not well conditioned wall) this can lead to a fast termination, with a fast

current quench (Valisa et al., 2006). A good conditioning of the plasma wall is therefore crucial. Moreover, even in good QSH states, in RFX-mod there is still a residual PWI associated with the phase locking of the secondary modes, with $7<n<23$. Correspondingly, the magnetic connection length to the wall presents a strong decrease ("hole") with increased PWI (by a factor ranging between 2 and 10), wich fortunately is not stationary thanks to the feedback control system. In the RFX-mod2 upgrade it has been calculated that secondary mode locking and associated PWI should be completely avoided (Scarin et al., 2019).

It has to be mentioned that in RFPs the footprint of PWI also shows a poloidal asymmetry between ion and electron drifts, withelectron and ion flows separately intercepted by the wall, due to the surface distortion (Ingraham et al., 1990),(Yagi et al., 1989),(Antoni et al., 1992), (Bergsåker et al., 1995). An example is shown in Fig. 8.4. Such asymmetry is more pronounced at low density, indicating that at low density a significant fraction of the poloidal current is due to suprathermal electrons (P. Innocente et al., 2017). The separate interception of ion and electron flows at the LM, is at the origin of halo currents which in RFX flow into the Inconel vessel with intensity up to 25 kA (Sonato et al., 1997), dissipating ≈4-5% of the total power input.

8.2 Recycling control

Due to the necessity of a close fitting conducting wall for MHD stability of current driven modes, the RFP devices presently in operation are not equipped with divertors. In the past some studies and experiments on small size devices have been produced to explore the impact of a divertor (poloidal and toroidal) on plasma stability and its capability in particle control (Sarff et al., 1989),(Hattori et al., 1995),(Hattori et al., 1994),(Iida et al., 1994) and heat control (Ishijima et al., 1995). Results, though not conclusive because obtained in devices not equipped with effective MHD control systems, showed in some cases some positive effects (decrease of light impurities), but also significant worsening of plasma performance, with increased fluctuations at the X-point and early termination of the discharge. As an alternative to divertors, the vented pump limiter has been proposed for the RFP as a means for actively controlling neutral particles at the wall (Sonato et al., 2002). The concept of the vented pump limiter, as applied in the Tore Supra tokamak (Loarer et al., 1996), is to provide a limiter head designed in such a way to be transparent (slots between blades) to recycled neutrals, which enter the limiter and can be extracted. Such an active particle control system has never been applied to RFP devices so far. The weak point could be the blade capability in sustaining power loads that can be locally very high, as happens in RFPs. An additional drawback is that, at least in RFX-mod, the edge topology is not stationary in time neither uniform along the angles, Θ and Φ, such that any tool designed for a Tokamak is of difficult application in a

RFP. A more viable solution is to exploit the similarity of the 3D field structures of RFPs and Stellarators. In fact, an interesting possibility, proposed in (Martines et al., 2010), exploits the peculiar topology of the RFP to produce a magnetic configuration resembling the island divertor of the Stellarator (Konig et al., 2002). The concept is based on the chain of m=0 magnetic islands that, in single helical axis states, develop at the reversal surface with the same helicity as the dominant mode. Due to the absence of significant asymmetries in helical states, the LCMS does not intercept the wall, while the X-points of m=0 islands act as the X-point of a divertor. In principle, divertor plates with pumping could be placed in such regularly spaced regions of interaction. The drawback is again that this technique requires stationary *m=0* modes, in principle achievable, given their strict phase relation with *m=1* modes, which can be feedback controlled.

In absence of systems providing active recycling control, in devices with carbon wall, the value of plasma density is determined by wall desorption rather than by the fuelling rate. In fact graphite is shot by shot saturated with trapped hydrogen/deuterium, so that the plasma density after the breakdown is completely sustained by atoms released by the wall, with a recycling coefficient R which can be greater than 1 (Bergsåker et al., 1995), (Puiatti et al., 2013a). The number of released particles depends both on the number of atoms stored in the graphite and on the power load on the wall, which makes density control very difficult, especially at high current. On the other hand, in RFPs, in addition to gas puffing, the only central fuelling is by pellet injection (no continuous direct core fuelling by neutral beams is applied), and the particle confinement times are relatively low (of the order of 10ms, see for example (Terranova et al., 2010)). As a consequence,very low recycling regimes cannot be sustained. In summary, a good density control can be obtained with R close to 1 with a not saturated first wall, which is an equilibrium more difficult to achieve in devices with a full graphite wall: indeed, when in EXTRAP T2R the carbon armour was replaced by molybdenum limiters, the density control improved (Brunsell et al., 2001).

In order to guarantee such conditions, in particular avoiding uncontrolled strong release of particles in high current discharges, effective wall conditioning treatments have been applied, including Glow Discharge Cleaning (GDC), Pulse Discharge Cleaning (PDC, repetition of short, low energy plasma discharges), operation with hot wall, boronization, lithization. GDC has been applied in devices with graphite wall (EXTRAP-T2, RFX, RFX-mod), mainly with Helium as working gas, to remove trapped Hydrogen or Deuterium; only occasionally GDC in H has been used to remove impurities (Bergsåker et al., 1997), (Canton et al., 2013). In RFX-mod, the effect of such kind of treatment has been characterised (Canton et al., 2013), showing a toroidal non-uniformity with respect to the positions of the electrodes: the ion flux to the wall features a distribution $\pm 30^0$ wide around the electrodes.

In RFX, to ensure the operation with a non saturated graphite as plasma facing material, the wall temperature has been raised up to 280^0 in some plasma sessions. A lower effective recycling characterized such pulses, but the wall response was still more unpredictable, with frequent sudden density build-ups and current quenches. This was associated with an easier overheating of graphite tiles in presence of high localized power loads, up to the carbon sublimation temperature (Bettella et al., 2000). Such uncontrolled events were instead avoided soon after a boronization. Boronization has been applied with different techniques on several RFP devices, including EXTRAP T2 ((Larsson et al., 1997)), MST ((Den Hartog et al., 1993), (Den Hartog and Kendrick, 1995),(Ko et al., 2013)), RFX((Sonato et al., 1996), (Sonato et al., 2002))and RFX-mod (M.E. Puiatti et al., 2013). A common result in all the experiments is that boronization is effective in reducing recycling, for a number of plasma shots that is dependent on the applied technique and boron layer thickness, on plasma regimes and on carbon redeposition rates. The analysis of samples exposed to the boronization treatments showed that a crucial issue is to obtain the deposition of a uniform layer (Barison et al., 2011; Fiameni et al., 2013), (Ko et al., 2013); in devices with a carbon wall and where boronization is periodically performed, as RFX and RFX-mod, its lifetime is mainly limited by carbon erosion and redeposition processes, decreasing with increasing power loads (Tramontin et al., 1999).

Two examples of the positive effects obtained by boronization in recycling control in MST and impurity decrease in RFX are given in Fig. 8.5 and Fig. 8.6, respectively. In MST, it has also been found that the operation with boronized wall can be associated to discharges featuring prolonged phases (up to 20ms) without sawthooth oscillations corresponding to MHD relaxation events. In such sawtooth-free phases, which are believed to be related to a lower plasma resistivity, the energy confinement time increases by a factor 3 (Chapman et al., 1996).

Following the experience of several Tokamaks (see for example (Mansfield et al., 1996), (Mazzitelli et al., 2010),(Zuo et al., 2012)) and Stellarators (Sánchez et al., 2009), conditioning by lithization has been implemeted on RFX-mod by a lithium capillary-pore system (M.E. Puiatti et al., 2013) and lithium pellet injection (Munaretto et al., 2015), (Innocente et al., 2015). A significant decrease of oxygen and carbon influxes and emissivities (carbon and oxygen are by far the prevailing impurities in RFX) has been found, for carbon in particular more pronounced than with boronization. The important effect was the improvement of density control, which was the main aim of the experimentation and allowed operation at high current ($\geq$ 1.5 MA) with higher density, up to $n/n_G \approx$ 0.5: an example is shown in Fig. 8.7. Despite a slight peaking of density profiles, confinement was not significantly improved.

Also in the case of lithization, a main issue remains the uniformity of Li deposition, though a more uniform layer has been obtained by multi-pellet injection (Innocente et al., 2015). An additional operational issue is related to the fact that, when the machine is vented and opened for maintenance, the formation of Li_2CO_3 (difficult to remove in a device lacking of a direct access to the first wall) must be prevented by a long boronization with argon flushing and careful minimization of the opening time (M.E. Puiatti et al., 2013).

8.3 Dust particles

Dust particles (small loose particles agglomerates, sized from tens of nanometers to millimeter) can be an issue in fusion plasma devices, as they potentially represent a safety hazard, an impurity source and a cause of surface damaging. In this respect, their behavior has been extensively studied in Tokamaks (see for example (Ratynskaia et al., 2011)), while only few relatively recent papers addressing this issue and related to the EXTRAP T2 and T2R device have been produced. Main results of such experimental and modelling studies can be summarized as follows:

a) the preferential origin of dust formation is related again to the high power load deposited in the locked mode region, where small agglomerates are ejected . In EXTRAP T2R, in discharges without active feedback more dust particles have been captured (by silica aerogel collectors) than in discharges with active feedback (Rubel et al., 2001), (Bergsåker et al., 2011);
b) post-mortem measurements indicate that most of dust particles are spheroids covered by deposits with granular morphology (Fig. 8.8 (b), (c)) and coated by corrugated layers containing Mo and stainless steel components, indicating that re-mobilization is an important element of intrinsic metal dust dynamics (Bykov et al., 2014);
c) some particles elongated and aligned with plasma flow have been also detected, (less than 20% of the total, see Fig. 8.8(a)) suggesting a relevant effect of ion drag (Bergsåker et al., 2011), (Bykov et al., 2014).

9 Current sustainment by oscillating field current drive

One of the most important attributes of the RFP configuration is large ohmic heating from its relatively large plasma current. This creates the possibility for ohmic ignition (Christiansen and Roberts, 1982). For a future reactor, inductive current drive via a transformer is simple and robust, and it does not introduce special plasma-boundary requirements or perforations in the blanket and shield. Low frequency induction also has the largest current drive efficiency.

The principal drawback of inductive current drive is that it is not strictly steady state as a consequence of Faraday's law of induction. While there is no fundamental reason why a pulsed-reactor concept cannot work, studies show pulsed operation tends to increase system size and cost [cf. PULSAR, (Werley and Bathke, 1994)]. Indeed a large emphasis in advanced tokamak research is placed on the development of steady-state scenarios that maximize the self-driven neoclassical

bootstrap current and minimize auxiliary current drive, and stellarator research aims to minimize or eliminate plasma current at the expense of toroidal symmetry.

A quasi-steady-state method of inductive current sustainment, called Oscillating Field Current Drive (OFCD), has been identified that could define an ohmic, steady-state sustainment scenario for the RFP. In OFCD, audio-range oscillatory toroidal and poloidal loop voltages are applied to the plasma, and the nonlinear relaxation processes (chap. 3) generate a dc current. Accumulation of magnetizing flux is avoided, and in principle the plasma current can be sustained indefinitely since the loop voltage has zero time-average, but a remnant ac ripple that appears in the equilibrium magnetic field. However, the amplitude of the ac ripple, which scales with the plasma's electrical resistance, is projected to be only a few percent at fusion reactor conditions. This creates an attractive, steady-state method for current sustainment that maintains the simplicity, robustness, and high current drive efficiency of conventional induction (Najmabadi et al., 1993).

It has to be mentioned that there have been a couple of experimental studies of OFCD on tokamak plasmas. The first was performed on the small Caltech tokamak without evidence for current drive (Bellan, 1989). There was also an attempt on the DIII-D tokamak using modulation of the plasma elongation to oscillate the toroidal flux, also without evidence for current drive (Yamaguchi et al., 1995) . Zero-dimensional relaxed-state modeling shows OFCD is less effective at high safety factor (Sprott, 1988) , in addition to the concern that tokamak plasmas may have limited access to small resistive instabilities that govern plasma relaxation.

The theoretical basis for OFCD has greatly matured as part of the development of nonlinear visco-resistive MHD modeling described in Chapter 3 . The physics basis and modeling specific to OFCD are reviewed in Sections 9.1 and 9.2. Several OFCD experiments have been conducted on RFP plasmas that are consistent with theoretical and modeling expectations, which are reviewed in Section 9.3. Unfortunately, a demonstration of full current drive by OFCD is not expected to be possible in present day RFP devices due to the scaling for the ac ripple that sets a limit on the equilibrium excursion during an OFCD cycle. Plasmas with larger Lundquist number, i.e., larger size and temperature, are necessary to test full current drive by OFCD. The demonstration of OFCD establishes an important goal for future RFP research..

9.1 Introduction to Oscillating Field Current Drive

The OFCD current drive method derives from the principle of a relaxed state, where (see chap. 3) the magnetic energy is minimized subject to the constraint of conserved total magnetic helicity, *K*.. The relaxed-state magnetic equilibrium satisfies $\nabla \times \mathbf{B} = \lambda \mathbf{B}$, with λ =constant. Conservation of magnetic helicity motivates a helicity balance, given by $\partial K/\partial t = 2V_T\,\Phi - 2\int \eta \boldsymbol{J}\cdot\boldsymbol{B}dV$, where V_T

is the toroidal loop voltage at the plasma surface and Φ is the toroidal magnetic flux embedded within the plasma. The first term is the rate of helicity injection, and the second term is ohmic dissipation of helicity resulting from the plasma's finite resistivity, η. Conventional induction injects magnetic helicity (and drives current) through a pulse of toroidal loop voltage generated by the transformer that links the torus.

There is close correspondence between magnetic helicity, plasma current, and the Poynting theorem for electromagnetic energy (Jensen and Chu, 1984). Bevir and Gray (Bevir M.K. and Gray J.W., 1981) recognized that, if the toroidal and poloidal loop voltages are sinusoidal, then net cycle-average helicity injection is possible, i.e., $\langle \partial K/\partial t \rangle = \left(\hat{V}_T \hat{V}_P/\omega\right)\sin\delta$, where ω is the oscillation frequency, δ is the relative phase between the loop voltages, and the over-hat identifies the ac amplitude of the loop voltages. Note that the poloidal loop voltage $V_P = -d\Phi/dt$, so there is a concomitant oscillation in the applied toroidal magnetic field. If the phase, $\delta = \pi/2$, then the rate of helicity injection is maximized. This corresponds to driving a net dc plasma current using purely ac loop voltages, hence the terminology "ac helicity injection" or Oscillating Field Current Drive. The frequency, ω, must be faster than the inverse resistive diffusion time, $\tau_R^{-1} = \eta/\mu_0 a^2$, but slower than the process that governs magnetic relaxation, i.e. , for the RFP, the resistive-Alfvenic hybrid timescale ($\sqrt{\tau_R \tau_A}$) associated with magnetic reconnection from tearing instability, typically in the audio frequency range. The principal concern for OFCD may be the impact on energy confinement, since the relaxation process happens through fluctuations : the scaling of these fluctuations is therefore important.

The formal connection between helicity injection and current drive has been developed in detail (Jensen and Chu, 1984), (Bellan, 1984) and includes dc helicity injection using electrodes which link magnetic flux. This is the basis for coaxial helicity injection (CHI) used extensively for spheromak formation (Jarboe, 1994), (Hooper et al., 2012) as well as non-inductive startup of low aspect ratio tokamaks (Redd et al., 2002), (Raman et al., 2001). It also applies to "localized helicity injection" using compact plasma sources inserted into the plasma. This approach was used on MST as a means for current profile control(Craig et al., 1997), (G. Fiksel et al., 1996) and has been further developed on the PEGASUS low aspect ratio tokamak as an alternative to CHI for tokamak startup (Battaglia et al., 2011). A version of ac helicity injection, called "steady inductive helicity injection", is also investigated to sustain spheromak plasmas, which aims to minimize the ac ripple by using loop voltages sources that are not toroidally symmetric (Jarboe, 2017) (Victor et al., 2011).

9.2 Modeling and scaling predictions

Nonlinear, resistive, 3D MHD models described in chap. 3 are briefly recalled here for the specific case of OFCD boundary conditions.

In a first simplified limit a global electromagnetic power balance is applied to plasmas that are assumed to maintain a relaxed-state instantaneously. The 3D dynamics are not resolved, but the effects on the magnetic equilibrium are revealed. This demonstrates OFCD on the basis of energy conservation and makes predictions for the evolution of a relaxed-state plasma. Because this approach resembles circuit analysis in some respects, it has also been referred to as zero-dimensional (0D) modeling (Schoenberg et al., 1982),(Schoenberg et al., 1984), (Sprott, 1988).

The distinctive feature of a relaxed-state plasma is a rigid (normalized) parallel current profile, $\lambda_{||}(r) = \mu_0 \mathbf{J} \cdot \mathbf{B}/B^2$, independent of varying electrical boundary conditions. Small amplitude fluctuations are assumed to provide a turbulent emf in just the right amount at each radius to maintain the relaxed profile. Any partially relaxed state that is time-space separable as $\lambda_{||}(r,t) = \lambda_0(t)\Lambda(r)$ is appropriate for this modeling, where λ_0 is the magnitude of $\lambda_{||}(t)$ at $r = 0$ and $\Lambda(r)$ is the spatial form of the rigid profile. The tendency toward a fixed $\Lambda(r)$ is the hallmark characteristic of relaxation dynamics in an RFP plasma. The gradient $d\Lambda/dr$ is proportional to the free energy for current-driven tearing instability, and dynamically there is a tendency to maintain marginal tearing stability at each instant in time via nonlinear feedback from the dynamo-like emf, $\langle \tilde{\mathbf{V}} \times \tilde{\mathbf{B}} \rangle_{||}$, in Ohm's law.

The evolution of a relaxed-state plasma is fully determined by a global magnetic energy balance. The Poynting theorem applied to a cylindrical relaxed-state plasma with radius, a, and length, $l = 2\pi R$, can be written with dimensionless quantities as (Ebrahimi et al., 2003)

$$\frac{\partial W}{\partial \lambda_0}\frac{\partial \lambda_0}{\partial t} = 2\Phi\left(\frac{a}{R}\Theta V_T - F V_P\right) - S^{-1}P_\Omega \qquad 9.1$$

where W is the magnetic energy, Φ is the toroidal flux, Θ is the pinch parameter, F is the reversal parameter, V_T is the toroidal (axial) loop voltage, V_P is the poloidal loop voltage, S is the Lundquist number, and P_Ω is the ohmic dissipation power. The resistivity profile is important for ohmic dissipation and must be included based on knowledge of the electron temperature's dependence on parameters like the plasma current and density (Stoneking et al., 1998), (Innocente et al., 2009). To simulate OFCD, the drive frequency, amplitudes, and relative phase of the loop voltages are specific, as well as values for the Lundquist number and aspect ratio. Equation 9.1 is time advanced until a steady-state time-average is attained.

The ac ripple in the equilibrium magnetic field derives primarily from the plasma's inductance since the resistive impedance is small, i.e., $V_T \approx L\, dI_p/dt$ with $L \approx \mu_o R$. Hence $\hat{V}_T \approx \mu_0 R\omega \hat{I}_p$, where the over-hat identifies the ac amplitude. Equating the time-average ac helicity injection rate in OFCD to the steady-induction helicity injection rate for the same plasma equilibrium yields a useful scaling prediction for the fractional ac ripple

$$\frac{\hat{I}_p}{\langle I_p \rangle} \sim S^{-1/4} \Omega_{mhd}^{-1/2} \left(\hat{V}_T/\hat{V}_P\right)^{1/2} (R/a)^{-1/2} \qquad 9.2$$

where $\langle I_p \rangle$ is the cycle-averaged plasma current and $\Omega_{mhd} = \omega\sqrt{\tau_R \tau_A}$ is the frequency normalized to the MHD tearing timescale. This relationship is obeyed reasonably well by the relaxed state modeling, for example the scaling with Lundquist number shown in Fig. 9.1(a). The scaling with S reveals the somewhat unfortunate behavior that the ac ripple in the plasma current decreases slowly with Lundquist number making it impractical to demonstrate 100% current sustainment by OFCD in present-day moderate-S experiments. Fig. 9.1(b) shows the projection for a large ripple in F unless S is very large, whereas $|F| < 0.5$ is typical for plasmas sustained by conventional induction.

A more sophisticated approach to study the dynamics of OFCD is based on a first-principle model at moderate $S = 10^5$ using 3D, nonlinear, resistive MHD simulations (DEBS code). The formalism is the same as for simulations of RFP plasmas sustained by conventional induction, but the boundary conditions include oscillating loop voltages. The evolution of the plasma current is shown in Fig. 9.2 for a case where OFCD is applied to a simulation that had reached steady conditions with conventional induction. The current settles into a new steady-state after a settling transition that lasts a couple of cycles. The simulations show that the current profile does not relax instantaneously, as represented by the cycle in $F - \Theta$ space. Instantaneous relaxation would have a trajectory like that in Fig. 9.2 (b, solid curve) (Ebrahimi et al., 2003).).

Analysis of Ohm's law provides insight into key differences between current drive with OFCD versus conventional induction. For simplicity consider the limit of single-fluid MHD, for which Ohm's law is $\mathbf{E} + \mathbf{V} \times \mathbf{B} = \eta \mathbf{J}$. In the zero-pressure limit, the current profile is governed by the component parallel to the mean-field $\mathbf{B}_0$, i.e., $E_{||} + \langle \tilde{\mathbf{V}} \times \tilde{\mathbf{B}} \rangle_{||} = \eta J_{||}$ where the angle brackets represent an average over a mean-field flux surface. The instantaneous alignment between $\mathbf{E}_0$ and $\mathbf{B}_0$ varies over an OFCD cycle, so one could cycle-average of Ohm's law and have non-zero cycle-averaged $E_{||}$, despite the loop voltage being oscillatory. An equivalent approach is to treat quantities instantaneously, in which case the OFCD mean-field current drive is represented by $\langle \mathbf{V}_0 \times \mathbf{B}_0 \rangle = \langle \hat{\mathbf{E}}_0 \cdot \hat{\mathbf{B}}_0 \rangle / B$, where the over-hat identifies the ac component. Fig. 9.3(a) shows the profile of the OFCD mean-field drive, which peaks in the outer region. For conventional induction, the mean

electric field peaks at $r = 0$. The average of the turbulent emf averaged over both the mean-field flux surface and OFCD cycle is shown in Fig. 9.3(b). For OFCD, the relaxation process transports inductively driven current that is largest in the outer region into the core. This is dynamically opposite to conventional induction, for which core-driven current is transported into the outer region of the plasma. Despite this opposite tendency, the parallel current profile is similar for both cases, consistent with the profile remaining close to marginal stability for current-driven tearing.

9.3 Experimental demonstrations of current drive by OFCD

The first OFCD experiments were conducted on the ZT-40M device at LANL in the 1980's (Schoenberg et al., 1988). High-power oscillators based on power triodes were developed that quickly ramped to full amplitude during a normal plasma pulse. The relative phase of the oscillators was tunable so that OFCD drive and anti-drive could be tested. The frequency was adjustable, $\omega/2\pi = 750$ Hz to 2 kHz, limited in part by the skin-time of the thin Inconel shell surrounding the plasma. Experiments were conducted in MST plasmas with current $I_p = 50$-180 kA. They were met with mixed success: there was clear evidence for current drive by OFCD with the correct dependence on oscillator phasing, the plasma response showed sufficient relaxation, but plasma-material interactions from the bare metal wall surrounding the plasma limited the OFCD current drive.

The most extensive experimental tests of OFCD have been performed on the MST device at UW-Madison. The minor radius and plasma temperature for MST plasmas are both significantly larger than for ZT-40M, which reduces the plasma resistance. High-power oscillators based on ignitron plasma-closing switches were developed that allowed turn-on at full oscillation amplitude (Nonn et al., 2011). The oscillator phasing was adjustable to examine the phase dependence in greater detail than in the ZT-40M experiments. Most of the experiments were performed with frequency $\omega/2\pi = 280$ Hz, since the oscillators were based on resonant tank circuits that were cumbersome to change. Experiments were conducted over a range of plasma current, but detailed studies were performed at 250 kA plasma current where the fractional drive by OFCD was maximum. The amount of OFCD-driven current is most sensitive to the oscillator voltages and frequency, and the added/subtracted current did not depend strongly on the background current available in MST ($I_p = 250$-500 kA).

The OFCD drive and anti-drive result from MST that is analogous to the ZT-40M experiment is shown in Fig. 9.4 (McCollam et al., 2006). The added current reaches 20 kA by the end of the current flattop. Note that the current rises continuously during the flattop period of the pulse, which is a consequence of the plasma's inductive back reaction, $L/R \approx 30$ ms. If the pulse duration were

longer, the anticipated OFCD-driven current would saturate at $\Delta I_p \approx 40$ kA, which is 15% of the total current.

The maximum OFCD-driven current in MST plasmas occurs for oscillator phasing $\delta = \pi/8$. The fractional increase in plasma current versus phase is shown in Fig. 9.5. There is a considerably more structure in this phase dependence than expected based on the global helicity balance formulation. The measured amplitude of magnetic fluctuations associated with tearing instabilities is also phase dependent, as shown in Fig. 9.6. The fluctuations are resolved for both poloidal mode numbers m=0 and m=1. Interestingly, the cycle-average amplitude of m=0 modes is somewhat smaller than for conventional flattop induction (dotted lines), with minimum the amplitude occurring for $\delta \approx \pi/8$.

Nonlinear, 3D, resistive MHD simulations with fractional OFCD current drive were performed to compare with the MST experimental results (McCollam et al., 2010). The green data points in Fig. 9.5 show that the fractional current drive in the simulations has a similar dependence on the relative. The lack of maximum current drive at $\delta = \pi/2$ is attributed to an increase in the dissipation of magnetic helicity. The experiments show an important additional effect in that the energy confinement is phase dependent, and not surprisingly maximum for $\delta \approx \pi/8$. This is shown in Fig. 9.7. The simulations used a fixed resistivity profile and did not include evolution of the thermal energy, so they could not make predictions regarding changes in confinement. Nevertheless, the good agreement between the simulations and experiment provide confidence that the OFCD physics basis is sound.

Since OFCD tends to drive current in the outer region of the plasma (Fig. 9.3) while conventional induction peaks in the core, their combination can lead to a flatter current drive profile. This creates a form of current profile control, which has been studied for optimization in nonlinear, 3D, resistive MHD modeling (Ebrahimi and Prager, 2004). The MST experiments have such a mixture of current drive, and the reduction in $m = 0$ tearing amplitude for $\delta = \pi/8$ phasing (Fig. 9.6) together with the cycle-averaged improvement in energy confinement (Fig. 9.7) is evidence for this control.

OFCD experiments have also been tested in RFX-mod: no clear evidence of a net current drive was found, possibly due to the limited available maximum oscillation amplitude, though MHD behavior suggested that the dynamo properties were affected (Bolzonella T et al., 2006).

9.4 Future directions

In summary, the visco-resistive, 3D MHD modeling together with experiments from MST and ZT-40M have substantially improved the physics basis for OFCD. The experiments on MST show that, while the basic expectations for OFCD hold, the dynamics associated with relaxation and confinement must be better understood to fully establish the OFCD concept. It is also necessary to

test OFCD in RFP plasmas with larger size and temperature, i.e., at larger Lundquist number. Fig. 9.1(b) illustrates the gap between MST and a typical reactor plasma. The plot shows the modulation in the F parameter, predicted by 1-D relaxed-state modeling versus Lundquist number. The ac ripple in the equilibrium magnetic field exceeds the range of normal operation by conventional induction for $S \lesssim 5 \times 10^7$. Hence, 100% current drive by OFCD in MST (or RFX-mod2) would have equilibrium excursions far beyond those of a reactor plasma, assuming there are no significant deleterious effects associated with such large excursions. This minimum ac ripple is a simple consequence of the inductive response to ac loop voltages, so this is not a subtle physics effect associated with relaxed-state dynamics. The ac ripple also quantifies a target for a next-step RFP experiment, since the demonstration of 100% OFCD is high leverage toward a goal to achieve an inductively sustained and ohmically ignited fusion plasma.

The tendency for RFP plasmas to enter the quasi-single-helicity (QSH) regime at high Lundquist number (Chapter 3) could have a substantial impact on the viability and efficacy of OFCD. This is especially true for a development path that relies on the QSH regime to achieve sufficient energy confinement in RFP plasmas. The current profile dynamics with OFCD is significantly different than for conventional induction, and this could change access to and stationarity of QSH. Computational studies with OFCD boundary conditions at very high Lundquist number and (could begin to address such questions, but such simulations are already state-of-the-art with modest Lundquist and Magnetic Prandtl numbers (especially relative to reactor parameters). F) fractional OFCD current drive experiments in RFX-mod2 at 2 MA could (begin to) probe the (physics related to the) compatibility and impact of and on QSH. Such experiments might require significant upgrades to the power supplies.

10 Conclusion

The last review paper on the RFP before the present one (Bodin, 1990) ended with the following statement: "…many new and important results can be expected in the next five years, with good progress in tackling the problems on which the fusion potential of this system depends". While that statement was reflecting a feeling of excessive optimism which was pervading the entire fusion community in those times, now we can look back and judge with realism and open mind whether important results have indeed been achieved and, above all, whether we are now able to make a firm statement on the fusion potential of the RFP.

Going through thirty years of research has been in fact a unique opportunity for the authors to review the field. Thanks to this exercise, we conclude that yes, over the last three decades the RFP

has obtained many very important results and underwent a number of transformational changes, which have led to a drastic improvement of its fusion performances.

A key transformational result is the experimental and reproducible evidence that the high level of magnetic fluctuations, leading to strong magnetic stochasticity and plaguing the confinement, is not intrinsic to the configuration sustainment. This happens either because the edge poloidal current which sustains field reversal can be actively driven from outside or because the magnetic self-organization which guarantees the configuration sustainment occurs with a gross topological modification that brings the plasma in a helical, low magnetic fluctuation state. The former is achieved reliably and repriducibly with Pulsed Poloidal Current Drive (PPCD), the latter with the access to Single Helicity States (SH). They bring substantially improved confinement. In several cases improved confinemet PPCD plasmas also corresponded to SH equilibria. The physics behind PPCD and SH has been explained by a broad set of nonlinear MHD simulations and theoretical work. The improved regimes have been achieved thanks to another transformational result, namely the demonstration of the reliable active control of magnetic instabilities in the RFP with active coils acting in a feedback process. RFP devices have pioneered active control of MHD stability by feedback controlled coils in the entire magnetic fusion community. Simultaneous cancellation of multiple Resistive Wall Modes (RWMs) has been achieved, as well as significant suppression of the tearing mode amplitude. RFP RWM control not only allows for reactor relevant magnetic front-end, since a thick passive conductive shell is not anymore relevant, but has also provided a large set of information for MHD control in advanced tokamak scenarios. Tearing control is a crucial ingredient for the achievement of SH states.

Following and to some extent anticipating the trend of development of numerical modelling in fusion, the RFP has been the test bed for a variety of codes and numerical simulations, which have profoundly influenced our comprehension of the configuration physics. They include – only to make a few examples - nonlinear MHD simulations, tools for the modelling of active control of stability, codes for the three-dimensional reconstruction of the RFP equilibria, for the study of turbulence and micro-instabilities and for the description of the dynamics of fast ions and runaway electrons.

The RFP devices have been a fertile environment for the realization of experiments and the development of tools, which have provided a significant impact on the other two configurations. Few examples, among many. The first deals with the access to the $q_{95}<2$ regime in tokamak, for times longer than the resistive diffusion time. The ample set of experimental and modelling tools developed for the RFX-mod active control has prompted the exploration of tokamak scenarios in RFX-mod, where $q_{95}<2$ plasmas have been produced. The same experiment has been proposed and

realized in the DIII-D tokamak (Piovesan et al., 2013). A second example concerns the upgrade of the VMEC code, a state of the art tool for the reconstruction of magnetic equilibria in the tokamak and stellarator: in (Piovesan et al., 2017) it has been shown that the MHD dynamo emf can be directly calculated from a reconstruction of the experimental 3D equilibrium in both Tokamak and RFP. Also the recent work aiming at a trans-configuration modelling of the density limit (Zanca et al., 2019) and the pioneering uninterrupted work carried out at MST on advanced diagnostic systems for fusion (see for example the last (VanMeter et al., 2019)) should be mentioned.

The question is now whether there will be a new review of RFP in the future or, to use a more scientific language, whether it is conceivable that the research on RFP as a fusion configuration will continue. Despite the positive results, a final assessment of "the fusion potential of this system", as wished in Bodin's 1990 review, needs a consolidation. This requires modifications and upgrades of the present machines, as already ongoing for RFX-mod, and further advancements of numerical studies.

Indeed scientific issues remain to be solved in order to make the RFP a strong candidate for fusion.

One concerns the scaling of confinement with current and size. The impressive increase of the confinement when pulsed poloidal current drive is applied leads to maximum values of $\tau_E \approx 12$ ms, well comparable with the Tokamak scaling laws, though transient up to now. Temperature and confinement have been found to increase with the current, concomitant to the reduction of magnetic chaos. In SH states at the highest current values ≥ 1.5 MA electron temperatures around 1.5 keV with confinement time ≈3ms have been obtained, with an almost linear scaling of τ_E with plasma current and secondary mode amplitude. This scaling is well-based, but whether it can be extrapolated to current values approaching those of reactor interest remains an open question Also, crucial is the assessment of how much the effect of residual magnetic chaos can be reduced: for example, also in quasi single helicity states a deformation related to phase locking of secondary modes is present and influences plasma-wall interaction, though in a non-stationary and much milder fashion than in the MH state. And an improved boundary could also have a significant effect on the performance when current profile control is applied. In addition, the possibility of obtaining helical states at high plasma density has still to be explored. Their experimental verification requires a milder plasma-wall interaction.

The active control of the plasma exhaust has to be assessed: the RFP has not developed a divertor concept, though innovative concepts for power exhaust have been proposed and should be experimentally tested .

None of the aforementioned issues appear at the moment to be show-stoppers. Some of them originate by uncertainty on the physics – and call therefore for fundamental theoretical and experimental work -, but others are due to a lack of experimental devices appropriate for the level reached by RFP physics. The RFP experiments are at least one generation behind the tokamak, mostly due to the smaller resources invested in this line. In the upgraded RFX-mod2 device the hardware limitations which make the magnetic front-end far from being optimal in RFX-mod will be removed. RFX-mod2 will allow the exploration of the 2 MA regime with a much smoother boundary. The level of stochasticity is expected to be substantially reduced, in order to confirm the strong dependence of confinement on magnetic fluctuations, thus providing a much more robust base and a leverage for confinement scaling.

All these considerations suggest that the RFP is still worth a significant scientific effort in the path toward fusion electricity, to help completing the fusion grand experiment, but also for its own fusion potential. It is important to remind that the RFP brings the advantage of a low toroidal magnetic field at the coils, of the absence of aspect ratio limitations and of the predominant ohmic heating. All of them are extremely valuable in terms of a power plant engineering. Future will tell us whether the community will be able to find efficient and smart ways to exploit the opportunity given by the RFP. Hopefully, keeping in mind the concept expressed by Enrico Fermi in 1947: "…the vocation of the scientist is to move forward the frontiers of our knowledge in all directions, not just along those that promise more immediate rewards or applauses".

Acknowledgements

The authors greatly appreciate the contribution by D.J. Den Hartog to this paper.

We also thank A.F. Almagri,T. Bolzonella, P. Brunsell, L. Carraro, S. Cappello, L. Frassinetti, F. Gnesotto, K. Hayase, H. Himura, Y. Hirano, M. Iida, R. Ikezoe, S. Kiyama, H. Koguchi, N. Mizuguchi, K. Oki, T. Onchi, H. Oshiyama, R. Paccagnella, R. Piovan, H. Sakakita, A. Sanpei, K.I. Satoh, S. Shiina, T. Shimada, P. Sonato, G. Spizzo, Y. Suzuki, D. Terranova, M. Valisa, M. Wakatani, K.Y. Watanabe, Y. Yagi, P.Zanca, M. Zuin and the EXTRAP-T2, MST, RELAX and RFX-mod teams.

Paolo Piovesan was a gifted scientist who gave seminal contributions to fusion physics. He had also a special talent to unite people and blend ideas. We thank and miss him.

References

Agostini, M., Scaggion, A., Scarin, P., Spizzo, G., Vianello, N., 2012. Interplay between edge magnetic topology, pressure profile and blobs in the edge of RFX-mod. Plasma Phys. Control. Fusion 54, 065003. https://doi.org/10.1088/0741-3335/54/6/065003

Agostini, M., Scarin, P., Cavazzana, R., Fassina, A., Alfier, A., Cervaro, V., 2010. Optical measurements for turbulence characterization in RFX-mod edge. Review of Scientific Instruments 81, 10D715. https://doi.org/10.1063/1.3478679

Agostini, M., Scarin, P., Cavazzana, R., Sattin, F., Serianni, G., Spolaore, M., Vianello, N., 2009. Edge turbulence characterization in RFX-mod with optical diagnostics. Plasma Phys. Control. Fusion 51, 105003. https://doi.org/10.1088/0741-3335/51/10/105003

Agostini, M., Scarin, P., Spizzo, G., Auriemma, F., Cappello, S., Carraro, L., Marrelli, L., Spagnolo, S., Spolaore, M., Veranda, M., Vianello, N., Zuin, M., RFX-mod Team, 2017. Edge plasma properties with 3D magnetic perturbations in RFX-mod. Nuclear Fusion 57, 076033. https://doi.org/10.1088/1741-4326/aa6ebe

Aguilera, A.M. de, Castejón, F., Ascasíbar, E., Blanco, E., Cal, E.D. la, Hidalgo, C., Liu, B., López-Fraguas, A., Medina, F., Ochando, M.A., Pastor, I., Pedrosa, M.Á., Milligen, B.V., Velasco, J.L., 2015. Magnetic well scan and confinement in the TJ-II stellarator. Nucl. Fusion 55, 113014. https://doi.org/10.1088/0029-5515/55/11/113014

Alfier, A., Pasqualotto, R., Spizzo, G., Canton, A., Fassina, A., Frassinetti, L., 2008. Electron temperature profiles in RFX-mod. Plasma Phys. Control. Fusion 50, 035013. https://doi.org/10.1088/0741-3335/50/3/035013

Almagri, A.F., Assadi, S., Prager, S.C., Sarff, J.S., Kerst, D.W., 1992. Locked modes and magnetic field errors in the Madison Symmetric Torus. Physics of Fluids B: Plasma Physics 4, 4080–4085. https://doi.org/10.1063/1.860473

Alper, B., 1990. A review of results from the HBTX reversed-field pinch. Physics of Fluids B: Plasma Physics B2, 1338–1341. https://doi.org/10.1063/1.859552

Alper, B., Bevir, M.K., Bodin, H.A.B., Bunting, C.A., Carolan, P.G., Cunnane, J., Evans, D.E., Gimblett, C.G., Hayden, R.J., Hender, T.C., Lazaros, A., Moses, R.W., Newton, A.A., Noonan, P.G., Paccagnella, R., Patel, A., Tsui, H.Y.W., Wilcock, P.D., 1989. RFP stability with a resistive shell in HBTX1C. Plasma Phys. Control. Fusion 31, 205–212. https://doi.org/10.1088/0741-3335/31/2/006

Anderson, J.K., Adney, J., Almagri, A., Blair, A., Brower, D.L., Cengher, M., Chapman, B.E., Choi, S., Craig, D., Demers, D.R., Hartog, D.J.D., Deng, B., Ding, W.X., Ebrahimi, F., Ennis, D., Fiksel, G., Forest, C.B., Franz, P., Goetz, J., Harvey, R.W., Holly, D., Hudson, B., Kaufman, M., Lovell, T., Marrelli, L., Martin, P., McCollam, K., Mirnov, V.V., Nonn, P., O'Connell, R., Oliva, S., Piovesan, P., Prager, S.C., Predebon, I., Sarff, J.S., Spizzo, G., Svidzinski, V., Thomas, M., Wyman, M.D., 2005. Dynamo-free plasma in the reversed-field pinch: Advances in understanding the reversed-field pinch improved confinement mode. Physics of Plasmas 12, 056118. https://doi.org/10.1063/1.1883666

Anderson, J.K., Almagri, A.F., Den Hartog, D.J., Eilerman, S., Forest, C.B., Koliner, J.J., Mirnov, V.V., Morton, L.A., Nornberg, M.D., Parke, E., Reusch, J.A., Sarff, J.S., Waksman, J., Belykh, V., Davydenko, V.I., Ivanov, A.A., Polosatkin, S.V., Tsidulko, Y.A., Lin, L., Liu, D., Fiksel, G., Sakakita, H., Spong, D.A., Titus, J., 2013. Fast ion confinement and stability in a neutral beam injected reversed field pinch. Physics of Plasmas 20, 056102. https://doi.org/10.1063/1.4801749

Anderson, J.K., Biewer, T.M., Forest, C.B., O'Connell, R., Prager, S.C., Sarff, J.S., 2004. Dynamo-free plasma in the reversed field pinch. Physics of Plasmas 11, L9–L12. https://doi.org/10.1063/1.1697399

Anderson, J.K., Capecchi, W., Eilerman, S., Koliner, J.J., Nornberg, M.D., Reusch, J.A., Sarff, J.S., Lin, L., 2014. Fast ion confinement in the three-dimensional helical reversed-field pinch.

Plasma Physics and Controlled Fusion 56, 094006. https://doi.org/10.1088/0741-3335/56/9/094006

Anderson, J.K., Forest, C.B., Biewer, T.M., Sarff, J.S., Wright, J.C., 2003. Equilibrium reconstruction in the Madison Symmetric Torus reversed field pinch. Nucl. Fusion 44, 162. https://doi.org/10.1088/0029-5515/44/1/018

Antoni, V., Bagatin, M., Martines, E., 1992. Energy transport and magnetic stochasticity at the edge of a plasma in RFP configuration. Plasma Physics and Controlled Fusion 34, 1639–1650. https://doi.org/10.1088/0741-3335/34/11/003

Antoni, V., Bartiromo, R., Carraro, L., Desideri, D., Martines, E., Puiatti, M.E., Sattin, F., Scarin, P., Serianni, G., Spolaore, M., Tramontin, L., Valisa, M., Zaniol, B., 2000a. Experimental measurements and modelling of the structure of the radial electric field in RFX. Czech J Phys 50, 1387–1396. https://doi.org/10.1023/A:1022843529120

Antoni, V., Cavazzana, R., Fattorini, L., Martines, E., Serianni, G., Spolaore, M., Tramontin, L., Vianello, N., 2000b. Effects of pulsed poloidal current drive on the edge region of a reversed field pinch plasma. Plasma Phys. Control. Fusion 42, 893. https://doi.org/10.1088/0741-3335/42/8/303

Antoni, V., Desideri, D., Martines, E., Serianni, G., Tramontin, L., 1997. Plasma Potential Well and Velocity Shear Layer at the Edge of Reversed Field Pinch Plasmas. Physical Review Letters 79, 4814–4817. https://doi.org/10.1103/PhysRevLett.79.4814

Antoni, V., Drake, J.R., Spada, E., Spolaore, M., Vianello, N., Bergsåker, H., Cavazzana, R., Cecconello, M., Martines, E., Serianni, G., 2006. Coherent structures and anomalous transport in reversed field pinch plasmas. Physica Scripta T122, 1–7. https://doi.org/10.1088/0031-8949/2006/T122/002

Antoni, V, Martines, E., Desideri, D., Fattorini, L., Serianni, G., Spolaore, M., Tramontin, L., Vianello, N., 2000. Electrostatic transport reduction induced by flow shear modification in a reversed field pinch plasma. Plasma Physics and Controlled Fusion 42, 83–90. https://doi.org/10.1088/0741-3335/42/2/301

Antoni, V., Merlin, D., Ortolani, S., Paccagnella, R., 1986. MHD stability analysis of force-free reversed field pinch configurations. Nucl. Fusion 26, 1711–1717. https://doi.org/10.1088/0029-5515/26/12/012

Antoni, V., Spada, E., Vianello, N., Spolaore, M., Cavazzana, R., Serianni, G., Martines, E., 2005. Shear flows generated by plasma turbulence and their influence on transport. Plasma Physics and Controlled Fusion 47, B13–B23. https://doi.org/10.1088/0741-3335/47/12B/S02

Auriemma, F., Hirano, Y., Koguchi, H., Canton, A., Innocente, P., Lorenzini, R., Puiatti, M.E., Terranova, D., Sakakita, H., 2009. Comparison of particle transport properties in TPE-RX standard and PPCD plasmas. Plasma Phys. Control. Fusion 51, 065012. https://doi.org/10.1088/0741-3335/51/6/065012

Auriemma, F., Lorenzini, R., Agostini, M., Carraro, L., Masi, G.D., Fassina, A., Gobbin, M., Martines, E., Innocente, P., Scarin, P., Schneider, W., Zuin, M., 2015. Characterization of particle confinement properties in RFX-mod at a high plasma current. Nuclear Fusion 55, 043010. https://doi.org/10.1088/0029-5515/55/4/043010

Auriemma, F., Zanca, P., Bergerson, W.F., Chapman, B.E., Ding, W.X., Brower, D.L., Franz, P., Innocente, P., Lorenzini, R., Momo, B., Terranova, D., 2011. Magnetic reconstruction of nonaxisymmetric quasi-single-helicity configurations in the Madison Symmetric Torus. Plasma Physics and Controlled Fusion 53, 105006. https://doi.org/10.1088/0741-3335/53/10/105006

Aydemir, A.Y., Barnes, D.C., 1984. Sustained Self-Reversal in the Reversed-Field Pinch. Phys. Rev. Lett. 52, 930–933. https://doi.org/10.1103/PhysRevLett.52.930

Baker, W., Dal Bello, S., Marcuzzi, D., Sonato, P., Zaccaria, P., 2002. Design of a new toroidal shell and support structure for RFX. Fusion Engineering and Design 63–64, 461–466. https://doi.org/10.1016/S0920-3796(02)00194-1

Barbui, T., Carraro, L., Den Hartog, D.J., Kumar, S.T.A., Nornberg, M., 2014. Impurity transport studies in the Madison Symmetric Torus reversed-field pinch during standard and pulsed poloidal current drive regimes. Plasma Physics and Controlled Fusion 56, 075012. https://doi.org/10.1088/0741-3335/56/7/075012

Barbui, T., Carraro, L., Franz, P., Innocente, P., Munaretto, S., Spizzo, G., 2015. Light impurity transport studies with solid pellet injections in the RFX-mod reversed-field pinch. Plasma Phys. Control. Fusion 57, 025006. https://doi.org/10.1088/0741-3335/57/2/025006

Barison, S., Canton, A., Dal Bello, S., Fiameni, S., Innocente, P., Alfier, A., Munaretto, S., Rossetto, F., 2011. Analysis of the interaction between plasmas and the graphite first wall in RFX-mod. Journal of Nuclear Materials 415, S274–S277. https://doi.org/10.1016/j.jnucmat.2010.12.311

Bartiromo, R., Antoni, V., Bolzonella, T., Buffa, A., Marrelli, L., Martin, P., Martines, E., Martini, S., Pasqualotto, R., 1999a. Improved confinement and transport studies in the reversed field experiment (RFX). Physics of Plasmas 6, 1830–1836. https://doi.org/10.1063/1.873441

Bartiromo, R., Bolzonella, T., Buffa, A., Chitarin, G., Martini, S., Masiello, A., Ortolani, S., Piovan, R., Sonato, P., Zollino, G., 1999b. Tearing Mode Rotation by External Field in a Reversed Field Pinch. Physical Review Letters 83, 1779–1782. https://doi.org/10.1103/PhysRevLett.83.1779

Bartiromo, R., Buffa, A., Canton, A., Carraro, L., Costa, S., Innoccente, P., Martines, E., Martini, S., Masiello, A., Murari, A., Ortolani, S., Piovan, R., Puiatti, M.E., Sattin, F., Scarin, P., Sonato, P., Spizzo, G., Valisa, M., Zaniol, B., 2000. Analysis of the high density limits in the RFX high current regimes, in: 27th EPS Conf. on Contr. Fus. Plasma Phys. ECA vol. 24B, 1380, Budapest, 12-16 June 2000, p. 1380.

Baruzzo, M., Bolzonella, T., Liu, Y.Q., Manduchi, G., Marchiori, G., Soppelsa, A., Takechi, M., Villone, F., 2012. RWM control studies on RFX-mod with a limited set of active coils. Nuclear Fusion 52, 103001. https://doi.org/10.1088/0029-5515/52/10/103001

Battaglia, D.J., Bongard, M.W., Fonck, R.J., Redd, A.J., 2011. Tokamak startup using outboard current injection on the Pegasus Toroidal Experiment. Nucl. Fusion 51, 073029. https://doi.org/10.1088/0029-5515/51/7/073029

Bellan, P.M., 1989. Non-observation of AC helicity injection. Nucl. Fusion 29, 78. https://doi.org/10.1088/0029-5515/29/1/008

Bellan, P.M., 1984. Physical model of current drive by ac helicity injection. The Physics of Fluids 27, 2191–2192. https://doi.org/10.1063/1.864846

Bellina, F., Chitarin, G., Fiorentin, P., Gaio, E., Marchiori, G., Sonato, P., Toigo, V., Zaccaria, P., Zollino, G., 1997. Feasibility analysis of an active local field control at the poloidal gap of RFX, in: Fusion Technology 1996. Elsevier, pp. 771–774. https://doi.org/10.1016/B978-0-444-82762-3.50162-2

Bergerson, W.F., Auriemma, F., Chapman, B.E., Ding, W.X., Zanca, P., Brower, D.L., Innocente, P., Lin, L., Lorenzini, R., Martines, E., Momo, B., Sarff, J.S., Terranova, D., 2011. Bifurcation to 3D Helical Magnetic Equilibrium in an Axisymmetric Toroidal Device. Phys. Rev. Lett. 107, 255001. https://doi.org/10.1103/PhysRevLett.107.255001

Bergsåker, H., Larsson, D., Brunsell, P., Möller, A., Tramontin, L., 1997. Wall conditioning and particle control in Extrap T2. Journal of Nuclear Materials 241–243, 993–997. https://doi.org/10.1016/S0022-3115(97)80180-8

Bergsåker, H., Menmuir, S., Rachlew, E., Brunsell, P.R., Frassinetti, L., Drake, J.R., 2008. Metal impurity fluxes and plasma-surface interactions in EXTRAP T2R. Journal of Physics: Conference Series 100, 062030. https://doi.org/10.1088/1742-6596/100/6/062030

Bergsåker, H., Möller, A., Li, G.X., Hellblom, G., Brzozowski, J.H., Emmoth, B., Gudowska, I., 1995. Edge plasma conditions and plasma-surface interactions in Extrap T1. Journal of Nuclear Materials 220–222, 712–716. https://doi.org/10.1016/0022-3115(94)00571-0

Bergsåker, H., Ratynskaia, S., Litnovsky, A., Ogata, D., Sahle, W., 2011. Studies of mobile dust in scrape-off layer plasmas using silica aerogel collectors. Journal of Nuclear Materials, Proceedings of the 19th International Conference on Plasma-Surface Interactions in Controlled Fusion 415, S1089–S1093. https://doi.org/10.1016/j.jnucmat.2011.01.052

Bevir M.K., Gray J.W., 1981. , in: Reversed Field Pinch Theory Workshop, Ed. Lweis & Gerwin, Los Alamos, Vol. III, A-3.

Bhattacharjee, A., Dewar, R.L., Monticello, D.A., 1980. Energy Principle with Global Invariants for Toroidal Plasmas. Physical Review Letters 45, 347–350. https://doi.org/10.1103/PhysRevLett.45.347

Biewer, T.M., Forest, C.B., Anderson, J.K., Fiksel, G., Hudson, B., Prager, S.C., Sarff, J.S., Wright, J.C., Brower, D.L., Ding, W.X., Terry, S.D., 2003. Electron Heat Transport Measured in a Stochastic Magnetic Field. Physical Review Letters 91. https://doi.org/10.1103/PhysRevLett.91.045004

Bilato, R., Volpe, F., Köhn, A., Paccagnella, R., Farina, D., Poli, E., Brambilla, M., 2009. Feasibility of electron Bernstein wave coupling via O-X-B mode conversion in the RFX-mod reversed field pinch device. Nuclear Fusion 49, 075020. https://doi.org/10.1088/0029-5515/49/7/075020

Bishop, C.M., 1989. An intelligent shell for the toroidal pinch. Plasma Physics and Controlled Fusion 31, 1179–1189. http://dx.doi.org/10.1088/0741-3335/31/7/012

Bodin, H.A.B., 1990. The reversed field pinch. Nuclear Fusion 30, 1717–1737. https://doi.org/10.1088/0029-5515/30/9/005

Bolzonella, T., Cavinato, M., Gaio, E., Grando, L., Luchetta, A., Manduchi, G., Marchiori, G., Marrelli, L., Paccagnella, R., Soppelsa, A., Zanca, P., 2007. Feedback control of resistive wall modes by saddle coils in RFX-mod. Fusion Engineering and Design 82, 1064–1072. https://doi.org/10.1016/j.fusengdes.2007.05.020

Bolzonella, T., Igochine, V., Guo, S.C., Yadikin, D., Baruzzo, M., Zohm, H., 2008. Resistive-Wall-Mode Active Rotation in the RFX-Mod Device. Phys. Rev. Lett. 101, 165003. https://doi.org/10.1103/PhysRevLett.101.165003

Bolzonella, T., Martin, P., Martini, S., Marrelli, L., Pasqualotto, R., Terranova, D., 2001. Quasistationary Magnetic Fluctuation Control in the Reversed Field Pinch: A Proof of Principle Experiment. Physical Review Letters 87. https://doi.org/10.1103/PhysRevLett.87.195001

Bolzonella, T., Terranova, D., 2002. Magnetic fluctuation spectra and non-linear MHD mode interaction in RFX. Plasma Phys. Control. Fusion 44, 2569. https://doi.org/10.1088/0741-3335/44/12/306

Bolzonella T, Terranova D, Zanotto L, Martini S, Sarff JS, 2006. Oscillating Field Current Drive experiments in RFX-mod, in: 33rd EPS Conference on Plasma Physics, Rome, 19-23 June 2006, Vol. 301, P-5.090.

Bondeson, A., Liu, Y., Gregoratto, D., Gribov, Y., Pustovitov, V.D., 2002. Active control of resistive wall modes in the large-aspect-ratio tokamak. Nucl. Fusion 42, 768–779. https://doi.org/10.1088/0029-5515/42/6/315

Bonfiglio, D., Cappello, S., Escande, D. F., 2006a. Impact of a uniform plasma resistivity in MHD modelling of helical solutions for the Reversed Field Pinch dynamo, in: Proc 13th International Congress on Plasma Physics, p. 126p.

Bonfiglio, D., Cappello, S., Escande, D.F., 2006b. Electrostatic dynamo in reversed field pinch plasmas: simple common fundamental nature of laminar and turbulent regimes, in: THEORY OF FUSION PLASMAS: Joint Varenna-Lausanne International Workshop AIP Conference Proceedings. Presented at the THEORY OF FUSION PLASMAS: Joint

Varenna-Lausanne International Workshop, AIP Publishing, pp. 3–14. https://doi.org/10.1063/1.2404535
Bonfiglio, D., Cappello, S., Escande, D.F., 2005. Dominant Electrostatic Nature of the Reversed Field Pinch Dynamo. Phys. Rev. Lett. 94, 145001. https://doi.org/10.1103/PhysRevLett.94.145001
Bonfiglio, D., Chacón, L., Cappello, S., 2010a. Nonlinear three-dimensional verification of the SPECYL and PIXIE3D magnetohydrodynamics codes for fusion plasmas. Physics of Plasmas (1994-present) 17, 082501. https://doi.org/10.1063/1.3462908
Bonfiglio, D., Escande, D.F., Zanca, P., Cappello, S., 2011. Necessary criterion for magnetic field reversal in the reversed-field pinch. Nuclear Fusion 51, 063016. https://doi.org/10.1088/0029-5515/51/6/063016
Bonfiglio, D., Veranda, M., Cappello, S., Chacón, L., Spizzo, G., 2010b. Magnetic chaos healing in the helical reversed-field pinch: indications from the volume-preserving field line tracing code NEMATO. J. Phys.: Conf. Ser. 260, 012003. https://doi.org/10.1088/1742-6596/260/1/012003
Bonfiglio, D., Veranda, M., Cappello, S., Escande, D.F., Chacón, L., 2015. Helical self-organization in 3D MHD modelling of fusion plasmas. Plasma Physics and Controlled Fusion 57, 044001. https://doi.org/10.1088/0741-3335/57/4/044001
Bonfiglio, D., Veranda, M., Cappello, S., Escande, D.F., Chacón, L., 2013. Experimental-like Helical Self-Organization in Reversed-Field Pinch Modeling. Physical Review Letters 111. https://doi.org/10.1103/PhysRevLett.111.085002
Bonofiglo, P. J., Anderson, J.K., Boguski, J., Kim, J., Egedal, J., Gobbin, M., Spong, D.A., Parke, E., 2019. Fast Ion Transport in the Three-Dimensional Reversed-Field Pinch. Physical Review Letters 123. https://doi.org/10.1103/PhysRevLett.123.055001
Bonofiglo, P. J., Anderson, J.K., Gobbin, M., Spong, D.A., Boguski, J., Parke, E., Kim, J., Egedal, J., 2019. Fast ion transport in the quasi-single helical reversed-field pinch. Physics of Plasmas 26, 022502. https://doi.org/10.1063/1.5084059
Bonomo, F., Alfier, A., Gobbin, M., Auriemma, F., Franz, P., Marrelli, L., Roberto Pasqualotto, Spizzo, G., Terranova, D., 2009. 2D characterization of core thermal topology changes in controlled RFX-mod QSH states. Nucl. Fusion 49, 045011. https://doi.org/10.1088/0029-5515/49/4/045011
Bonomo, F., Bonfiglio, D., Piovesan, P., Piron, L., Zaniol, B., Cappello, S., Carraro, L., Cavazzana, R., M. Gobbin, Marrelli, L., Martines, E., Momo, B., Puiatti, M.E., Valisa, M., 2011. Flow measurements and modelling in helical RFX-mod equilibria. Nucl. Fusion 51, 123007. https://doi.org/10.1088/0029-5515/51/12/123007
Brower, D.L., Ding, W.X., Terry, S.D., Anderson, J.K., Biewer, T.M., Chapman, B.E., Craig, D., Forest, C.B., Prager, S.C., Sarff, J.S., 2003. Laser polarimetric measurement of equilibrium and fluctuating magnetic fields in a reversed field pinch (invited). Review of Scientific Instruments 74, 1534–1540. https://doi.org/10.1063/1.1526927
Brower, D.L., Ding, W.X., Terry, S.D., Anderson, J.K., Biewer, T.M., Chapman, B.E., Craig, D., Forest, C.B., Prager, S.C., Sarff, J.S., 2002. Measurement of the Current-Density Profile and Plasma Dynamics in the Reversed-Field Pinch. Physical Review Letters 88. https://doi.org/10.1103/PhysRevLett.88.185005
Brunsell, P.R., Bergsåker, H., Cecconello, M., Drake, J.R., Gravestijn, R.M., Hedqvist, A., Malmberg, J.-A., 2001. Initial results from the rebuilt EXTRAP T2R RFP device. Plasma Phys. Control. Fusion 43, 1457. https://doi.org/10.1088/0741-3335/43/11/303
Brunsell, P.R., Malmberg, J.-A., Yadikin, D., Cecconello, M., 2003. Resistive wall modes in the EXTRAP T2R reversed-field pinch. Physics of Plasmas 10, 3823. https://doi.org/10.1063/1.1604775
Brunsell, P.R., Yadikin, D., Gregoratto, D., Paccagnella, R., Bolzonella, T., Cavinato, M., Cecconello, M., Drake, J.R., Luchetta, A., Manduchi, G., Marchiori, G., Marrelli, L.,

Martin, P., Masiello, A., Milani, F., Ortolani, S., Spizzo, G., Zanca, P., 2004. Feedback Stabilization of Multiple Resistive Wall Modes. Physical Review Letters 93. https://doi.org/10.1103/PhysRevLett.93.225001

Brunsell, P.R., Yadikin, D., Gregoratto, D., Paccagnella, R., Liu, Y.Q., Bolzonella, T., Cecconello, M., Drake, J.R., Kuldkepp, M., Manduchi, G., Marchiori, G., Marrelli, L., Martin, P., Menmuir, S., Ortolani, S., Rachlew, E., Spizzo, G., Zanca, P., 2005. Active control of multiple resistive wall modes. Plasma Physics and Controlled Fusion 47, B25–B36. https://doi.org/10.1088/0741-3335/47/12B/S03

Brunsell, P.R., Yagi, Y., Hirano, Y., Maejima, Y., Shimada, T., 1993a. Coherent magnetic field fluctuations and locked modes in a reversed-field pinch. Physics of Fluids B: Plasma Physics (1989-1993) 5, 885–895. https://doi.org/10.1063/1.860939

Brunsell, P.R., Yagi, Y., Hirano, Y., Maejima, Y., Shimada, T., 1993b. Coherent magnetic field fluctuations and locked modes in a reversed-field pinch. Physics of Fluids B: Plasma Physics (1989-1993) 5, 885–895. https://doi.org/10.1063/1.860939

Budny, R.V., Bell, M.G., Biglari, H., Bitter, M., Bush, C.E., Cheng, C.Z., Fredrickson, E.D., Grek, B., Hill, K.W., Hsuan, H., Janos, A.C., Jassby, D.L., Johnson, D.W., Johnson, L.C., LeBlanc, B., McCune, D.C., Mikkelsen, D.R., Park, H.K., Ramsey, A.T., Sabbagh, S.A., Scott, S.D., Schivell, J.F., Strachan, J.D., Stratton, B.C., Synakowski, E.J., Taylor, G., Zarnstorff, M.C., Zweben, S.J., 1992. Simulations of deuterium-tritium experiments in TFTR. Nuclear Fusion 32, 429–447. https://doi.org/10.1088/0029-5515/32/3/I07

Buffa, A., Gnesotto, F., Antoni, V., et al., 1994. Magnetic field configuration and locked modes in RFX, in: 21. EPS Conference on Controlled Fusion and Plasma Physics, Montpellier (France) 1994. Presented at the 21. EPS conference on controlled fusion and plasma physics, Montpellier (France) 1994, p. 458.

Burke, D.R., Goetz, J.A., Kaufman, M.C., Almagri, A.F., Anderson, J.K., Forest, C.B., Prager, S.C., Ryan, P.M., Rasmussen, D., 2007. Diagnosis of Lower Hybrid on MST, in: AIP Conference Proceedings. Presented at the RADIO FREQUENCY POWER IN PLASMAS: 17th Topical Conference on Radio Frequency Power in Plasmas, AIP, Clearwater (Florida), pp. 313–316. https://doi.org/10.1063/1.2800501

Bykov, I., Vignitchouk, L., Ratynskaia, S., Banon, J.-P., Tolias, P., Bergsåker, H., Frassinetti, L., Brunsell, P.R., 2014. Transport asymmetry and release mechanisms of metal dust in the reversed-field pinch configuration. Plasma Physics and Controlled Fusion 56, 035014. https://doi.org/10.1088/0741-3335/56/3/035014

Canton, A., Dal Bello, S., Agostini, M., Carraro, L., Cavazzana, R., Fiameni, S., Grando, L., Rais, B., Spolaore, M., Zuin, M., 2013. Studies of spatial uniformity of glow discharge cleaning plasmas on the RFX-mod device. Journal of Nuclear Materials 438, S1164–S1167. https://doi.org/10.1016/j.jnucmat.2013.01.257

Canton, A., Hirano, Y., Innocente, P., Koguchi, H., Lorenzini, R., 2004. Electron density behaviour in the TPE-RX reversed field pinch experiment and comparison with the particle transport model of the RFX experiment. Plasma Phys. Control. Fusion 46, 23. https://doi.org/10.1088/0741-3335/46/1/003

Cappello, S., 2004. Bifurcation in the MHD behaviour of a self-organizing system: the reversed field pinch (RFP). Plasma Phys. Control. Fusion 46, B313. https://doi.org/10.1088/0741-3335/46/12B/027

Cappello, S., Biskamp, D., 1996. Reconnection processes and scaling laws in reversed field pinch magnetohydrodynamics. Nucl. Fusion 36, 571. https://doi.org/10.1088/0029-5515/36/5/I05

Cappello, S., Biskamp, D., 1996. Nonlinear MHD sustainment dynamics of the reversed field pinch (RFP) configuration at different values of the pinch parameter, in: 1996 Int. Conf. on Plasma Physics. Presented at the ICPP Nagoya, P.E. Stott (Bristol: Institute of Physics Publishing), Nagoya, Japan, pp. 854–857.

Cappello, S., Bonfiglio, D., Chacon, L., Ciaccio, G., Escande, D. F., Guo, S., Liu, S. F., Predebon, I., Sattin, F., Veranda, M., Wang, Z. R., 2012. Nonlinear Modeling for Helical Configurations in Toroidal Pinch Systems, in: Proceedings of the 24th IAEA Fusion Energy Conference, San Diego, USA. p. TH/P2-16.

Cappello, S., Bonfiglio, D., Escande, D.F., 2006. Magnetohydrodynamic dynamo in reversed field pinch plasmas: Electrostatic drift nature of the dynamo velocity fielda). Physics of Plasmas (1994-present) 13, 056102. https://doi.org/10.1063/1.2177198

Cappello, S., Bonfiglio, D., Escande, D.F., Guo, S.C., Alfier, A., Lorenzini, R., Team, R.F.X., 2008. The Reversed Field Pinch toward magnetic order: a genuine self-organization, in: AIP Conference Proceedings. Presented at the THEORY OF FUSION PLASMAS, AIP Publishing, pp. 27–39. https://doi.org/10.1063/1.3033714

Cappello, S., Bonfiglio, D., Escande, D.F., Guo, S.C., Predebon, I., Sattin, F., Veranda, M., Zanca, P., C. Angioni, Chacón, L., Dong, J.Q., Garbet, X., Liu, S.F., 2011. Equilibrium and transport for quasi-helical reversed field pinches. Nucl. Fusion 51, 103012. https://doi.org/10.1088/0029-5515/51/10/103012

Cappello, S., Escande, D.F., 2000. Bifurcation in Viscoresistive MHD: The Hartmann Number and the Reversed Field Pinch. Phys. Rev. Lett. 85, 3838–3841. https://doi.org/10.1103/PhysRevLett.85.3838

Cappello, S., Paccagnella, R., 1992. Nonlinear plasma evolution and sustainment in the reversed field pinch. Physics of Fluids B: Plasma Physics (1989-1993) 4, 611–618. https://doi.org/10.1063/1.860471

Cappello, S., Paccagnella, R., 1990. , in: Proc. Workshop on Theory of Fusion Plasmas. Sindoni, E. Compositori, Bologna, p. 595.

Caramana, E.J., Nebel, R.A., 1988. Reversed-field pinch Ohmic equilibria during current decay and termination. The Physics of Fluids 31, 3322–3329. https://doi.org/10.1063/1.866946

Caramana, E.J., Nebel, R.A., Schnack, D.D., 1983. Nonlinear, single-helicity magnetic reconnection in the reversed-field pinch. Physics of Fluids (1958-1988) 26, 1305–1319. https://doi.org/10.1063/1.864253

Carmody, D., Pueschel, M.J., Anderson, J.K., Terry, P.W., 2015. Microturbulence studies of pulsed poloidal current drive discharges in the reversed field pinch. Physics of Plasmas 22, 012504. https://doi.org/10.1063/1.4905709

Carmody, D., Pueschel, M.J., Terry, P.W., 2013. Gyrokinetic studies of microinstabilities in the reversed field pinch. Physics of Plasmas 20, 052110. https://doi.org/10.1063/1.4803509

Carraro, L., Alfier, A., Bonomo, F., Fassina, A., Gobbin, M., Lorenzini, R., Piovesan, P., Puiatti, M.E., G. Spizzo, Terranova, D., Valisa, M., Zuin, M., Canton, A., Franz, P., Innocente, P., Pasqualotto, R., Auriemma, F., S. Cappello, Guo, S.C., Marrelli, L., Martines, E., Spolaore, M., Zanotto, L., 2009. Improved confinement with internal electron transport barriers in RFX-mod. Nucl. Fusion 49, 055009. https://doi.org/10.1088/0029-5515/49/5/055009

Carraro, L., Casarotto, E., Pasqualotto, R., Puiatti, M.E., Sattin, F., Scarin, P., Valisa, M., 1995. Impurity influx studies in the RFX reversed field pinch. Journal of Nuclear Materials, Plasma-Surface Interactions in Controlled Fusion Devices 220–222, 646–649. https://doi.org/10.1016/0022-3115(94)00557-5

Carraro, L., Casarotto, E., Puiatti, M.E., Scarin, P., Valisa, M., 1995. Impurity influxes and production mechanism in RFX, in: 22nd EPS Conf. Contr. Fus. and Plasma Phys., Vol.19c,Part II, 317.

Carraro, L., Costa, S., Puiatti, M.E., Sattin, F., Scarin, P., Telesca, G., Tokar', M.Z., Valisa, M., Franz, P., Marrelli, L., 2000a. Radiation and confinement properties of impurity seeded discharges in the reversed field pinch RFX. Nuclear Fusion 40, 1983–1991. https://doi.org/10.1088/0029-5515/40/12/303

Carraro, L., Costa, S., Puiatti, M.E., Sattin, F., Scarin, P., Valisa, M., 2000b. Reconstruction of the radiation emitted by the intrinsic impurities in the RFX reversed field pinch. Plasma Physics and Controlled Fusion 42, 731–741. https://doi.org/10.1088/0741-3335/42/6/308

Carraro, L., Innocente, P., Auriemma, F., Cavazzana, R., Fassina, A., Franz, P., Gobbin, M., Predebon, I., A. Ruzzon, Spizzo, G., Terranova, D., Bolzonella, T., Canton, A., Bello, S.D., Grando, L., Lorenzini, R., L. Marrelli, Martines, E., Puiatti, M.E., Scarin, P., Soppelsa, A., Valisa, M., Zanotto, L., Zuin, M., 2013. Advances in understanding RFX-mod helical plasmas. Nucl. Fusion 53, 073048. https://doi.org/10.1088/0029-5515/53/7/073048

Carraro, L., Puiatti, M.E., Sattin, F., Scarin, P., Valisa, M., 2002. Impurity transport during pulsed poloidal current drive experiment in the reversed field pinch experiment RFX. Plasma Physics and Controlled Fusion 44, 2135–2148. https://doi.org/10.1088/0741-3335/44/10/305

Carraro, L., Puiatti, M.E., Sattin, F., Scarin, P., Valisa, M., 1998. Toroidal and poloidal plasma rotation in the reversed field pinch RFX. Plasma Phys. Control. Fusion 40, 1021. https://doi.org/10.1088/0741-3335/40/6/009

Carraro, L., Puiatti, M.E., Sattin, F., Scarin, P., Valisa, M., DePol, G., Pasqualotto, R., Pugno, R., Telesca, G., 1999. Impurity screening in the RFX reversed field pinch. Journal of Nuclear Materials 266–269, 446–451. https://doi.org/10.1016/S0022-3115(98)00827-7

Carraro, L., Puiatti, M.E., Sattin, F., Scarin, P., Valisa, M., Mattioli, M., 1996. Carbon and oxygen behaviour in the reversed field pinch RFX. Nuclear Fusion 36, 1623–1632. https://doi.org/10.1088/0029-5515/36/12/I03

Carreras, B.A., Lynch, V.E., Ichiguchi, K., Wakatani, M., Tatsuno, T., 2001. On the applicability of local asymptotic stability criteria to stellarator stability. Physics of Plasmas (1994-present) 8, 990–996. https://doi.org/10.1063/1.1349877

Caspary, K.J., 2014. DENSITY AND BETA LIMITS IN THE MADISON SYMMETRIC TORUS REVERSED-FIELD PINCH (Ph.D. Thesis). University of Wisconsin - Madison, Madison, US.

Cavinato, M., Manduchi, G., Luchetta, A., Marchiori, G., Taliercio, C., 2006a. Distributed real time control in RFX-mod nuclear fusion experiment: commissioning and first results. IEEE Transactions on Nuclear Science 53, 1015–1021. https://doi.org/10.1109/TNS.2006.873531

Cavinato, M., Manduchi, G., Luchetta, A., Taliercio, C., 2006b. General-purpose framework for real time control in nuclear fusion experiments. IEEE Trans. Nucl. Sci. 53, 1002–1008. https://doi.org/10.1109/TNS.2006.873002

Cecconello, M., Malmberg, J.-A., Spizzo, G., Chapman, B.E., Gravestjin, R.M., Franz, P., Piovesan, P., Martin, P., Drake, J.R., 2003. Current profile modification experiments in EXTRAP T2R. Plasma Phys. Control. Fusion 46, 145. https://doi.org/10.1088/0741-3335/46/1/009

Cengher, M., Anderson, J.K., Svidzinski, V., Forest, C.B., 2006. Coupling to the electron Bernstein wave using a phased array of waveguides in MST reversed field pinch. Nuclear Fusion 46, 521–531. https://doi.org/10.1088/0029-5515/46/5/004

Chacón, L., 2008. An optimal, parallel, fully implicit Newton–Krylov solver for three-dimensional viscoresistive magnetohydrodynamics. Physics of Plasmas 15, 056103. https://doi.org/10.1063/1.2838244

Chacón, L., 2004. A non-staggered, conservative, , finite-volume scheme for 3D implicit extended magnetohydrodynamics in curvilinear geometries. Computer Physics Communications 163, 143–171. https://doi.org/10.1016/j.cpc.2004.08.005

Chang, Z., 1995. Observation of Nonlinear Neoclassical Pressure-Gradient–Driven Tearing Modes in TFTR. Phys. Rev. Lett. 74, 4663–4666. https://doi.org/10.1103/PhysRevLett.74.4663

Chapman, B.E., 1997. FLUCTUATION REDUCTION AND ENHANCED CONFINEMENT IN THE MST REVERSED FIELD PINCH (Ph.D. Thesis). University of Wisconsin - Madison, madison, US.

Chapman, B.E., Ahn, J.W., Almagri, A.F., Anderson, J.K., Bonomo, F., Brower, D.L., Burke, D.R., Caspary, K., Clayton, D.J., Combs, S.K., Cox, W.A., Craig, D., Deng, B.H., Hartog, D.J.D., Ding, W.X., Ebrahimi, F., Ennis, D.A., Fiksel, G., Forest, C.B., Foust, C.R., Franz, P., Gangadhara, S., Goetz, J.A., Kaufman, M.C., Kulpin, J.G., Kuritsyn, A., Magee, R.M., Miller, M.C., Mirnov, V.V., Nonn, P.D., O'Connell, R., Oliva, S.P., Prager, S.C., Reusch, J.A., Sarff, J.S., Stephens, H.D., Wyman, M.D., Yates, T., 2009. Improved-confinement plasmas at high temperature and high beta in the MST RFP. Nucl. Fusion 49, 104020. https://doi.org/10.1088/0029-5515/49/10/104020

Chapman, B.E., Almagri, A.F., Anderson, J.K., Biewer, T.M., Chattopadhyay, P.K., Chiang, C.-S., Craig, D., Den Hartog, D.J., Fiksel, G., Forest, C.B., Hansen, A.K., Holly, D., Lanier, N.E., O'Connell, R., Prager, S.C., Reardon, J.C., Sarff, J.S., Wyman, M.D., Brower, D.L., Ding, W.X., Jiang, Y., Terry, S.D., Franz, P., Marrelli, L., Martin, P., 2002. High confinement plasmas in the Madison Symmetric Torus reversed-field pinch. Physics of Plasmas 9, 2061–2068. https://doi.org/10.1063/1.1456930

Chapman, B.E., Almagri, A.F., Anderson, J.K., Brower, D.L., Caspary, K.J., Clayton, D.J., Craig, D., Hartog, D.J.D., Ding, W.X., Ennis, D.A., Fiksel, G., Gangadhara, S., Kumar, S., Magee, R.M., O'Connell, R., Parke, E., Prager, S.C., Reusch, J.A., Sarff, J.S., Stephens, H.D., Yang, Y.M., 2010. Generation and confinement of hot ions and electrons in a reversed-field pinch plasma. Plasma Physics and Controlled Fusion 52, 124048. https://doi.org/10.1088/0741-3335/52/12/124048

Chapman, B.E., Almagri, A.F., Anderson, J.K., Chiang, C.-S., Craig, D., Fiksel, G., Lanier, N.E., Prager, S.C., Sarff, J.S., Stoneking, M.R., Terry, P.W., 1998a. E×B flow shear and enhanced confinement in the Madison Symmetric Torus reversed-field pinch. Physics of Plasmas 5, 1848–1854. https://doi.org/10.1063/1.872855

Chapman, B.E., Almagri, A.F., Cekic, M., Den Hartog, D.J., Prager, S.C., Sarff, J.S., 1996. Sawteeth and energy confinement in the Madison Symmetric Torus reversed-field pinch. Physics of Plasmas 3, 709–711. https://doi.org/10.1063/1.871775

Chapman, B.E., Anderson, J.K., Biewer, T.M., Brower, D.L., Castillo, S., Chattopadhyay, P.K., Chiang, C.-S., Craig, D., Hartog, D.J.D., Fiksel, G., Fontana, P.W., Forest, C.B., Gerhardt, S., Hansen, A.K., Holly, D., Jiang, Y., Lanier, N.E., Prager, S.C., Reardon, J.C., Sarff, J.S., 2001. Reduced Edge Instability and Improved Confinement in the MST Reversed-Field Pinch. Phys. Rev. Lett. 87, 205001. https://doi.org/10.1103/PhysRevLett.87.205001

Chapman, B.E., Biewer, T.M., Chattopadhyay, P.K., Chiang, C.-S., Craig, D.J., Crocker, N.A., Den Hartog, D.J., Fiksel, G., Fontana, P.W., Prager, S.C., Sarff, J.S., 2000. Modifications to the edge current profile with auxiliary edge current drive and improved confinement in a reversed-field pinch. Physics of Plasmas 7, 3491–3494. https://doi.org/10.1063/1.1287913

Chapman, B.E., Chiang, C.-S., Prager, S.C., Sarff, J.S., Stoneking, M.R., 1998b. Strong E × B Flow Shear and Reduced Fluctuations in a Reversed-Field Pinch. Physical Review Letters 80, 2137–2140. https://doi.org/10.1103/PhysRevLett.80.2137

Chapman, B.E., Fitzpatrick, R., Craig, D., Martin, P., Spizzo, G., 2004. Observation of tearing mode deceleration and locking due to eddy currents induced in a conducting shell. Physics of Plasmas 11, 2156–2171. https://doi.org/10.1063/1.1689353

Chattopadhyay, P.K., Anderson, J.K., Biewer, T.M., Craig, D., Forest, C.B., Harvey, R.W., Smirnov, A.P., 2002. Electron Bernstein wave emission from an overdense reversed field pinch plasma. Physics of Plasmas 9, 752–755. https://doi.org/10.1063/1.1447253

Chirikov, B.V., 1979. A universal instability of many-dimensional oscillator systems. Physics Reports 52, 263–379. https://doi.org/10.1016/0370-1573(79)90023-1

Christiansen, J.P., Roberts, K.V., 1982. Power balance in an Ohmically heated fusion reactor. Nuclear Fusion 22, 77–88. https://doi.org/10.1088/0029-5515/22/1/008

Connor, J.W., Taylor, J.B., 1984. Resistive fluid turbulence and energy confinement. Physics of Fluids 27, 2676. https://doi.org/10.1063/1.864570

Craig, D., Almagri, A.F., Anderson, J.K., Chapman, J.T., Chiang, C.-S., Crocker, N.A., Den Hartog, D.J., Fiksel, G., Prager, S.C., Sarff, J.S., Stoneking, M.R., 1997. Enhanced Confinement with Plasma Biasing in the MST Reversed Field Pinch. Physical Review Letters 79, 1865–1868. https://doi.org/10.1103/PhysRevLett.79.1865

Craig, D., Fiksel, G., Prager, S.C., Sarff, J.S., 2001. Control of magnetic fluctuations in the reversed field pinch with edge current drive. Physics of Plasmas 8, 1463–1466. https://doi.org/doi:10.1063/1.1365103

Cravotta, A., Spizzo, G., Terranova, D., Bolzonella, T., Franz, P., Marrelli, L., Martin, P., Martini, S., Ortolani, S., 2003. A statistical analysis of pulsed poloidal current drive in the Reversed Field eXperiment. Physics of Plasmas (1994-present) 10, 705–712. https://doi.org/10.1063/1.1538594

Dahlin, J.-E, Scheffel, J., 2007. Numerical studies of confinement scalings for the dynamo-free reversed-field pinch. Nuclear Fusion 47, 9–16. https://doi.org/10.1088/0029-5515/47/1/002

Dahlin, Jon-Erik, Scheffel, J., 2007. Ultra-high beta in numerical simulations of a tearing-mode reduced reversed-field pinch. Nuclear Fusion 47, 1184–1188. https://doi.org/10.1088/0029-5515/47/9/015

Dahlin, J.-E., Scheffel, J., 2005. A novel feedback algorithm for simulating controlled dynamics and confinement in the advanced reversed-field pinch. Physics of Plasmas 12, 062502. https://doi.org/10.1063/1.1924556

Dahlin, J.-E., Scheffel, J., Anderson, J.K., 2007. Numerical studies of active current profile control in the reversed-field pinch. Plasma Physics and Controlled Fusion 49, 183–195. https://doi.org/10.1088/0741-3335/49/2/008

D'Angelo, F., Paccagnella, R., 1996. The stochastic diffusion process in reversed-field pinch. Physics of Plasmas 3, 2353. https://doi.org/10.1063/1.871919

De Masi, G. et al., 2012. Edge flow and radiation in Helium discharges in RFX, in: 39th EPS Conf. & 16th Int. Congress on Plasma Physics. Presented at the 39th EPS / 16th ICPP, Stockholm.

Delzanno, G.L., Chacón, L., Finn, J.M., 2008. Electrostatic mode associated with the pinch velocity in reversed field pinch simulations. Physics of Plasmas 15, 122102. https://doi.org/10.1063/1.3026714

Den Hartog, D.J., Cekic, M., Fiksel, G., Hokin, S.A., Kendrick, R.D., Prager, S.C., Stoneking, M.R., 1993. B4C solid target boronization of the MST reversed-field pinch. Journal of Nuclear Materials 200, 177–183. https://doi.org/10.1016/0022-3115(93)90328-V

Den Hartog, D.J., Chapman, J.T., Craig, D., Fiksel, G., Fontana, P.W., Prager, S.C., Sarff, J.S., 1999. Measurement of core velocity fluctuations and the dynamo in a reversed-field pinch. Physics of Plasmas 6, 1813–1821. https://doi.org/10.1063/1.873439

Den Hartog, D.J., Kendrick, R.D., 1995. Solid target boronization of the MST reversed-field pinch during pulsed discharge cleaning. Journal of Nuclear Materials 220–222, 631–635. https://doi.org/10.1016/0022-3115(94)00554-0

Dennis, G.R., Hudson, S.R., Terranova, D., Franz, P., Dewar, R.L., Hole, M.J., 2013. Minimally Constrained Model of Self-Organized Helical States in Reversed-Field Pinches. Phys. Rev. Lett. 111, 055003. https://doi.org/10.1103/PhysRevLett.111.055003

Dexter, R.N., Kerst, D.W., Lovell, T.W., Prager, S.C., Sprott, J.C., 1991. The Madison Symmetric Torus. Fusion Technology 19, 131–139. https://doi.org/10.13182/FST91-A29322

Di Giannatale, G., Falessi, M.V., Grasso, D., Pegoraro, F., Schep, T.J., Veranda, M., Bonfiglio, D., Cappello, S., 2018. Lagrangian Coherent Structures as a new frame to investigate the particle transport in highly chaotic magnetic systems. Journal of Physics: Conference Series 1125, 012008-. https://doi.org/10.1088/1742-6596/1125/1/012008

Ding, W.X., Brower, D.L., Craig, D., Chapman, B.E., Ennis, D., Fiksel, G., Gangadhara, S., Den Hartog, D.J., Mirnov, V.V., Prager, S.C., Sarff, J.S., Svidzinski, V., Terry, P.W., Yates, T., 2008a. Stochastic magnetic field driven charge transport and zonal flow during magnetic reconnection. Physics of Plasmas 15, 055901. https://doi.org/10.1063/1.2837047

Ding, W.X., Brower, D.L., Terry, S.D., Craig, D., Prager, S.C., Sarff, J.S., Wright, J.C., 2003. Measurement of Internal Magnetic Field Fluctuations in a Reversed-Field Pinch by Faraday Rotation. Physical Review Letters 90. https://doi.org/10.1103/PhysRevLett.90.035002

Ding, W.X., Brower, D.L., Yates, T.Y., 2008b. Measurement of magnetic fluctuation-induced particle flux (invited). Review of Scientific Instruments 79, 10E701. https://doi.org/10.1063/1.2953437

Drake, J.R., Bolzonella, T., Olofsson, K.E.J., Baruzzo, T.M., Brunsell, P.R., Frassinetti, L., Guo, S.C., Igochine, V., Liu, Y.Q., Marchiori, G., others, 2008. Reversed-field pinch contributions to resistive wall mode physics and control, in: Proc. 22nd International Conference on Fusion Energy. Presented at the 22nd Fusion Energy Conference, IAEA, p. EX P9-7.

Drake, J.R., Brunsell, P.R., Yadikin, D., Cecconello, M., Malmberg, J.A., Gregoratto, D., Paccagnella, R., Bolzonella, T., Manduchi, G., Marrelli, L., Ortolani, S., Spizzo, G., Zanca, P., Bondeson, A., Liu, Y.Q., 2005. Experimental and theoretical studies of active control of resistive wall mode growth in the EXTRAP T2R reversed-field pinch. Nucl. Fusion 45, 557–564. https://doi.org/10.1088/0029-5515/45/7/002

Ebrahimi, F., 2007. Momentum Transport from Current-Driven Reconnection in the Reversed Field Pinch. Phys. Rev. Lett. 99. https://doi.org/10.1103/PhysRevLett.99.075003

Ebrahimi, F., Prager, S.C., 2004. Current profile control by alternating current magnetic helicity injection. Physics of Plasmas 11, 2014–2025. https://doi.org/10.1063/1.1690304

Ebrahimi, F., Prager, S.C., Sarff, J.S., Wright, J.C., 2003. The three-dimensional magnetohydrodynamics of ac helicity injection in the reversed field pinch. Physics of Plasmas 10, 999–1014. https://doi.org/doi:10.1063/1.1555622

Escande, D. F., 2015. What is a Reversed Field Pinch?, in: Rotation and Momentum Transport in Magnetized Plasmas. Diamond P. H. , Garbet X., Ghendrih P., and Sarazin Y. (World Scientific).

Escande, D. F., Bénisti, D., 1997. , in: Proc. of the 7th European Fusion Theory Conference. Rogister, A., Forschungzentrum KFA Jülich, p. 127.

Escande, D.F., Cappello, S., D'Angelo, F., Martin, P., Ortolani, S., Paccagnella, R., 2000a. Single helicity: a new paradigm for the reversed field pinch. Plasma Phys. Control. Fusion 42, B243. https://doi.org/10.1088/0741-3335/42/12B/319

Escande, D.F., Martin, P., Ortolani, S., Buffa, A., Franz, P., Marrelli, L., Martines, E., Spizzo, G., Cappello, S., Murari, A., Pasqualotto, R., Zanca, P., 2000b. Quasi-Single-Helicity Reversed-Field-Pinch Plasmas. Phys. Rev. Lett. 85, 1662–1665. https://doi.org/10.1103/PhysRevLett.85.1662

Escande, D.F., Paccagnella, R., Cappello, S., Marchetto, C., D'Angelo, F., 2000c. Chaos Healing by Separatrix Disappearance and Quasisingle Helicity States of the Reversed Field Pinch. Phys. Rev. Lett. 85, 3169–3172. https://doi.org/10.1103/PhysRevLett.85.3169

Evans, T.E., Moyer, R.A., Thomas, P.R., Watkins, J.G., Osborne, T.H., Boedo, J.A., Doyle, E.J., Fenstermacher, M.E., Finken, K.H., Groebner, R.J., Groth, M., Harris, J.H., La Haye, R.J., Lasnier, C.J., Masuzaki, S., Ohyabu, N., Pretty, D.G., Rhodes, T.L., Reimerdes, H., Rudakov, D.L., Schaffer, M.J., Wang, G., Zeng, L., 2004. Suppression of Large Edge-Localized Modes in High-Confinement DIII-D Plasmas with a Stochastic Magnetic Boundary. Phys. Rev. Lett. 92, 235003. https://doi.org/10.1103/PhysRevLett.92.235003

Fassina, A., Alfier, A., Agostini, M., Auriemmal, F., Brombin, M., Franz, P., Lorenzini, R., Marrelli, L., Martines, E., Spizzo, G., Zanca, P., 2013. Electron Pressure and Transport Analysis During QSH States in RFX-mod. IEEE Transactions on Plasma Science 41, 2–11. https://doi.org/10.1109/TPS.2012.2224871

Fiameni, S., Barison, S., Canton, A., Bello, S.D., Innocente, P., Pagura, C., Fabrizio, M., Daolio, S., 2013. SIMS analysis of the interaction between plasmas and the graphite first wall in RFX-

mod: SIMS analysis of graphite first wall in RFX-mod. Surf. Interface Anal. 45, 423–426. https://doi.org/10.1002/sia.5063

Fiksel, G., Almagri, A.F., Chapman, B.E., Mirnov, V.V., Ren, Y., Sarff, J.S., Terry, P.W., 2009. Mass-Dependent Ion Heating during Magnetic Reconnection in a Laboratory Plasma. Physical Review Letters 103. https://doi.org/10.1103/PhysRevLett.103.145002

Fiksel, G., Almagri, A.F., Craig, D., Iida, M., Prager, S.C., Sarff, J.S., 1996. High current plasma electron emitter. Plasma Sources Sci. Technol. 5, 78. https://doi.org/10.1088/0963-0252/5/1/010

Fiksel, G, Bengtson, R.D., Cekic, M., Hartog, D.D., Prager, S.C., Pribyl, P., Sarff, J., Sovinec, C., Stoneking, M.R., Taylor, R.J., Terry, P.W., Tynan, G.R., Wootton, A.J., 1996. Measurement of magnetic fluctuation-induced heat transport in tokamaks and RFP. Plasma Physics and Controlled Fusion 38, A213–A225. https://doi.org/10.1088/0741-3335/38/12A/016

Fiksel, G., Hudson, B., Den Hartog, D.J., Magee, R.M., O'Connell, R., Prager, S.C., Beklemishev, A.D., Davydenko, V.I., Ivanov, A.A., Tsidulko, Yu.A., 2005. Observation of Weak Impact of a Stochastic Magnetic Field on Fast-Ion Confinement. Physical Review Letters 95. https://doi.org/10.1103/PhysRevLett.95.125001

Fiksel, G., Prager, S.C., Shen, W., Stoneking, M.R., 1994. Measurement of magnetic fluctuation induced energy transport. Physical Review Letters 72, 1028–1031. https://doi.org/10.1103/PhysRevLett.72.1028

Filonenko, N.N., Sagdeev, R.Z., Zaslavsky, G.M., 1967. Destruction of magnetic surfaces by magnetic field irregularities: Part II. Nucl. Fusion 7, 253. https://doi.org/10.1088/0029-5515/7/4/009

Finn, J.M., Guzdar, P.N., Chernikov, A.A., 1992a. Particle transport and rotation damping due to stochastic magnetic field lines. Physics of Fluids B: Plasma Physics 4, 1152–1155. https://doi.org/10.1063/1.860123

Finn, J.M., Nebel, R., Bathke, C., 1992b. Single and multiple helicity Ohmic states in reversed-field pinches. Physics of Fluids B: Plasma Physics (1989-1993) 4, 1262–1279. https://doi.org/10.1063/1.860082

Fitzpatrick, R., 1999. Formation and locking of the "slinky mode" in reversed-field pinches. Physics of Plasmas 6, 1168–1193. https://doi.org/10.1063/1.873361

Fitzpatrick, R., 1993. Interaction of tearing modes with external structures in cylindrical geometry (plasma). Nucl. Fusion 33, 1049–1084. https://doi.org/10.1088/0029-5515/33/7/I08

Fitzpatrick, R., Guo, S.C., Den Hartog, D.J., Hegna, C.C., 1999. Effect of a resistive vacuum vessel on dynamo mode rotation in reversed field pinches. Physics of Plasmas 6, 3878–3889. https://doi.org/10.1063/1.873650

Fitzpatrick, R., Yu, E.P., 1999. Feedback stabilization of resistive shell modes in a reversed field pinch. Physics of Plasmas 6, 3536–3547.

Fitzpatrick, R., Zanca, P., 2002. Phase-locking of tearing modes in the reversed field experiment. Physics of Plasmas 9, 2707–2724. https://doi.org/10.1063/1.1481057

Fontana, P.W., 2000. Spectroscopic Observation of Fluctuation-Induced Dynamo in the Edge of the Reversed-Field Pinch. Phys. Rev. Lett. 85, 566–569. https://doi.org/10.1103/PhysRevLett.85.566

Forest, C.B., Chattopadhyay, P.K., Harvey, R.W., Smirnov, A.P., 2000. Off-midplane launch of electron Bernstein waves for current drive in overdense plasmas. Physics of Plasmas 7, 1352–1355. https://doi.org/10.1063/1.873951

Franz, P., Gobbin, M., Marrelli, L., Ruzzon, A., Fassina, A., Martines, E., Spizzo, G., 2013. Experimental investigation of electron temperature dynamics of helical states in the RFX-Mod reversed field pinch. Nuclear Fusion 53, 053011. https://doi.org/10.1088/0029-5515/53/5/053011

Franz, P., Marrelli, L., Piovesan, P., Chapman, B.E., Martin, P., Predebon, I., Spizzo, G., White, R.B., Xiao, C., 2004. Observations of Multiple Magnetic Islands in the Core of a Reversed Field Pinch. Physical Review Letters 92. https://doi.org/10.1103/PhysRevLett.92.125001

Franz, P., Marrelli, L., Piovesan, P., Predebon, I., Bonomo, F., Frassinetti, L., Martin, P., Spizzo, G., Chapman, B.E., Craig, D., Sarff, J.S., 2006. Tomographic imaging of resistive mode dynamics in the Madison Symmetric Torus reversed-field pinch. Physics of Plasmas (1994-present) 13, 012510. https://doi.org/10.1063/1.2160519

Frassinetti, L., Alfier, A., Pasqualotto, R., Bonomo, F., Innocente, P., 2008. Heat diffusivity model and temperature simulations in RFX-mod. Nuclear Fusion 48, 045007. https://doi.org/10.1088/0029-5515/48/4/045007

Frassinetti, L., Brunsell, P.R., Cecconello, M., Drake, J.R., 2009a. Heat transport modelling in EXTRAP T2R. Nucl. Fusion 49, 025002. https://doi.org/10.1088/0029-5515/49/2/025002

Frassinetti, L., Brunsell, P.R., Drake, J.R., 2009b. Experiments and modelling of active quasi-single helicity regime generation in a reversed field pinch. Nucl. Fusion 49, 075019. https://doi.org/10.1088/0029-5515/49/7/075019

Frassinetti, L., Brunsell, P.R., Drake, J.R., Menmuir, S., Cecconello, M., 2007. Spontaneous quasi single helicity regimes in EXTRAP T2R reversed-field pinch. Physics of Plasmas (1994-present) 14, 112510. https://doi.org/10.1063/1.2805450

Frassinetti, L., Gobbin, M., Marrelli, L., Piovesan, P., Franz, P., Martin, P., Chapman, B.E., 2005a. Perturbative transport studies in the reversed-field pinch. Nucl. Fusion 45, 1342. https://doi.org/10.1088/0029-5515/45/11/015

Frassinetti, L., Sun, Y., Fridström, R., Menmuir, S., Olofsson, K.E.J., Brunsell, P.R., Khan, M.W.M., Liang, Y., Drake, J.R., 2015. Braking due to non-resonant magnetic perturbations and comparison with neoclassical toroidal viscosity torque in EXTRAP T2R. Nuclear Fusion 55, 112003. https://doi.org/10.1088/0029-5515/55/11/112003

Frassinetti, L, Terranova, D., Hirano, Y., Koguchi, H., Auriemma, F., Yambe, K., Sakakita, H., 2007a. Cold pulse propagation in a reversed-field pinch. Nuclear Fusion 47, 135–145. https://doi.org/10.1088/0029-5515/47/2/007

Frassinetti, L., Yagi, Y., Koguchi, H., Shimada, T., Hirano, Y., 2004. Performance improvement conditions and their physical origin in the pulsed poloidal current drive regime of the reversed-field pinch device TPE-RX. Physics of Plasmas 11, 5229–5238. https://doi.org/10.1063/1.1796731

Frassinetti, L., Yagi, Y., Koguchi, H., Shimada, T., Hirano, Y., Sakakita, H., 2006. Toroidally localized soft x-ray expulsion at the termination of the improved confinement regime in the TPE-RX reversed-field pinch experiment. Physics of Plasmas (1994-present) 13, 042502. https://doi.org/10.1063/1.2188397

Frassinetti, L., Yagi, Y., Koguchi, H., Shimada, T., Hirano, Y., Sakakita, H., 2005b. Role of locked mode in the effectiveness of pulsed poloidal current drive regime in the reversed-field pinch. Physics of Plasmas (1994-present) 12, 100703. https://doi.org/10.1063/1.2107027

Frassinetti, L., Yagi, Y., Martin, P., Koguchi, H., Shimada, T., Hirano, Y., Sakakita, H., Asai, T., 2003. Operating Conditions to Achieve High Performance in PPCD in a Reversed-Field Pinch Plasma. J. Phys. Soc. Jpn. 72, 3297–3298. https://doi.org/10.1143/JPSJ.72.3297

Frassinetti, L, Yambe, K., Kiyama, S., Hirano, Y., Koguchi, H., Sakakita, H., 2007b. Turbulence and particle confinement in a reversed-field pinch plasma. Plasma Physics and Controlled Fusion 49, 199–209. https://doi.org/10.1088/0741-3335/49/3/001

Freidberg, J.P., 2013. Ideal magnetohydrodynamics. Springer-Verlag New York, New York.

Fridström, R., Chapman, B.E., Almagri, A.F., Frassinetti, L., Brunsell, P.R., Nishizawa, T., Sarff, J.S., 2018. Dependence of Perpendicular Viscosity on Magnetic Fluctuations in a Stochastic Topology. Phys. Rev. Lett. 120, 225002. https://doi.org/10.1103/PhysRevLett.120.225002

Gaio, E., Luchetta, A., Manduchi, G., Marchiori, G., Peruzzo, S., Toigo, V., 1999. Upgrade for full control of radial magnetic field errors in RFX poloidal gaps, in: 18th IEEE/NPSS

Symposium on Fusion Engineering. Symposium Proceedings (Cat. No.99CH37050). Presented at the 18th IEEE/NPSS Symposium on Fusion Engineering. Symposium Proceedings, IEEE, Albuquerque, NM, USA, pp. 579–582. https://doi.org/10.1109/FUSION.1999.849906

Galante, M.E., Reusch, L.M., Den Hartog, D.J., Franz, P., Johnson, J.R., McGarry, M.B., Nornberg, M.D., Stephens, H.D., 2015. Determination of Z_{eff} by integrating measurements from x-ray tomography and charge exchange recombination spectroscopy. Nuclear Fusion 55, 123016. https://doi.org/10.1088/0029-5515/55/12/123016

Gangadhara, S., Craig, D., Ennis, D.A., Den Hartog, D.J., Fiksel, G., Prager, S.C., 2008. Ion heating during reconnection in the Madison Symmetric Torus reversed field pinch. Physics of Plasmas 15, 056121. https://doi.org/10.1063/1.2884038

Gangadhara, S., Craig, D., Ennis, D.A., Hartog, D.J.D., Fiksel, G., Prager, S.C., 2007. Spatially Resolved Measurements of Ion Heating during Impulsive Reconnection in the Madison Symmetric Torus. Physical Review Letters 98. https://doi.org/10.1103/PhysRevLett.98.075001

Gatto, R., Terry, P.W., Hegna, C.C., 2002. Tearing mode stability with equilibrium flows in the reversed-field pinch. Nuclear Fusion 42, 496–509. https://doi.org/10.1088/0029-5515/42/5/302

Gnesotto, F., Sonato, P., Baker, W.R., Doria, A., Elio, F., Fauri, M., Fiorentin, P., Marchiori, G., Zollino, G., 1995. The plasma system of RFX. Fusion Engineering and Design 25, 335–372. https://doi.org/10.1016/0920-3796(94)00280-K

Gobbin, M., Bonfiglio, D., Boozer, A.H., Cooper, A.W., Escande, D.F., Hirshman, S.P., Lore, J., Lorenzini, R., Marrelli, L., Martin, P., Martines, E., Momo, B., Pomphrey, N., Predebon, I., Puiatti, M.E., Sanchez, R., Spizzo, G., Spong, D.A., Terranova, D., Team, R., 2011a. Three-dimensional equilibria and transport in RFX-mod: A description using stellarator toolsa). Physics of Plasmas (1994-present) 18, 062505. https://doi.org/10.1063/1.3602083

Gobbin, M., Bonfiglio, D., Escande, D.F., Fassina, A., Marrelli, L., Alfier, A., Martines, E., Momo, B., Terranova, D., 2011b. Vanishing Magnetic Shear And Electron Transport Barriers In The RFX-Mod Reversed Field Pinch. Physical Review Letters 106. https://doi.org/10.1103/PhysRevLett.106.025001

Gobbin, M., Carraro, L., Puiatti, M.E., Valisa, M., Franz, P., Momo, B., Terranova, D., 2017. Effect of a helical core topology on impurity behavior in RFX-mod plasmas. Plasma Physics and Controlled Fusion 59, 055011. https://doi.org/10.1088/1361-6587/aa645c

Gobbin, M., Franz, P., Auriemma, F., Lorenzini, R., Marrelli, L., 2015. Spontaneous versus induced hydrogen and deuterium helical shaped plasmas with electron internal transport barriers. Plasma Phys. Control. Fusion 57, 095004. https://doi.org/10.1088/0741-3335/57/9/095004

Gobbin, M., Franz, P., Lorenzini, R., Predebon, I., Ruzzon, A., Fassina, A., Marrelli, L., Momo, B., Terranova, D., 2013. Heat transport in helical RFX-mod plasmas by electron temperature dynamics from soft-x-ray diagnostics. Plasma Phys. Control. Fusion 55, 105010. https://doi.org/10.1088/0741-3335/55/10/105010

Gobbin, M., Guazzotto, L., Guo, S., Predebon, I., Sattin, F., Spizzo, G., Zanca, P., Cappello, S., 2009. Trapped Particles in the Reversed Field Pinch. Journal of Plasma Fusion Research SERIES 8, 1147.

Gobbin, M., Marrelli, L., Martin, P., White, R.B., 2007. Ion and electron local transport inside single helicity islands in the reversed field pinch. Physics of Plasmas (1994-present) 14, 072305. https://doi.org/10.1063/1.2747631

Gobbin, M., Spizzo, G., Marrelli, L., White, R.B., 2010. Neoclassical Transport in the Helical Reversed-Field Pinch. Phys. Rev. Lett. 105, 195006. https://doi.org/10.1103/PhysRevLett.105.195006

Goforth, R.R., Carlstrom, T.N., Chu, C., Curwen, B., Graumann, D., Lee, P.S.C., Nilles, E.J., Ohkawa, T., Schaffer, M.J., Tamano, T., Taylor, P.L., Taylor, T.S., Register, D.F., 1986.

Reversed-field pinch experiments with a resistive shell. Nucl. Fusion 26, 515–517. https://doi.org/10.1088/0029-5515/26/4/011
Greene, P., Robertson, S., 1993a. Spectra and Growth rates of resistive wall modes in a reversed field pinch. Physics of Fluids B: Plasma Physics B5, 556–563. https://doi.org/10.1063/1.860541
Greene, P., Robertson, S., 1993b. Locking of kink modes in a reversed-field pinch. Physics of Fluids B: Plasma Physics 5, 550–555. https://doi.org/10.1063/1.860540
Greenwald, M., 2002. Density limits in toroidal plasmas. Plasma Phys. Control. Fusion 44, R27. https://doi.org/10.1088/0741-3335/44/8/201
Gregoratto, D., Drake, J.R., Yadikin, D., Liu, Y.Q., Paccagnella, R., Brunsell, P.R., Bolzonella, T., Marchiori, G., Cecconello, M., 2005. Studies on the response of resistive-wall modes to applied magnetic perturbations in the EXTRAP T2R reversed field pinch. Physics of Plasmas 12, 092510. https://doi.org/10.1063/1.2061447
Gregoratto, D., Garzotti, L., Innocente, P., Martini, S., Canton, A., 1998. Behaviour of electron density profiles and particle transport analysis in the RFX reversed field pinch. Nuclear Fusion 38, 1199–1213. https://doi.org/10.1088/0029-5515/38/8/307
Guazzotto, L., Betti, R., Manickam, J., Kaye, S., 2004. Numerical study of tokamak equilibria with arbitrary flow. Physics of Plasmas. https://doi.org/10.1063/1.1637918
Guazzotto, L., Paccagnella, R., 2009. Magnetic field profiles in fusion plasmas in the presence of equilibrium flow. Plasma Physics and Controlled Fusion 51, 065013. https://doi.org/10.1088/0741-3335/51/6/065013
Guo, S.C., 2008. Stability threshold of ion temperature gradient driven mode in reversed field pinch plasmas. Physics of Plasmas 15, 122510. https://doi.org/10.1063/1.3039895
Guo, S.C., Chu, M.S., 2004. Study on wall locking of multiple tearing modes in reversed field pinch plasmas. Physics of Plasmas 11, 4050–4063. https://doi.org/10.1063/1.1768553
Guo, S.C., Freidberg, J.P., Nachtrieb, R., 1999. Stability of resistive wall modes in reversed field pinches with longitudinal flow and dissipative effects. Physics of Plasmas 6, 3868–3877. https://doi.org/10.1063/1.873191
Guo, S.C., Xu, X.Y., Wang, Z.R., Liu, Y.Q., 2013. Does shaping bring an advantage for reversed field pinch plasmas? Nucl. Fusion 53, 113035. https://doi.org/10.1088/0029-5515/53/11/113035
Hansen, A.K., Almagri, A.F., Den Hartog, D.J., Prager, S.C., Sarff, J.S., 1998. Locking of multiple resonant mode structures in the reversed-field pinch. Physics of Plasmas 5, 2942–2946. https://doi.org/10.1063/1.873017
Harvey, R.W., McCoy, M.G., Hsu, J.Y., Mirin, A.A., 1981. Electron Dynamics Associated with Stochastic Magnetic and Ambipolar Electric Fields. Physical Review Letters 47, 102–105. https://doi.org/10.1103/PhysRevLett.47.102
Hattori, K., Hayase, K., Sato, Y., 1995. First results of the toroidal divertor experiment on the TPE-2M reversed field pinch. Nuclear Fusion 35, 981–987. https://doi.org/10.1088/0029-5515/35/8/I06
Hattori, K., Hayase, K., Sato, Y., 1994. Poloidal-Open Divertor Experiments on TPE-2M Reversed Field Pinch. Journal of the Physical Society of Japan 63, 2177–2184. https://doi.org/10.1143/JPSJ.63.2177
Hattori, K., Hirano, Y., Shimada, T., Yagi, Y., Maejima, Y., Hirota, I., Ogawa, K., 1991. Behavior of magnetic field fluctuations during dynamo activity and its effect on energy confinement in a reversed-field pinch. Physics of Fluids B: Plasma Physics 3, 3111–3124. https://doi.org/10.1063/1.859791
Hedin, G., 1998. MHD behaviour in a resistive-shell reversed-field pinch. Plasma Phys. Control. Fusion 40, 1529–1539. https://doi.org/10.1088/0741-3335/40/8/006
Hegna, C.C., 1998. Self-consistent mean-field forces in turbulent plasmas: Current and momentum relaxation. Physics of Plasmas 5, 2257–2263. https://doi.org/10.1063/1.873032

Hegna, C.C., 1996. Nonlinear tearing mode interactions and mode locking in reversed-field pinches. Physics of Plasmas 3, 4646–4657. https://doi.org/10.1063/1.872033

Hendries, E.R., Anderson, J.K., Diem, S., Forest, C.B., Harvey, R.W., Reusch, J.A., Seltzman, A.H., Sovinec, C.R., 2014. MHD simulation of RF current drive in MST. AIP Conference Proceedings 1580, 510–513. https://doi.org/10.1063/1.4864600

Hirano, Y., Koguchi, H., Yambe, K., Sakakita, H., Kiyama, S., 2006. Quasi-single helicity state by a small positive pulse of toroidal magnetic field in TPE-RX reversed field pinch experiment. Physics of Plasmas (1994-present) 13, 122511. https://doi.org/10.1063/1.2405343

Hirano, Y., Maejima, Y., Shimada, T., Hirota, I., Yagi, Y., 1996. Improved confinement in a high pinch parameter region of the reversed field pinch plasma. Nucl. Fusion 36, 721. https://doi.org/10.1088/0029-5515/36/6/I04

Hirano, Y., Paccagnella, R., Koguchi, H., Frassinetti, L., Sakakita, H., Kiyama, S., Yagi, Y., 2005. Quasi-single helicity state at shallow reversal in TPE-RX reversed-field pinch experiment. Physics of Plasmas (1994-present) 12, 112501. https://doi.org/10.1063/1.2118728

Hirano, Y., Yagi, Y., Maejima, Y., Shimada, T., Hirota, I., 1997. Self-organization and its effect on confinement in a reversed field pinch plasma. Plasma Phys. Control. Fusion 39, A393. https://doi.org/10.1088/0741-3335/39/5A/036

Hirshman, S.P., 1988. Finite-aspect-ratio effects on the bootstrap current in tokamaks. Physics of Fluids (1958-1988) 31, 3150–3152. https://doi.org/10.1063/1.866973

Ho, Y.L., 1991. Numerical simulation of fluctuation suppression via DC helicity injection in a reversed field pinch. Nucl. Fusion 31, 341. https://doi.org/10.1088/0029-5515/31/2/009

Ho, Y.L., Prager, S.C., 1988. Stability of a reversed field pinch with resistive and distant boundaries. Phys. Fluids 31, 1673. https://doi.org/10.1063/1.866705

Ho, Y.L., Prager, S.C., Schnack, D.D., 1989. Nonlinear behavior of the reversed field pinch with nonideal boundary conditions. Physical Review Letters 62, 1504–1507. https://doi.org/10.1103/PhysRevLett.62.1504

Hokin, S., Almagri, A., Assadi, S., Beckstead, J., Chartas, G., Crocker, N., Cudzinovic, M., Hartog, D.D., Dexter, R., Holly, D., Prager, S., Rempel, T., Sarff, J., Scime, E., Shen, W., Spragins, C., Sprott, C., Starr, G., Stoneking, M., Watts, C., Nebel, R., 1991. Global confinement and discrete dynamo activity in the MST reversed-field pinch. Physics of Fluids B: Plasma Physics (1989-1993) 3, 2241–2246. https://doi.org/10.1063/1.859642

Holmes, J.A., Carreras, B.A., Hender, T.C., Hicks, H.R., Lynch, V.E., An, Z.G., Diamond, P.H., 1985. Nonlinear interaction of tearing modes: A comparison between the tokamak and the reversed field pinch configurations. Physics of Fluids (1958-1988) 28, 261–270. https://doi.org/10.1063/1.865194

Hooper, E.B., Bulmer, R.H., Cohen, B.I., Hill, D.N., Holcomb, C.T., Hudson, B., McLean, H.S., Pearlstein, L.D., Romero-Talamás, C.A., Sovinec, C.R., Stallard, B.W., Wood, R.D., Woodruff, S., 2012. Sustained Spheromak Physics Experiment (SSPX): design and physics results. Plasma Phys. Control. Fusion 54, 113001. https://doi.org/10.1088/0741-3335/54/11/113001

Hörling, P., Hedin, G., Brzozowski, J.H., Tennfors, E., Mazur, S., 1996. Ion temperature, heating and scaling relations at the Extrap-T1 reversed-field pinch. Plasma Phys. Control. Fusion 38, 1725. https://doi.org/10.1088/0741-3335/38/10/003

Howell, R.B., Ingraham, J.C., Wurden, G.A., Weber, P.G., Buchenauer, C.J., 1987. Asymmetric magnetic flux generation, m=1 activity, and edge phenomena on a reversed-field pinch. Phys. Fluids 30, 1828. https://doi.org/10.1063/1.866198

Hudson, B.F., 2006. FAST ION CONFINEMENT IN THE REVERSED FIELD PINCH (Ph.D. Thesis). University of Wisconsin - Madison, Madison, US.

Iida, M., Miyagi, T., Ishijima, D., Mori, A., Ohta, K., Masamune, S., Oshiyama, H., 1994. First results from the poloidal divertor experiment in the STE-2 reversed field pinch. Plasma Physics and Controlled Fusion 36, 153–161. https://doi.org/10.1088/0741-3335/36/1/013

Ikezoe, R., Masamune, S., Oki, K., Sanpei, A., Himura, H., Onchi, T., Hirose, A., 2012. Phase Locking and Unlocking Associated with Transition to Quasi-Single Helicity State in the RELAX Reversed-Field Pinch. J. Phys. Soc. Jpn. 81, 115001. https://doi.org/10.1143/JPSJ.81.115001

Ingraham, J.C., Ellis, R.F., Downing, J.N., Munson, C.P., Weber, P.G., Wurden, G.A., 1990. Energetic electron measurements in the edge of a reversed-field pinch. Physics of Fluids B: Plasma Physics 2, 143–159. https://doi.org/10.1063/1.859526

Innocente, P., Alfier, A., Canton, A., Pasqualotto, R., 2009. Plasma performance and scaling laws in the RFX-mod reversed-field pinch experiment. Nucl. Fusion 49, 115022. https://doi.org/10.1088/0029-5515/49/11/115022

Innocente, P., Alfier, A., Carraro, L., Lorenzini, R., Pasqualotto, R., Terranova, D., Team, the R., 2007. Transport and confinement studies in the RFX-mod reversed-field pinch experiment. Nucl. Fusion 47, 1092. https://doi.org/10.1088/0029-5515/47/9/004

Innocente, P., Bufferand, H., Canton, A., Ciraolo, G., Visonà, N., 2017. Heat flux measurements and modelling in the RFX-mod experiment. Nuclear Materials and Energy 12, 1199–1204. https://doi.org/10.1016/j.nme.2017.01.020

Innocente, P, Lorenzini, R., Terranova, D., Zanca, P., 2017. FLiT: a field line trace code for magnetic confinement devices. Plasma Physics and Controlled Fusion 59, 045014. https://doi.org/10.1088/1361-6587/aa5cc4

Innocente, P., Mansfield, D.K., Roquemore, A.L., Agostini, M., Barison, S., Canton, A., Carraro, L., Cavazzana, R., De Masi, G., Fassina, A., Fiameni, S., Grando, L., Rais, B., Rossetto, F., Scarin, P., 2015. Lithium wall conditioning by high frequency pellet injection in RFX-mod. Journal of Nuclear Materials, PLASMA-SURFACE INTERACTIONS 21Proceedings of the 21st International Conference on Plasma-Surface Interactions in Controlled Fusion Devices Kanazawa, Japan May 26-30, 2014 463, 1138–1141. https://doi.org/10.1016/j.jnucmat.2014.11.088

Innocente, P., Martini, S., Canton, A., Tasinato, L., 1997. Upgrade of the RFX CO_2 interferometer using in-vessel optics for extended edge resolution. Review of Scientific Instruments 68, 694–697. https://doi.org/10.1063/1.1147677

Innocente, P., Zanca, P., Zuin, M., Bolzonella, T., Zaniol, B., 2014. Tearing modes transition from slow to fast rotation branch in the presence of magnetic feedback. Nuclear Fusion 54, 122001. https://doi.org/10.1088/0029-5515/54/12/122001

Intravaia, A., Marrelli, L., Martin, P., Pasqualotto, R., Franz, P., Murari, A., Spizzo, G., Bolzonella, T., Canton, A., Innocente, P., Martini, S., Puiatti, M.E., Scarin, P., Terranova, D., Valisa, M., 1999. Scaling of Local Core Transport with Lundquist Number in the Reversed Field Pinch. Physical Review Letters 83, 5499–5502. https://doi.org/10.1103/PhysRevLett.83.5499

Ishijima, D., Iida, M., Masamune, S., Oda, N., Tanonaka, A., Oshiyama, H., 1995. Heat flux studies in a poloidal-divertor reversed-field pinch. Plasma Physics and Controlled Fusion 37, 657–666. https://doi.org/10.1088/0741-3335/37/6/005

Jarboe, T.R., 2017. Steady Inductive Helicity Injection and Its Application to a High-Beta Spheromak. Fusion Technology. https://doi.org/10.13182/FST99-A94

Jarboe, T.R., 1994. Review of spheromak research. Plasma Physics and Controlled Fusion 36, 945–990. https://doi.org/10.1088/0741-3335/36/6/002

Jensen, T.H., Chu, M.S., 1984. Current drive and helicity injection. The Physics of Fluids 27, 2881–2885. https://doi.org/10.1063/1.864602

Ji, H., 1994. Time-Resolved Observation of Discrete and Continuous Magnetohydrodynamic Dynamo in the Reversed-Field Pinch Edge. Phys. Rev. Lett. 73, 668–671. https://doi.org/10.1103/PhysRevLett.73.668

Ji, H., Prager, S.C., Almagri, A.F., Sarff, J.S., Yagi, Y., Hirano, Y., Hattori, K., Toyama, H., 1996. Measurement of the dynamo effect in a plasma. Physics of Plasmas 3, 1935–1942. https://doi.org/10.1063/1.871989

Ji, H, Prager, S.C., Sarff, J.S., 1995, 1995. Conservation of Magnetic helicity during Plasma Relaxation. Phys. Rev. Lett. 74, 2945.

Jiang, Z.X., Bondeson, A., Paccagnella, R., 1995. Stability of current-driven modes in reversed field pinches with resistive walls and plasma rotation. Physics of Plasmas 2, 442–449. https://doi.org/10.1063/1.870969

Kaufman, M.C., 2005. Lower Hybrid Experiments on MST, in: AIP Conference Proceedings. Presented at the RADIO FREQUENCY POWER IN PLASMAS: 16th Topical Conference on Radio Frequency Power in Plasmas, AIP, Park City, Utah (USA), pp. 319–322. https://doi.org/10.1063/1.2098248

Kaufman, M.C., Goetz, J.A., Burke, D.R., Almagri, A.F., Oliva, S.P., Kulpin, J.G., Ryan, P.M., Rasmussen, D., 2007. Validating the Lower Hybrid Interdigital-line Antenna on MST, in: AIP Conference Proceedings. Presented at the RADIO FREQUENCY POWER IN PLASMAS: 17th Topical Conference on Radio Frequency Power in Plasmas, AIP, Clearwater (Florida), pp. 309–312. https://doi.org/10.1063/1.2800500

Kim, J.-H., Terry, P.W., 2012. Magnetic turbulence suppression by a helical mode in a cylindrical geometry. Physics of Plasmas 19, 122304. https://doi.org/10.1063/1.4769369

King, J.R., Sovinec, C.R., Mirnov, V.V., 2011. First-order finite-Larmor-radius effects on magnetic tearing in pinch configurations. Physics of Plasmas (1994-present) 18, 042303. https://doi.org/10.1063/1.3571599

Kislov, D.A., Esipchuk, Y.V., Kirneva, N.A., Klimanov, I.V., Pavlov, Y.D., Subbotin, A.A., Alikaev, V.V., Borshegovskiy, A.A., Gott, Y.V., Kakurin, A.M., Krilov, S.V., Myalton, T.B., Roy, I.N., Trukhina, E.V., Volkov, V.V., Team, T.-10, 2001. Beta limit due to resistive tearing modes in T-10. Nucl. Fusion 41, 1619. https://doi.org/10.1088/0029-5515/41/11/311

K nig, R., Grigull, P., McCormick, K., Feng, Y., Kisslinger, J., Komori, A., Masuzaki, S., Matsuoka, K., Obiki, T., Ohyabu, N., Renner, H., Sardei, F., Wagner, F., Werner, A., 2002. The divertor program in stellarators. Plasma Physics and Controlled Fusion 44, 2365–2422. https://doi.org/10.1088/0741-3335/44/11/306

Ko, J., Den Hartog, D.J., Goetz, J.A., Weix, P.J., Limbach, S.T., 2013. First gaseous boronization during pulsed discharge cleaning. Journal of Nuclear Materials 432, 146–151. https://doi.org/10.1016/j.jnucmat.2012.07.040

Koguchi, H., Sakakita, H., Kiyama, S., Yambe, K., Asai, T., Hirano, Y., Auriemma, F., Terranova, D., Innocente, P., 2009. High Beta and High Density Operation in TPE-RX. Plasma and Fusion Research 4, 022–022. https://doi.org/10.1585/pfr.4.022

Koguchi, H., Terranova, D., Innocente, P., Lorenzini, R., Sakakita, H., Asai, T., Yagi, Y., Hirano, Y., Yambe, K., 2006. Deuterium Ice Pellet Injection during Pulsed Poloidal Current Drive Operation in Toroidal Pinch Experiment-RX Reversed-Field Pinch Device. Jpn. J. Appl. Phys. 45, L1124. https://doi.org/10.1143/JJAP.45.L1124

Koliner, J.J., Forest, C.B., Sarff, J.S., Anderson, J.K., Liu, D., Nornberg, M.D., Waksman, J., Lin, L., Brower, D.L., Ding, W.X., Spong, D.A., 2012. Fast-Particle-Driven Alfvénic Modes in a Reversed Field Pinch. Physical Review Letters 109. https://doi.org/10.1103/PhysRevLett.109.115003

Koslowski, H.R., Fuchs, G., Jaspers, R., Krämer-Flecken, A., Messiaen, A.M., Ongena, J., Rapp, J., Schüller, F.C., Tokar', M.Z., 2000. MHD activity at the beta limit in RI mode discharges on TEXTOR-94. Nucl. Fusion 40, 821. https://doi.org/10.1088/0029-5515/40/4/307

Kuldkepp, M., Brunsell, P.R., Cecconello, M., Dux, R., Menmuir, S., Rachlew, E., 2006. Measurements and modeling of transport and impurity radial profiles in the EXTRAP T2R reversed field pinch. Physics of Plasmas 13, 092506. https://doi.org/10.1063/1.2349304

Kumar, S.T.A., Den Hartog, D.J., Mirnov, V.V., Caspary, K.J., Magee, R.M., Brower, D.L., Chapman, B.E., Craig, D., Ding, W.X., Eilerman, S., Fiksel, G., Lin, L., Nornberg, M., Parke, E., Reusch, J.A., Sarff, J.S., 2012a. Classical confinement and outward convection of impurity ions in the MST RFP. Physics of Plasmas 19, 056121. https://doi.org/10.1063/1.4718310

Kumar, S.T.A., Den Hartog, D.J., Caspary, K.J., Magee, R.M., Mirnov, V.V., Chapman, B.E., Craig, D., Fiksel, G., Sarff, J.S., 2012b. Classical Impurity Ion Confinement in a Toroidal Magnetized Fusion Plasma. Physical Review Letters 108. https://doi.org/10.1103/PhysRevLett.108.125006

Kusano, K., Sato, T., 1990. Simulation study of the self-sustainment mechanism in the reversed field pinch configuration. Nucl. Fusion 30, 2075–2096. https://doi.org/10.1088/0029-5515/30/10/009

Kusano, K., Sato, T., 1986. Simulation study of the self-reversal process in the reversed-field pinch based on a non-linearly driven reconnection model. Nuclear Fusion 26, 1051–1061. https://doi.org/10.1088/0029-5515/26/8/005

Kusano, K., Tamano, T., Sato, T., 1991. MHD simulation of the toroidal phase locking mechanism in a reversed field pinch plasma. Nuclear Fusion 31, 1923–1932. https://doi.org/10.1088/0029-5515/31/10/010

La Haye, R.J., Lee, P.S., Schaffer, M.J., Tamano, T., Taylor, P.L., 1988. Magnetic fluctuation measurements in the thin resistive shell OHTE device operated as a reversed field pinch. Nuclear Fusion Letters 28, 918–922.

Lanier, N.E., Craig, D., Anderson, J.K., Biewer, T.M., Chapman, B.E., Den Hartog, D.J., Forest, C.B., Prager, S.C., Brower, D.L., Jiang, Y., 2001. An investigation of density fluctuations and electron transport in the Madison Symmetric Torus reversed-field pinch. Physics of Plasmas 8, 3402–3410. https://doi.org/10.1063/1.1378328

Lanier, N.E., Craig, D., Anderson, J.K., Biewer, T.M., Chapman, B.E., Den Hartog, D.J., Forest, C.B., Prager, S.C., Brower, D.L., Jiang, Y., 2000. Control of Density Fluctuations and Electron Transport in the Reversed-Field Pinch. Physical Review Letters 85, 2120–2123. https://doi.org/10.1103/PhysRevLett.85.2120

Larsson, D., Bergsåker, H., Hokin, S., Brunsell, P., Drake, J., Möller, A., 1997. Surface modification by solid target boronisation in the Extrap T2 experiment. Vacuum 48, 693–695. https://doi.org/10.1016/S0042-207X(97)00058-4

Lei, J., Schoch, P.M., Demers, D.R., Shah, U., Connor, K.A., Anderson, J.K., Crowley, T.P., 2002. Core Electrostatic Fluctuations and Particle Transport in a Reversed-Field Pinch. Physical Review Letters 89. https://doi.org/10.1103/PhysRevLett.89.275001

Li, G., Drake, J.R., Bergsåker, H., Brzozowski, J.H., Hellblom, G., Mazur, S., Möller, A., Nordlund, P., 1995. Correlation between internal tearing modes and edge electrostatic fluctuations in a reversed-field pinch. Physics of Plasmas 2, 2615–2617. https://doi.org/10.1063/1.871224

Lianghua, Y., Dawei, Z., Beibin, F., Chengyuan, C., Yan, Z., Xiaoyu, H., Yonggao, L., Bucalossi, J., Xuru, D., 2010. Comparison of Supersonic Molecular Beam Injection from Both Low Field Side and High Field Side of HL-2A. Plasma Sci. Technol. 12, 529. https://doi.org/10.1088/1009-0630/12/5/04

Lipschultz, B., 1987. Review of MARFE phenomena in tokamaks. Journal of Nuclear Materials 145–147, 15–25. https://doi.org/10.1016/0022-3115(87)90306-0

Liu, S.F., Guo, S.C., Zhang, C.L., Dong, J.Q., Carraro, L., Wang, Z.R., 2011. Impurity effects on the ion temperature gradient mode in reversed-field pinch plasmas. Nucl. Fusion 51, 083021. https://doi.org/10.1088/0029-5515/51/8/083021

Liu, Y.Q., Bondeson, A., Fransson, C.M., Lennartson, B., Breitholtz, C., 2000. Feedback stabilization of nonaxisymmetric resistive wall modes in tokamaks. I. Electromagnetic model. Physics of Plasmas 7, 3681. https://doi.org/10.1063/1.1287744

Loarer, T., Tsitrone, E., Pegourie, B., Owen, L.W., Chappuis, P., Chatelier, M., Cordier, J.J., Ghendrih, P., A. Grosman, Guilhem, D., Mioduszewski, P.K., 1996. Particle exhaust with a vented pump limiter on Tore Supra. Nucl. Fusion 36, 225. https://doi.org/10.1088/0029-5515/36/2/I09

Lorenzini, R., Agostini, M., Alfier, A., Antoni, V., Apolloni, L., Auriemma, F., Barana, O., Baruzzo, M., Bettini, P., Bonfiglio, D., Bolzonella, T., Bonomo, F., Brombin, M., Buffa, A., Canton, A., Cappello, S., Carraro, L., Cavazzana, R., Chitarin, G., Bello, S.D., Lorenzi, A.D., Masi, G.D., Escande, D.F., Fassina, A., Franz, P., Gaio, E., Gazza, E., Giudicotti, L., Gnesotto, F., Gobbin, M., Grando, L., Guo, S.C., Innocente, P., Luchetta, A., Manduchi, G., Marchiori, G., Marcuzzi, D., Marrelli, L., Martin, P., Martini, S., Martines, E., Milani, F., Moresco, M., Novello, L., Ortolani, S., Paccagnella, R., Pasqualotto, R., Peruzzo, S., Piovan, R., Piovesan, P., Piron, L., Pizzimenti, A., Pomaro, N., Predebon, I., Puiatti, M.E., Rostagni, G., Sattin, F., Scarin, P., Serianni, G., Sonato, P., Spada, E., Soppelsa, A., Spagnolo, S., Spizzo, G., Spolaore, M., Taliercio, C., Terranova, D., Toigo, V., Valisa, M., Veltri, P., Vianello, N., Zaccaria, P., Zaniol, B., Zanotto, L., Zilli, E., Zuin, M., 2009a. Improvement of the magnetic configuration in the reversed field pinch through successive bifurcationsa). Physics of Plasmas (1994-present) 16, 056109. https://doi.org/10.1063/1.3082821

Lorenzini, R., Agostini, M., Auriemma, F., Carraro, L., Masi, G.D., Fassina, A., Franz, P., Gobbin, M., P. Innocente, Puiatti, M.E., Scarin, P., Zaniol, B., Zuin, M., 2015. The isotope effect in the RFX-mod experiment. Nucl. Fusion 55, 043012. https://doi.org/10.1088/0029-5515/55/4/043012

Lorenzini, R., Alfier, A., Auriemma, F., Fassina, A., Franz, P., Innocente, P., López-Bruna, D., Martines, E., Momo, B., Pereverzev, G., Piovesan, P., Spizzo, G., Spolaore, M., Terranova, D., 2012. On the energy transport in internal transport barriers of RFP plasmas. Nuclear Fusion 52, 062004. https://doi.org/10.1088/0029-5515/52/6/062004

Lorenzini, R., Auriemma, F., Fassina, A., Martines, E., Terranova, D., Sattin, F., 2016. Internal Transport Barrier Broadening through Subdominant Mode Stabilization in Reversed Field Pinch Plasmas. Physical Review Letters 116. https://doi.org/10.1103/PhysRevLett.116.185002

Lorenzini, R, Auriemma, F., Innocente, P., Martines, E., Martini, S., Terranova, D., 2008. Confinement loss during dynamo relaxation event in RFX-mod. Plasma Physics and Controlled Fusion 50, 035004. https://doi.org/10.1088/0741-3335/50/3/035004

Lorenzini, R., Garzotti, L., Pégourié, B., Innocente, P., Martini, S., 2002. Analysis and modelling of plasma response to pellet injection in RFX. Plasma Physics and Controlled Fusion 44, 233–252. https://doi.org/10.1088/0741-3335/44/2/307

Lorenzini, R., Martines, E., Piovesan, P., Terranova, D., Zanca, P., Zuin, M., Alfier, A., Bonfiglio, D., Bonomo, F., Canton, A., Cappello, S., Carraro, L., Cavazzana, R., Escande, D.F., Fassina, A., Franz, P., Gobbin, M., Innocente, P., Marrelli, L., Pasqualotto, R., Puiatti, M.E., Spolaore, M., Valisa, M., Vianello, N., Martin, P., Apolloni, L., Adamek, J., Agostini, M., Annibaldi, S.V., Antoni, V., Auriemma, F., Barana, O., Baruzzo, M., Bettini, P., Bolzonella, T., Brombin, M., Brotankova, J., Buffa, A., Buratti, P., Cavinato, M., Chapman, B.E., Chitarin, G., Bello, S.D., Lorenzi, A.D., Masi, G.D., Ferro, A., Gaio, E., Gazza, E., Giudicotti, L., Gnesotto, F., Grando, L., Guazzotto, L., Guo, S.C., Igochine, V., Liu, Y.Q., Luchetta, A., Manduchi, G., Marchiori, G., Marcuzzi, D., Martini, S., McCollam, K., Milani, F., Moresco, M., Novello, L., Ortolani, S., Paccagnella, R., Peruzzo, S., Piovan, R., Piron, L., Pizzimenti, A., Pomaro, N., Predebon, I., Reusch, J.A., Rostagni, G., Rubinacci, G., Sarff, J.S., Sattin, F., Scarin, P., Serianni, G., Sonato, P., Spada, E., Soppelsa, A., Spagnolo, S., Spizzo, G., Taliercio, C., Toigo, V., Villone, F., White, R.B., Yadikin, D., Zaccaria, P., Zamengo, A., Zaniol, B., Zanotto, L., Zilli, E., Zohm, H., 2009b. Self-

organized helical equilibria as a new paradigm for ohmically heated fusion plasmas. Nat Phys 5, 570–574. https://doi.org/10.1038/nphys1308

Lorenzini, R., Terranova, D., Alfier, A., Innocente, P., Martines, E., Pasqualotto, R., Zanca, P., 2008. Single-Helical-Axis States in Reversed-Field-Pinch Plasmas. Phys. Rev. Lett. 101, 025005. https://doi.org/10.1103/PhysRevLett.101.025005

Malmberg, J.-A., Brunsell, P.R., Yagi, Y., Koguchi, H., 2000. Locked modes in two reversed-field pinch devices of different size and shell system. Physics of Plasmas 7, 4184–4196. https://doi.org/10.1063/1.1290281

Mansfield, D.K., Hill, K.W., Strachan, J.D., Bell, M.G., Scott, S.D., Budny, R., Marmar, E.S., Snipes, J.A., Terry, J.L., Batha, S., Bell, R.E., Bitter, M., Bush, C.E., Chang, Z., Darrow, D.S., Ernst, D., Fredrickson, E., Grek, B., Herrmann, H.W., Janos, A., Jassby, D.L., Jobes, F.C., Johnson, D.W., Johnson, L.C., Levinton, F.M., Mikkelsen, D.R., Mueller, D., Owens, D.K., Park, H., Ramsey, A.T., Roquemore, A.L., Skinner, C.H., Stevenson, T., Stratton, B.C., Synakowski, E., Taylor, G., von Halle, A., von Goeler, S., Wong, K.L., Zweben, S.J., TFTR Group, 1996. Enhancement of Tokamak Fusion Test Reactor performance by lithium conditioning. Physics of Plasmas 3, 1892–1897. https://doi.org/10.1063/1.871984

Marchiori, G., Baruzzo, M., Bolzonella, T., Liu, Y.Q., Soppelsa, A., Villone, F., 2012. Dynamic simulator of RWM control for fusion devices: modelling and experimental validation on RFX-mod. Nuclear Fusion 52, 023020. https://doi.org/10.1088/0029-5515/52/2/023020

Marrelli, L., Cavazzana, R., Bonfiglio, D., Gobbin, M., Marchiori, G., Peruzzo, S., Puiatti, M.E., Spizzo, G., Voltolina, D., Zanca, P., Zuin, M., Berton, G., Bettini, P., Bolzonella, T., Canton, A., Cappello, S., Carraro, L., Cordaro, L., Dal Bello, S., Dalla Palma, M., De Masi, G., Fassina, A., Gnesotto, F., Grando, L., Innocente, P., Lunardon, F., Manduchi, G., Marcuzzi, D., Marconato, N., Piovan, R., Pomaro, N., Rigoni, A., Rizzolo, A., Scarin, P., Siragusa, M., Sonato, P., Spagnolo, S., Spolaore, M., Terranova, D., the RFX-Mod Team, 2019. Upgrades of the RFX-mod reversed field pinch and expected scenario improvements. Nuclear Fusion 59, 076027. https://doi.org/10.1088/1741-4326/ab1c6a

Marrelli, L., Frassinetti, L., Martin, P., Craig, D., Sarff, J.S., 2005. Reduced intermittency in the magnetic turbulence of reversed field pinch plasmas. Physics of Plasmas 12, 030701. https://doi.org/10.1063/1.1850475

Marrelli, Lionello, Marchiori, G., Bettini, P., Cavazzana, R., Kapidani, B., Grando, L., Marconato, N., Specogna, R., Voltolina, D., 2019. Optimization of RFX-mod2 gap configuration by estimating the magnetic error fields due to the passive structure currents. Fusion Engineering and Design 146, 680–683. https://doi.org/10.1016/j.fusengdes.2019.01.054

Marrelli, L., Martin, P., Spizzo, G., Franz, P., Chapman, B.E., Craig, D., Sarff, J.S., Biewer, T.M., Prager, S.C., Reardon, J.C., 2002. Quasi-single helicity spectra in the Madison Symmetric Torus. Physics of Plasmas (1994-present) 9, 2868–2871. https://doi.org/10.1063/1.1482766

Marrelli, L., Zanca, P., Martin, P., Martini, S., Murari, A., 1999. Edge localised asymmetric radiative phenomena in RFX. Journal of Nuclear Materials 266–269, 877–883. https://doi.org/10.1016/S0022-3115(98)00554-6

Marrelli, L, Zanca, P., Valisa, M., Marchiori, G., Alfier, A., Bonomo, F., Gobbin, M., Piovesan, P., Terranova, D., Agostini, M., Alessi, C., Antoni, V., Apolloni, L., Auriemma, F., Barana, O., Bettini, P., Bolzonella, T., Bonfiglio, D., Brombin, M., Buffa, A., Canton, A., Cappello, S., Carraro, L., Cavazzana, R., Cavinato, M., Chitarin, G., Dal Bello, S., De Lorenzi, A., Escande, D.F., Fassina, A., Franz, P., Gadani, G., Gaio, E., Gazza, E., Giudicotti, L., Gnesotto, F., Grando, L., Guo, S.C., Innocente, P., Lorenzini, R., Luchetta, A., Malesani, G., Manduchi, G., Marcuzzi, D., Martin, P., Martini, S., Martines, E., Masiello, A., Milani, F., Moresco, M., Murari, A., Novello, L., Ortolani, S., Paccagnella, R., Pasqualotto, R., Peruzzo, S., Piovan, R., Pizzimenti, A., Pomaro, N., Predebon, I., Puiatti, M.E., Rostagni, G., Sattin, F., Scarin, P., Serianni, G., Sonato, P., Spada, E., Soppelsa, A., Spizzo, G., Spolaore, M., Taccon, C., Taliercio, C., Toigo, V., Vianello, N., Zaccaria, P., Zaniol, B.,

Zanotto, L., Zilli, E., Zollino, G., Zuin, M., 2007. Magnetic self organization, MHD active control and confinement in RFX-mod. Plasma Physics and Controlled Fusion 49, B359–B369. https://doi.org/10.1088/0741-3335/49/12B/S33

Marrelli, L., Zanca, P., Valisa, M., Marchiori, G., Alfier, A., Bonomo, F., Gobbin, M., Piovesan, P., Terranova, D., M Agostini, Alessi, C., Antoni, V., Apolloni, L., Auriemma, F., Barana, O., Bettini, P., Bolzonella, T., Bonfiglio, D., M Brombin, Buffa, A., Canton, A., Cappello, S., Carraro, L., Cavazzana, R., Cavinato, M., Chitarin, G., Bello, S.D., Lorenzi, A.D., Escande, D.F., Fassina, A., Franz, P., Gadani, G., Gaio, E., Gazza, E., Giudicotti, L., Gnesotto, F., Grando, L., Guo, S.C., Innocente, P., Lorenzini, R., Luchetta, A., Malesani, G., Manduchi, G., Marcuzzi, D., Martin, P., Martini, S., E Martines, Masiello, A., Milani, F., Moresco, M., Murari, A., Novello, L., Ortolani, S., Paccagnella, R., Pasqualotto, R., S Peruzzo, Piovan, R., Pizzimenti, A., Pomaro, N., Predebon, I., Puiatti, M.E., Rostagni, G., Sattin, F., Scarin, P., G Serianni, Sonato, P., Spada, E., Soppelsa, A., Spizzo, G., Spolaore, M., Taccon, C., Taliercio, C., Toigo, V., Vianello, N., P Zaccaria, Zaniol, B., Zanotto, L., Zilli, E., Zollino, G., Zuin, M., 2007. Magnetic self organization, MHD active control and confinement in RFX-mod. Plasma Phys. Control. Fusion 49, B359. https://doi.org/10.1088/0741-3335/49/12B/S33

Martin, P., 2011. Lessons from the RFP on Magnetic Feedback Control of Plasma Stability. Fusion Science and Technology 59, 602–616. https://doi.org/10.13182/FST11-A11700

Martin, P., 1999. Magnetic and thermal relaxation in the reversed field pinch. Plasma Phys. Control. Fusion 41, A247. https://doi.org/10.1088/0741-3335/41/3A/018

Martin, P., 133 others, 2011. Overview of the RFX fusion science program. Nuclear Fusion 51, 094023. https://doi.org/10.1088/0029-5515/51/9/094023

Martin, P., Apolloni, L., Puiatti, M.E., Adamek, J., Agostini, M., Alfier, A., Annibaldi, S.V., Antoni, V., F. Auriemma, Barana, O., Baruzzo, M., Bettini, P., Bolzonella, T., Bonfiglio, D., Bonomo, F., Brombin, M., J. Brotankova, Buffa, A., Buratti, P., Canton, A., Cappello, S., Carraro, L., Cavazzana, R., Cavinato, M., B.E. Chapman, Chitarin, G., Bello, S.D., Lorenzi, A.D., Masi, G.D., Escande, D.F., Fassina, A., Ferro, A., P. Franz, Gaio, E., Gazza, E., Giudicotti, L., Gnesotto, F., Gobbin, M., Grando, L., Guazzotto, L., Guo, S.C., V. Igochine, Innocente, P., Liu, Y.Q., Lorenzini, R., Luchetta, A., Manduchi, G., Marchiori, G., Marcuzzi, D., L. Marrelli, Martini, S., Martines, E., McCollam, K., Menmuir, S., Milani, F., Moresco, M., Novello, L., S. Ortolani, Paccagnella, R., Pasqualotto, R., Peruzzo, S., Piovan, R., Piovesan, P., Piron, L., Pizzimenti, A., N. Pomaro, Predebon, I., Reusch, J.A., Rostagni, G., Rubinacci, G., Sarff, J.S., Sattin, F., Scarin, P., G. Serianni, Sonato, P., Spada, E., Soppelsa, A., Spagnolo, S., Spolaore, M., Spizzo, G., Taliercio, C., D. Terranova, Toigo, V., Valisa, M., Vianello, N., Villone, F., White, R.B., Yadikin, D., Zaccaria, P., Zamengo, A., P. Zanca, Zaniol, B., Zanotto, L., Zilli, E., Zohm, H., Zuin, M., 2009. Overview of RFX-mod results. Nucl. Fusion 49, 104019. https://doi.org/10.1088/0029-5515/49/10/104019

Martin, P., Buffa, A., Cappello, S., D'Angelo, F., Escande, D.F., Franz, P., Marrelli, L., Martines, E., Ortolani, S., Spizzo, G., Bilato, R., Bolzonella, T., Costa, S., Murari, A., Paccagnella, R., Pasqualotto, R., Terranova, D., Zanca, P., 2000. Quasi-single helicity states in the reversed field pinch: Beyond the standard paradigm. Physics of Plasmas (1994-present) 7, 1984–1992. https://doi.org/10.1063/1.874054

Martin, P., Marrelli, L., Spizzo, G., Franz, P., Piovesan, P., Predebon, I., Bolzonella, T., Cappello, S., A. Cravotta, Escande, D.F., Frassinetti, L., Ortolani, S., Paccagnella, R., Terranova, D., team, the R., B.E. Chapman, Craig, D., Prager, S.C., Sarff, J.S., team, the M., Brunsell, P., Malmberg, J.-A., Drake, J., team, the E.T., Yagi, Y., Koguchi, H., Hirano, Y., team, the T.-R., White, R.B., Sovinec, C., Xiao, C., Nebel, R.A., D.D. Schnack, 2003. Overview of quasi-single helicity experiments in reversed field pinches. Nucl. Fusion 43, 1855. https://doi.org/10.1088/0029-5515/43/12/028

Martin, P., Martini, S., Antoni, V., Apolloni, L., Bagatin, M., Baker, W., Barana, O., Bartiromo, R., Bettini, P., A. Boboc, Bolzonella, T., Buffa, A., Canton, A., Cappello, S., Carraro, L., Cavazzana, R., Chitarin, G., Costa, S., F. D'Angelo, Bello, S.D., Lorenzi, A.D., Desideri, D., Escande, D., Fattorini, L., Fiorentin, P., Franz, P., E. Gaio, Garzotti, L., Giudicotti, L., Gnesotto, F., Grando, L., Guo, S.C., Innoccente, P., Intravaia, A., R. Lorenzini, Luchetta, A., Malesani, G., Manduchi, G., Marchiori, G., Marrelli, L., Martines, E., Maschio, A., A. Masiello, Milani, F., Moresco, M., Murari, A., Nielsen, P., O'Gorman, M., Ortolani, S., Paccagnella, R., R. Pasqualotto, Pégourié, B., Peruzzo, S., Piovan, R., Pomaro, N., Ponno, A., Preti, G., Puiatti, M.E., Rostagni, G., F. Sattin, Scarin, P., Serianni, G., Sonato, P., Spada, E., Spizzo, G., Spolaore, M., Taliercio, C., Telesca, G., D. Terranova, Toigo, V., Tramontin, L., Valisa, M., Vianello, N., Viterbo, M., Zabeo, L., Zaccaria, P., Zanca, P., B. Zaniol, Zanotto, L., Zilli, E., Zollino, G., 2002. New insights into MHD dynamics of magnetically confined plasmas from experiments in RFX. Nucl. Fusion 42, 247. https://doi.org/10.1088/0029-5515/42/3/304

Martines, E., Lorenzini, R., Momo, B., Munaretto, S., Innocente, P., Spolaore, M., 2010. The plasma boundary in single helical axis RFP plasmas. Nucl. Fusion 50, 035014. https://doi.org/10.1088/0029-5515/50/3/035014

Martines, E., Lorenzini, R., Momo, B., Terranova, D., Zanca, P., Alfier, A., Bonomo, F., Canton, A., Fassina, A., Franz, P., Innocente, P., 2011. Equilibrium reconstruction for single helical axis reversed field pinch plasmas. Plasma Phys. Control. Fusion 53, 035015. https://doi.org/10.1088/0741-3335/53/3/035015

Martines, E., Spagnolo, S., 2008. One-dimensional simulations of reversed field pinch discharges. Physics of Plasmas 15, 122506. https://doi.org/10.1063/1.3040015

Martini, S., Agostini, M., Alessi, C., Alfier, A., Antoni, V., Apolloni, L., Auriemma, F., Bettini, P., Bolzonella, T., Bonfiglio, D., Bonomo, F., Brombin, M., Buffa, A., Canton, A., Cappello, S., Carraro, L., Cavazzana, R., Cavinato, M., Chitarin, G., Cravotta, A., Bello, S.D., Lorenzi, A.D., Pasqual, L.D., Escande, D.F., Fassina, A., Franz, P., Gadani, G., Gaio, E., Garzotti, L., Gazza, E., Giudicotti, L., Gnesotto, F., Gobbin, M., Grando, L., Guo, S.C., Innocente, P., Lorenzini, R., Luchetta, A., Malesani, G., Manduchi, G., Marchiori, G., Marcuzzi, D., Marrelli, L., Martin, P., Martines, E., Masiello, A., Milani, F., Moresco, M., Murari, A., Novello, L., Ortolani, S., Paccagnella, R., Pasqualotto, R., Peruzzo, S., Piovan, R., Piovesan, P., Pizzimenti, A., Pomaro, N., Puiatti, M.E., Rostagni, G., Sattin, F., Scarin, P., Serianni, G., Sonato, P., Spada, E., Soppelsa, A., Spizzo, G., Spolaore, M., Taccon, C., Taliercio, C., Terranova, D., Toigo, V., Valisa, M., Vianello, N., Zaccaria, P., Zanca, P., Zaniol, B., Zanotto, L., Zilli, E., Zollino, G., Zuin, M., 2007. Active MHD control at high currents in RFX-mod. Nucl. Fusion 47, 783. https://doi.org/10.1088/0029-5515/47/8/008

Martini, S. et al., 1999a. Oscillating Poloidal Current Drive Experiments in RFX, in: 26th EPS Conf. on Contr. Fusion and Plasma Physics. Presented at the 26th EPS Conf. on Contr. Fusion and Plasma Physics, Maastricht 14-18 June 1999, p. ECA 23J, 1137-1140.

Martini, S., Terranova, D., Innocente, P., Bolzonella, T., 1999b. Spontaneous and driven reduced turbulence modes in the RFX reversed field pinch. Plasma Phys. Control. Fusion 41, A315. https://doi.org/10.1088/0741-3335/41/3A/025

Masamune, S, Iida, M., Ohfuji, Y., Ohta, K., Oshiyama, H., 1998. RFP plasma response to external helical perturbations. Plasma Physics and Controlled Fusion 40, 127–137. https://doi.org/10.1088/0741-3335/40/1/007

Masamune, Sadao, Iida, M., Ohta, K., Oshiyama, H., 1998. Magnetic Island in Helically Perturbed Force-Free Equilibrium. J. Phys. Soc. Jpn. 67, 2977–2980. https://doi.org/10.1143/JPSJ.67.2977

Masamune, S., Sanpei, A., Ikezoe, R., Onchi, T., Murata, K.-I., Oki, K., Shimazu, H., Yamashita, T., Himura, H., 2007. Characterization of Initial Low-Aspect Ratio RFP Plasmas in "RELAX." J. Phys. Soc. Jpn. 76, 123501. https://doi.org/10.1143/JPSJ.76.123501

Masi, G.D., Martines, E., Spolaore, M., Vianello, N., Cavazzana, R., Innocente, P., Momo, B., Spagnolo, S., Zuin, M., 2013. Electrostatic properties and active magnetic topology modification in the RFX-mod edge plasma. Nuclear Fusion 53, 083026. https://doi.org/10.1088/0029-5515/53/8/083026

Mazzitelli, G., Apicella, M.L., Ridolfini, V.P., Apruzzese, G., De Angelis, R., Frigione, D., Giovannozzi, E., Gabellieri, L., Granucci, G., Mazzotta, C., Marinucci, M., Romano, A., Tudisco, O., Alekseyev, A., Ljublinski, I., Vertkov, A., 2010. Review of FTU results with the liquid lithium limiter. Fusion Engineering and Design 85, 896–901. https://doi.org/10.1016/j.fusengdes.2010.08.038

McCollam, K.J., Anderson, J.K., Blair, A.P., Craig, D., Den Hartog, D.J., Ebrahimi, F., O'Connell, R., Reusch, J.A., Sarff, J.S., Stephens, H.D., Stone, D.R., Brower, D.L., Deng, B.H., Ding, W.X., 2010. Equilibrium evolution in oscillating-field current-drive experiments. Physics of Plasmas 17, 082506-082506–13. https://doi.org/doi:10.1063/1.3461167

McCollam, K.J., Blair, A.P., Prager, S.C., Sarff, J.S., 2006. Oscillating-Field Current-Drive Experiments in a Reversed Field Pinch. Phys. Rev. Lett. 96, 035003. https://doi.org/10.1103/PhysRevLett.96.035003

Menmuir, S., Carraro, L., Alfier, A., Bonomo, F., Fassina, A., Spizzo, G., Vianello, N., 2010. Impurity transport studies in RFX-mod multiple helicity and enhanced confinement QSH regimes. Plasma Phys. Control. Fusion 52, 095001. https://doi.org/10.1088/0741-3335/52/9/095001

Mercier, C., 1960. A necessary condition for hydromagnetic stability of plasma with axial symmetry. Nucl. Fusion 1, 47. https://doi.org/10.1088/0029-5515/1/1/004

Merlin, D., Ortolani, S., Paccagnella, R., Scapin, M., 1989. Linear resistive magnetohydrodynamic stability analysis of reversed field pinch configurations at finite beta. Nuclear Fusion 29, 1153–1160. https://doi.org/10.1088/0029-5515/29/7/007

Miyazawa, J., Masuzaki, S., Yamada, H., Sakamoto, R., Peterson, B.J., Shoji, M., Ohyabu, N., Komori, A., Motojima, O., LHD Experimental Group, Grigull, P., Feng, Y., McCormick, K., Sardei, F., Igitkhanov, Y., W7-As Team, 2006. Detachment Phenomena in LHD Compared to W7-AS. Fusion Science and Technology 50, 192–200. https://doi.org/10.13182/FST06-A1235

Momo, B., Martines, E., Escande, D.F., Gobbin, M., 2011. Magnetic coordinate systems for helical SHAx states in reverse field pinch plasmas. Plasma Phys. Control. Fusion 53, 125004. https://doi.org/10.1088/0741-3335/53/12/125004

Morales, J.A., Bos, W.J.T., Schneider, K., Montgomery, D.C., 2014. The effect of toroidicity on reversed field pinch dynamics. Plasma Phys. Control. Fusion 56, 095024. https://doi.org/10.1088/0741-3335/56/9/095024

Munaretto, S., Chapman, B.E., Holly, D.J., Nornberg, M.D., Norval, R.J., Den Hartog, D.J., Goetz, J.A., McCollam, K.J., 2015. Control of 3D equilibria with resonant magnetic perturbations in MST. Plasma Physics and Controlled Fusion 57, 104004. https://doi.org/10.1088/0741-3335/57/10/104004

Munaretto, S., Dal Bello, S., Innocente, P., Agostini, M., Auriemma, F., Barison, S., Canton, A., Carraro, L., De Masi, G., Fiameni, S., Scarin, P., Terranova, D., 2012. RFX-mod wall conditioning by lithium pellet injection. Nuclear Fusion 52, 023012. https://doi.org/10.1088/0029-5515/52/2/023012

Najmabadi, F., Conn, R.W., Krakowski, R.A., Schultz, K.R., Steiner, D., Bartlit, J.R., Bathke, C.G., Blanchard, J.P., Cheng, E.T., Chu, Y.-Y., Cooke, P.I.H., Creedon, R.L., Duggan, W.P., Gierszewski, P.J., Ghoniem, N.M., Grotz, S.P., Hasan, M.Z., Hoot, C.G., Kelleher, W.P., Kessel, C.E., Kevton, O.K., Martin, R.C., Miller, R.L., Prinja, A.K., Orient, G.O., Sharafat, S., Vold, E.L., Werley, K.A., Wong, C.P.C., Sze, D.-K., 1993. Introduction and synopsis of the TITAN reversed-field-pinch fusion-reactor study. Fusion Engineering and Design 23, 69–80. https://doi.org/10.1016/0920-3796(93)90124-Z

Nebel, R.A., Schnack, D.D., Gianakon, T.A., 2002. Self-similar decaying profiles for reversed-field pinches. Physics of Plasmas 9, 4968–4984. https://doi.org/10.1063/1.1521713

Newcomb, W.A., 1960. Hydromagnetic stability of a diffuse linear pinch. Annals of Physics 10, 232–267. https://doi.org/10.1016/0003-4916(60)90023-3

Nonn, P.D., Blair, A.P., McCollam, K.J., Sarff, J.S., Stone, D.R., 2011. Powered oscillator using ignitron switches. Review of Scientific Instruments 82, 064701-064701–7. https://doi.org/doi:10.1063/1.3589266

Nordlund, P., Mazur, S., 1994. Nonlinear dynamics of kink-tearing modes and their interaction with the current profiles in a reversed-field pinch. Physics of Plasmas (1994-present) 1, 4032–4042. https://doi.org/10.1063/1.870873

O'Connell, R., Hartog, D.J.D., Forest, C.B., Anderson, J.K., Biewer, T.M., Chapman, B.E., Craig, D., Fiksel, G., Prager, S.C., Sarff, J.S., Terry, S.D., Harvey, R.W., 2003. Observation of Velocity-Independent Electron Transport in the Reversed Field Pinch. Physical Review Letters 91. https://doi.org/10.1103/PhysRevLett.91.045002

Okamura, S., Matsuoka, K., Akiyama, R., Darrow, D.S., Ejiri, A., Fujisawa, A., Fujiwara, M., Goto, M., Ida, K., Idei, H., Iguchi, H., Inoue, N., Isobe, M., Itoh, K., Kado, S., Khlopenkov, K., Kondo, T., Kubo, S., Lazaros, A., Lee, S., Matsunaga, G., Minami, T., Morita, S., Murakami, S., Nakajima, N., Nikai, N., Nishimura, S., Nomura, I., Ohdachi, S., Ohkuni, K., Osakabe, M., Pavlichenko, R., Peterson, B.J., Sakamoto, R., Sanuki, H., Sasao, M., Shimizu, A., Shirai, Y., Sudo, S., Takagi, S., Takahashi, C., Takayama, S., Takechi, M., Tanaka, K., Toi, K., Watari, T., Yamazaki, K., Yokoyama, M., Yoshimura, Y., 1999. Confinement physics study in a small low aspect ratio helical device: CHS. Nucl. Fusion 39, 1337. https://doi.org/10.1088/0029-5515/39/9Y/310

Oki, K., Fukahori, D., Deguchi, K., Nakaki, S., Sanpei, A., Himura, H., Masamune, S., Paccagnella, R., 2012. Characterization of Quasi-Single-Helicity States in a Low-Aspect-Ratio RFP. Plasma and Fusion Research 7, 1402028–1402028. https://doi.org/10.1585/pfr.7.1402028

Oki, K., Sanpei, A., Himura, H., Masamune, S., 2013. Dependence of Properties of Quasi-Single-Helicity States on Field Reversal Parameter in a Low-Aspect-Ratio Reversed Field Pinch. Fusion Science and Technology 63, 386–388. https://doi.org/10.13182/FST13-A16963

Olofsson, E., Brunsell, P., Drake, J., 2009. Closed-loop direct parametric identification of magnetohydrodynamic normal modes spectra in EXTRAP-T2R reversed-field pinch, in: 2009 IEEE International Conference on Control Applications. Presented at the 2009 IEEE International Conference on Control Applications (CCA), IEEE, St. Petersburg, Russia, pp. 1449–1454. https://doi.org/10.1109/CCA.2009.5281183

Olofsson, K.E.J., Brunsell, P.R., Drake, J.R., 2013a. Experimental modal analysis of resistive wall toroidal pinch plasma dynamics. Nuclear Fusion 53, 072003. https://doi.org/10.1088/0029-5515/53/7/072003

Olofsson, K.E.J., Brunsell, P.R., Drake, J.R., Frassinetti, L., 2012. A first attempt at few coils and low-coverage resistive wall mode stabilization of EXTRAP T2R. Plasma Physics and Controlled Fusion 54, 094005. https://doi.org/10.1088/0741-3335/54/9/094005

Olofsson, K.E.J., Brunsell, P.R., Rojas, C.R., Drake, J.R., Hjalmarsson, H., 2011. Predictor-based multivariable closed-loop system identification of the EXTRAP T2R reversed field pinch external plasma response. Plasma Physics and Controlled Fusion 53, 084003. https://doi.org/10.1088/0741-3335/53/8/084003

Olofsson, K.E.J., Soppelsa, A., Bolzonella, T., Marchiori, G., 2013b. Subspace identification analysis of RFX and T2R reversed-field pinches. Control Engineering Practice 21, 917–929. https://doi.org/10.1016/j.conengprac.2013.03.004

Onofri, M., 2011. Single-helicity states in compressible magnetohydrodynamics simulations of the reversed-field pinch with nonuniform resistivity. Nucl. Fusion 51, 112003. https://doi.org/10.1088/0029-5515/51/11/112003

Onofri, M., Malara, F., 2013. Effects of the resistivity profile on the formation of a reversed configuration and single helicity states in compressible simulations of the reversed-field pinch. Physics of Plasmas (1994-present) 20, 102514. https://doi.org/10.1063/1.4826222

Onofri, M., Malara, F., Veltri, P., 2010a. Temperature evolution in a magnetohydrodynamics simulation of a reversed-field pinch. Nucl. Fusion 50, 055003. https://doi.org/10.1088/0029-5515/50/5/055003

Onofri, M., Malara, F., Veltri, P., 2010b. Effects of Anisotropic Thermal Conductivity in Magnetohydrodynamics Simulations of a Reversed-Field Pinch. Phys. Rev. Lett. 105, 215006. https://doi.org/10.1103/PhysRevLett.105.215006

Onofri, M., Malara, F., Veltri, P., 2009. Effects of compressibility and heating in magnetohydrodynamics simulations of a reversed field pinch. Physics of Plasmas (1994-present) 16, 052508. https://doi.org/10.1063/1.3139248

Onofri, M., Malara, F., Veltri, P., 2008. Compressibility Effects in the Dynamics of the Reversed-Field Pinch. Phys. Rev. Lett. 101, 255002. https://doi.org/10.1103/PhysRevLett.101.255002

Ortolani, S., Rostagni, G., 1983. Density limits and scaling laws in reversed field pinches. Nuclear Instruments and Methods in Physics Research 207, 35–48. https://doi.org/10.1016/0167-5087(83)90221-1

Ortolani, S., Schnack, D.D., 1993. Magnetohydrodynamics of plasma relaxation. World Scientific, Singapore.

Ortolani, S., team, the R., 2006. Active MHD control experiments in RFX-mod. Plasma Physics and Controlled Fusion 48, B371–B381. https://doi.org/10.1088/0741-3335/48/12B/S34

Paccagnella, R., 2016. Aspect ratio scaling of the single helical states in the reversed field pinch plasmas. Nuclear Fusion 56, 046010. https://doi.org/10.1088/0029-5515/56/4/046010

Paccagnella, Roberto, 2016. Relaxation models for single helical reversed field pinch plasmas. Physics of Plasmas 23, 092512. https://doi.org/10.1063/1.4963677

Paccagnella, R., 2014. Pressure-driven reconnection and quasi periodical oscillations in plasmas. Physics of Plasmas (1994-present) 21, 032307. https://doi.org/10.1063/1.4868728

Paccagnella, R., 2013. Pressure driven tearing and interchange modes in the reversed field pinch. Physics of Plasmas (1994-present) 20, 012119. https://doi.org/10.1063/1.4789446

Paccagnella, R., 1998. Linear magnetohydrodynamic stability in reversed field pinch with distant and multiple resistive walls. Nuclear Fusion 38, 1067–1081. https://doi.org/10.1088/0029-5515/38/7/309

Paccagnella, R., Bondeson, A., Lütjens, H., 1991. Ideal toroidal stability beta limits and shaping effects for reversed field pinch configurations. Nucl. Fusion 31, 1899. https://doi.org/10.1088/0029-5515/31/10/008

Paccagnella, R., Gregoratto, D., Bondeson, A., 2002a. Feedback control of resistive wall modes in reversed field pinches. Nucl. Fusion 42, 1102–1109. https://doi.org/10.1088/0029-5515/42/9/308

Paccagnella, R., Ortolani, S., Zanca, P., Alfier, A., Bolzonella, T., Marrelli, L., Puiatti, M.E., Serianni, G., Terranova, D., Valisa, M., Agostini, M., Apolloni, L., Auriemma, F., Bonomo, F., Canton, A., Carraro, L., Cavazzana, R., Cavinato, M., Franz, P., Gazza, E., Grando, L., Innocente, P., Lorenzini, R., Luchetta, A., Manduchi, G., Marchiori, G., Martini, S., Pasqualotto, R., Piovesan, P., Pomaro, N., Scarin, P., Spizzo, G., Spolaore, M., Taliercio, C., Vianello, N., Zaniol, B., Zanotto, L., Zuin, M., 2006. Active-Feedback Control of the Magnetic Boundary for Magnetohydrodynamic Stabilization of a Fusion Plasma. Phys. Rev. Lett. 97, 075001. https://doi.org/10.1103/PhysRevLett.97.075001

Paccagnella, R., Schnack, D.D., Chu, M.S., 2002b. Feedback studies on resistive wall modes in the reversed-field pinch. Physics of Plasmas 9, 234–242. https://doi.org/10.1063/1.1427725

Pegoraro, F., Bonfiglio, D., Cappello, S., Giannatale, G.D., Falessi, M.V., Grasso, D., Veranda, M., 2019. Coherent magnetic structures in self-organized plasmas. Plasma Physics and Controlled Fusion 61, 044003. https://doi.org/10.1088/1361-6587/ab03b5

Perkins, F.W., Hulse, R.A., 1985. On the Murakami density limit in tokamaks and reversed-field pinches. Phys. Fluids 28, 1837. https://doi.org/10.1063/1.864927

Peruzzo, S., Agostini, M., Agostinetti, P., Bernardi, M., Bettini, P., Bolzonella, T., Canton, A., Carraro, L., Cavazzana, R., Dal Bello, S., Dalla Palma, M., De Masi, G., Delogu, R., Fassina, A., Grando, L., Innocente, P., Marchiori, G., Marconato, N., Marrelli, L., Patel, N., Puiatti, M.E., Scarin, P., Siragusa, M., Sonato, P., Spolaore, M., Trevisan, L., Valisa, M., Vallar, M., Vincenzi, P., Zamengo, A., Zanca, P., Zanotto, L., 2017. Design concepts of machine upgrades for the RFX-mod experiment. Fusion Engineering and Design 123, 59–62. https://doi.org/10.1016/j.fusengdes.2017.03.056

Peruzzo, S., Bernardi, M., Berton, G., Cavazzana, R., Dal Bello, S., Dalla Palma, M., Grando, L., Iafrati, M., Marcuzzi, D., Rizzetto, D., Rizzolo, A., Rossetto, F., Siragusa, M., Spolaore, M., Trevisan, L., Utili, M., Zuin, M., 2019. Technological challenges for the design of the RFX-mod2 experiment. Fusion Engineering and Design 146, 692–696. https://doi.org/10.1016/j.fusengdes.2019.01.057

Piovesan, P., Almagri, A., Chapman, B.E., Craig, D., Marrelli, L., Martin, P., Prager, S.C., Sarff, J.S., 2008. Filamentary current structures in the Madison Symmetric Torus. Nuclear Fusion 48, 095003. https://doi.org/10.1088/0029-5515/48/9/095003

Piovesan, P., Bonfiglio, D., Auriemma, F., Bonomo, F., Carraro, L., Cavazzana, R., Masi, G.D., Fassina, A., Franz, P., Gobbin, M., Marrelli, L., Martin, P., Martines, E., Momo, B., Piron, L., Valisa, M., Veranda, M., Vianello, N., Zaniol, B., Agostini, M., Baruzzo, M., Bolzonella, T., Canton, A., Cappello, S., Chacón, L., Ciaccio, G., Escande, D.F., Innocente, P., Lorenzini, R., Paccagnella, R., Puiatti, M.E., Scarin, P., Soppelsa, A., Spizzo, G., Spolaore, M., Terranova, D., Zanca, P., Zanotto, L., Zuin, M., 2013. RFX-mod: A multi-configuration fusion facility for three-dimensional physics studiesa). Physics of Plasmas (1994-present) 20, 056112. https://doi.org/10.1063/1.4806765

Piovesan, P., Bonfiglio, D., Bonomo, F., Cappello, S., Carraro, L., Cavazzana, R., Gobbin, M., Marrelli, L., Martin, P., E Martines, Momo, B., Piron, L., Puiatti, M.E., Soppelsa, A., Valisa, M., Zanca, P., Zaniol, B., team, the R., 2011a. Influence of external 3D magnetic fields on helical equilibrium and plasma flow in RFX-mod. Plasma Phys. Control. Fusion 53, 084005. https://doi.org/10.1088/0741-3335/53/8/084005

Piovesan, P., Bonfiglio, D., Bonomo, F., Cappello, S., Carraro, L., Cavazzana, R., Gobbin, M., Marrelli, L., Martin, P., E Martines, Momo, B., Piron, L., Puiatti, M.E., Soppelsa, A., Valisa, M., Zanca, P., Zaniol, B., team, the R., 2011b. Influence of external 3D magnetic fields on helical equilibrium and plasma flow in RFX-mod. Plasma Phys. Control. Fusion 53, 084005. https://doi.org/10.1088/0741-3335/53/8/084005

Piovesan, P., Bonfiglio, D., Cianciosa, M., Luce, T.C., Taylor, N.Z., Terranova, D., Turco, F., Wilcox, R.S., Wingen, A., Cappello, S., Chrystal, C., Escande, D.F., Holcomb, C.T., Marrelli, L., Paz-Soldan, C., Piron, L., Predebon, I., Zaniol, B., The DIII-D, RFX-Mod Teams, 2017. Role of a continuous MHD dynamo in the formation of 3D equilibria in fusion plasmas. Nuclear Fusion 57, 076014. https://doi.org/10.1088/1741-4326/aa700b

Piovesan, P., Craig, D., Marrelli, L., Cappello, S., Martin, P., 2004a. Measurements of the MHD Dynamo in the Quasi-Single-Helicity Reversed-Field Pinch. Phys. Rev. Lett. 93, 235001. https://doi.org/10.1103/PhysRevLett.93.235001

Piovesan, P., Hanson, J.M., Martin, P., Navratil, G.A., Turco, F., Bialek, J., Ferraro, N.M., La Haye, R.J., Lanctot, M.J., Okabayashi, M., 2014. Tokamak Operation with Safety Factor q 95 < 2 via Control of MHD Stability. Physical Review Letters 113. https://doi.org/10.1103/PhysRevLett.113.045003

Piovesan, P., Spizzo, G., Yagi, Y., Koguchi, H., Shimada, T., Hirano, Y., Martin, P., 2004b. Self-organization towards helical states in the Toroidal Pinch Experiment reversed-field pinch. Physics of Plasmas (1994-present) 11, 151–157. https://doi.org/10.1063/1.1629693

Piovesan, P., Zuin, M., Alfier, A., Bonfiglio, D., Bonomo, F., Canton, A., Cappello, S., Carraro, L., R. Cavazzana, Escande, D.F., Fassina, A., Gobbin, M., Lorenzini, R., Marrelli, L., Martin, P., Martines, E., R. Pasqualotto, Puiatti, M.E., Spolaore, M., Valisa, M., Vianello, N., Zanca, P., Team, the R., 2009. Magnetic order and confinement improvement in high-current regimes of RFX-mod with MHD feedback control. Nucl. Fusion 49, 085036. https://doi.org/10.1088/0029-5515/49/8/085036

Piron, L., Marrelli, L., Piovesan, P., Zanca, P., 2010. Model-based design of multi-mode feedback control in the RFX-mod experiment. Nucl. Fusion 50, 115011. https://doi.org/10.1088/0029-5515/50/11/115011

Portone, A., Villone, F., Liu, Y., Albanese, R., Rubinacci, G., 2008. Linearly perturbed MHD equilibria and 3D eddy current coupling via the control surface method. Plasma Phys. Control. Fusion 50, 085004. https://doi.org/10.1088/0741-3335/50/8/085004

Prager, S.C., 1999. Dynamo and anomalous transport in the reversed field pinch. Plasma Phys. Control. Fusion 41, A129. https://doi.org/10.1088/0741-3335/41/3A/008

Prager, S.C., 1990. Transport and fluctuations in reversed field pinches. Plasma Physics and Controlled Fusion 32, 903–916. https://doi.org/10.1088/0741-3335/32/11/006

Predebon, I., Angioni, C., Guo, S.C., 2010a. Gyrokinetic simulations of ion temperature gradient modes in the reversed field pinch. Physics of Plasmas (1994-present) 17, 012304. https://doi.org/10.1063/1.3290173

Predebon, I., Carraro, L., Angioni, C., 2011. On the mutual effect of ion temperature gradient instabilities and impurity peaking in the reversed field pinch. Plasma Phys. Control. Fusion 53, 125009. https://doi.org/10.1088/0741-3335/53/12/125009

Predebon, I., Marrelli, L., White, R.B., Martin, P., 2004. Particle-Transport Analysis in Reversed Field Pinch Helical States. Phys. Rev. Lett. 93, 145001. https://doi.org/10.1103/PhysRevLett.93.145001

Predebon, I., Sattin, F., 2013. On the linear stability of collisionless microtearing modes. Physics of Plasmas 20, 040701. https://doi.org/10.1063/1.4799980

Predebon, I., Sattin, F., Veranda, M., Bonfiglio, D., Cappello, S., 2010b. Microtearing Modes in Reversed Field Pinch Plasmas. Phys. Rev. Lett. 105, 195001. https://doi.org/10.1103/PhysRevLett.105.195001

Predebon, I., Xanthopoulos, P., 2015. Ion temperature gradient turbulence in helical and axisymmetric RFP plasmas. Physics of Plasmas (1994-present) 22, 052308. https://doi.org/10.1063/1.4921645

Puiatti, M.E., Alfier, A., Auriemma, F., Cappello, S., Carraro, L., Cavazzana, R., Bello, S.D., Fassina, A., Escande, D.F., P Franz, Gobbin, M., Innocente, P., Lorenzini, R., Marrelli, L., Martin, P., Piovesan, P., Predebon, I., Sattin, F., Spizzo, G., D Terranova, Valisa, M., Zaniol, B., Zanotto, L., Zuin, M., Agostini, M., Antoni, V., Apolloni, L., Baruzzo, M., Bolzonella, T., D Bonfiglio, Bonomo, F., Boozer, A., Brombin, M., Canton, A., Delogu, R., Masi, G.D., Gaio, E., Gazza, E., Giudicotti, L., L Grando, Guo, S.C., Manduchi, G., Marchiori, G., Martines, E., Martini, S., Menmuir, S., Momo, B., Moresco, M., Munaretto, S., L Novello, Paccagnella, R., Pasqualotto, R., Piovan, R., Piron, L., Pizzimenti, A., Pomphrey, N., Scarin, P., Serianni, G., E Spada, Soppelsa, A., Spagnolo, S., Spolaore, M., Taliercio, C., Vianello, N., Zamengo, A., Zanca, P., 2009a. Helical equilibria and magnetic structures in the reversed field pinch and analogies to the tokamak and stellarator. Plasma Phys. Control. Fusion 51, 124031. https://doi.org/10.1088/0741-3335/51/12/124031

Puiatti, M.E., Bello, S.D., Marrelli, L., Martin, P., Agostinetti, P., Agostini, M., Antoni, V., Auriemma, F., M. Barbisan, Barbui, T., Baruzzo, M., Battistella, M., Belli, F., Bettini, P., Bigi, M., Bilel, R., Boldrin, M., T. Bolzonella, Bonfiglio, D., Brombin, M., Buffa, A., Canton, A., Cappello, S., Carraro, L., Cavazzana, R., D. Cester, Chacon, L., Chapman, B.E., Chitarin, G., Ciaccio, G., Cooper, W.A., Palma, M.D., Deambrosis, S., R. Delogu, Lorenzi, A.D., Masi, G.D., Dong, J.Q., Escande, D.F., Esposito, B., Fassina, A., Fellin, F., Ferro, A.,

C. Finotti, Franz, P., Frassinetti, L., Palumbo, M.F., Gaio, E., Ghezzi, F., Giudicotti, L., Gnesotto, F., M. Gobbin, Gonzales, W.A., Grando, L., Guo, S.C., Hanson, J.D., Hirshman, S.P., Innocente, P., Jackson, J.L., S. Kiyama, Komm, M., Laguardia, L., Li, C., Liu, S.F., Liu, Y.Q., Lorenzini, R., Luce, T.C., Luchetta, A., A. Maistrello, Manduchi, G., Mansfield, D.K., Marchiori, G., Marconato, N., Marocco, D., Marcuzzi, D., E. Martines, Martini, S., Matsunaga, G., Mazzitelli, G., Miorin, E., Momo, B., Moresco, M., Okabayashi, M., E. Olofsson, Paccagnella, R., Patel, N., Pavei, M., Peruzzo, S., Pilan, N., Pigatto, L., Piovan, R., Piovesan, P., C. Piron, Piron, L., Predebon, I., Rea, C., Recchia, M., Rigato, V., Rizzolo, A., Roquemore, A.L., Rostagni, G., C Ruset, Ruzzon, A., Sajò-Bohus, L., Sakakita, H., Sanchez, R., Sarff, J.S., Sartori, E., Sattin, F., Scaggion, A., P. Scarin, Schmitz, O., Sonato, P., Spada, E., Spagnolo, S., Spolaore, M., Spong, D.A., Spizzo, G., Stevanato, L., M. Takechi, Taliercio, C., Terranova, D., Trevisan, G.L., Urso, G., Valente, M., Valisa, M., Veranda, M., N. Vianello, Viesti, G., Villone, F., Vincenzi, P., Visona', N., Wang, Z.R., White, R.B., Xanthopoulos, P., Xu, X.Y., V. Yanovskiy, Zamengo, A., Zanca, P., Zaniol, B., Zanotto, L., Zilli, E., Zuin, M., 2015. Overview of the RFX-mod contribution to the international Fusion Science Program. Nucl. Fusion 55, 104012. https://doi.org/10.1088/0029-5515/55/10/104012

Puiatti, M.E., Cappello, S., Lorenzini, R., Martini, S., Ortolani, S., Paccagnella, R., Sattin, F., D. Terranova, Bolzonella, T., Buffa, A., Canton, A., Carraro, L., Escande, D.F., Garzotti, L., Innocente, P., L. Marrelli, Martines, E., Scarin, P., Spizzo, G., Valisa, M., Zanca, P., Antoni, V., Apolloni, L., Bagatin, M., W. Baker, Barana, O., Bettella, D., Bettini, P., Cavazzana, R., Cavinato, M., Chitarin, G., Cravotta, A., F. D'Angelo, Bello, S.D., Lorenzi, A.D., Desideri, D., Fiorentin, P., Franz, P., Frassinetti, L., Gaio, E., L. Giudicotti, Gnesotto, F., Grando, L., Guo, S.C., Luchetta, A., Malesani, G., Manduchi, G., Marchiori, G., D. Marcuzzi, Martin, P., Masiello, A., Milani, F., Moresco, M., Murari, A., Nielsen, P., Pasqualotto, R., B. Pégourie, Peruzzo, S., Piovan, R., Piovesan, P., Pomaro, N., Preti, G., Regnoli, G., Rostagni, G., Serianni, G., P. Sonato, Spada, E., Spolaore, M., Taliercio, C., Telesca, G., Toigo, V., Vianello, N., Zaccaria, P., Zaniol, B., L. Zanotto, Zilli, E., Zollino, G., Zuin, M., 2003. Analysis and modelling of the magnetic and plasma profiles during PPCD experiments in RFX. Nucl. Fusion 43, 1057. https://doi.org/10.1088/0029-5515/43/10/006

Puiatti, M.E., Scarin, P., Spizzo, G., Valisa, M., Agostini, M., Alfier, A., Canton, A., Carraro, L., Gazza, E., Lorenzini, R., Paccagnella, R., Predebon, I., Terranova, D., Bonfiglio, D., Cappello, S., Cavazzana, R., Bello, S.D., Innocente, P., Marrelli, L., Piovan, R., Piovesan, P., Sattin, F., Zanca, P., 2009b. High density physics in reversed field pinches: comparison with tokamaks and stellarators. Nucl. Fusion 49, 045012. https://doi.org/10.1088/0029-5515/49/4/045012

Puiatti, M.E., Scarin, P., Spizzo, G., Valisa, M., Paccagnella, R., Predebon, I., Agostini, M., Alfier, A., Canton, A., Cappello, S., Carraro, L., Gazza, E., Innocente, P., Lorenzini, R., Marrelli, L., Terranova, D., 2009c. High density limit in reversed field pinches. Physics of Plasmas (1994-present) 16, 012505. https://doi.org/10.1063/1.3063060

Puiatti, M. E., Spizzo, G., Agostini, M., Auriemma, F., Bonfiglio, D., Canton, A., Cappello, S., Carraro, L., Cavazzana, R., G Ciaccio, Masi, G.D., Fassina, A., Franz, P., Gobbin, M., Guo, S.C., Innocente, P., Lorenzini, R., Marrelli, L., Martin, P., L Piron, Paccagnella, R., Predebon, I., Scaggion, A., Scarin, P., Terranova, D., Valisa, M., Vianello, N., Zaniol, B., M Zuin, Team, the R., 2013. Interaction between magnetic boundary and first wall recycling in the reversed field pinch. Plasma Phys. Control. Fusion 55, 124013. https://doi.org/10.1088/0741-3335/55/12/124013

Puiatti, M.E., Spizzo, G., Auriemma, F., Carraro, L., Cavazzana, R., De Masi, G., Gobbin, M., Innocente, P., Predebon, I., Scarin, P., Agostini, M., Canton, A., Dal Bello, S., Fassina, A., Franz, P., Grando, L., Mansfield, D., Marrelli, L., Martin, P., Mazzitelli, G., Munaretto, S., Roquemore, L., Ruzzon, A., Terranova, D., Valisa, M., Vertkov, A., Zaniol, B., the RFX-

mod Team, 2013. Wall conditioning and density control in the reversed field pinch RFX-mod. Nuclear Fusion 53, 073001. https://doi.org/10.1088/0029-5515/53/7/073001

Puiatti, M.E., Tramontin, L., Antoni, V., Bartiromo, R., Carraro, L., Desideri, D., Martines, E., Sattin, F., Scarin, P., Serianni, G., Spolaore, M., Valisa, M., Zaniol, B., 2001. Plasma rotation and structure of the radial electric field in RFX. Journal of Nuclear Materials 290–293, 696–700. https://doi.org/10.1016/S0022-3115(00)00529-8

Puiatti, M.E., Valisa, M., Agostini, M., Auriemma, F., Bonomo, F., Carraro, L., Fassina, A., Gobbin, M., R. Lorenzini, Momo, B., Scaggion, A., Zaniol, B., Alfier, A., Apolloni, L., Baruzzo, M., Bolzonella, T., D. Bonfiglio, Canton, A., Cappello, S., Cavazzana, R., Bello, S.D., Masi, G.D., Escande, D.F., Franz, P., E. Gazza, Guo, S., Innocente, P., Marchiori, G., Marrelli, L., Martin, P., Martines, E., Martini, S., Menmuir, S., L. Novello, Paccagnella, R., Piovesan, P., Piron, L., Predebon, I., Ruzzon, A., Sattin, F., Scarin, P., Soppelsa, A., G. Spizzo, Spagnolo, S., Spolaore, M., Terranova, D., Veranda, M., Vianello, N., Zanca, P., Zanotto, L., Zuin, M., 2011. Internal and external electron transport barriers in the RFX-mod reversed field pinch. Nucl. Fusion 51, 073038. https://doi.org/10.1088/0029-5515/51/7/073038

Pustovitov, V.D., 1982. Evolution equations of a stabilized helical pinch. JETP Letters 1.

Raman, R., Jarboe, T.R., Mueller, D., Schaffer, M.J., Maqueda, R., Nelson, B.A., Sabbagh, S.A., Bell, M.G., R. Ewig, Fredrickson, E.D., Gates, D.A., Hosea, J.C., Jardin, S.C., Ji, H., Kaita, R., Kaye, S.M., Kugel, H.W., L.L. Lao, Maingi, R., Menard, J., Ono, M., Orvis, D., Paoletti, F., Paul, S.F., Peng, Y.-K.M., Skinner, C.H., J.B. Wilgen, Zweben, S.J., Team, N.R., 2001. Non-inductive current generation in NSTX using coaxial helicity injection. Nucl. Fusion 41, 1081. https://doi.org/10.1088/0029-5515/41/8/311

Ratynskaia, S., Castaldo, C., Bergsåker, H., Rudakov, D., 2011. Diagnostics of mobile dust in scrape-off layer plasmas. Plasma Physics and Controlled Fusion 53, 074009. https://doi.org/10.1088/0741-3335/53/7/074009

Rea, C., Vianello, N., Agostini, M., Cavazzana, R., De Masi, G., Martines, E., Momo, B., Scarin, P., Spagnolo, S., Spizzo, G., Spolaore, M., Zuin, M., 2015. Comparative studies of electrostatic turbulence induced transport in presence of resonant magnetic perturbations in RFX-mod. Nuclear Fusion 55, 113021. https://doi.org/10.1088/0029-5515/55/11/113021

Rechester, A.B., Rosenbluth, M.N., 1978. Electron Heat Transport in a Tokamak with Destroyed Magnetic Surfaces. Physical Review Letters 40, 38–41. https://doi.org/10.1103/PhysRevLett.40.38

Redd, A.J., Nelson, B.A., Jarboe, T.R., Gu, P., Raman, R., Smith, R.J., McCollam, K.J., 2002. Current drive experiments in the helicity injected torus (HIT-II). Physics of Plasmas 9, 2006. https://doi.org/10.1063/1.1448832

Reusch, J.A., Anderson, J.K., Den Hartog, D.J., Ebrahimi, F., Schnack, D.D., Stephens, H.D., Forest, C.B., 2011. Experimental Evidence for a Reduction in Electron Thermal Diffusion due to Trapped Particles. Physical Review Letters 107. https://doi.org/10.1103/PhysRevLett.107.155002

Reynolds, J.M., Sovinec, C.R., Prager, S.C., 2008. Nonlinear magnetohydrodynamics of pulsed parallel current drive in reversed-field pinches. Physics of Plasmas 15, 062512. https://doi.org/10.1063/1.2937770

Ricci, P., Halpern, F.D., Jolliet, S., Loizu, J., Mosetto, A., Fasoli, A., Furno, I., Theiler, C., 2012. Simulation of plasma turbulence in scrape-off layer conditions: the GBS code, simulation results and code validation. Plasma Phys. Control. Fusion 54, 124047. https://doi.org/10.1088/0741-3335/54/12/124047

Riva, F., Vianello, N., Spolaore, M., Ricci, P., Cavazzana, R., Marrelli, L., Spagnolo, S., 2018. Three-dimensional simulations of plasma turbulence in the RFX-mod scrape-off layer and comparison with experimental measurements. Physics of Plasmas 25, 022305. https://doi.org/10.1063/1.5008803

Robinson, D.C., 1978. Tearing-mode-stable diffuse-pinch configurations. Nucl. Fusion 18, 939–953. https://doi.org/10.1088/0029-5515/18/7/006

Robinson, D.C., 1971. High-β diffuse pinch configurations. Plasma Phys. 13, 439. https://doi.org/10.1088/0032-1028/13/6/001

Rosenbluth, M.N., Sagdeev, R.Z., Taylor, J.B., Zaslavski, G.M., 1966. Destruction of magnetic surfaces by magnetic field irregularities. Nucl. Fusion 6, 297. https://doi.org/10.1088/0029-5515/6/4/008

Rubel, M., Cecconello, M., Malmberg, J.A., Sergienko, G., Biel, W., Drake, J.R., Hedqvist, A., Huber, A., Philipps, V., 2001. Dust particles in controlled fusion devices: morphology, observations in the plasma and influence on the plasma performance. Nuclear Fusion 41, 1087–1099. https://doi.org/10.1088/0029-5515/41/8/312

Rusbridge, M.G., 1991. The relationship between the "tangled discharge" and "dynamo" models of the magnetic relaxation process. Plasma Physics and Controlled Fusion 33, 1381–1389. https://doi.org/10.1088/0741-3335/33/12/004

Rutherford, P.H., 1973. Nonlinear growth of the tearing mode. Phys. Fluids 16, 1903. https://doi.org/10.1063/1.1694232

Sakakibara, S., Watanabe, K.Y., Takemura, Y., Okamoto, M., Ohdachi, S., Suzuki, Y., Narushima, Y., Ida, K., M. Yoshinuma, Tanaka, K., Tokuzawa, T., Yamada, I., Yamada, H., Takeiri, Y., 2015. Characteristics of MHD instabilities limiting the beta value in LHD. Nucl. Fusion 55, 083020. https://doi.org/10.1088/0029-5515/55/8/083020

Sakakita, H., Yagi, Y., Koguchi, H., Hirano, Y., Shimada, T., Canton, A.M., Innocente, P., 2004. Electron Density Control Using Fast Gas Puffing in Reversed-field Pinch Device, TPE-RX. Jpn. J. Appl. Phys. 43, L1184. https://doi.org/10.1143/JJAP.43.L1184

Sánchez, J., Acedo, M., Alonso, A., Alonso, J., Alvarez, P., Ascasíbar, E., Baciero, A., Balbín, R., Barrera, L., E. Blanco, Botija, J., Bustos, A. de, Cal, E. de la, Calvo, I., Cappa, A., Carmona, J.M., Carralero, D., R. Carrasco, Carreras, B.A., Castejón, F., Castro, R., Catalán, G., Chmyga, A.A., Chamorro, M., Eliseev, L., L. Esteban, Estrada, T., Fernández, A., Fernández-Gavilán, R., Ferreira, J.A., Fontdecaba, J.M., Fuentes, C., L. García, García-Cortés, I., García-Gómez, R., García-Regaña, J.M., Guasp, J., Guimarais, L., Happel, T., J. Hernanz, Herranz, J., Hidalgo, C., Jiménez, J.A., Jiménez-Denche, A., Jiménez-Gómez, R., Jiménez-Rey, D., I. Kirpitchev, Komarov, A.D., Kozachok, A.S., Krupnik, L., Lapayese, F., Liniers, M., López-Bruna, D., A. López-Fraguas, López-Rázola, J., López-Sánchez, A., Lysenko, S., Marcon, G., Martín, F., Maurin, V., K.J. McCarthy, Medina, F., Medrano, M., Melnikov, A.V., Méndez, P., Milligen, B. van, Mirones, E., Nedzelskiy, I.S., M. Ochando, Olivares, J., Pablos, J.L. de, Pacios, L., Pastor, I., Pedrosa, M.A., Peña, A. de la, Pereira, A., G. Pérez, Pérez-Risco, D., Petrov, A., Petrov, S., Portas, A., Pretty, D., Rapisarda, D., Rattá, G., Reynolds, J.M., E. Rincón, Ríos, L., Rodríguez, C., Romero, J.A., Ros, A., Salas, A., Sánchez, M., Sánchez, E., Sánchez-Sarabia, E., K. Sarksian, Sebastián, J.A., Silva, C., Schchepetov, S., Skvortsova, N., Solano, E.R., Soleto, A., Tabarés, F., D. Tafalla, Tarancón, A., Taschev, Y., Tera, J., Tolkachev, A., Tribaldos, V., Vargas, V.I., Vega, J., G. Velasco, Velasco, J.L., Weber, M., Wolfers, G., Zurro, B., 2009. Confinement transitions in TJ-II under Li-coated wall conditions. Nucl. Fusion 49, 104018. https://doi.org/10.1088/0029-5515/49/10/104018

Sanpei, A., Oki, K., Ikezoe, R., Onchi, T., Murata, K.-I., Shimazu, H., Yamashita, T., Fujita, S., Himura, H., Masamune, S., K. Anderson, J., 2009. Equilibrium Reconstruction and Estimation of Neoclassical Effect in Low-Aspect-Ratio Reversed Field Pinch Experiments on RELAX. Journal of the Physical Society of Japan 78, 013501. https://doi.org/10.1143/JPSJ.78.013501

Sarff, J.S., Almagri, A.F., Anderson, J.K., Biewer, T.M., Blair, A.P., Cengher, M., Chapman, B.E., P.K. Chattopadhyay, Craig, D., Hartog, D.J.D., Ebrahimi, F., Fiksel, G., Forest, C.B., Goetz, J.A., Holly, D., B. Hudson, Lovell, T.W., McCollam, K.J., Nonn, P.D., O'Connell, R.,

Oliva, S.P., Prager, S.C., Reardon, J.C., M.A. Thomas, Wyman, M.D., Brower, D.L., Ding, W.X., Terry, S.D., Carter, M.D., Davydenko, V.I., Ivanov, A.A., R.W. Harvey, Pinsker, R.I., Xiao, C., 2003a. Tokamak-like confinement at a high beta and low toroidal field in the MST reversed field pinch. Nucl. Fusion 43, 1684. https://doi.org/10.1088/0029-5515/43/12/014

Sarff, J.S., Almagri, A.F., Anderson, J.K., Borchardt, M., Cappechi, W., Carmody, D., Caspary, K., B.E. Chapman, Hartog, D.J.D., Duff, J., Eilerman, S., Falkowski, A., Forest, C.B., Galante, M., Goetz, J.A., D.J. Holly, Koliner, J., Kumar, S., Lee, J.D., Liu, D., McCollam, K.J., McGarry, M., Mirnov, V.V., Morton, L., S. Munaretto, Nornberg, M.D., Nonn, P.D., Oliva, S.P., Parke, E., Pueschel, M.J., Reusch, J.A., Sauppe, J., A. Seltzman, Sovinec, C.R., Stone, D., Theucks, D., Thomas, M., Triana, J., Terry, P.W., Waksman, J., Whelan, G.C., D.L. Brower, Ding, W.X., Lin, L., Demers, D.R., Fimognari, P., Titus, J., Auriemma, F., Cappello, S., Franz, P., P. Innocente, Lorenzini, R., Martines, E., Momo, B., Piovesan, P., Puiatti, M., Spolaore, M., Terranova, D., P. Zanca, Davydenko, V.I., Deichuli, P., Ivanov, A.A., Polosatkin, S., Stupishin, N.V., Spong, D., Craig, D., H. Stephens, Harvey, R.W., Cianciosa, M., Hanson, J.D., Breizman, B.N., Li, M., Zheng, L.J., 2015. Overview of results from the MST reversed field pinch experiment. Nucl. Fusion 55, 104006. https://doi.org/10.1088/0029-5515/55/10/104006

Sarff, J.S., Almagri, A.F., Anderson, J.K., Borchardt, M., Carmody, D., Caspary, K., Chapman, B.E., Hartog, D.J.D., Duff, J., Eilerman, S., Falkowski, A., Forest, C.B., Goetz, J.A., Holly, D.J., Kim, J.-H., King, J., Ko, J., J. Koliner, Kumar, S., Lee, J.D., Liu, D., Magee, R., McCollam, K.J., McGarry, M., Mirnov, V.V., Nornberg, M.D., P.D. Nonn, Oliva, S.P., Parke, E., Reusch, J.A., Sauppe, J.P., Seltzman, A., Sovinec, C.R., Stephens, H., Stone, D., D. Theucks, Thomas, M., Triana, J., Terry, P.W., Waksman, J., Bergerson, W.F., Brower, D.L., Ding, W.X., Lin, L., D.R. Demers, Fimognari, P., Titus, J., Auriemma, F., Cappello, S., Franz, P., Innocente, P., Lorenzini, R., E. Martines, Momo, B., Piovesan, P., Puiatti, M., Spolaore, M., Terranova, D., Zanca, P., Belykh, V., V.I. Davydenko, Deichuli, P., Ivanov, A.A., Polosatkin, S., Stupishin, N.V., Spong, D., Craig, D., Harvey, R.W., M. Cianciosa, Hanson, J.D., 2013. Overview of results from the MST reversed field pinch experiment. Nucl. Fusion 53, 104017. https://doi.org/10.1088/0029-5515/53/10/104017

Sarff, J.S., Almagri, A.F., Assadi, S., Den Hartog, D.J., Dexter, R.N., Prager, S.C., Sprott, J.C., 1989. Studies of a reversed field pinch in a poloidal divertor configuration. Nuclear Fusion 29, 104–108. https://doi.org/10.1088/0029-5515/29/1/014

Sarff, J.S., Almagri, A.F., Cekic, M., Chaing, C. -S., Craig, D., Den Hartog, D.J., Fiksel, G., Hokin, S.A., Harvey, R.W., Ji, H., Litwin, C., Prager, S.C., Sinitsyn, D., Sovinec, C.R., Sprott, J.C., Uchimoto, E., 1995. Transport reduction by current profile control in the reversed-field pinch. Physics of Plasmas 2, 2440–2446. https://doi.org/10.1063/1.871268

Sarff, J.S., Anderson, J.K., Biewer, T.M., Brower, D.L., Chapman, B.E., Chattopadhyay, P.K., Craig, D., Deng, B., Hartog, D.J.D., Ding, W.X., Fiksel, G., Forest, C.B., Goetz, J.A., O'Connell, R., Prager, S.C., Thomas, M.A., 2003b. Tokamak-like confinement at high beta and low field in the reversed field pinch. Plasma Phys. Control. Fusion 45, A457. https://doi.org/10.1088/0741-3335/45/12A/029

Sarff, J.S., Hokin, S.A., Ji, H., Prager, S.C., Sovinec, C.R., 1994. Fluctuation and transport reduction in a reversed field pinch by inductive poloidal current drive. Phys. Rev. Lett. 72, 3670–3673. https://doi.org/10.1103/PhysRevLett.72.3670

Sarff, J.S., Lanier, N.E., Prager, S.C., Stoneking, M.R., 1997. Increased Confinement and $\mathit{\ensuremath{\beta}}$ by Inductive Poloidal Current Drive in the Reversed Field Pinch. Phys. Rev. Lett. 78, 62–65. https://doi.org/10.1103/PhysRevLett.78.62

Sätherblom, H.-E., Mazur, S., Nordlund, P., 1996. Resistivity profile effects in numerical magnetohydrodynamic simulations of the reversed-field pinch. Plasma Physics and Controlled Fusion 38, 2205–2214. https://doi.org/10.1088/0741-3335/38/12/012

Sattin, F., Garbet, X., Guo, S.C., 2010. Study of ion-temperature-gradient modes in RFX-mod using TRB code. Plasma Physics and Controlled Fusion 52, 105002. https://doi.org/10.1088/0741-3335/52/10/105002

Sattin, F., Scarin, P., Agostini, M., Cavazzana, R., Serianni, G., Spolaore, M., Vianello, N., 2006. Statistical features of edge turbulence in RFX-mod from gas puffing imaging. Plasma Physics and Controlled Fusion 48, 1033–1051. https://doi.org/10.1088/0741-3335/48/7/011

Sattin, F., Vianello, N., Lorenzini, R., Gobbin, M., Bonomo, F., 2011. Modelling the temperature plateau in RFX-mod single-helical-axis (SHAx) states. Plasma Phys. Control. Fusion 53, 025013. https://doi.org/10.1088/0741-3335/53/2/025013

Sauppe, J.P., Sovinec, C.R., 2017. Extended MHD modeling of tearing-driven magnetic relaxation. Physics of Plasmas 24, 056107. https://doi.org/10.1063/1.4977540

Sauppe, J.P., Sovinec, C.R., 2016. Two-fluid and finite Larmor radius effects on helicity evolution in a plasma pinch. Physics of Plasmas 23, 032303. https://doi.org/10.1063/1.4942761

Sauter, O., Angioni, C., Lin-Liu, Y.R., 1999. Neoclassical conductivity and bootstrap current formulas for general axisymmetric equilibria and arbitrary collisionality regime. Physics of Plasmas. https://doi.org/10.1063/1.873240

Scarin, P., Agostini, M., Spizzo, G., Veranda, M., Zanca, P., the RFX-Mod Team, 2019. Helical plasma-wall interaction in the RFX-mod: effects of high- *n* mode locking. Nuclear Fusion 59, 086008. https://doi.org/10.1088/1741-4326/ab2071

Scarin, P., Vianello, N., Agostini, M., Spizzo, G., Spolaore, M., Zuin, M., Cappello, S., Carraro, L., R. Cavazzana, Masi, G.D., Martines, E., Moresco, M., Munaretto, S., Puiatti, M.E., Valisa, M., Team, the R., 2011. Topology and transport in the edge region of RFX-mod helical regimes. Nucl. Fusion 51, 073002. https://doi.org/10.1088/0029-5515/51/7/073002

Scheffel, J., Dahlin, J.-E., 2006. Confinement scaling in the advanced reversed-field pinch. Plasma Physics and Controlled Fusion 48, L97–L104. https://doi.org/10.1088/0741-3335/48/11/L01

Scheffel, J., Liu, D., 1997. Magnetic fluctuation driven cross-field particle transport in the reversed-field pinch. Physics of Plasmas 4, 3620–3628. https://doi.org/10.1063/1.872257

Scheffel, J., Schnack, D.D., 2000a. Confinement Scaling Laws for the Conventional Reversed-Field Pinch. Physical Review Letters 85, 322–325. https://doi.org/10.1103/PhysRevLett.85.322

Scheffel, J., Schnack, D.D., 2000b. Numerical studies of confinement scaling in the conventional reversed field pinch. Nucl. Fusion 40, 1885. https://doi.org/10.1088/0029-5515/40/11/308

Scheffel, J., Schnack, D.D., Mirza, A.A., 2013. Static current profile control and RFP confinement. Nuclear Fusion 53, 113007. https://doi.org/10.1088/0029-5515/53/11/113007

Schnack, D., 1992. Advances in Reversed Field Pinch Theory and Computation. Presented at the Plasma Physics and Controlled Nuclear Fusion Research, p. 553.

Schnack, D.D., 2009. Lectures in Magnetohydrodynamics, Lecture Notes in Physics. Springer Berlin Heidelberg, Berlin, Heidelberg. https://doi.org/10.1007/978-3-642-00688-3

Schnack, D.D., Barnes, D.C., Mikic, Z., Harned, D.S., Caramana, E.J., 1987. Semi-implicit magnetohydrodynamic calculations. Journal of Computational Physics 70, 330–354. https://doi.org/10.1016/0021-9991(87)90186-0

Schnack, D.D., Caramana, E.J., Nebel, R.A., 1985. Three-dimensional magnetohydrodynamic studies of the reversed-field pinch. Physics of Fluids (1958-1988) 28, 321–333. https://doi.org/10.1063/1.865151

Schnack, D.D., Ortolani, S., 1990. Computational modelling of the effect of a resistive shell on the RFX reversed field pinch experiment. Nucl. Fusion 30, 277–296. https://doi.org/10.1088/0029-5515/30/2/007

Schoenberg, K.F., Gribble, R.F., Baker, D.A., 1984. Oscillating field current drive for reversed field pinch discharges. Journal of Applied Physics 56, 2519–2529. https://doi.org/10.1063/1.334316

Schoenberg, K.F., Gribble, R.F., Phillips, J.A., 1982. Zero-dimensional simulations of reversed-field pinch experiments. Nucl. Fusion 22, 1433. https://doi.org/10.1088/0029-5515/22/11/003

Schoenberg, K.F., Ingraham, J.C., Munson, C.P., Weber, P.G., Baker, D.A., Gribble, R.F., Howell, R.B., Miller, G., Reass, W.A., Schofield, A.E., Shinohara, S., Wurden, G.A., 1988. Oscillating field current drive experiments in a reversed field pinch. The Physics of Fluids 31, 2285–2291. https://doi.org/10.1063/1.866629

Scime, E., Cekic, M., Den Hartog, D.J., Hokin, S., Holly, D.J., Watts, C., 1992. Ion heating and magnetohydrodynamic dynamo fluctuations in the reversed-field pinch. Physics of Fluids B: Plasma Physics 4, 4062–4071. https://doi.org/10.1063/1.860313

Seltzman, A.H., Anderson, J.K., DuBois, A.M., Almagri, A., Forest, C.B., 2016. X-ray analysis of electron Bernstein wave heating in MST. Rev. Sci. Instrum. 87, 11E329. https://doi.org/10.1063/1.4960161

Setiadi, A.C., Brunsell, P.R., Frassinetti, L., 2015. Implementation of model predictive control for resistive wall mode stabilization on EXTRAP T2R. Plasma Physics and Controlled Fusion 57, 104005. https://doi.org/10.1088/0741-3335/57/10/104005

Shiina, S., Kondoh, Y., Saito, K., Shimada, T., Maekawa, T., 1995. Theoretical investigation on r.f. current drive in reversed-field pinch plasma. Fusion Engineering and Design 26, 259–276. https://doi.org/10.1016/0920-3796(94)00193-B

Shiina, S., Nagamine, Y., Taguchi, M., Aizawa, M., Osanai, Y., Yagi, Y., Hirano, Y., Ashida, H., Koguchi, H., Saito, K., Sakakita, H., Sugimoto, H., Watanabe, M., 2005. Neoclassical reversed-field pinch equilibrium with dominant self-induced plasma current. Physics of Plasmas 12, 080702. https://doi.org/10.1063/1.2001407

Sonato, P., Antoni, V., Bagatin, M., Baker, W.R., Peruzzo, S., Tramontin, L., Zaccaria, P., Zollino, G., 1997. Investigation of plasma facing components and vacuum vessel in RFX. Journal of Nuclear Materials 241–243, 982–987. https://doi.org/10.1016/S0022-3115(97)80178-X

Sonato, P., Antoni, V., Baker, W.R., Bertoncello, R., Buffa, A., Carraro, L., Costa, S., Della Mea, G., Marrelli, L., Murari, A., Puiatti, M.E., Rigato, V., Scarin, P., Tramontin, L., Valisa, M., Zandolin, S., 1996. Boronization with trimethylboron in the reversed field pinch RFX. Journal of Nuclear Materials 227, 259–265. https://doi.org/10.1016/0022-3115(95)00161-1

Sonato, P., Antoni, V., Carraro, L., Puiatti, M., Serianni, G., Scarin, P., Spolaore, M., Valisa, M., Zaccaria, P., 2002. Particle control systems at the edge of RFP experiments. Plasma Phys. Control. Fusion 44, 627. https://doi.org/10.1088/0741-3335/44/6/301

Sonato, P., Chitarin, G., Zaccaria, P., Gnesotto, F., Ortolani, S., Buffa, A., Bagatin, M., Baker, W.R., Dal Bello, S., Fiorentin, P., Grando, L., Marchiori, G., Marcuzzi, D., Masiello, A., Peruzzo, S., Pomaro, N., Serianni, G., 2003. Machine modification for active MHD control in RFX. Fusion Engineering and Design 66–68, 161–168. https://doi.org/10.1016/S0920-3796(03)00177-7

Soppelsa, A., Marchiori, G., Marrelli, L., Villone, F., 2009. Integrated identification of RFX-mod active control system from experimental data and finite element model. Fusion Engineering and Design 84, 1784–1788. https://doi.org/10.1016/j.fusengdes.2008.11.025

Sovinec, C.R., 1995. Magnetohydrodynamics simulations of noninductive helicity injection in the Reversed field Pinch and Tokamak, Ph. D. Thesis. University of Wisconsin.

Sovinec, C.R., Gianakon, T.A., Held, E.D., Kruger, S.E., Schnack, D.D., NIMROD Team, 2003. NIMROD: A computational laboratory for studying nonlinear fusion magnetohydrodynamics. Physics of Plasmas 10, 1727. https://doi.org/10.1063/1.1560920

Sovinec, C.R., Glasser, A.H., Gianakon, T.A., Barnes, D.C., Nebel, R.A., Kruger, S.E., Schnack, D.D., Plimpton, S.J., Tarditi, A., Chu, M.S., 2004. Nonlinear magnetohydrodynamics simulation using high-order finite elements. Journal of Computational Physics 195, 355–386. https://doi.org/10.1016/j.jcp.2003.10.004

Sovinec, C.R., Prager, S.C., 1999. Magnetohydrodynamic effects of current profile control in reversed field pinches. Nucl. Fusion 39, 777. https://doi.org/10.1088/0029-5515/39/6/306
Spitzer L, Jr. (1962), n.d. Physics of Fully Ionized Gases, 2nd ed. Interscience, New York, 1962.
Spizzo, G., Agostini, M., Scarin, P., Vianello, N., White, R.B., Cappello, S., Puiatti, M.E., Valisa, M., Team, the R., 2012. Edge topology and flows in the reversed-field pinch. Nucl. Fusion 52, 054015. https://doi.org/10.1088/0029-5515/52/5/054015
Spizzo, G., Cappello, S., Cravotta, A., Escande, D.F., Predebon, I., Marrelli, L., Martin, P., White, R.B., 2006. Transport Barrier inside the Reversal Surface in the Chaotic Regime of the Reversed-Field Pinch. Physical Review Letters 96. https://doi.org/10.1103/PhysRevLett.96.025001
Spizzo, G., Franz, P., Marrelli, L., Martin, P., Murari, A., Bolzonella, T., Terranova, D., Zanca, P., 2001. Mitigation of plasma–wall interaction during quasi-single helicity states in RFX. Journal of Nuclear Materials, 14th Int. Conf. on Plasma-Surface Interactions in Controlled Fusion D evices 290–293, 1018–1022. https://doi.org/10.1016/S0022-3115(00)00462-1
Spizzo, G., Pucella, G., Tudisco, O., Zuin, M., Agostini, M., Alessi, E., Auriemma, F., Bin, W., Buratti, P., Carraro, L., Cavazzana, R., Ciaccio, G., Masi, G.D., Esposito, B., Galperti, C., Garavaglia, S., Granucci, G., Marinucci, M., Marrelli, L., Martines, E., Mazzotta, C., Minelli, D., Moro, A., Puiatti, M.E., Scarin, P., Sozzi, C., Spolaore, M., Schmitz, O., Vianello, N., White, R.B., 2015. Density limit studies in the tokamak and the reversed-field pinch. Nucl. Fusion 55, 043007. https://doi.org/10.1088/0029-5515/55/4/043007
Spizzo, G., Scarin, P., Agostini, M., Alfier, A., Auriemma, F., Bonfiglio, D., Cappello, S., Fassina, A., Franz, P., Piron, L., Piovesan, P., Puiatti, M.E., Valisa, M., Vianello, N., 2010. Investigation on the relation between edge radial electric field asymmetries in RFX-mod and density limit. Plasma Phys. Control. Fusion 52, 095011. https://doi.org/10.1088/0741-3335/52/9/095011
Spizzo, G., Vianello, N., White, R.B., Abdullaev, S.S., Agostini, M., Cavazzana, R., Ciaccio, G., Puiatti, M.E., Scarin, P., Schmitz, O., Spolaore, M., Terranova, D., Teams, R. and T., 2014. Edge ambipolar potential in toroidal fusion plasmasa). Physics of Plasmas (1994-present) 21, 056102. https://doi.org/10.1063/1.4872173
Spizzo, G., White, R.B., Cappello, S., 2007. Chaos generated pinch effect in toroidal confinement devices. Physics of Plasmas 14, 102310. https://doi.org/10.1063/1.2776907
Spizzo, G., White, R.B., Cappello, S., Marrelli, L., 2009. Nonlocal transport in the reversed field pinch. Plasma Phys. Control. Fusion 51, 124026. https://doi.org/10.1088/0741-3335/51/12/124026
Spolaore, M., Antoni, V., Spada, E., Bergsåker, H., Cavazzana, R., Drake, J.R., Martines, E., Regnoli, G., Serianni, G., Vianello, N., 2004. Vortex-Induced Diffusivity In Reversed Field Pinch Plasmas. Physical Review Letters 93. https://doi.org/10.1103/PhysRevLett.93.215003
Spolaore, M., Vianello, N., Furno, I., Carralero, D., Agostini, M., Alonso, J.A., Avino, F., Cavazzana, R., De Masi, G., Fasoli, A., Hidalgo, C., Martines, E., Momo, B., Scaggion, A., Scarin, P., Spagnolo, S., Spizzo, G., Theiler, C., Zuin, M., 2015. Electromagnetic turbulent structures: A ubiquitous feature of the edge region of toroidal plasma configurations. Physics of Plasmas 22, 012310. https://doi.org/10.1063/1.4906869
Spong, D.A., Sanchez, R., Weller, A., 2003. Shear Alfvén continua in stellarators. Physics of Plasmas 10, 3217–3224. https://doi.org/10.1063/1.1590316
Sprott, J.C., 1988. Electrical circuit modeling of reversed field pinches. The Physics of Fluids 31, 2266–2275. https://doi.org/10.1063/1.866627
Stabler, A., McCormick, K., Mertens, V., Muller, E.R., Neuhauser, J., Niedermeyer, H., Steuer, K.-H., Zohm, H., Dollinger, F., Eberhagen, A., Fussmann, G., Gehre, O., Gernhardt, J., Hartinger, T., Hofmann, J.V., Kakoulidis, E., Kaufmann, M., Kyriakakis, G., Lang, R.S., Murmann, H.D., Poschenrieder, W., Ryter, F., Sandmann, W., Schneider, U., Siller, G.,

Soldner, F.X., Tsois, N., Vollmer, O., Wagner, F., 1992. Density limit investigations on ASDEX. Nucl. Fusion 32, 1557. https://doi.org/10.1088/0029-5515/32/9/I05

Steinhauer, L.C., Ishida, A., 1997. Relaxation of a Two-Specie Magnetofluid. Physical Review Letters 79, 3423–3426. https://doi.org/10.1103/PhysRevLett.79.3423

Stephens, H.D., Den Hartog, D.J., Hegna, C.C., Reusch, J.A., 2010. Electron thermal transport within magnetic islands in the reversed-field pinch. Physics of Plasmas 17, 056115. https://doi.org/10.1063/1.3388374

Stoneking, M.R., Chapman, J.T., Hartog, D.J.D., Prager, S.C., Sarff, J.S., 1998. Experimental scaling of fluctuations and confinement with Lundquist number in the reversed-field pinch. Physics of Plasmas (1994-present) 5, 1004–1014. https://doi.org/10.1063/1.872670

Stoneking, M.R., Lanier, N.E., Prager, S.C., Sarff, J.S., Sinitsyn, D., 1997. Fivefold confinement time increase in the Madison Symmetric Torus using inductive poloidal current drive. Physics of Plasmas 4, 1632–1637. https://doi.org/10.1063/1.872324

Sudo, S., Takeiri, Y., Zushi, H., Sano, F., Itoh, K., Kondo, K., Iiyoshi, A., 1990. Scalings of energy confinement and density limit in stellarator/heliotron devices. Nuclear Fusion 30, 11–21. https://doi.org/10.1088/0029-5515/30/1/002

Svidzinski, V.A., Prager, S.C., 2007. On the Physics of Improved Confinement During Pulsed Poloidal Current Drive in MST Reversed-Field Pinch. J Fusion Energ 26, 215–220. https://doi.org/10.1007/s10894-006-9041-6

Sykes, A., Wesson, J., 1977. Field reversal in pinches. Presented at the 8th European Conf. on Controlled Fusion and Plasma Phys., Czechoslovak Academy of Sciences, Prague, 1977, Prague, p. 80.

Tamano, T., Bard, W.D., Chu, C., Kondoh, Y., La Haye, R.J., Lee, P.S., Saito, M., Schaffer, M.J., Taylor, P.L., 1987. Observation of a new toroidally localized kink mode and its role in reverse-field--pinch plasmas. Phys. Rev. Lett. 59, 1444–1447. https://doi.org/10.1103/PhysRevLett.59.1444

Tassi, E., Militello, F., Porcelli, F., Hastie, R.J., 2008. Saturation of tearing modes in reversed field pinches with locally linear force-free magnetic fields and its application to quasi-single-helicity states. Physics of Plasmas 15, 052104. https://doi.org/10.1063/1.2913263

Taylor, J.B., 1986. Relaxation and magnetic reconnection in plasmas. Rev. Mod. Phys. 58, 741–763. https://doi.org/10.1103/RevModPhys.58.741

Telesca, G., Tokar, M.Z., 2004. Modelling of PPCD in the reversed field pinch RFX by the transport code RITM. Nucl. Fusion 44, 303. https://doi.org/10.1088/0029-5515/44/2/012

Terranova, D., Alfier, A., Bonomo, F., Franz, P., Innocente, P., Pasqualotto, R., 2007. Enhanced Confinement and Quasi-Single-Helicity Regimes Induced by Poloidal Current Drive. Phys. Rev. Lett. 99, 095001. https://doi.org/10.1103/PhysRevLett.99.095001

Terranova, D., Auriemma, F., Canton, A., Carraro, L., Lorenzini, R., Innocente, P., 2010. Experimental particle transport studies by pellet injection in helical equilibria. Nucl. Fusion 50, 035006. https://doi.org/10.1088/0029-5515/50/3/035006

Terranova, D., Bolzonella, T., Cappello, S., Innocente, P., Marrelli, L., Pasqualotto, R., 2000. Study of the scaling of magnetic fluctuations in the RFX reversed field pinch [1]. Plasma Physics and Controlled Fusion 42, 843–854. https://doi.org/10.1088/0741-3335/42/7/307

Terranova, D., Marrelli, L., Hanson, J.D., Hirshman, S.P., Cianciosa, M., Franz, P., 2013. Helical equilibrium reconstruction with V3FIT in the RFX-mod Reversed Field Pinch. Nuclear Fusion 53, 113014. https://doi.org/10.1088/0029-5515/53/11/113014

Terry, P.W., Carmody, D., Doerk, H., Guttenfelder, W., Hatch, D.R., Hegna, C.C., Ishizawa, A., Jenko, F., Nevins, W.M., Predebon, I., Pueschel, M.J., Sarff, J.S., Whelan, G.G., 2015. Overview of gyrokinetic studies of finite- β microturbulence. Nuclear Fusion 55, 104011. https://doi.org/10.1088/0029-5515/55/10/104011

Terry, P.W., Fiksel, G., Ji, H., Almagri, A.F., Cekic, M., Den Hartog, D.J., Diamond, P.H., Prager, S.C., Sarff, J.S., Shen, W., Stoneking, M., Ware, A.S., 1996. Ambipolar magnetic

fluctuation-induced heat transport in toroidal devices. Physics of Plasmas 3, 1999–2005. https://doi.org/10.1063/1.871996

Terry, P.W., Whelan, G.G., 2014. Time-dependent behavior in a transport-barrier model for the quasi-single helcity state. Plasma Phys. Control. Fusion 56, 094002. https://doi.org/10.1088/0741-3335/56/9/094002

Terry, S.D., Brower, D.L., Ding, W.X., Anderson, J.K., Biewer, T.M., Chapman, B.E., Craig, D., Forest, C.B., O'Connell, R., Prager, S.C., Sarff, J.S., 2004. Measurement of current profile dynamics in the Madison Symmetric Torus. Physics of Plasmas 11, 1079–1086. https://doi.org/10.1063/1.1643917

Tramontin, L., Antoni, V., Bagatin, M., Boscarino, D., Cattaruzza, E., Rigato, V., Zandolin, S., 1999. Erosion, redeposition and boronization lifetime in RFX. Journal of Nuclear Materials 266–269, 709–713. https://doi.org/10.1016/S0022-3115(98)00837-X

Uchimoto, E., Cekic, M., Harvey, R.W., Litwin, C., Prager, S.C., Sarff, J.S., Sovinec, C.R., 1994. Lower-hybrid poloidal current drive for fluctuation reduction in a reversed field pinch. Physics of Plasmas 1, 3517–3519. https://doi.org/10.1063/1.870886

Valisa, M., Auriemma, F., Canton, A., Carraro, L., Lorenzini, R., Ortolani, S., Paccagnella, R., Puiatti, M.E., Sattin, F., Scarin, P., Spizzo, G., Spolaore, M., Vianello, N., 2004. The Greenwald density limit in the Reversed Field Pinch, in: Proc. 20th IAEA Fusion Energy Conf. IAEA, Vienna, 2004, Vilamoura, Portugal, p. EX/P4-13.

Valisa, M., Bartiromo, R., Bettella, D., Carraro, L., Costa, S., Martin, P., Martini, S., Pasqualotto, R., Puiatti, M.E., Scarin, P., Sattin, F., Telesca, G., Zanca, P., Zaniol, B., 2001. Issues in the plasma wall interactions in RFX. Journal of Nuclear Materials, 14th Int. Conf. on Plasma-Surface Interactions in Controlled Fusion D evices 290–293, 980–984. https://doi.org/10.1016/S0022-3115(00)00545-6

Valisa, M., Bolzonella, T., Buratti, P., Carraro, L., Cavazzana, R., Bello, S.D., Martin, P., Pasqualotto, R., Sarff, J.S., M Spolaore, Zanca, P., Zanotto, L., Agostini, M., Alfier, A., Antoni, V., Apolloni, L., Auriemma, F., Barana, O., Baruzzo, M., P Bettini, Bonfiglio, D., Bonomo, F., Brombin, M., Buffa, A., Canton, A., Cappello, S., Cavinato, M., Chitarin, G., Lorenzi, A.D., Masi, G.D., Escande, D.F., Fassina, A., Franz, P., Gaio, E., Gazza, E., Giudicotti, L., Gnesotto, F., Gobbin, M., L Grando, Guazzotto, L., Guo, S.C., Igochine, V., Innocente, P., Lorenzini, R., Luchetta, A., Manduchi, G., Marchiori, G., D Marcuzzi, Marrelli, L., Martini, S., Martines, E., McCollam, K., Milani, F., Moresco, M., Novello, L., Ortolani, S., R Paccagnella, Peruzzo, S., Piovan, R., Piron, L., Pizzimenti, A., Piovesan, P., Pomaro, N., Predebon, I., Puiatti, M.E., G Rostagni, Sattin, F., Scarin, P., Serianni, G., Sonato, P., Spada, E., Soppelsa, A., Spagnolo, S., Spizzo, G., Taliercio, C., D Terranova, Toigo, V., Vianello, N., Yadikin, D., Zaccaria, P., Zaniol, B., Zilli, E., Zuin, M., 2008. High current regimes in RFX-mod. Plasma Phys. Control. Fusion 50, 124031. https://doi.org/10.1088/0741-3335/50/12/124031

Valisa, M., Bolzonella, T., Carraro, L., Casarotto, E., Costa, S., Garzotti, L., Innocente, P., Martini, S., Pasqualotto, R., Puiatti, M.E., Pugno, R., Scarin, P., 1997. Locked modes induced plasma-wall interactions in RFX. Journal of Nuclear Materials 241–243, 988–992. https://doi.org/10.1016/S0022-3115(97)80179-1

VanMeter, P.D., Delgado-Aparicio, L.F., Reusch, L.M., Hartog, D.J.D., 2019. A versatile multi-energy soft x-ray diagnostic for T_e measurements in the Madison Symmetric Torus. Journal of Instrumentation 14, C09009–C09009. https://doi.org/10.1088/1748-0221/14/09/C09009

Veranda, M., Bonfiglio, D., Cappello, S., Chacón, L., Escande, D.F., 2013. Impact of helical boundary conditions on nonlinear 3D magnetohydrodynamic simulations of reversed-field pinch. Plasma Physics and Controlled Fusion 55, 074015. https://doi.org/10.1088/0741-3335/55/7/074015

Veranda, M., Bonfiglio, D., Cappello, S., di Giannatale, G., Escande, D.F., 2020. Helically self-organized pinches: dynamical regimes and magnetic chaos healing. Nuclear Fusion 60, 016007. https://doi.org/10.1088/1741-4326/ab4863

Veranda, M., Bonfiglio, D., Cappello, S., Escande, D.F., Auriemma, F., Borgogno, D., Chacón, L., Fassina, A., Franz, P., Gobbin, M., Grasso, D., Puiatti, M.E., 2017. Magnetohydrodynamics modelling successfully predicts new helical states in reversed-field pinch fusion plasmas. Nuclear Fusion 57, 116029. https://doi.org/10.1088/1741-4326/aa7f46

Vianello, N, Antoni, V., Spada, E., Spolaore, M., Serianni, G., Cavazzana, R., Bergsåker, H., Cecconello, M., Drake, J.R., 2005. Reynolds and Maxwell stress measurements in the reversed field pinch experiment Extrap-T2R. Nuclear Fusion 45, 761–766. https://doi.org/10.1088/0029-5515/45/8/001

Vianello, N., Martines, E., Agostini, M., Alfier, A., Canton, A., Cavazzana, R., Masi, G.D., Fassina, A., R. Lorenzini, Scarin, P., Serianni, G., Spagnolo, S., Spizzo, G., Spolaore, M., Zuin, M., Team, the R., 2009. Transport mechanisms in the outer region of RFX-mod. Nucl. Fusion 49, 045008. https://doi.org/10.1088/0029-5515/49/4/045008

Vianello, N., Rea, C., Agostini, M., Cavazzana, R., Ciaccio, G., Masi, G.D., Martines, E., Mazzi, A., Momo, B., Spizzo, G., P Scarin, Spolaore, M., Zanca, P., Zuin, M., Carraro, L., Innocente, P., Marrelli, L., Puiatti, M.E., Terranova, D., 2015. Magnetic perturbations as a viable tool for edge turbulence modification. Plasma Phys. Control. Fusion 57, 014027. https://doi.org/10.1088/0741-3335/57/1/014027

Vianello, N., Spada, E., Antoni, V., Spolaore, M., Serianni, G., Regnoli, G., Cavazzana, R., Bergsåker, H., Drake, J.R., 2005. Self-Regulation of Flow Shear via Plasma Turbulence. Physical Review Letters 94. https://doi.org/10.1103/physrevlett.94.135001

Vianello, N., Spolaore, M., Agostini, M., Cavazzana, R., Masi, G.D., Martines, E., Momo, B., Scarin, P., Spagnolo, S., Zuin, M., 2016. On the statistics and features of turbulent structures in RFX-mod. Plasma Phys. Control. Fusion 58, 044009. https://doi.org/10.1088/0741-3335/58/4/044009

Victor, B.S., Jarboe, T.R., Hossack, A.C., Ennis, D.A., Nelson, B.A., Smith, R.J., Akcay, C., Hansen, C.J., Marklin, G.J., Hicks, N.K., Wrobel, J.S., 2011. Evidence for Separatrix Formation and Sustainment with Steady Inductive Helicity Injection. Physical Review Letters 107. https://doi.org/10.1103/PhysRevLett.107.165005

Villone, F., Liu, Y.Q., Paccagnella, R., Bolzonella, T., Rubinacci, G., 2008. Effects of Three-Dimensional Electromagnetic Structures on Resistive-Wall-Mode Stability of Reversed Field Pinches. Physical Review Letters 100, 255005. https://doi.org/10.1103/PhysRevLett.100.255005

Volpe, F.A., Frassinetti, L., Brunsell, P.R., Drake, J.R., Olofsson, K.E.J., 2013. Error field assessment from driven rotation of stable external kinks at EXTRAP-T2R reversed field pinch. Nuclear Fusion 53, 043018. https://doi.org/10.1088/0029-5515/53/4/043018

Waksman, J., Anderson, J.K., Nornberg, M.D., Parke, E., Reusch, J.A., Liu, D., Fiksel, G., Davydenko, V.I., Ivanov, A.A., Stupishin, N., Deichuli, P.P., Sakakita, H., 2012. Neutral beam heating of a RFP plasma in MST. Physics of Plasmas 19, 122505. https://doi.org/10.1063/1.4772763

Watterson, P., Gimblett, C.G., 1983. Catching voltage prescriptions for the RFP, theoretical Physics Note 83/10.

Weber, P.G., 1985. Spectroscopic investigation of a reversed field pinch operated without limiters. Physics of Fluids 28, 3136. https://doi.org/10.1063/1.865355

Weller, A., Sakakibara, S., Watanabe, K.Y., Toi, K., Geiger, J., Zarnstorff, M.C., Hudson, S.R., Reiman, A., Werner, A., Nührenberg, C., Ohdachi, S., Suzuki, Y., Yamada, H., W7-AS Team, LHD Team, 2006. Significance of MHD Effects in Stellarator Confinement. Fusion Science and Technology 50, 158–170. https://doi.org/10.13182/FST06-A1231

Werley, K.A., 1991. Reversed field pinch ignition requirements. Nuclear Fusion 31, 567–582. https://doi.org/10.1088/0029-5515/31/3/015

Werley, K.A., Bathke, C.G., 1994. Startup and Shutdown of the PULSAR Tokamak Reactor. Fusion Technology 26, 582–587. https://doi.org/10.13182/FST94-A40220

Werley, K.A., Nebel, R.A., Wurden, G.A., 1985. Transport description of the rise time of sawtooth oscillations in reversed-field pinches. The Physics of Fluids 28, 1450–1453. https://doi.org/10.1063/1.864979

Wesson, J.A., 2004. Tokamaks - third Edition, Clarendon Press-Oxford. ed. Clarendon Press-Oxford.

White, R.B., Chance, M.S., 1984. Hamiltonian guiding center drift orbit calculation for plasmas of arbitrary cross section. Physics of Fluids (1958-1988) 27, 2455–2467. https://doi.org/10.1063/1.864527

Wyman, M.D., Chapman, B.E., Ahn, J.W., Almagri, A.F., Anderson, J.K., Bonomo, F., Brower, D.L., Combs, S.K., Craig, D., Den Hartog, D.J., Deng, B.H., Ding, W.X., Ebrahimi, F., Ennis, D.A., Fiksel, G., Foust, C.R., Franz, P., Gangadhara, S., Goetz, J.A., O'Connell, R., Oliva, S.P., Prager, S.C., Reusch, J.A., Sarff, J.S., Stephens, H.D., Yates, T., 2009. Plasma behaviour at high β and high density in the Madison Symmetric Torus RFP. Nuclear Fusion 49, 015003. https://doi.org/10.1088/0029-5515/49/1/015003

Wyman, M.D., Chapman, B.E., Ahn, J.W., Almagri, A.F., Anderson, J.K., Bonomo, F., Brower, D.L., Combs, S.K., Craig, D., Hartog, D.J.D., Deng, B.H., Ding, W.X., Ebrahimi, F., Ennis, D.A., Fiksel, G., Foust, C.R., Franz, P., Gangadhara, S., Goetz, J.A., O'Connell, R., Oliva, S.P., Prager, S.C., Reusch, J.A., Sarff, J.S., Stephens, H.D., Yates, T., 2008a. High-β, improved confinement reversed-field pinch plasmas at high density. Physics of Plasmas (1994-present) 15, 010701. https://doi.org/10.1063/1.2835439

Wyman, M.D., Chapman, B.E., Ahn, J.W., Almagri, A.F., Anderson, J.K., Bonomo, F., Brower, D.L., Combs, S.K., Craig, D., Hartog, D.J.D., Deng, B.H., Ding, W.X., Ebrahimi, F., Ennis, D.A., Fiksel, G., Foust, C.R., Franz, P., Gangadhara, S., Goetz, J.A., O'Connell, R., Oliva, S.P., Prager, S.C., Reusch, J.A., Sarff, J.S., Stephens, H.D., Yates, T., 2008b. Plasma behaviour at high β and high density in the Madison Symmetric Torus RFP. Nucl. Fusion 49, 015003. https://doi.org/10.1088/0029-5515/49/1/015003

Yagi, Y., Koguchi, H., Hirano, Y., Sakakita, H., Frassinetti, L., 2005. An empirical scaling law for improved confinement in reversed-field pinch plasmas. Nuclear Fusion 45, 138–142. https://doi.org/10.1088/0029-5515/45/2/007

Yagi, Y., Koguchi, H., Hirano, Y., Sakakita, H., Shimada, T., Sekine, S., 2002. Figure of Merit for the Improvement of Confinement in Pulsed Poloidal Current Drive Experiments in Reversed-Field Pinch Devices. J. Phys. Soc. Jpn. 71, 2574–2575. https://doi.org/10.1143/JPSJ.71.2574

Yagi, Y., Koguchi, H., Hirano, Y., Shimada, T., Sakakita, H., Sekine, S., Chapman, B.E., Sarff, J.S., 2003. Increased confinement improvement in a reversed-field pinch using double-pulsed poloidal current drive. Physics of Plasmas (1994-present) 10, 2925–2931. https://doi.org/10.1063/1.1581883

Yagi, Yasuyuki, Koguchi, H., Sakakita, H., Sekine, S., Maejima, Y., Nilsson, J.-A.B., Bolzonella, T., Zanca, P., 1999. Mode-locking phenomena in the TPE-RX reversed-field pinch plasma. Physics of Plasmas 6, 3824–3837. https://doi.org/10.1063/1.873647

Yagi, Y., Sekine, S., Shimada, T., Masiello, A., Hayase, K., Hirano, Y., Hirota, I., Kiyama, S., Koguchi, H., Maejima, Y., Sakakita, H., Sato, Y., Sugisaki, K., Hasegawa, M., Yamane, M., Sato, F., Oyabu, I., Kuno, K., Minato, T., Kiryu, A., Takagi, S., Sako, K., Kudough, F., Urata, K., Kaguchi, H., Orita, J., Sago, H., Ishigami, Y., 1999. Front-end system of the TPE-RX reversed-field pinch machine. Fusion Engineering and Design 45, 421–436. https://doi.org/10.1016/S0920-3796(99)00056-3

Yagi, Y., Shimada, T., Hirota, I., Maejima, Y., Hirano, Y., Ogawa, K., Namiki, K., Ioki, K., 1989. Movable limiter experiment on tpe-1rm15 reversed field pinch machine. Journal of Nuclear Materials 162, 702–709. https://doi.org/10.1016/0022-3115(89)90351-6

Yamaguchi, S., Schaffer, M., Kondoh, Y., 1995. Preliminary oscillating fluxes current drive experiment in DIII-D tokamak. Fusion Engineering and Design 26, 121–132. https://doi.org/10.1016/0920-3796(94)00177-9

Yambe, K., Hirano, Y., Sakakita, H., Koguchi, H., 2014. Improved confinement region without large magnetohydrodynamic activity in TPE-RX reversed-field pinch plasma. Physics of Plasmas 21, 114502. https://doi.org/10.1063/1.4901350

Zanca, P., 2010. Feedback control of dynamo tearing modes in a reversed field pinch: comparison between out-vessel and in-vessel active coils. Plasma Physics and Controlled Fusion 52, 115002. https://doi.org/10.1088/0741-3335/52/11/115002

Zanca, P., 2009. Avoidance of tearing modes wall-locking in a reversed field pinch with active feedback coils. Plasma Physics and Controlled Fusion 51, 015006. https://doi.org/10.1088/0741-3335/51/1/015006

Zanca, P., 2007. Self-similar current decay experiment in RFX-mod. Plasma Phys. Control. Fusion 49, 113. https://doi.org/10.1088/0741-3335/49/2/002

Zanca, P., Bettella, D., Martini, S., Valisa, M., 2001a. Non-axisymmetric perturbation of the plasma surface in RFX: analysis of magnetic data versus CCD images of plasma–wall interaction. Journal of Nuclear Materials 290–293, 990–994. https://doi.org/10.1016/S0022-3115(00)00474-8

Zanca, P., Marchiori, G., Marrelli, L., Piron, L., the RFX-mod team, 2012a. Advanced feedback control of magnetohydrodynamic instabilities: comparison of compensation techniques for radial sensors. Plasma Physics and Controlled Fusion 54, 124018. https://doi.org/10.1088/0741-3335/54/12/124018

Zanca, P., Marrelli, L., Manduchi, G., Marchiori, G., 2007. Beyond the intelligent shell concept: the clean-mode-control. Nuclear Fusion 47, 1425–1436. https://doi.org/10.1088/0029-5515/47/11/004

Zanca, P., Marrelli, L., Paccagnella, R., Soppelsa, A., Baruzzo, M., Bolzonella, T., Marchiori, G., Martin, P., Piovesan, P., 2012b. Feedback control model of the $m = 2$, $n = 1$ resistive wall mode in a circular plasma. Plasma Phys. Control. Fusion 54, 094004. https://doi.org/10.1088/0741-3335/54/9/094004

Zanca, P., Martines, E., Bolzonella, T., Cappello, S., Guo, S.C., Martin, P., Martini, S., Ortolani, S., Paccagnella, R., Terranova, D., Viterbo, M., 2001b. Analysis of phase locking of tearing modes in reversed field pinch plasmas. Physics of Plasmas 8, 516–524. https://doi.org/10.1063/1.1339835

Zanca, P., Martini, S., 1999. Reconstruction of the plasma surface in a RFP in the presence of non-axisymmetric perturbations. Plasma Physics and Controlled Fusion 41, 1251–1275. https://doi.org/10.1088/0741-3335/41/10/304

Zanca, P., Sattin, F., Escande, D.F., JET Contributors, 2019. A power-balance model of the density limit in fusion plasmas: application to the L-mode tokamak. Nuclear Fusion 59, 126011. https://doi.org/10.1088/1741-4326/ab3b31

Zanca, P., Sattin, F., Escande, D.F., Pucella, G., Tudisco, O., 2017. A unified model of density limit in fusion plasmas. Nuclear Fusion 57, 056010. https://doi.org/10.1088/1741-4326/aa6230

Zanca, P., Terranova, D., 2004. Reconstruction of the magnetic perturbation in a toroidal reversed field pinch. Plasma Phys. Control. Fusion 46, 1115. https://doi.org/10.1088/0741-3335/46/7/011

Zanca, P., Terranova, D., Valisa, M., Dal Bello, S., 2007. Plasma wall interactions in RFX-mod with virtual magnetic boundary. Journal of Nuclear Materials 363–365, 733–737. https://doi.org/10.1016/j.jnucmat.2007.01.072

Zheng, J., Song, Y., Yang, Q., Liu, X., Xiao, B., Luo, Z., Ding, W., Liu, W., Du, S., Li, H., Zhang, J., Zhao, W., 2012. Preliminary design of KTX magnet system. Fusion Engineering and Design 87, 1853–1860. https://doi.org/10.1016/j.fusengdes.2012.09.001

Zonca, F., Chen, L., Dong, J.Q., Santoro, R.A., 1999. Existence of ion temperature gradient driven shear Alfvén instabilities in tokamaks. Physics of Plasmas 6, 1917–1924. https://doi.org/10.1063/1.873449

Zuin, M., Dal Bello, S., Marrelli, L., Puiatti, M.E., Agostinetti, P., Agostini, M., Antoni, V., Auriemma, F., Barbisan, M., Barbui, T., Baruzzo, M., Belli, F., Bettini, P., Bigi, M., Bilel, R., Boldrin, M., Bolzonella, T., Bonfiglio, D., Brombin, M., Buffa, A., Bustreo, C., Canton, A., Cappello, S., Carraro, L., Cavazzana, R., Cester, D., Chacon, L., Chitarin, G., Cooper, W.A., Cordaro, L., Dalla Palma, M., Deambrosis, S., Delogu, R., De Lorenzi, A., De Masi, G., Dong, J.Q., Escande, D.F., Fassina, A., Felici, F., Ferro, A., Finotti, C., Franz, P., Frassinetti, L., Gaio, E., Ghezzi, F., Giudicotti, L., Gnesotto, F., Gobbin, M., Gonzalez, W.A., Grando, L., Guo, S.C., Hanson, J.D., Hirshman, S.P., Innocente, P., Jackson, J.L., Kiyama, S., Komm, M., Kudlacek, O., Laguardia, L., Li, C., Liu, B., Liu, S.F., Liu, Y.Q., López- Bruna, D., Lorenzini, R., Luce, T.C., Luchetta, A., Maistrello, A., Manduchi, G., Mansfield, D.K., Marchiori, G., Marconato, N., Marcuzzi, D., Martin, P., Martines, E., Martini, S., Mazzitelli, G., McCormack, O., Miorin, E., Momo, B., Moresco, M., Narushima, Y., Okabayashi, M., Paccagnella, R., Patel, N., Pavei, M., Peruzzo, S., Pilan, N., Pigatto, L., Piovan, R., Piovesan, P., Piron, C., Piron, L., Predebon, I., Pucella, G., Rea, C., Recchia, M., Rizzolo, A., Rostagni, G., Ruset, C., Sajò-Bohus, L., Sakakita, H., Sanchez, R., Sarff, J.S., Sattin, F., Scarin, P., Schmitz, O., Schneider, W., Siragusa, M., Sonato, P., Spada, E., Spagnolo, S., Spolaore, M., Spong, D.A., Spizzo, G., Stevanato, L., Suzuki, Y., Taliercio, C., Terranova, D., Tudisco, O., Urso, G., Valente, M., Valisa, M., Vallar, M., Veranda, M., Vianello, N., Villone, F., Vincenzi, P., Visonà, N., White, R.B., Xanthopoulos, P., Xu, X.Y., Yanovskiy, V., Zamengo, A., Zanca, P., Zaniol, B., Zanotto, L., Zhang, Y., Zilli, E., 2017. Overview of the RFX-mod fusion science activity. Nuclear Fusion 57, 102012. https://doi.org/10.1088/1741-4326/aa61cc

Zuin, M., Spagnolo, S., Paccagnella, R., Martines, E., Cavazzana, R., Serianni, G., Spolaore, M., Vianello, N., 2010. Resistive g-modes in a reversed-field pinch plasma. Nucl. Fusion 50, 052001. https://doi.org/10.1088/0029-5515/50/5/052001

Zuin, M., Spagnolo, S., Predebon, I., Sattin, F., Auriemma, F., Cavazzana, R., Fassina, A., Martines, E., Paccagnella, R., Spolaore, M., Vianello, N., 2013. Experimental Observation of Microtearing Modes in a Toroidal Fusion Plasma. Physical Review Letters 110. https://doi.org/10.1103/PhysRevLett.110.055002

Zuin, M., Vianello, N., Spolaore, M., Antoni, V., Bolzonella, T., Cavazzana, R., Martines, E., Serianni, G., Terranova, D., 2009. Current sheets during spontaneous reconnection in a current-carrying fusion plasma. Plasma Phys. Control. Fusion 51, 035012. https://doi.org/10.1088/0741-3335/51/3/035012

Zuo, G.Z., Hu, J.S., Zhen, S., Li, J.G., Mansfield, D.K., Cao, B., Wu, J.H., Zakharov, L.E., the EAST Team, 2012. Comparison of various wall conditionings on the reduction of H content and particle recycling in EAST. Plasma Physics and Controlled Fusion 54, 015014. https://doi.org/10.1088/0741-3335/54/1/015014

Figures

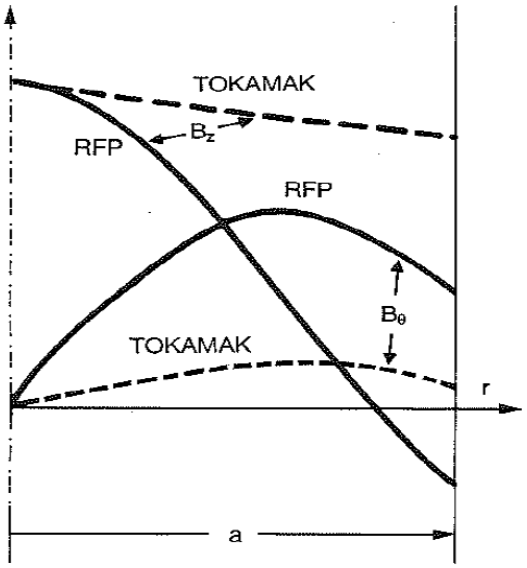

Fig. 2.1) The Toroidal (B_ϕ) and poloidal (B_Θ) magnetic field profile in Reversed Field Pinch and Tokamak. From (Ortolani and Schnack, 1993)

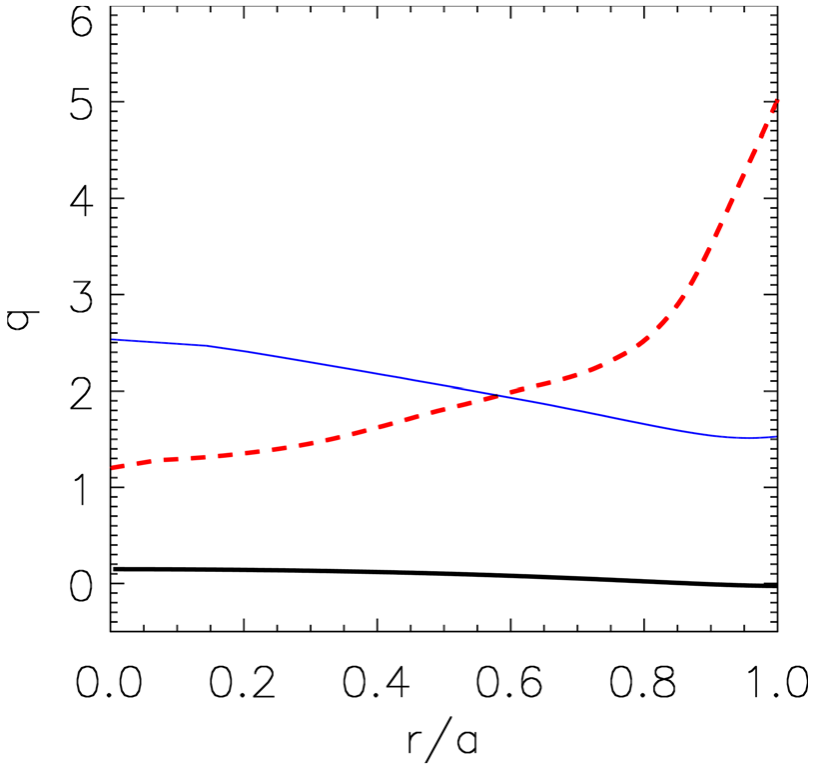

Fig. 2.2) Safety factor profiles for three different fusion plasma configurations: the RFP (black thick line), the tokamak (dashed red line), the stellarator (blue thin line). From (Gobbin et al., 2011a)

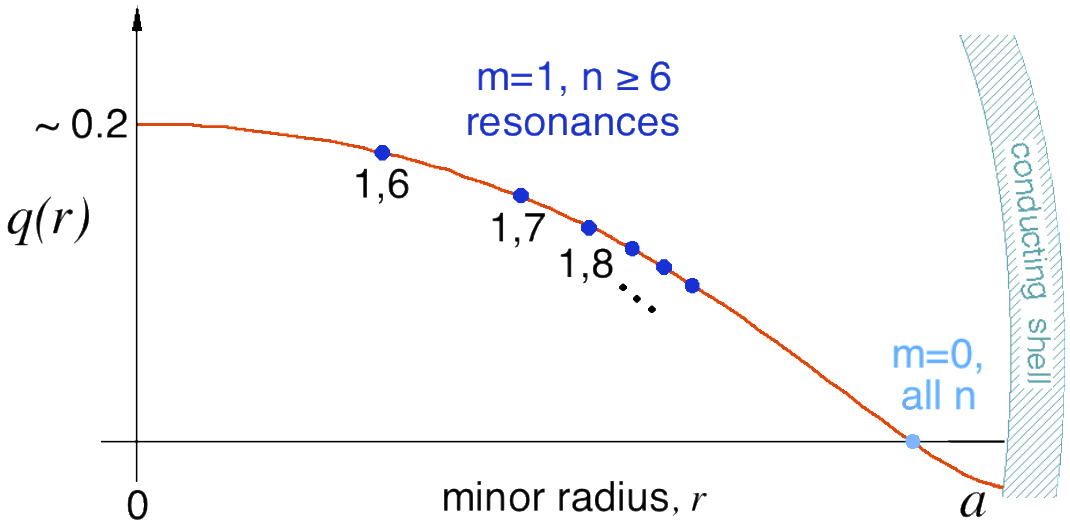

Fig. 2.3) The safety factor profile $q(r) = rB_\phi/RB_\theta$ for a typical RFP. The multiple $m = 1$ Fourier modes resonant in the core and the $m = 0$ modes resonant at the $q = 0$ surface underlie the nonlinear dynamics of the RFP.

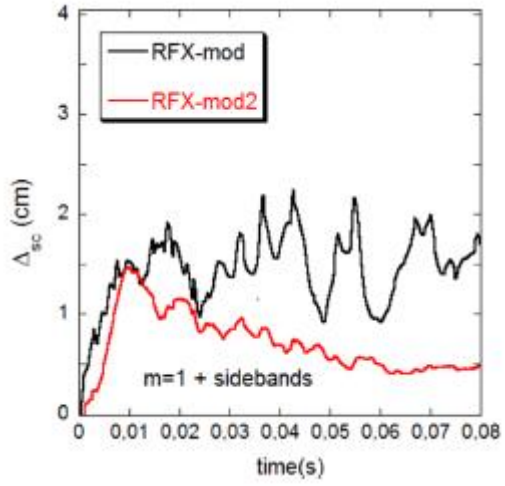

Fig. 2.4) Deformation of the LCMS, with the vacuum vessel removed (red) and with vacuum vessel (black). Taken from (Zuin et al., 2017)

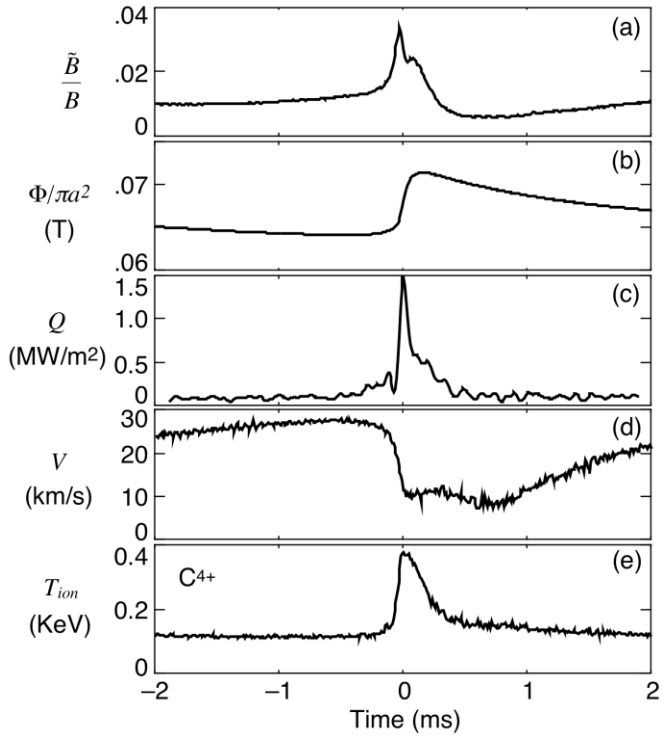

Fig. 3.1) A prototypical RFP sawtooth, ensemble averaged from a large number of similar events recorded on the MST RFP. Time $t = 0$ *is a marker at the peak of sawtooth activity. Each panel represents the change in a key parameter during a sawtooth event. a) relative amplitude of magnetic fluctuations, illustrating tearing mode growth; b) toroidal magnetic flux density, illustrating RFP dynamo activity; c) heat flux, indicative of magnetic stochastic transport; d) plasma flow, indicative of momentum transport; and e) ion temperature; demonstrating ion heating.*

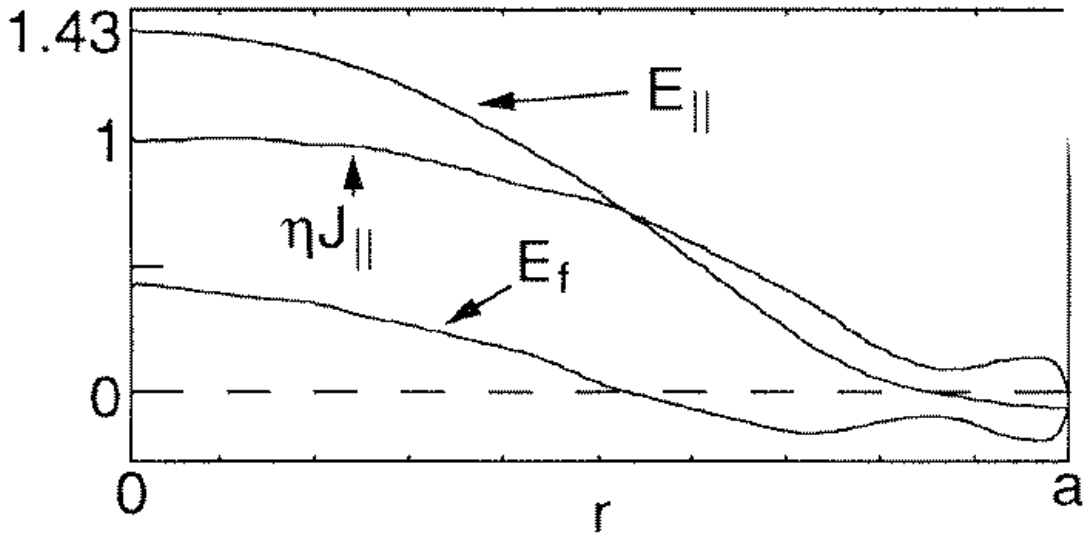

Fig. 3.2) Parallel electric field profiles for the RFP from a 3D visco-resistive MHD simulation. $E_{\|}$ is externally applied, $E_{f\|}$ is the MHD dynamo, and $J_{\|}$ is the resulting current density profile. Taken from (Ho, 1991).

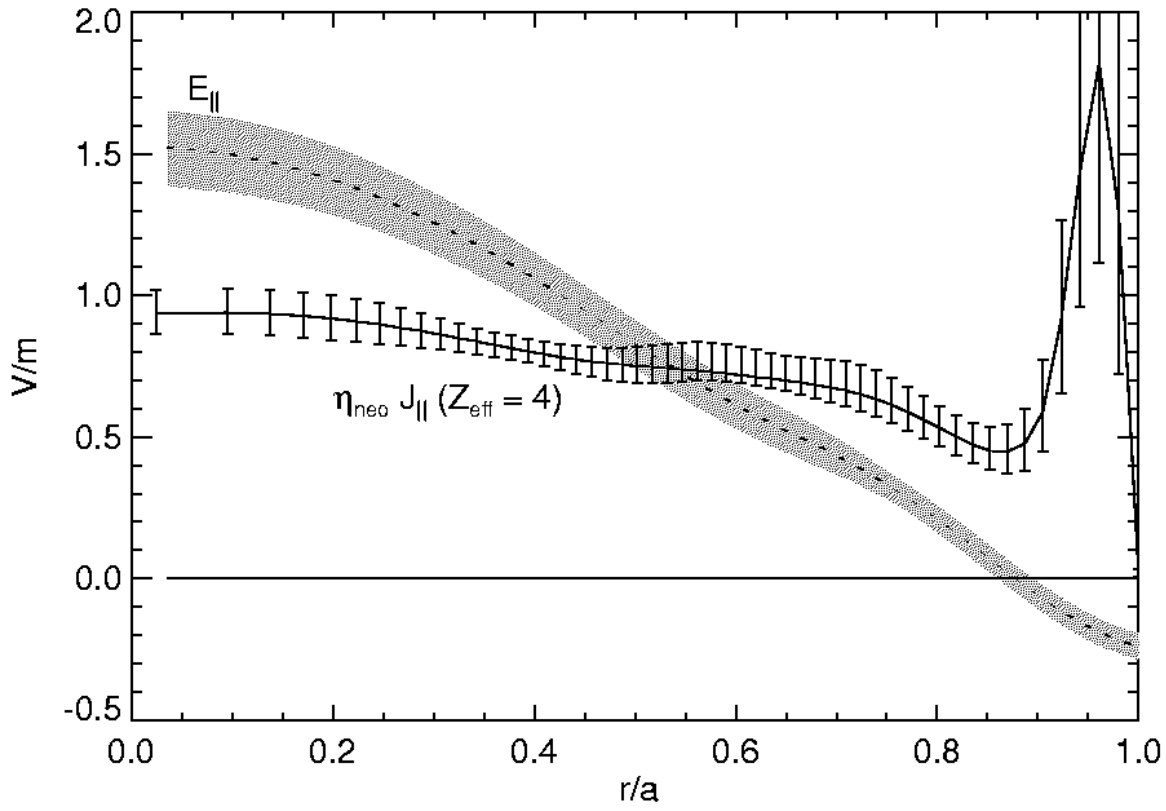

Fig. 3.3) Results from an equilibrium reconstruction illustrating that $E_{\|} \neq \eta J_{\|}$ in standard multiple-helicity RFP operation. In particular, the existence of a radial location with zero applied electric field and finite current density makes clear the need for dynamo drive. [From (Anderson et al., 2004).]

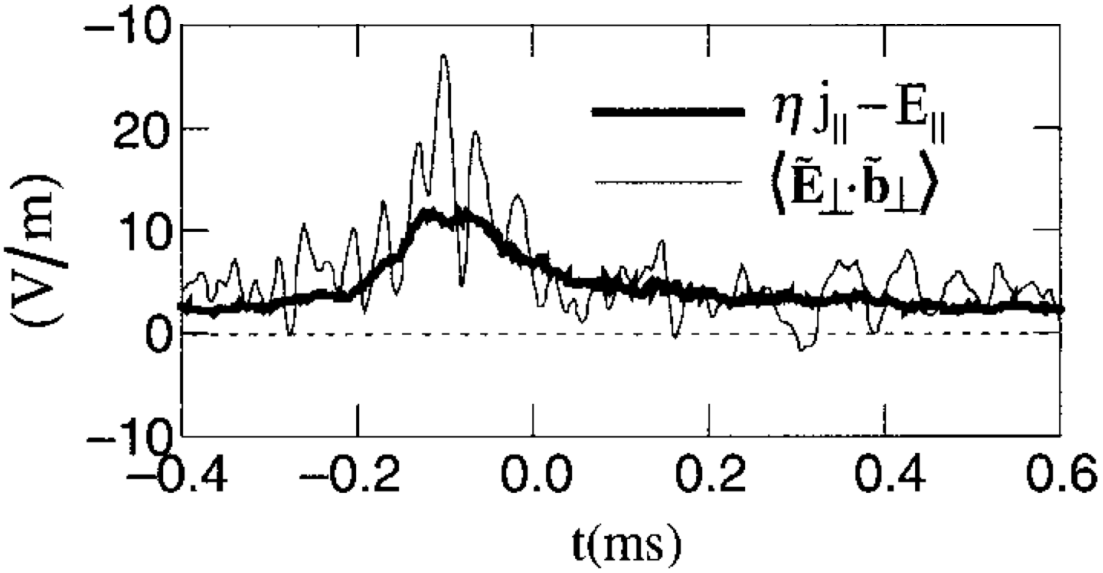

Fig. 3.4) Comparison of the dynamo electric field $\langle \widetilde{\boldsymbol{E}}_{\perp} \cdot \widetilde{\boldsymbol{b}}_{\perp} \rangle$ *to* $\eta \boldsymbol{J}_{\parallel} - E_{\parallel}$ *from an ensemble of sawtooth relaxation events in the MST RFP. Time t = 0 is a reproducible time marker for aligning individual sawtooth events during ensemble averaging. [From (Ji et al., 1996)]*

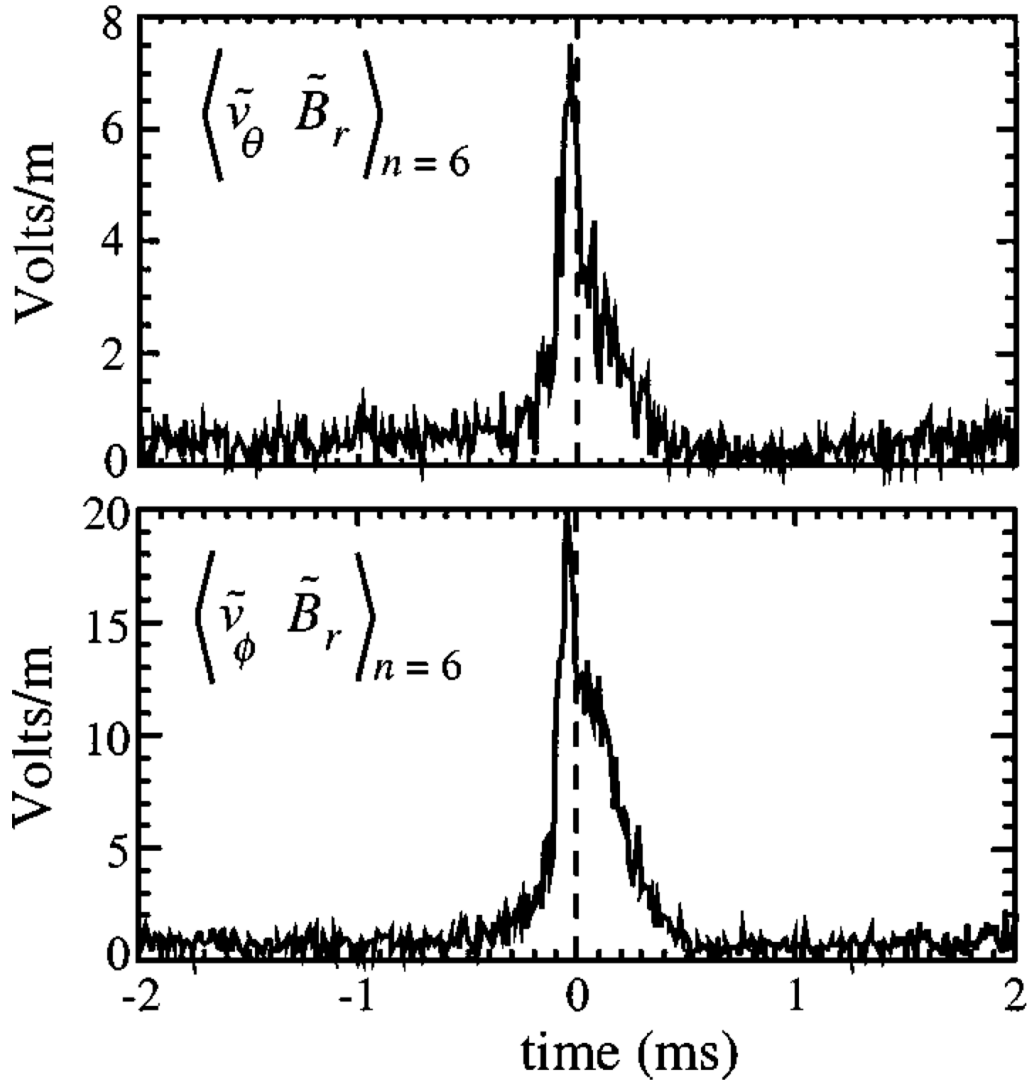

Fig. 3.5) Two m = 1, n = 6 components of the dynamo, both of which suppress parallel current in the core of MST. The velocity and magnetic fluctuations reach peak coherence at the sawtooth event (t = 0) and are nearly in phase, maximizing the dynamo product. Taken from (Den Hartog et al., 1999)

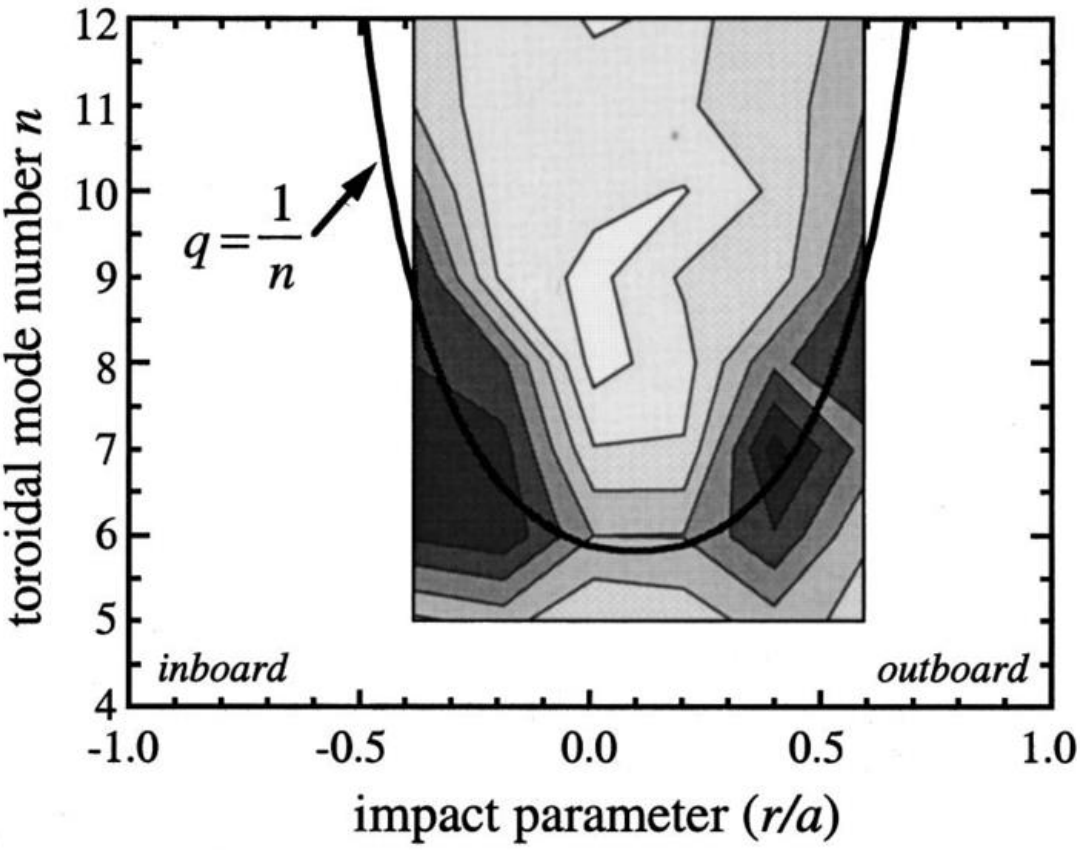

Fig. 3.6) Amplitude contours of the mode-resolved poloidal velocity fluctuation $\left\{\sqrt{\tilde{v}_\theta^2}\right\}_n$. *The velocity fluctuation amplitude for a particular n-mode peaks approximately at the impact parameter where that mode is expected to be resonant (estimated from the q profile). [From (Den Hartog et al., 1999)]*

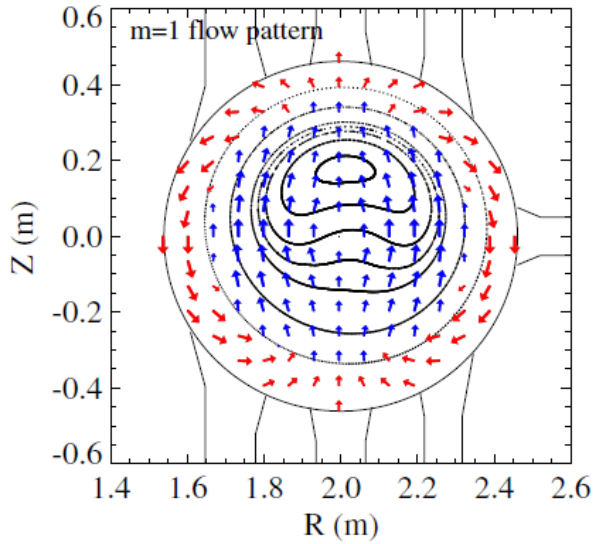

Fig. 3.7) 2D reconstruction of the flow pattern in RFX-mod from multichord Doppler shift measurements. Data refer to a 1.2 MA plasma discharge. The flow is radially directed towards the helical magnetic axis in the core and changes the sign moving to the edge . The helical axis is represented by the reconstructed helical magnetic surfaces. From (Bonomo et al., 2011).

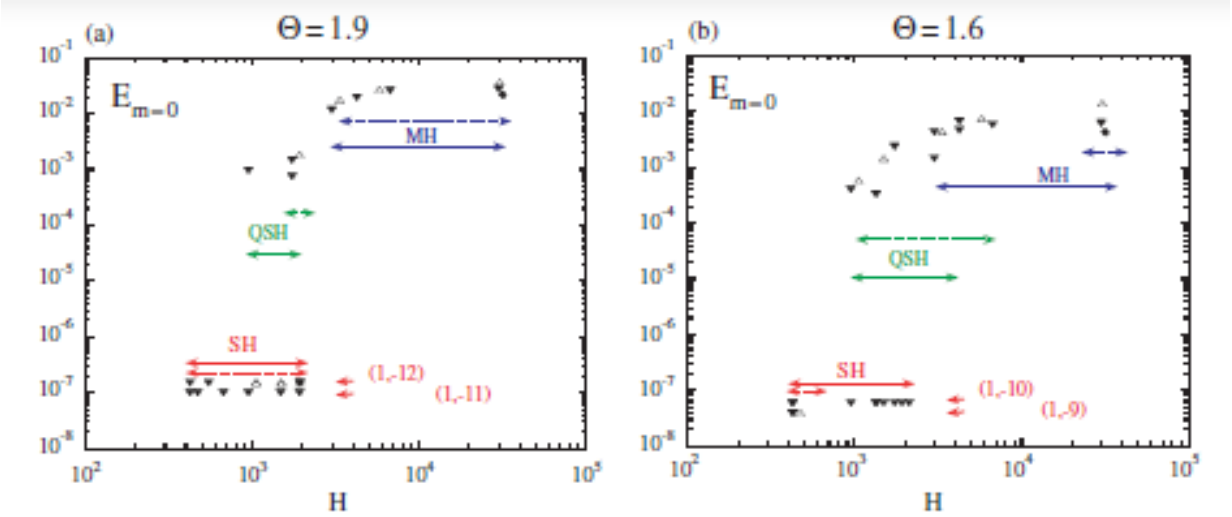

Fig. 3.8) Transition diagrams at two values of the pinch parameter: a) Θ = 1:9, b) Θ = 1:6. $E_{m=0}$ is the time averaged magnetic energy of the m = 0 modes and H is the Hartmann number. The open triangles correspond to S = 3.3 10^3 with P = [0.012, 50], black triangles to S = 3.0 10^4 with P = [1, 5000], and black circles to S = 10^5 with P = 10. The vanishing SH m = 0 modes energy is represented as a finite conventional value with different offsets associated to the different preferred helicities (from (Cappello, 2004)).

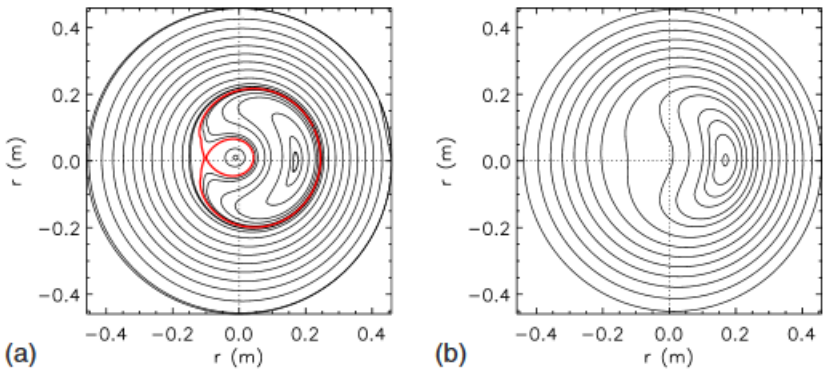

Fig. 3.9) Magnetic topology reconstructed using only the axi-symmetric fields and the eigenfunction of the dominant mode: (a) QSH with a magnetic island; (b) SHAx state (from (Lorenzini et al., 2009a))

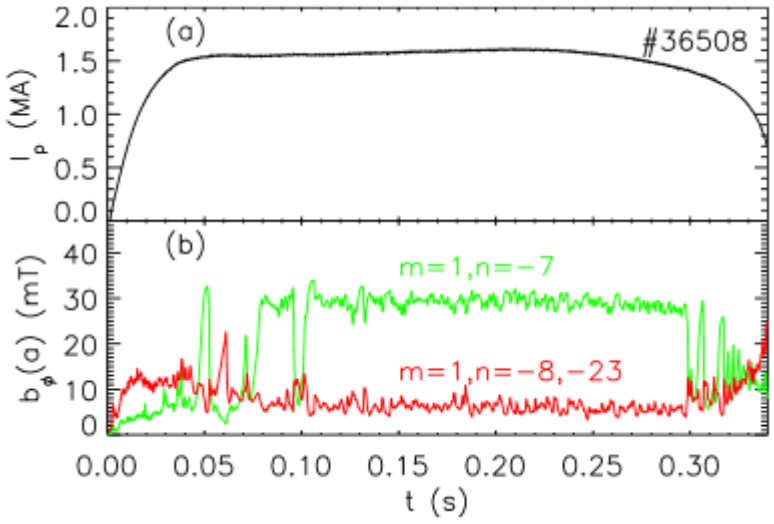

Fig. 3.10) Example of a spontaneous long-lasting QSH in RFX-mod; (top) time evolution of plasma current;(bottom) amplitude of dominant m=1,n=7 tearing mode (red) and averaged amplitude of secondary modes. Adapted from (Lorenzini et al., 2015)

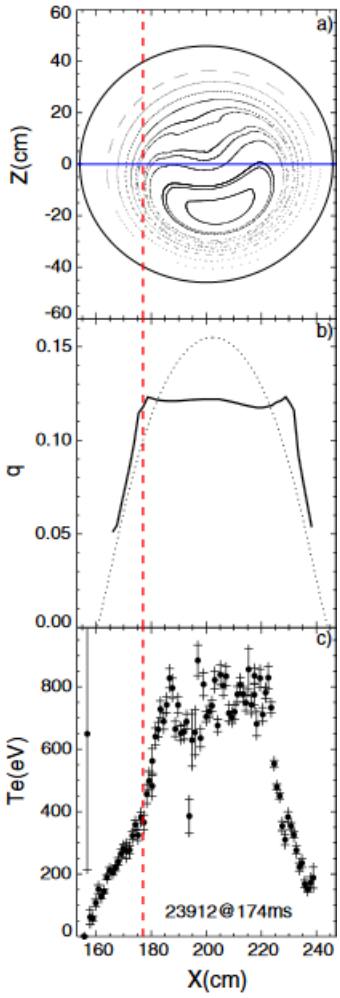

Fig. 3.11) For a SHAx in RFX-mod: (a) Poincare' plot; (b) safety factor profile (plain line) compared to the axisymmetric case (dashed); (c) temperature profile from Thomson scattering as measured along a diameter (blue line in plot (a).(From (Gobbin et al., 2011b))

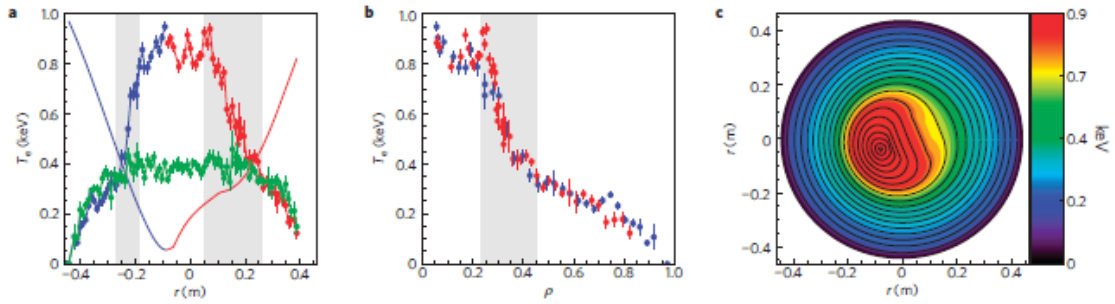

Fig. 3.12) InRFX-mod, mapping of measured electron temperature Te on helical flux surfaces.(a) Te profile as measured by Thomson scattering, with the continuous line corresponding to the helical coordinate ρ, (b) te profile mapped on the helical coordinate ρ; (c) 2-d map of te on the poloidal plane, with helical flux surfaces superimposed. From (Lorenzini et al., 2009b)

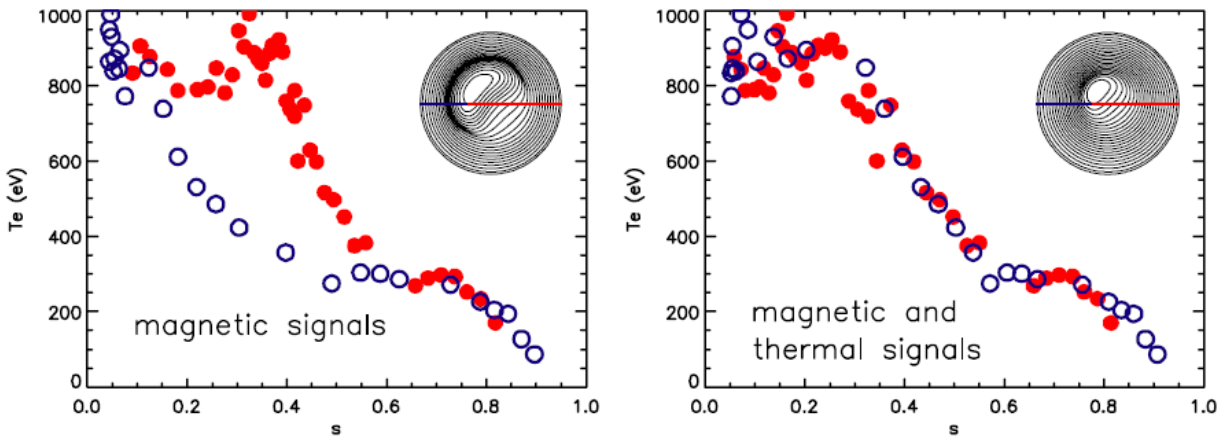

Fig. 3.13) Remapping of electron temperature measurements on magnetic flux surfaces (see small plots) as obtained by the V3FIT code. Empty and full circles refer to different sides with respect to the helical axis. Left plot: force-free equilibrium obtained using only magnetic measurements. Right plot equilibrium with pressure consistent with temperature and density measurements. From (Terranova et al., 2013)

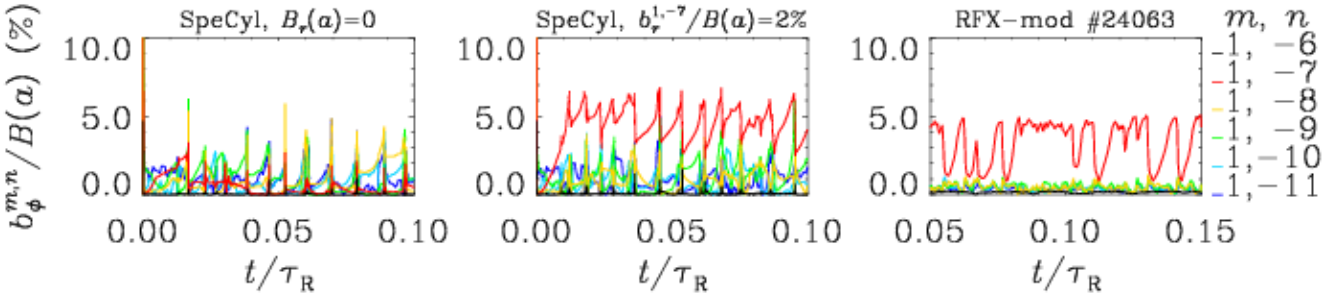

Fig. 3.14) Simulation of the time evolution of the m=1 tearing modes by the Specyl code; (left) with ideal boundary conditions; (middle) with 2% perturbation; (left) comparison with a RFX-mod experiment. The Lundquist number in the simulation is about the experimental one (10^7) (from (Puiatti et al., 2015))

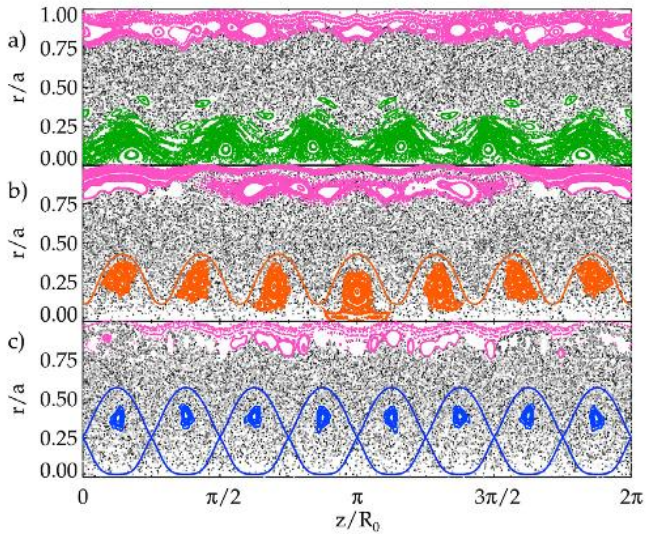

Fig. 3.15) Poincare' maps from simulations at θ=0 with a 2% magnetic perturbation (MP) as boundary condition.; (top) MP with helicity m=1,n=6, non resonant; (middle) MP with helicity m=1,n=6; (bottom) MP with helicity m=1,n=8. The n=6 case shows larger areas of conserved surfaces. (From (Veranda et al., 2017))

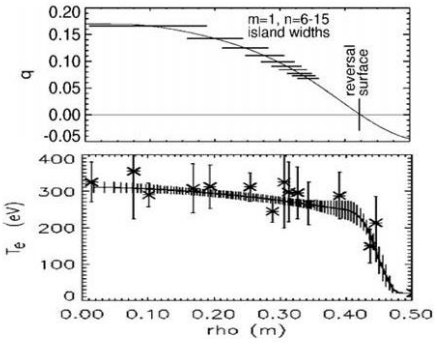

Fig. 4.1) (top) radial extent of magnetic islands in a MST MH discharge, superimposed to the q profile; (bottom) corresponding temperature profile. Adapted from (Biewer et al., 2003)

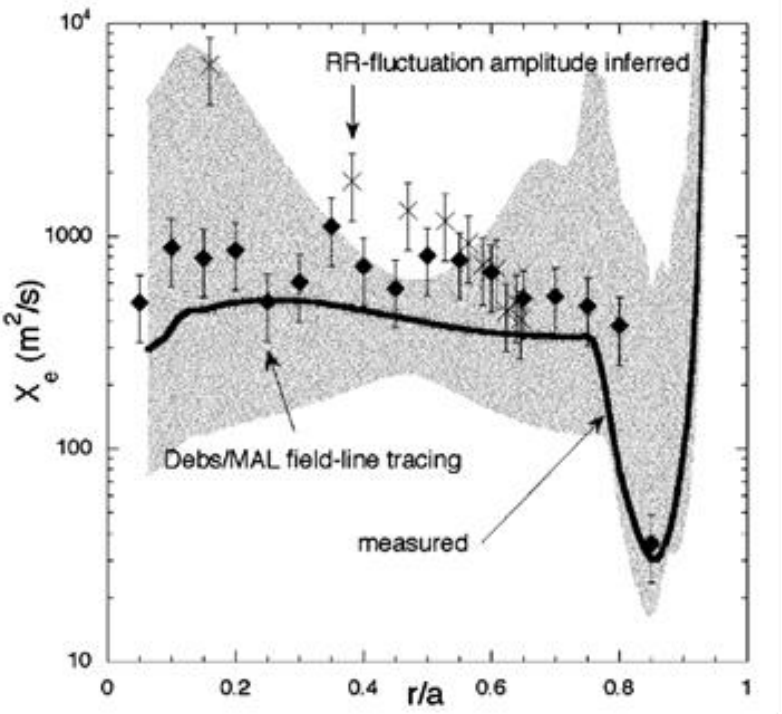

Fig. 4.2) Measured profile of electron thermal diffusivity in MST (solid line), compared with DEBS simulations (diamonds) and Rechester and Rosenbluth theory (crosses). The grey region is representative on the uncertainty in the measurements. From (Biewer et al., 2003)

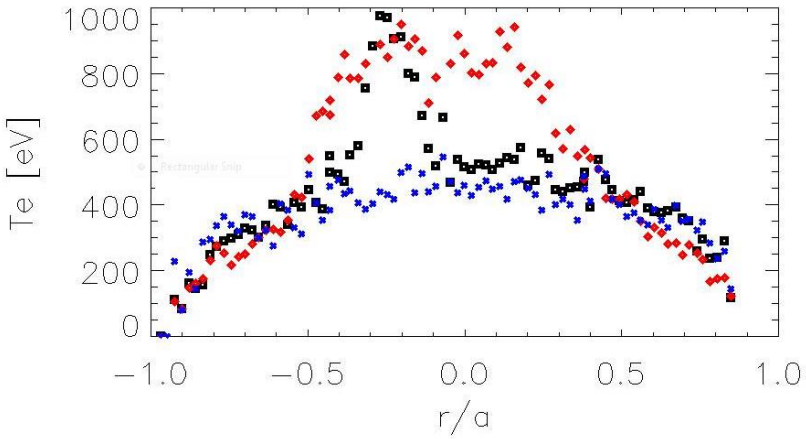

Fig. 4.3) Comparison of the electron temperature profile in RFX-mod Quasi Single Helicity (black squares DAx, red diamonds SHAx states) and MH (blue squares) plasmas

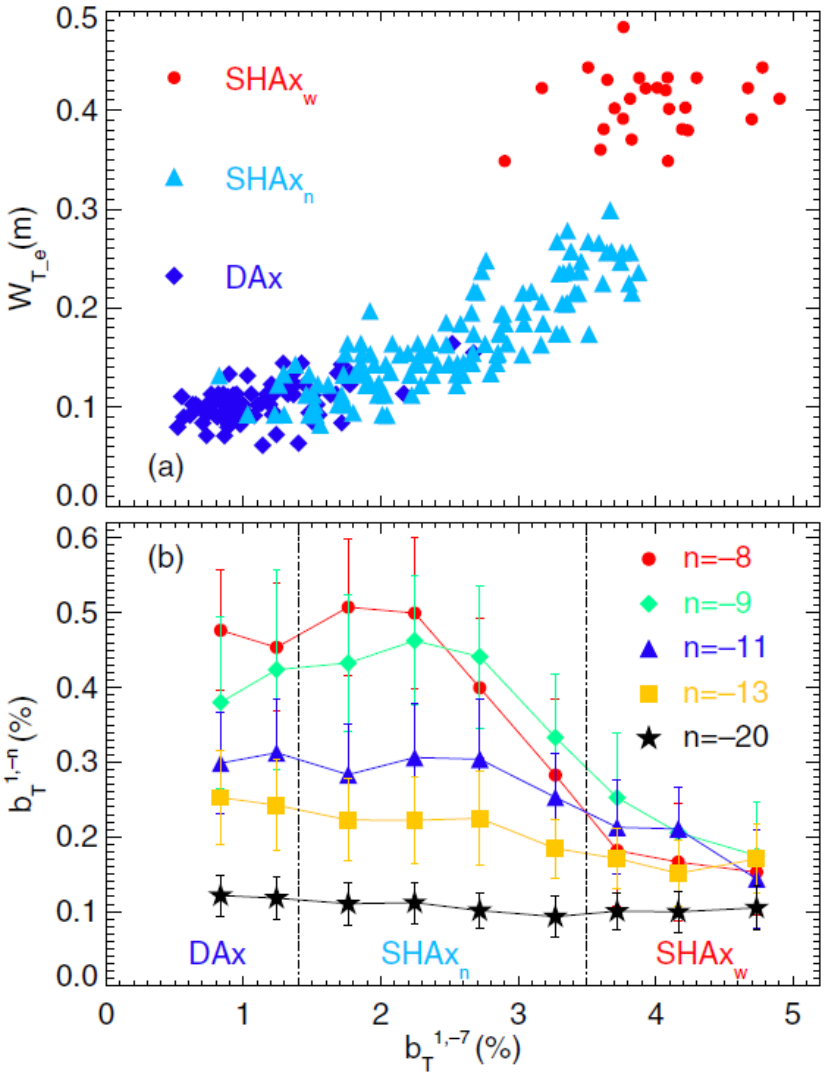

Fig. 4.4) (a) Thermal structure width W_{Te} versus the dominant mode amplitude $b^{1;-7}{}_T$. (b) Ensemble-averaged amplitude of selected secondary modes versus $b^{1;-7}{}_T$. From (Lorenzini et al., 2016)

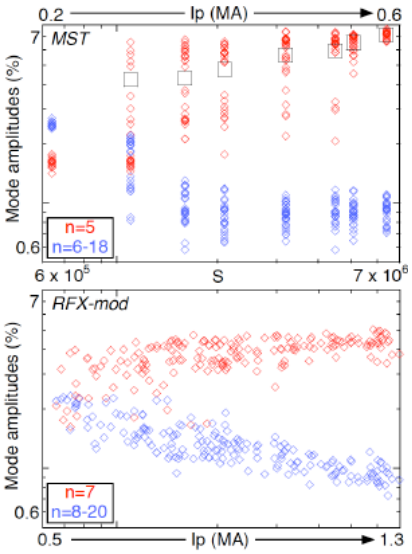

Fig. 4.5) Dominant and secondary mode scaling with the current and Lundquist number S (middle of figure) in MST (top) and RFX-mod (bottom). Open squares in MST data correspond to averages over innermost mode amplitude. Presented by B.E. Chapman at 24th IAEA Fusion Energy Conference, October 8-13, 2012, San Diego, USA, paper EX/P6-01

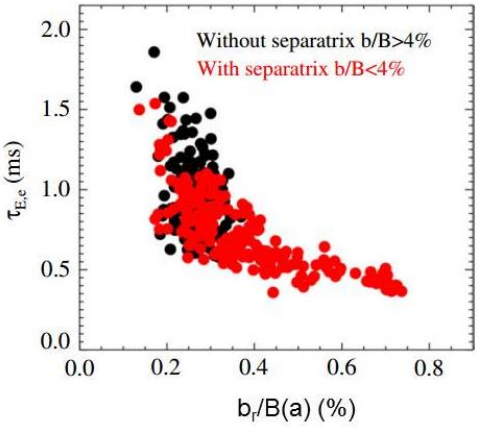

Fig. 4.6) Electron energy confinement time as a function of average secondary mode amplitude in RFX-mod; black points correspond to SHAxs, red points to DAxs (from (Carraro et al., 2013))

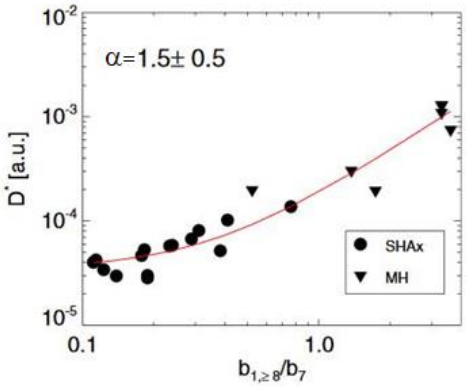

Fig. 4.7) Effective core particle diffusivity normalized to the ion thermal velocity as a function of the ratio between secondary and dominant modes (from (Auriemma et al., 2015))

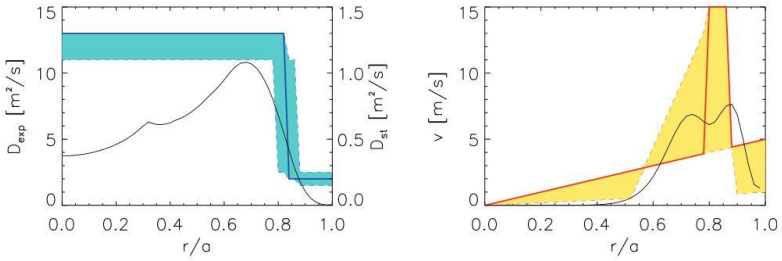

Fig. 4.8) Carbon diffusion coefficient (left) and pinch velocity (right) in RFX-mod MH; blue and red lines are the experimental values, obtained by the combination of measurements with the simulation by a collisional-radiative 1-dim transport code; coloured areas are the estimated uncertainties in the determination. Black solid lines are the values computed according to the stochastic theory. From (Barbui et al., 2015)

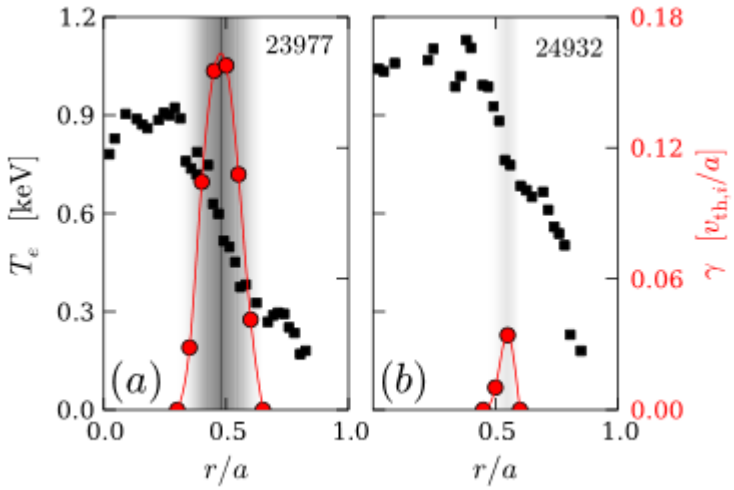

Fig. 4.9) Growth rate of the most unstable microtearing mode as obtained code for two RFX-mod plasmas by the GS2 code modified to include the RFP geometry. The grey tone corresponds to the mode growth rate. From (Predebon et al., 2010b)

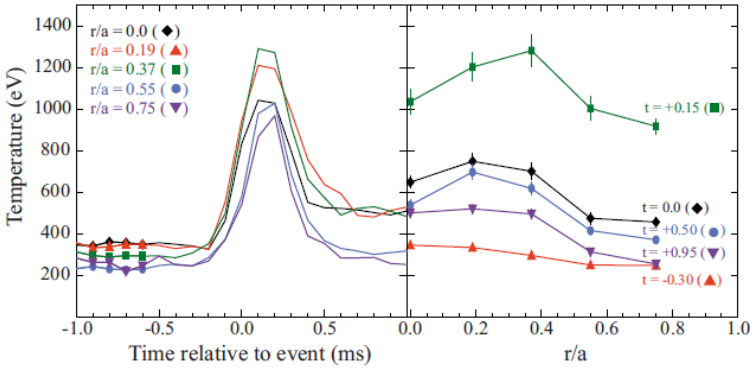

Fig. 4.10) Ensemble- averaged impurity ion temperature from charge-exchange spectroscopy in MST (Ip=390 kA, ne=1 1019 m-3) during a reconnection event: (left) time evolution at five radial locations; (right) radial profile at five times. From (Gangadhara et al., 2008)

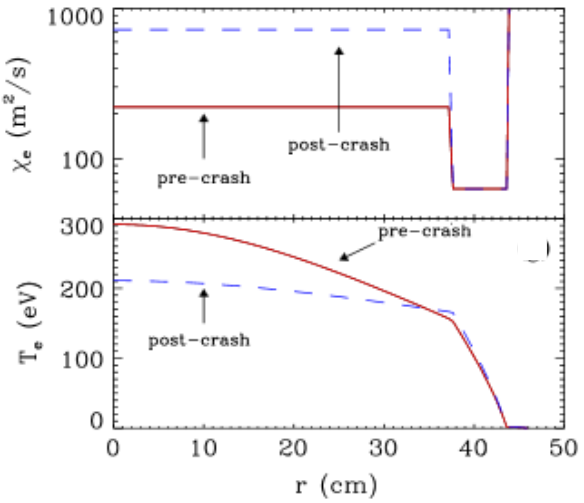

Fig. 4.11) Simulation of electron temperature and thermal diffusivity profiles before and after a reconnection event in RFX-mod. From (Frassinetti et al., 2008)

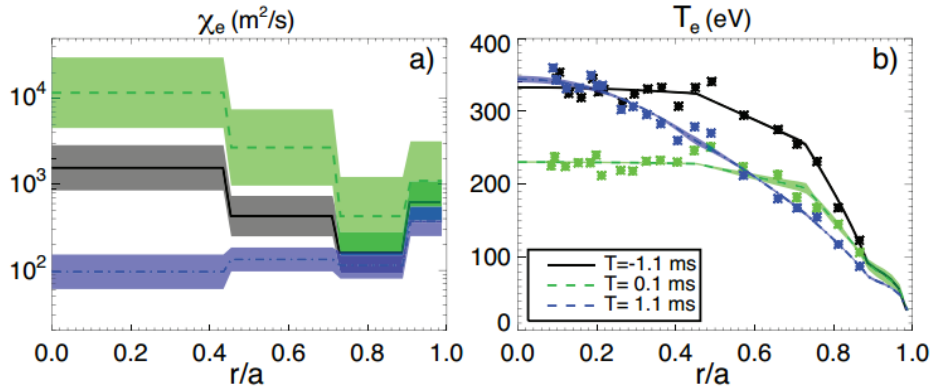

Fig. 4.12) electron thermal diffusivity (a) and tenmperature (b) in MST at three times. Black:1.1 ms before a reconnection event (RE), green: 0.1 ms after RE; blur: 1.1ms after RE. From (Reusch et al., 2011)

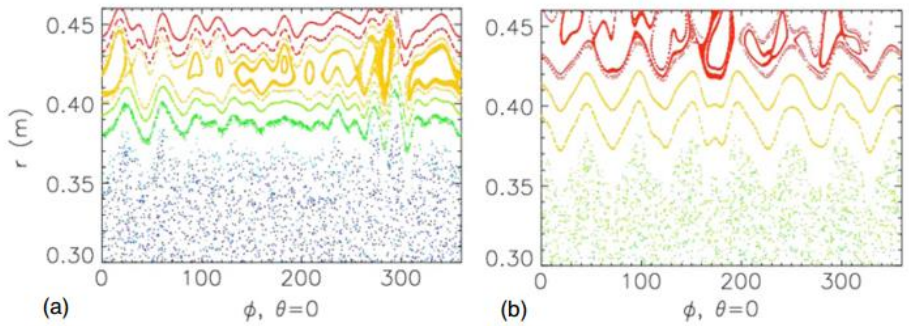

Fig. 4.13) Poincarè plot in the r-ϕ plane of the magnetic field lines in RFX-mod MH (a) and QSH (b) plasmas. From(Vianello et al., 2009)

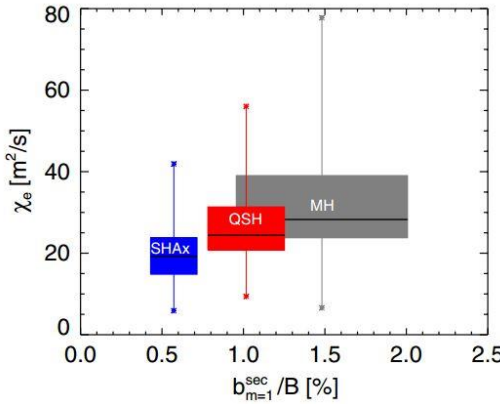

Fig. 4.14) Edge electron thermal conductivity as a function of secondary mode amplitude in RFX-mod; boxes encompass the 25% and 75% percentile of the statistical population of the measured values; bars indicate the minimum and maximum values (Vianello et al., 2009)

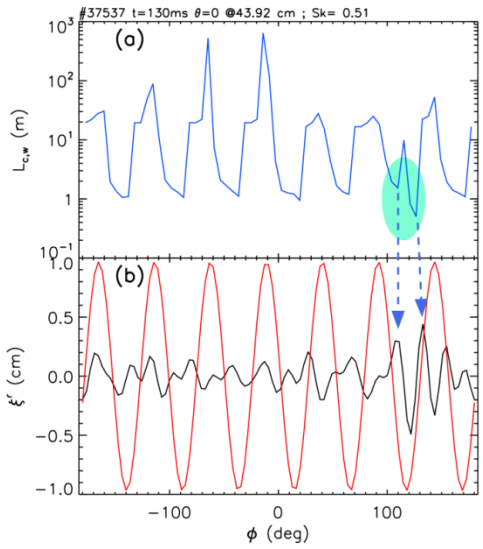

Fig. 4.15) From a RFX-mod QSH discharge: (a) magnetic field connection length in the edge (in meters, logarithmic plot) as a function of the toroidal angle; (b) displacement of the dominant (red) and secondary modes (black). The arrows indicate the interference pattern at the locking angle. From (Scarin et al., 2019)

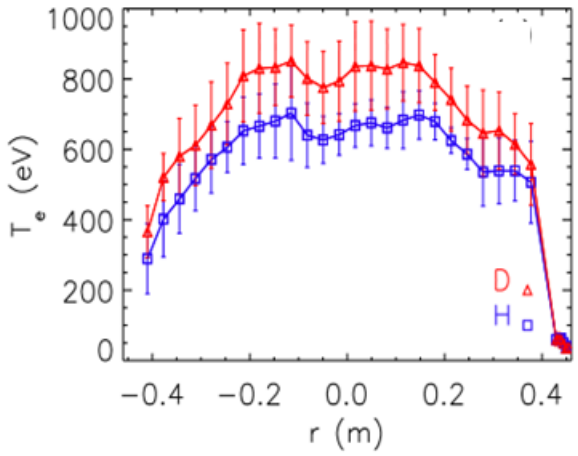

Fig. 4.16) Example of electron temperature measurements obtained in RFX-mod discharges with hydrogen (blue) and deuterium (red) as filling gas at the same electron density . In deuterium, the temperature is higher up to r ≈ 0.365m (r/a=0.8). From (Lorenzini et al., 2015)

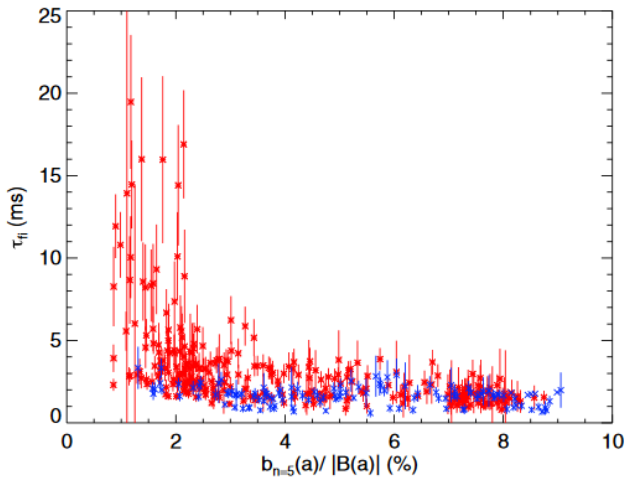

Fig. 4.17) Fast ion confinement time as a function of the normalized amplitude of the most-core resonant mode in MST (lowest values correspond to MH regimes, high values to QSH). Red points: co-injected beam; blue points: counter-injected beam. From (Anderson et al., 2014)

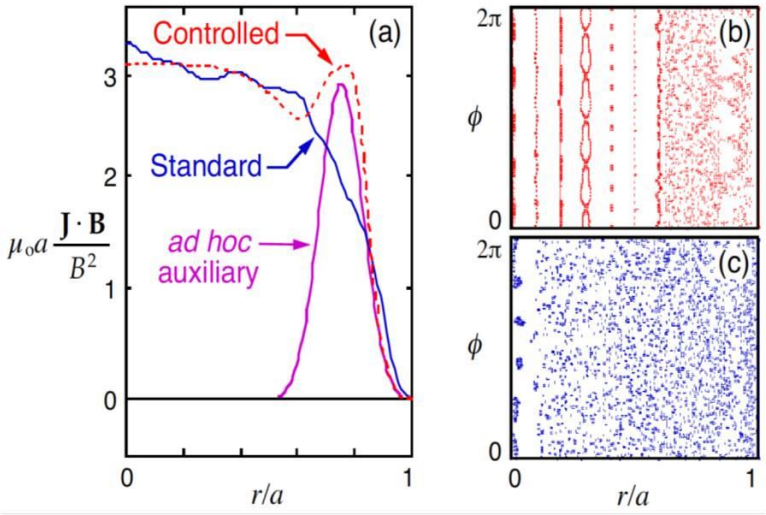

Fig. 5.1) From DEBS code: (a) $J_{//}B$ radial profile in the standard steady toroidal induction case (blue) compared to the controlled case (red) with an auxiliary ad-hoc parallel electron force (magenta). Poincaré plot of magnetic field line in controlled (b) and standard (c) cases. Adapted from (Prager, 1999)

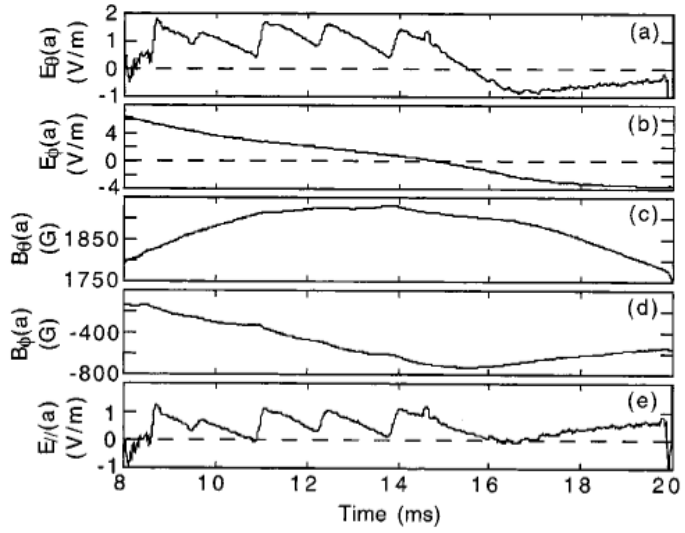

Fig. 5.2) MST 500 kA plasma with PPCD: time evolution of (a) poloidal and (b) toroidal electric fields, (c) poloidal and (d) toroidal magnetic fields and (e) parallel electric field. PPCD is applied at 8.5 ms. From (Chapman et al., 2002)

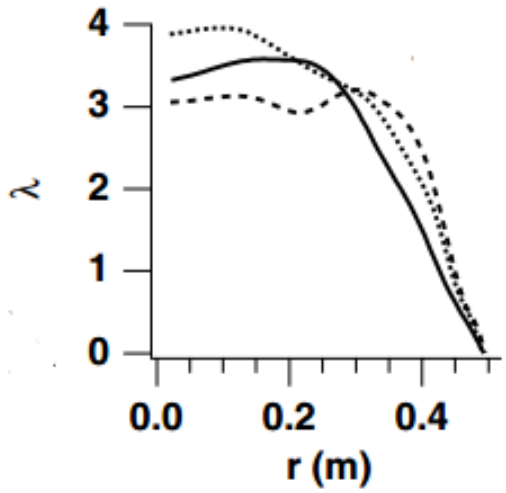

Fig. 5.3) Radial profiles of $\lambda = -\mu_0 a J_{||}/B$ in MST; (solid line) 0.25 ms before a sawtooth crash; (long dashed line) 0.25 ms after a sawtooth crash; (short dashed line) during PPCD. From (Brower et al., 2002).

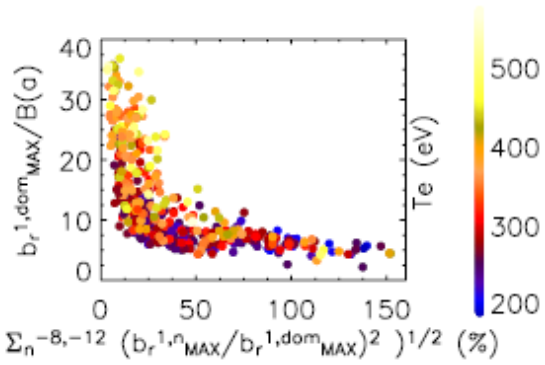

Fig. 5.4) from RFX-mod OPCD discharges, maximum of the dominant mode as a function of the ratio between the maximum of secondary modes to the maximum of the dominant one. The behavior of electron temperature is also reported. From (Terranova et al., 2007)

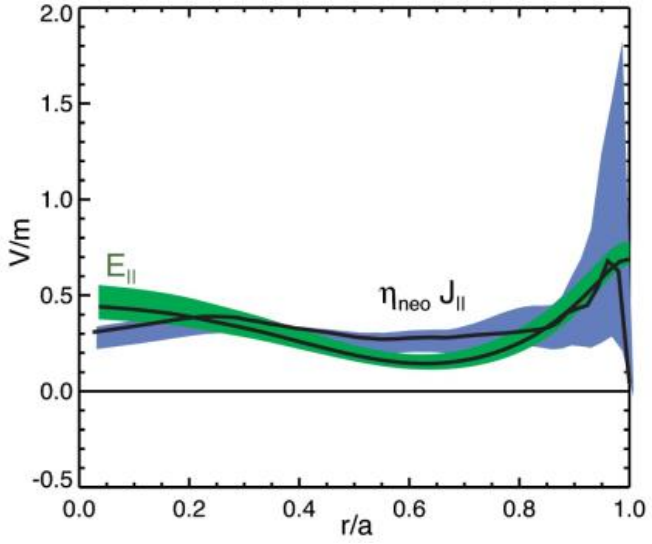

Fig. 5.5) From an MST plasma with PPCD, profile of inductive parallel electric field and product of neoclassical resistivity and parallel current. From (Anderson et al., 2005)

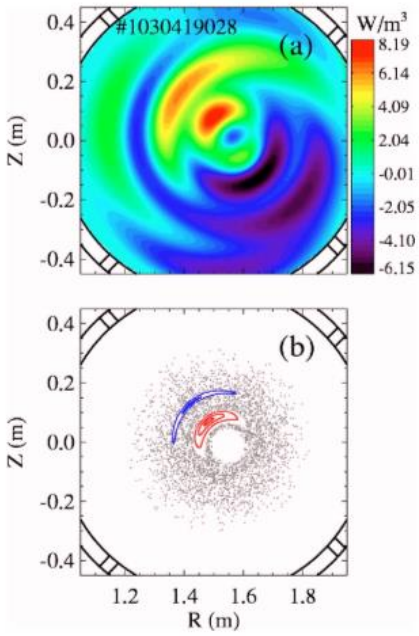

Fig. 5.6) During a MST PPCD plasma showing (a) SXR emissivity tomographic reconstruction showing (1,-6) and (1,-7) islands appearing simoultaneously in the core and (b) the corresponding reconstruction of the magnetic field lines by the ORBIT code. From (Franz et al., 2006)

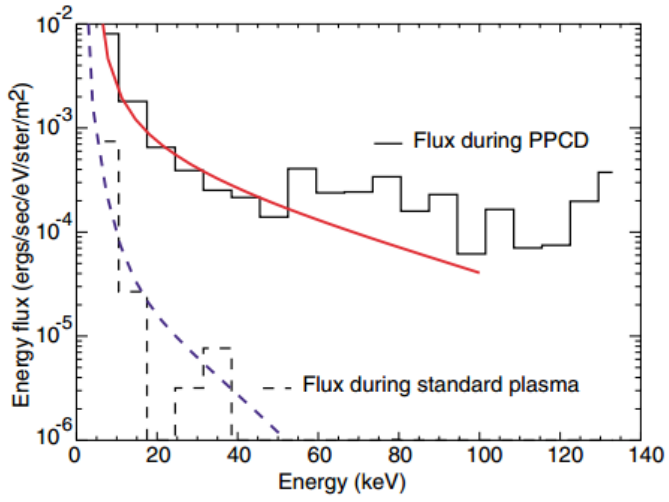

Fig. 5.7) X-ray measurements in MST PPCD and steady induction plasmas. Curves are fits of data with electron diffusion cofficients independent of (PPCD) and proportional to (steady induction) the parallel electron velocity. From (O'Connell et al., 2003)

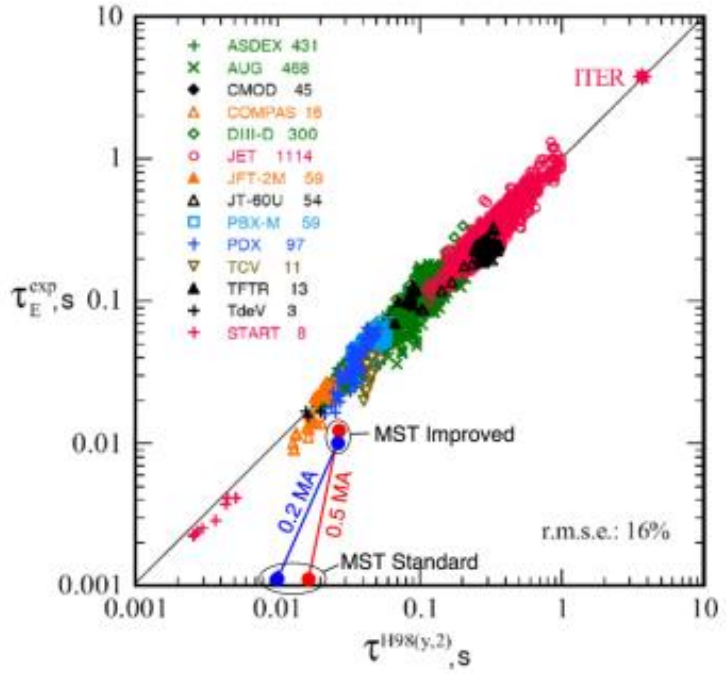

Fig. 5.8) MST confinement time compared to a "fiducial" tokamak specified by the IPB98(y,2) ELMy-H mode empirical scaling (ITER Physics Guidelines, ITER report N. 19 FDR 1 01-07-13 R 0.1). From (Chapman et al., 2010)

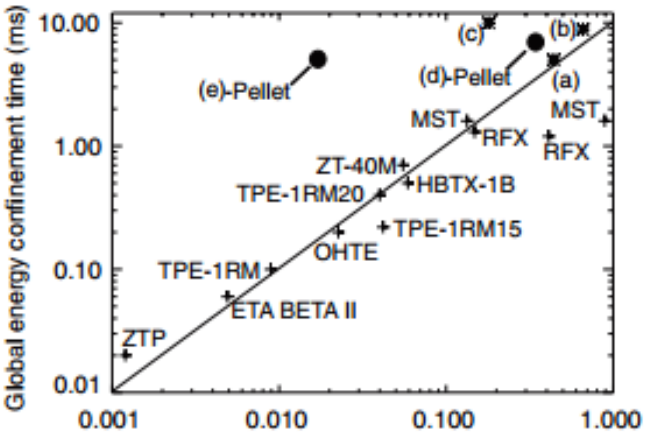

Fig. 5.9) Connor-Taylor scaling of confinement for various RFP devices including steady induction plasmas (+) and PPCD plasmas at low (*) and high (•) density. From (Wyman et al., 2009)

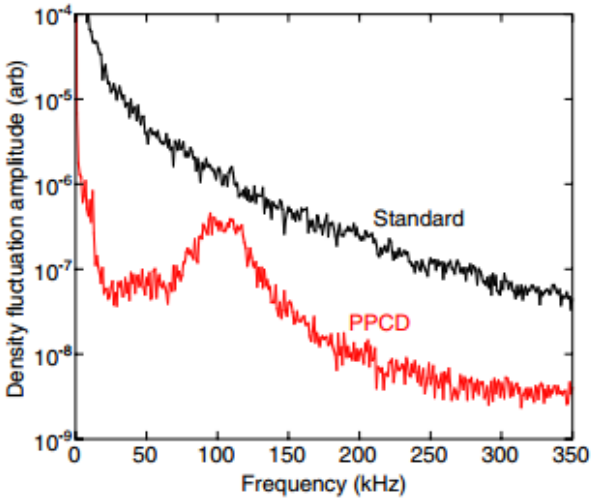

Fig. 5.10) Comparison of density fluctuation spectra at r/a ≈ 0.8 measured by FIR forward scattering in MST in steady induction and PPCD plasmas. From (Sarff et al., 2015)

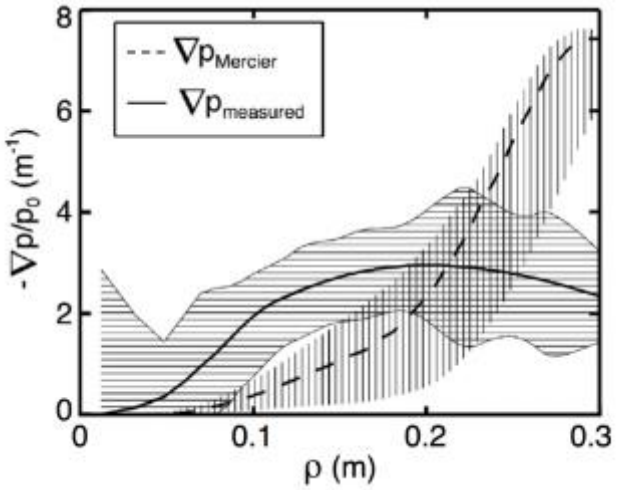

Fig. 6.1) Profile of the measured pressure gradients (solid line) in a MST discharge with pellet injection where β =26% is achieved. Dashed line is the critical Mercier pressure gradients, which is exceeded in the core plasma. Shaded regions indicate the uncertainties. From (Chapman et al., 2009)

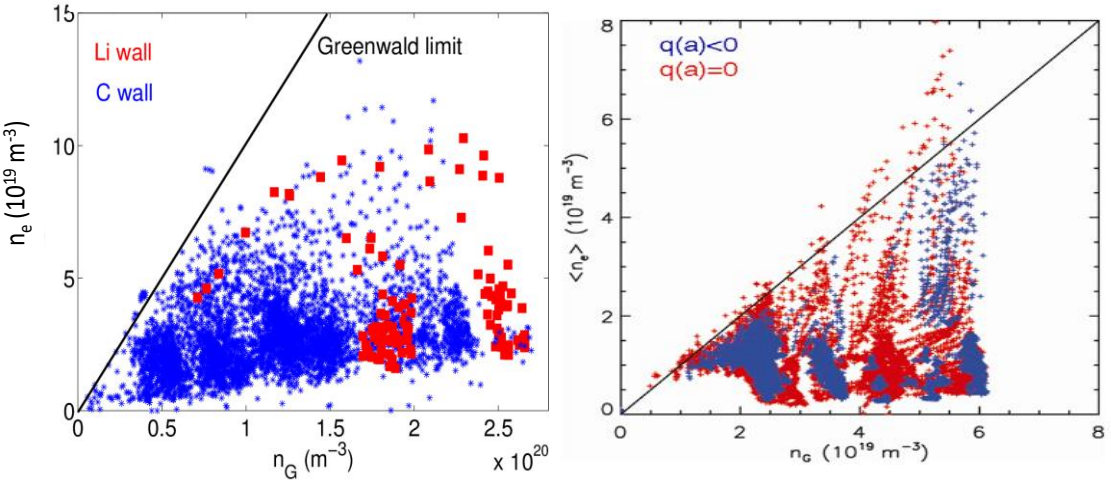

Fig. 6.2) Greenwald plot in RFX-mod (left) and MST (right). From (Sarff et al., 2015)

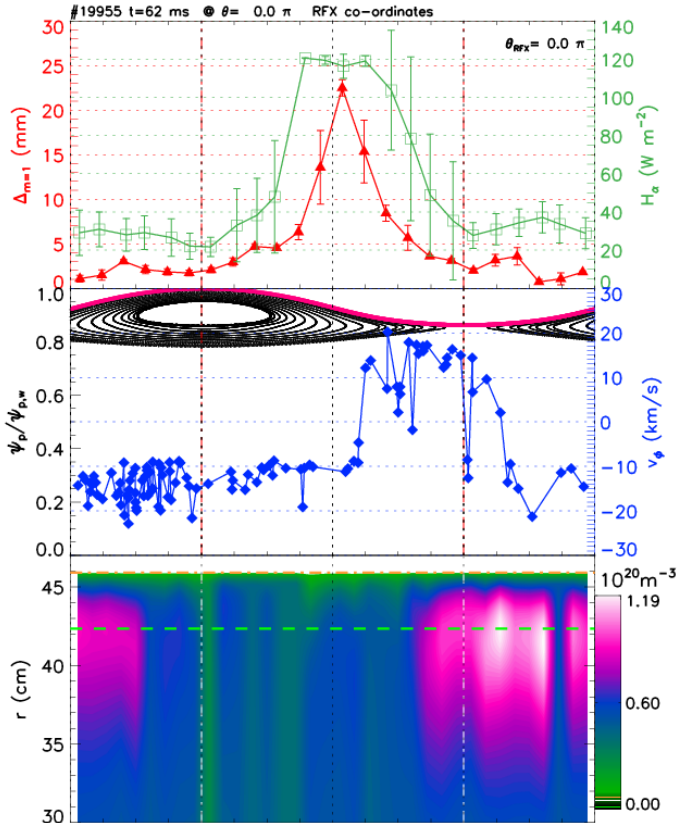

Fig. 6.3) from top to bottom: H_α emissivity (green) and plasma displacement associated to m=1 modes (red); m=0, n=1 edge island (black) and plasma edge flow (blue); (bottom): electron density profile. Data are plotted as a function of the helical angle $u(\theta, \varphi; t) = m\theta - n\varphi + \omega t$ (from (M.E. Puiatti et al., 2013))

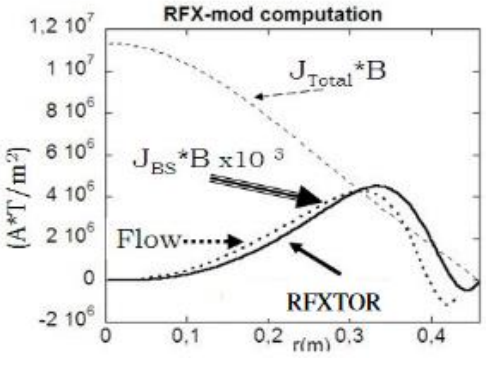

Fig. 6.4) total and bootstrap parallel current profiles calculated for RFX- J_{BS} is multiplied by 10^3. mod (from (Gobbin et al., 2009).

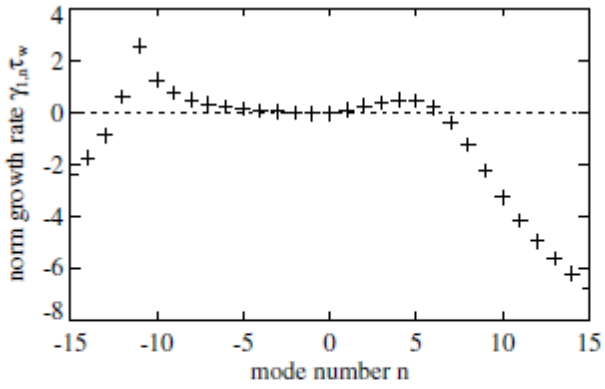

Fig. 7.1) RWM growth rates normalized to the long wall time constant $\gamma^{m,n}\tau^{m,n}$ for m=1 modes as a function of the toroidal mode number n (from (Brunsell et al., 2005))

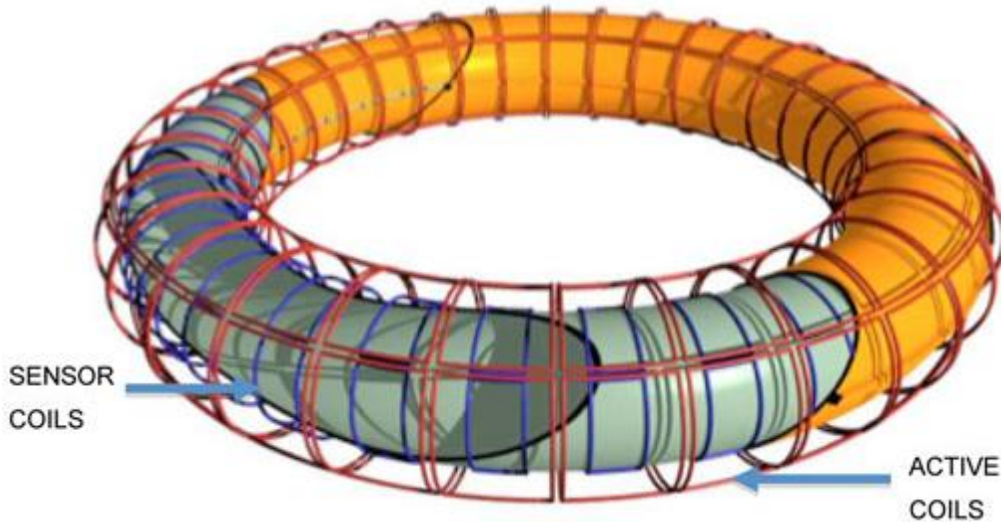

Fig. 7.2) EXTRAP T2R illustration showing the vacuum vessel (grey), the resistive wall (orange), the radial magnetic field sensors placed between the vessel and resistive wall (blue) and the active coils outside the resistive wall (red). (from Fig 2 of (Martin, 2011))

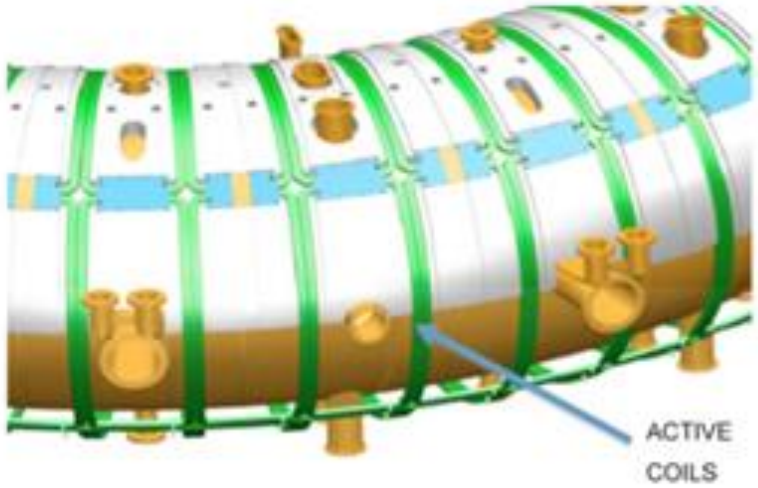

Fig. 7.3) A section of the RFX-mod mechanical and magnetic front end, highlighting active saddle coils. In each toroidal location there are 4 coils, for a total of 48 toroidal locations (from Fig 2 of (Martin, 2011))

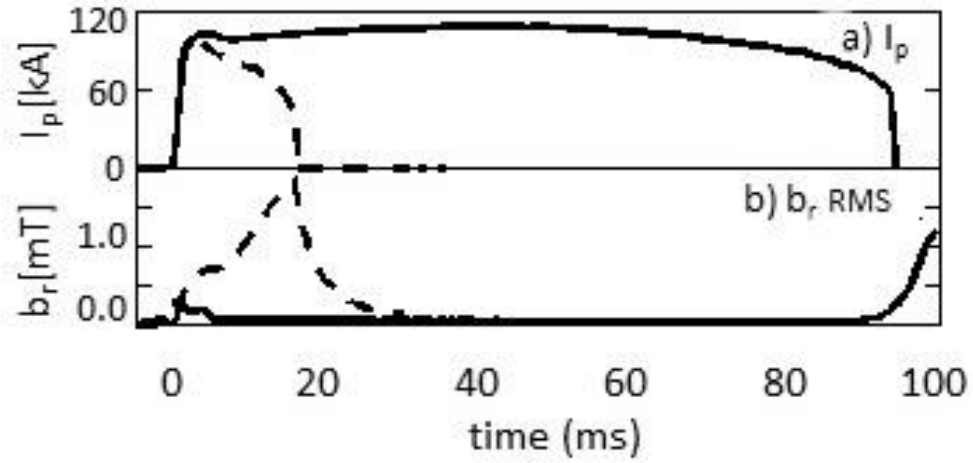

Fig. 7.4) EXTRAP T2R pulse showing the discharge current and total radial field amplitude at the sensor coil array for a discharge without control (dashed line) and with active control (line).(from (Drake et al., 2008)).

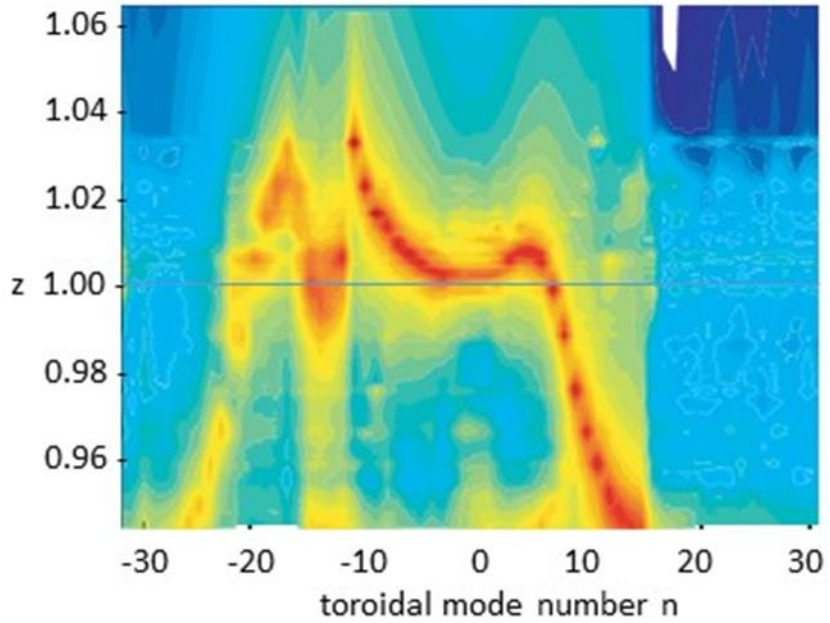

Fig. 7.5) Empirical RWM dispersion relation for T2R. Red color indicates high modal density (highly probable location of the plasma response eigenvalues; z<1 indicates stability, z>1 indicates instability. (from (Olofsson et al., 2013a)).

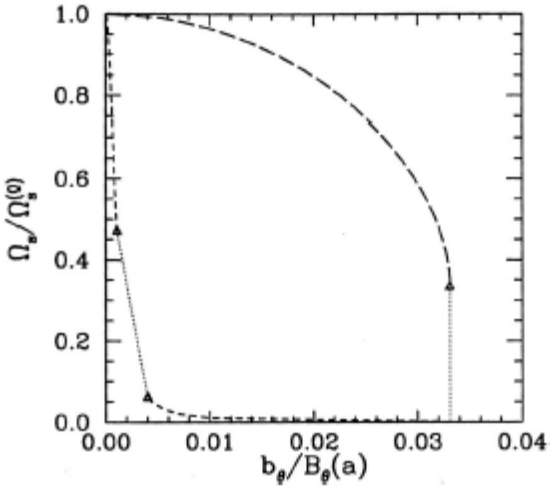

Fig. 7.6) The toroidal angular phase velocity Ω_s of the characteristic dynamo mode (normalized to the corresponding velocity Ω_s (0) in the absence of vacuum vessel eddy currents) as a function of the associated perturbed poloidal magnetic field b_θ seen at the Mirnov coils [normalized with respect to the edge equilibrium magnetic field B_θ (a)] calculated for MST (longdashed Line) and RFX (short-dashed line). (from (Fitzpatrick et al., 1999))

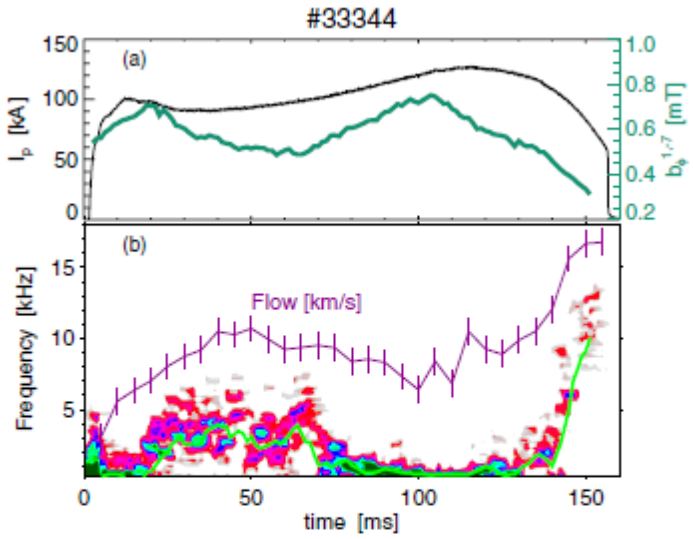

Fig. 7.7) Time traces from shot 33344 for the m = 1, n = −7 TM. Top: time traces for plasma current (black line) and toroidal field harmonic amplitude (green line). Bottom: spectrogram of the mode frequency (the light green line is the estimated time behaviour) and line-averaged plasma flow toroidal velocity from spectroscopic measurements (purple line). (from (Innocente et al., 2014)).

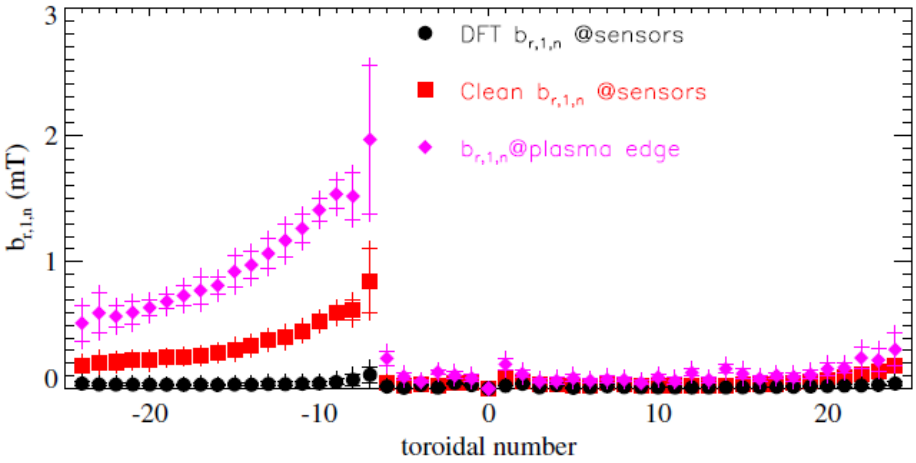

Fig. 7.8) Ensemble averaged spectra of the radial field for the m = 1 harmonics: (circles) DFT harmonics of the measurements; (squares) clean Fourier harmonics; (diamonds) harmonics extrapolated at plasma radius. A set of reproducible VS discharges is considered. Averages are taken during plasma current flat-top times, 60 < t < 120 ms, I_p = 0.79 ± 0.04 MA, $n_e = 2.1 \times 10^{19} \pm 0.2 \times 10^{19}$ m−3 and similar equilibrium. (from (L Marrelli et al., 2007))

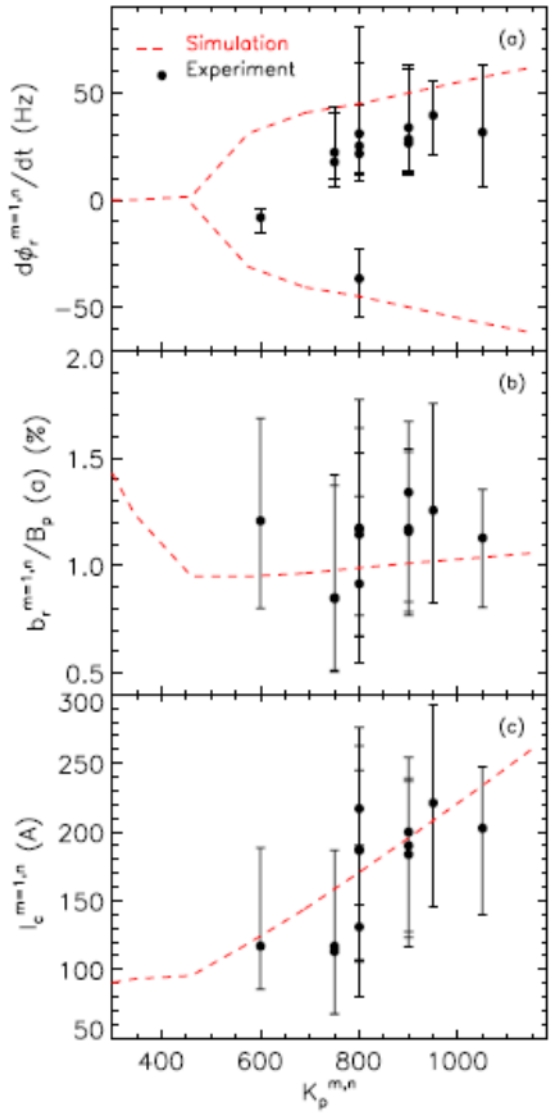

Fig. 7.9) Effect of a proportional gain scan on (a) the (1,−7) mode angular frequency, (b) the (1,−7) normalized edge radial magnetic field and (c) the (1,−7) coil current amplitude. Each point represents a flattop average and the experimental points are from a set of 1.4MA reproducible discharges. The error bars are 25th and the 75th percentiles of the data. They represent the variation of the above quantities due to the natural mode dynamics, not measurement errors. The red dashed curve represents the RFXlocking core prediction. Taken from (Piron et al., 2010)

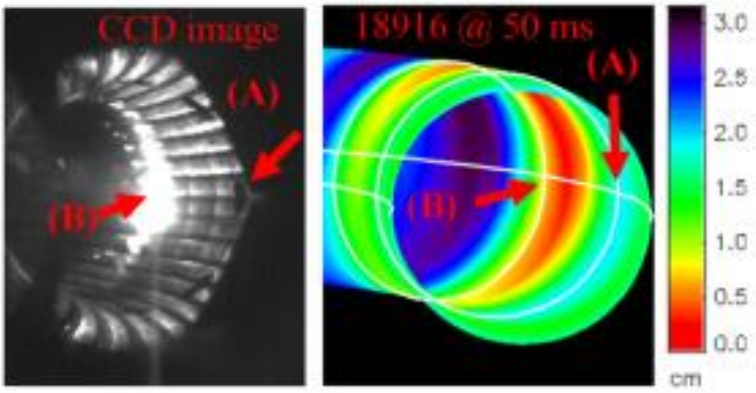

Fig. 8.1) (left) footprint of the perturbation associated to locked modes in a RFX-mod discharge as observed by a CCD camera; (right) magnetic reconstruction of the perturbation. Color code refers to the plasma-wall distance. Adapted from (P. Zanca et al., 2007)

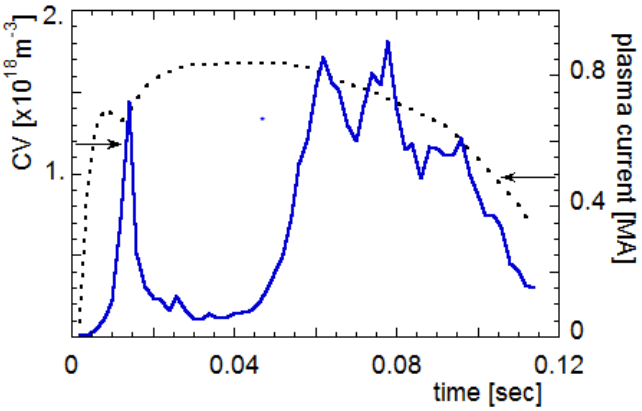

Fig. 8.2) Time evolution of plasma current (dashed) and C V density in a RFX discharge with carbon blooming, manifesting as a strong carbon enhancement and corresponding current decrease. Adapted from (Carraro et al., 1996)

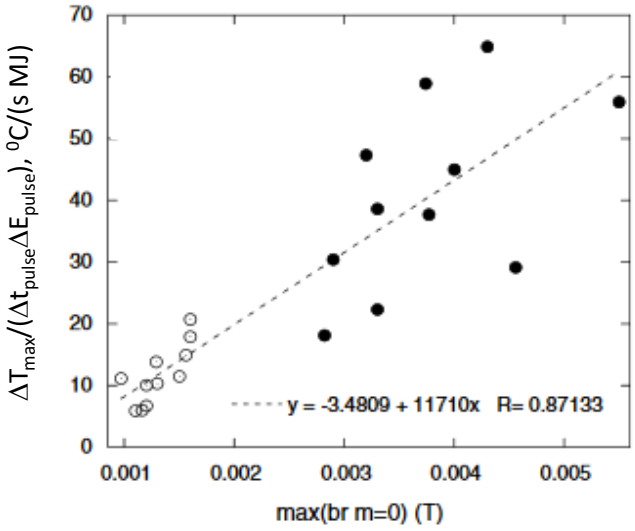

Fig. 8.3) Evolution of maximum wall temperature in RFX-mod as a function of m=0 maximum radial field. Empty circles: with feedback; black circles: without feedback. From (P. Zanca et al., 2007)

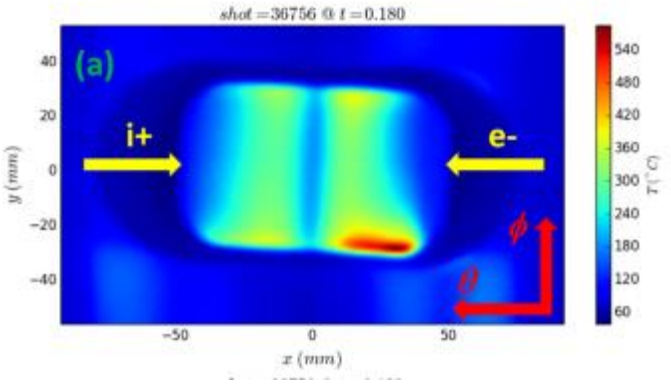

Fig. 8.4) Graphite temperature by an IR camera in RFX-mod; the x axis corresponds to the poloidal direction, the y axis to the toroidal one. From (P. Innocente et al., 2017)

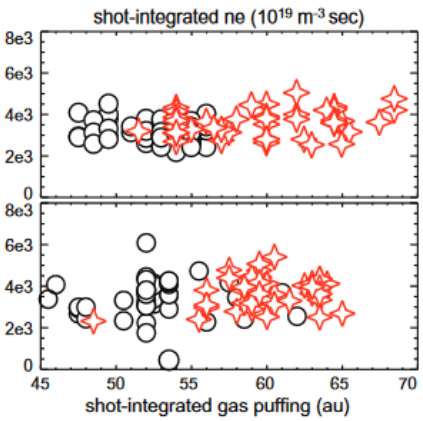

Fig. 8.5) Electron density integrated during the current flat-top as a function of the total number of particles puffed in the MST device before (black circles) and after (red stars) boronisation. From (Ko et al., 2013)

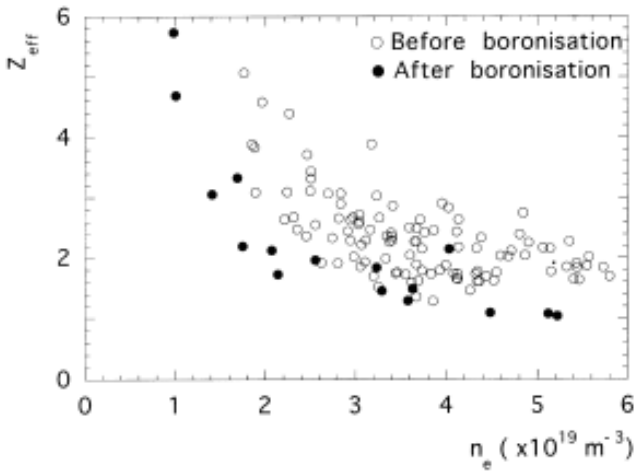

Fig. 8.6) Effect of boronisation on Zeff in the RFX device. From (Carraro et al., 1999)

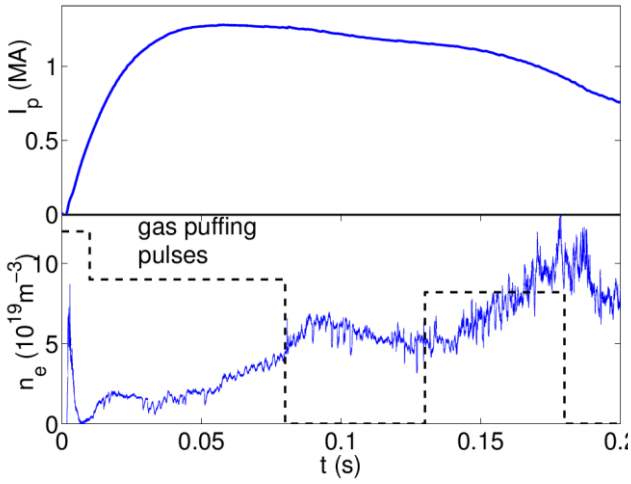

Fig. 8.7) Time evolution of plasma current (top) and electron density (bottom) after lithization in RFX-mod. Pulses of puffed gas are superimposed (dashed), showing the good response of density. From (M.E. Puiatti et al., 2013)

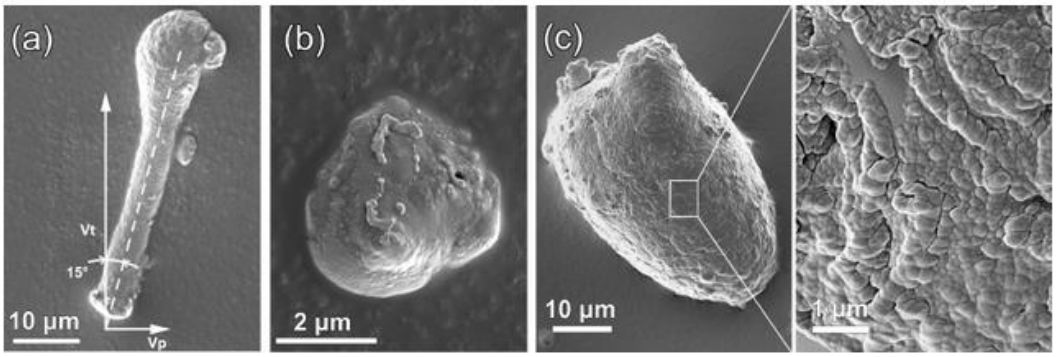

Fig. 8.8) Examples of SEM analysis of dust particles collected post-mortem in EXTRAP T2R.by adhesive tape.Particles are mainly spheroids covered by deposits (b) with granular morphology (b) and (c). Few elongated particles also observed (a). From (Bykov et al., 2014)

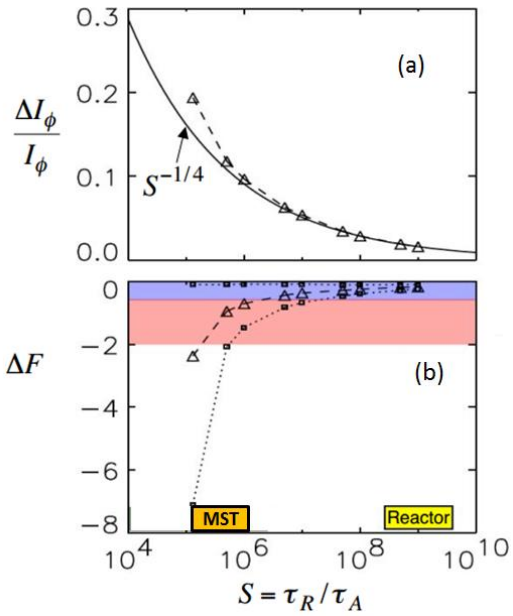

Fig. 9.1) In OFCD plasmas, (a) fractional axial current and (b) F parameter variation as a function of S. Triangles in (b) are time averaged mean values, squares on dotted curves F-oscillation extremes. The red region identifies the PPCD parameter space, the blue region the standard space. S ranges relative to MST, and the extrapolation to the reactor are highlighted. Adapted from (Ebrahimi et al., 2003)

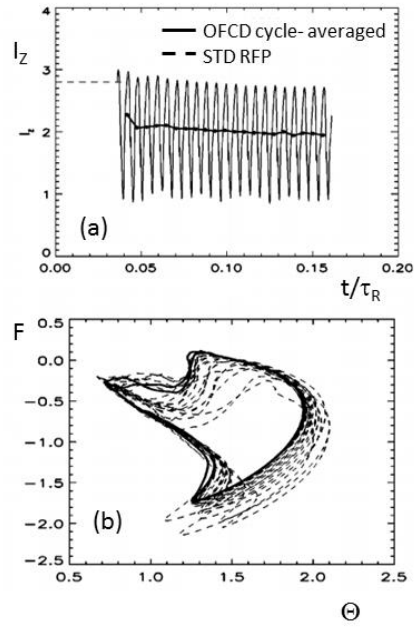

Fig. 9.2) (a) Toroidal current and (b) F-Θ trajectory for OFCD sustained plasma; simulation with S= 5 10^5 . The solid curve shows the F-Θ limit cycle.From (Ebrahimi et al., 2003)

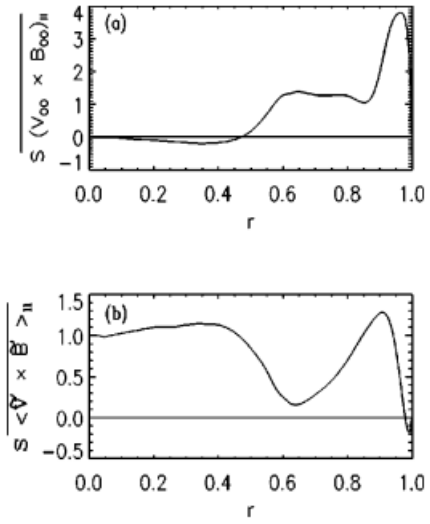

Fig. 9.3) Cycle- averaged dynamo terms from (a) symmetric oscillations and (b) asymmetric tearing dynamo terms $\langle \tilde{\boldsymbol{v}} \, x \, \tilde{\boldsymbol{B}} \rangle_{||}$. *From (Ebrahimi et al., 2003)*

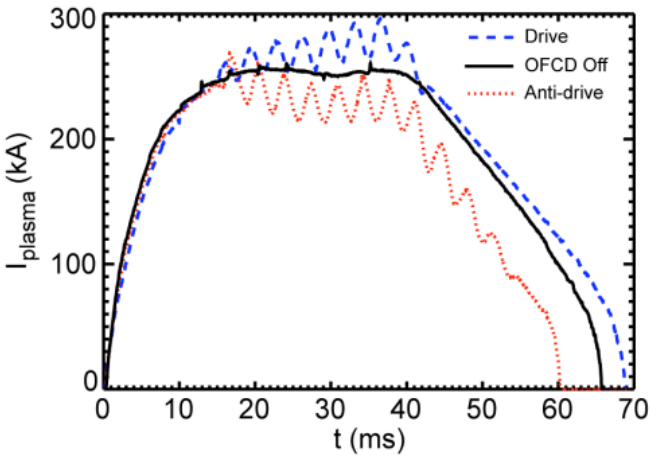

Fig. 9.4) Time evolution of plasma current in MST discharges with OFCD (drive and antidrive) compared to the case without OFCD . From (McCollam et al., 2006)

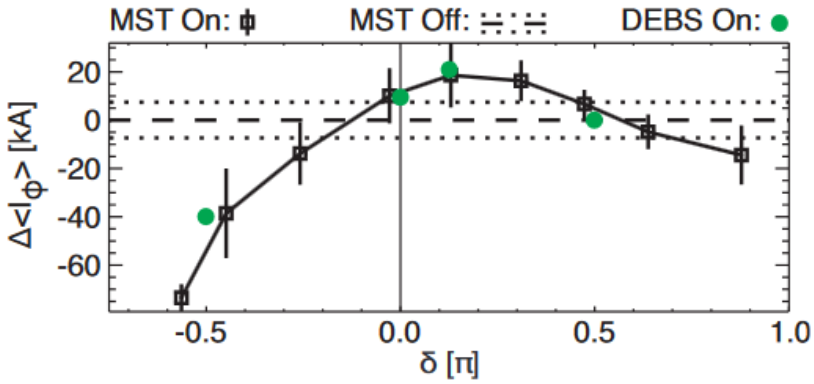

Fig. 9.5) Phase dependence of the plasma current change (cycle averaged) in MST OFCD experiments (squares) compared to a DEBS numerical simulation (green circles) and to the case without OFCD (dashed line with dotted uncertainties). From (McCollam et al., 2010)

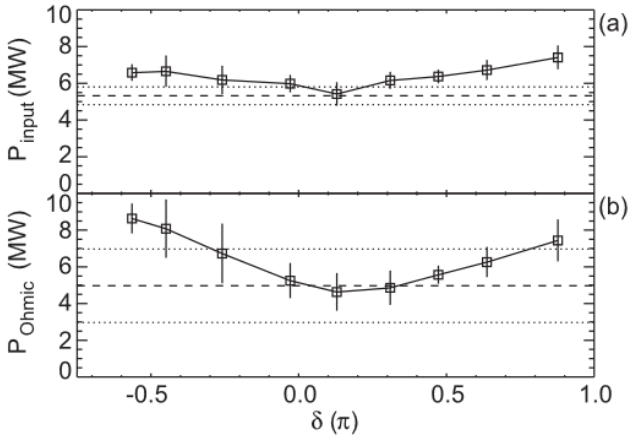

Fig. 9.6) During a MST OFCD pulse: phase dependence of m/n=0/1-4 (a) and m/n=1/6-15 (b) tearing mode amplitude during the OFCD discharges.Error bars indicate the pulse-to-pulse variability. The OFCD off case is shown for comparison (dashed lines, with dotted lines pulse-to pulse variability). From (McCollam et al., 2006)

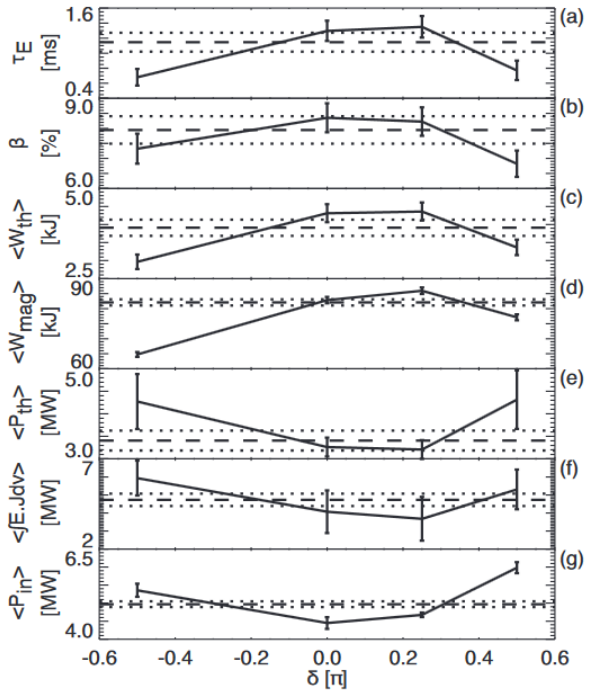

Fig. 9.7) In MST, phase dependence of (a) energy confinement time, (b) plasma thermal pressure, (c) thermal energy, (d) magnetic energy, (e)thermal input power, (f) power transfer from magnetic field, (g) total input power for discharge ensambles with OFCD (solid) and without (dashed, with dotted uncertainties). All quantities are cycle averages. From (McCollam et al., 2010)